

**OPTIMISATION AND DESIGN OF TWO MICRO-HYDRO TURBINES FOR  
MEDIUM AND LOW HEAD APPLICATIONS**

by  
**Julian Randelhoff**

Thesis submitted in partial fulfillment of the academic requirements for the degree of  
Master of Science in engineering in the department of  
Mechanical Engineering

University of Natal  
Durban  
2000

## ABSTRACT

The necessity to develop an automated process for the design of micro-hydro power systems was based on the increasing demand for hydropower as a renewable energy source and to develop cost effective power supplies to rural areas. The application of the formula for the design of these systems is then to simplify the selection of the turbine sizing and is made possible by the similarity laws that exist within turbine and pump families. In addition the sizing of the supply and exhaust piping is also a matter of scaling. No selection process of turbine type is included due to the limitations of cost effectiveness and the category of size into which the turbine was specified. Furthermore, a new approach to turbine design was separately undertaken to satisfy low head and low flow-rate conditions. However, it was only designed up to a cost analysis with no manufacturing having been undertaken.

The axial flow turbine, which was most suited for micro-hydro was designed and built as a prototype with a standardized mounting frame. The initial conditions used to generate the velocity vectors and angles were specific to the installation site and used to computationally generate the rotor and stator blades. This required an analysis of the different profiles available as well as research into their design. Once the blade profile stacking had been determined, this was translated into a software program that developed the blades from site-specific initial conditions. However, the design of the blades was interdependent on the dimensioning of the rest of the turbine components and designing these in parallel proved to be an intricate task. With the design complete, the turbine was then installed and testing proceeded with the use of pressure gauges and the results of torque and rpm obtained from a dynamometer. Analysis of the results was undertaken and presented in graphical format with comments on both the design and results.

## ACKNOWLEDGEMENTS

The author wishes to express his gratitude to the following people:

- The Workshop staff in the Department of Mechanical Engineering for their assistance and invaluable advice.
- Gary Austin for his professional approach to his work and his standard of excellence
- Patrick Morewood for his tireless insight and application of the fabrication of the blades.
- Jack Coombie for his assistance in the development of the turbine blades.
- Dr. Sagren Govender, Fred Cooper and Les Tessororf of Natal Foundary Supplies for their considerable input of information regarding the investment casting process.
- Prof. G D J Smith who supervised the project for his time and the concerted effort with which he administered advice and guidance throughout each phase of the project.
- Gary Austin, Jack Coombie and Geraldine Touche Du Poujol for their time and effort in photographing the turbine
- Prof. Saneshan Govender for his role as supervisor in the marking stage of the completion of the thesis
- My Father God without whom none of this would have been possible

## TABLE OF CONTENTS

	Page
ABSRTACT	ii
ACKNOWLEDGEMENTS	iii
NOMENCLATURE	x
CHAPTER 1 INTRODUCTION	1
CHAPTER 2 LITERATURE REVIEW	3
CHAPTER 3 DESIGNING THE TURBINE	37
CHAPTER 4 PROGRAMMING FOR BLADE DESIGN	77
CHAPTER 5 EXPERIMENTAL RESULTS	88
CHAPTER 6 CONCLUSIONS AND RECOMMENDATIONS	112
CHAPTER 7 APPENDIX	120
CHAPTER 8 REFERENCES	166
CHAPTER 9 DRAWINGS AND SKETCHES	167

<b>1</b>	<b>INTRODUCTION.....</b>	<b>1</b>
<b>2</b>	<b>LITERATURE REVIEW.....</b>	<b>3</b>
<b>2.1</b>	<b>Hydrodynamic Drag .....</b>	<b>3</b>
2.1.1	Skin Friction.....	3
2.1.2	Critical Reynolds Number .....	3
2.1.3	Surface Roughness.....	4
2.1.4	Pressure Drag .....	4
2.1.5	Drag Characteristics in Cavitating Flow.....	5
<b>2.2</b>	<b>Airfoil Data for Blade Design.....</b>	<b>5</b>
2.2.1	Types of Airfoil Section.....	5
2.2.2	Lift.....	6
2.2.3	Pitching moment .....	6
2.2.4	Drag.....	6
2.2.5	Flow Deflection in Cascade Airfoils.....	6
2.2.6	Flow Deflection in Fan Blades.....	7
2.2.7	Isolated Airfoil Data.....	8
2.2.8	Cascade Airfoil Data.....	10
2.2.9	Effect of Reynold's Number on Airfoil Data.....	10
<b>2.3</b>	<b>Fundamentals of Hydraulics.....</b>	<b>11</b>
2.3.1	Introduction.....	11
2.3.2	The pressure distribution.....	12
2.3.3	Airfoil Characteristics .....	12
2.3.4	Airfoil blade design methods for turbines.....	12
2.3.5	Minimum spacing of airfoil blades .....	13
2.3.6	Work done on airfoil blades.....	14
2.3.7	Effect of blade pitch on Lift and Drag .....	15
<b>2.4</b>	<b>Axial Flow Turbines .....</b>	<b>16</b>

2.4.1	Propeller turbines .....	16
2.4.2	Turbine constants and empirical equations.....	17
2.4.3	Experience Curves .....	20
2.4.4	Runner Speed .....	21
2.4.5	Runner Diameter .....	21
2.4.6	Turbine efficiency .....	22
2.4.7	Cavitation and Turbine Setting .....	22
2.4.8	Cavitation Coefficient.....	23
2.4.9	Control of Cavitation .....	26
2.4.10	Selection of the Turbine Setting.....	27
2.4.11	Draft Tubes .....	29
<b>2.5</b>	<b>Diffuser design for small turbines .....</b>	<b>30</b>
2.5.1	Effect of the draft tube on performance.....	31
2.5.2	Turbine-Draft tube matching .....	33
2.5.3	Draft tube performance .....	34
<b>3</b>	<b>DESIGNING THE TURBINE.....</b>	<b>37</b>
<b>3.1</b>	<b>Site specific parameters.....</b>	<b>37</b>
<b>3.2</b>	<b>Piping .....</b>	<b>38</b>
3.2.1	Supply .....	38
3.2.2	Penstock .....	39
3.2.3	Diffuser .....	39
<b>3.3</b>	<b>Stuffing Box .....</b>	<b>40</b>
3.3.1	Design conditions.....	40
3.3.2	Design Options.....	40
<b>3.4</b>	<b>Drive Train .....</b>	<b>41</b>
<b>3.5</b>	<b>Bearing Selection.....</b>	<b>42</b>

3.5.1	Bearing types.....	42
3.5.2	Final selection .....	42
3.5.3	Pre-load spring .....	43
<b>3.6</b>	<b>Bearing Pedestal.....</b>	<b>44</b>
3.6.1	Design options.....	44
3.6.2	Final selection .....	45
<b>3.7</b>	<b>Main support frame.....</b>	<b>46</b>
<b>3.8</b>	<b>Rotor and Stator.....</b>	<b>47</b>
3.8.1	Shaping the blade.....	49
3.8.2	Defining the pressure distribution.....	50
3.8.3	Location of the transition point.....	51
3.8.4	Flow conditions.....	52
<b>3.9</b>	<b>Draft tube design considerations .....</b>	<b>53</b>
3.9.1	General design.....	53
3.9.2	Draft tube bend.....	53
3.9.3	Choice of speed and setting .....	56
3.9.4	Selection of the turbine setting.....	66
3.9.5	Manufacturing procedures .....	68
<b>3.10</b>	<b>Manufacturing the master patterns .....</b>	<b>72</b>
3.10.1	Defining the blade.....	72
3.10.2	Profile fabrication .....	73
3.10.3	Producing a master pattern.....	74
3.10.4	The blades .....	75
<b>4</b>	<b>PROGRAMMING FOR BLADE DESIGN.....</b>	<b>77</b>
<b>4.1</b>	<b>The governing equations .....</b>	<b>77</b>
<b>4.2</b>	<b>Program structure.....</b>	<b>78</b>

4.3	Profile Selection.....	83
4.4	Geometric Representation.....	85
<b>5</b>	<b>EXPERIMENTAL RESULTS .....</b>	<b>88</b>
5.1	Experimental apparatus.....	88
5.2	Objectives.....	88
5.3	Experimental procedure.....	89
5.3.1	Methods of water flow measurement.....	89
5.3.2	Obtaining results .....	89
5.4	Experimental results.....	92
5.5	Precautions for the analysis .....	99
5.6	Analysis of the results .....	100
<b>6</b>	<b>CONCLUSIONS AND RECOMMENDATIONS.....</b>	<b>112</b>
6.1	Conclusions about the design.....	112
6.2	Conclusions about the experimental results .....	113
6.3	Recommendations .....	117
<b>7</b>	<b>APPENDIX.....</b>	<b>120</b>
7.1	Curtain plate.....	120
7.2	Bearing Design .....	122
7.3	Pre-load spring.....	124



<b>7.4</b>	<b>Bearing pedestal design .....</b>	<b>126</b>
7.4.1	Design of the diaphragm plates.....	126
7.4.2	Calculating the stress of the plate supporting the thrust bearing .....	127
<b>7.5</b>	<b>Drive Train Shaft Design.....</b>	<b>128</b>
<b>7.6</b>	<b>Shaft Design.....</b>	<b>129</b>
<b>7.7</b>	<b>Rotor and Stator design.....</b>	<b>132</b>
7.7.1	Determining the axial flow velocity.....	132
7.7.2	Determining the solidity.....	134
7.7.3	Characteristics of the diffuser .....	136
7.7.4	Design considerations .....	138
7.7.5	Determining a suitable rotor speed .....	148
7.7.6	Cavitation.....	151
<b>7.8</b>	<b>Programming for blade development .....</b>	<b>159</b>
7.8.1	Stator and rotor blade geometry.....	159
7.8.2	Plotting the camber line .....	159
7.8.3	Circular arc hub and tip caps.....	159
7.8.4	Defining the solidity.....	160
7.8.5	Developing the projected and interpolated points.....	160
7.8.6	Plotting the figures .....	160
7.8.7	Designing the diffuser.....	160
<b>7.9</b>	<b>Manufacturing Procedure.....</b>	<b>161</b>
7.9.1	Job schedule task list.....	161
<b>7.10</b>	<b>Inventory.....</b>	<b>163</b>
<b>8</b>	<b>REFERENCES.....</b>	<b>166</b>
<b>9</b>	<b>DRAWINGS.....</b>	<b>167</b>

## Nomenclature:

### Latin

- $c$  = length of chord of airfoil blade [m]  
 $\Delta C_w$  = change in tangential component [ $\text{ms}^{-1}$ ]  
 $C_D$  = Coefficient of drag  
 $C_L$  = Coefficient of lift  
 $C_f$  = coefficient of drag of the reference area  $t^2$   
 $D_h, D_t$  = hub and tip diameters respectively [m]  
 $En 8$  = grade of plain carbon steel  
 $H = H_{\text{net}}$  [m]  
 $h_{f2-3}$  = head loss between points 2 and 3 [m]  
 $h_L$  = head loss summed across the stator and rotor [m]  
 $\dot{m}$  = mass flow rate [ $\text{kgs}^{-1}$ ]  
 $M$  = moment [Nm]  
 $M_t$  = torque [Nm]  
 $n_s, N_s$  = specific speed  
 $P$  = power [kW, W]  
 $P_2$  = pressure at point 2, [kPa]  
 $P_3$  = pressure at point 3, [kPa]  
 $P.C.D.$  = pitch diameter  
 $P_H$  = hydraulic power [kW] {based on  $m \cdot U_b \cdot C_w$ }  
 $Q$  = volume flow rate [ $\text{m}^3 \text{s}^{-1}$ ]  
 $Re$  = Reynolds Number  
 $RF$  = reserve factor  
 $S_e$  = endurance strength [MPa]  
 $S_u$  = ultimate tensile strength [MPa]  
 $S_y$  = yield strength [MPa]  
 $T$  = torque produced [Nm]  
 $\vec{U}$  = cross sectional average velocity vector with magnitude  $U$   
 $U_b$  = tangential velocity of blade [ $\text{ms}^{-1}$ ]  
 $V_2$  = water velocity at point 2, [ $\text{ms}^{-2}$ ]  
 $V_3$  = water velocity at point 3, [ $\text{ms}^{-2}$ ]  
 $V_A, C_x$  = axial velocity [ $\text{ms}^{-1}$ ]  
 $V_{\text{abs}}$  = absolute velocity component [ $\text{ms}^{-1}$ ]  
 $V_{\text{rel}}$  = relative velocity component [ $\text{ms}^{-1}$ ]  
 $V_{\text{tan}}$  = tangential component [ $\text{ms}^{-1}$ ]  
 $z_2$  = elevation of point 2 above the reference datum, [m]  
 $z_3$  = elevation of point 3 above the reference datum, [m]

### Greek

- $\alpha_1$  = angle of blade @ stator absolute outlet [degrees]  
 $\alpha_2$  = angle of blade @ rotor absolute outlet [degrees]  
 $\beta_1$  = angle of stator relative outlet velocity [degrees]  
 $\beta_2$  = angle of rotor relative outlet velocity [degrees]  
 $\gamma$  = specific weight of water, [ $\text{kgm}^{-3}$ ]

$\rho$  = density [ $\text{kgm}^{-3}$ ]  
 $\sigma$  = cavitation coefficient  
 $\sigma_{alt}$  = alternating stress [MPa]  
 $\sigma_m$  = mean stress [MPa]  
 $\omega$  =  $\text{rads}^{-1}$

#### Subscripts

*abs* = absolute  
*rel* = relative  
*tan* = tangential  
*CS* = control surface

## CHAPTER 1

### INTRODUCTION

From the increase in rural settlements has arisen the need for the development of structured grids providing water and electricity. The development of the automation of a water turbine designing process may serve to facilitate such urbanization. The advantage of drawing power from a hydroelectric turbine over typical grids is the reduction in the cost of power and the fact that it serves as a renewable energy source. Considering the initial cost of installation can be recovered after a period of approximately 3 years, the cost of maintaining the turbine thereafter provides power at a very cost-effective level.

The power output of the turbine is limited by the available flow rate of water measured against its potential energy gradient and micro-hydro is typically in the power range of 0-100kW. Its applications can be extended from supplying electricity, to irrigation and further to simply pump water to areas not in the immediate vicinity of a river. Applications such as irrigation and water supply are currently the most suitable since the supply of electricity in the form of 50Hz, 220V AC requires that the turbine be governed; a technical challenge which has yet to be overcome at a level appropriate to rural communities. Governing of the electricity generated may take the form of simple bob weight mechanical controllers or by creating a DC voltage buffer and then converting to AC as is applied for wind power generators. Variation in the power output is caused by the change in the flow rate of the supply to the turbine and furthermore the change in load introduces severe transients.

The selection of the axial flow propeller turbine in the current research was a decision based firstly on; application, cost effectiveness, low maintenance and the ability to standardize the working components were also considered. The automation of the design process is governed primarily by the similarity laws pertaining to turbines. These laws allow the turbine to be scaled and have, in the past, applied mostly to prototyping. Using the site conditions as the design criteria, it is possible to build a turbine that is directly suited to a particular combination of head and flow rate.

The turbine was designed with fixed blades, the angles of which were to be specified by a program incorporating the initial conditions at the point of maximum efficiency. Therefore the fixed blade design does not accommodate any changes in flow conditions, which result in inefficient operation and a consequential decrease in the power output from the optimum. The design of the blade profile was adapted from airfoil predictions as applied to hydrofoil applications where consideration was given to the optimum ratio of drag to lift coefficients. The logistics of the supply piping used by the research turbine has been determined external to the scope of the project, where a cost analysis is provided weighing up the cost of piping versus the power developed by the flow. This is necessary since the pipe diameter is critical in determining the friction losses associated with the velocity, which causes a decrease in the total pressure driving the turbine. The selection of suitable irrigation or reservoir pumps can then be tailored to the mechanical output of the turbine and its delivery piping designed according to the aforementioned dissertation.

Coupling these designs together in a single program relating the turbine sizing to both the supply and delivery piping as well as the pump or generator selection shall prove to be a powerful tool enabling fast efficient implementation of hydropower systems.

The first sites to be exploited are those in which at least one of the entities of flow rate or pressure head has to be significant to provide the energy for the turbine. The author also considered a particular site where both a low flow rate and a low-pressure head existed, with a shallow river depth over a wide area. Hence the author designed a unique turbine that recovered energy from negligible head by rely on a large swept area. Although it was intended that it be built, the design was not pursued past a cost analysis.

## CHAPTER 2

### LITERATURE REVIEW

#### 2.1 Hydrodynamic Drag

##### 2.1.1 Skin Friction

There is basically very little conceptual difference between water and air when it comes to frictional drag, if using the non-dimensional formulation of drag coefficient  $C_f$  as a function of the Reynolds Number in the following equations, Hoerner (1965).

$$\log (Re_1 C_f) = 0.242 / \sqrt{C_f} \quad \& \quad C_f = C_f / (1 + 3.59 \sqrt{C_f}) \quad (2.1.1)$$

A simplifying formula approximating this one to within  $\pm 2\%$  is:

$$1 / \sqrt{C_f} = 3.46 \log Re_1 - 5.6 \quad (2.1.2)$$

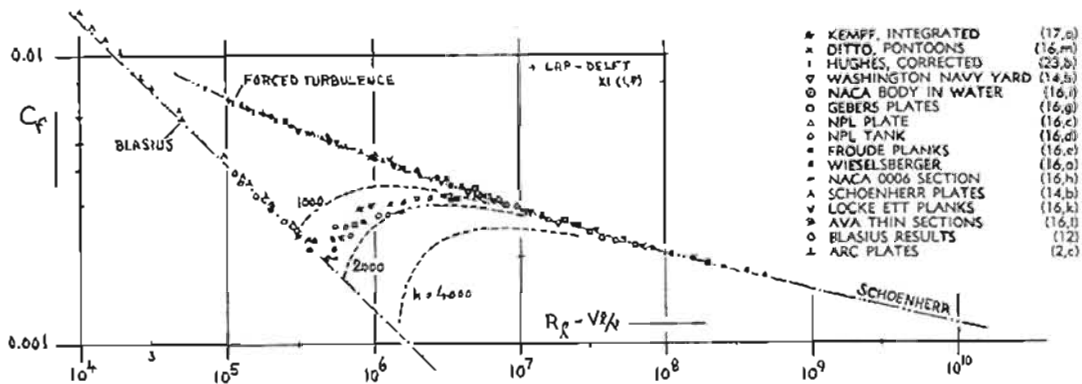


Figure 2.1. 1 Average or total skin friction coefficient in air and in water, Hoerner (1965)

##### 2.1.2 Critical Reynolds Number

Disregarding forced stimulation of turbulence, there appears to be some systematic difference in the transition Reynolds numbers as found in water and in air. The plot of the Reynolds Number against the critical speed  $V_{crit}$ . Figure 2.1. 2 shows that the critical number in water is approximately half that of air.

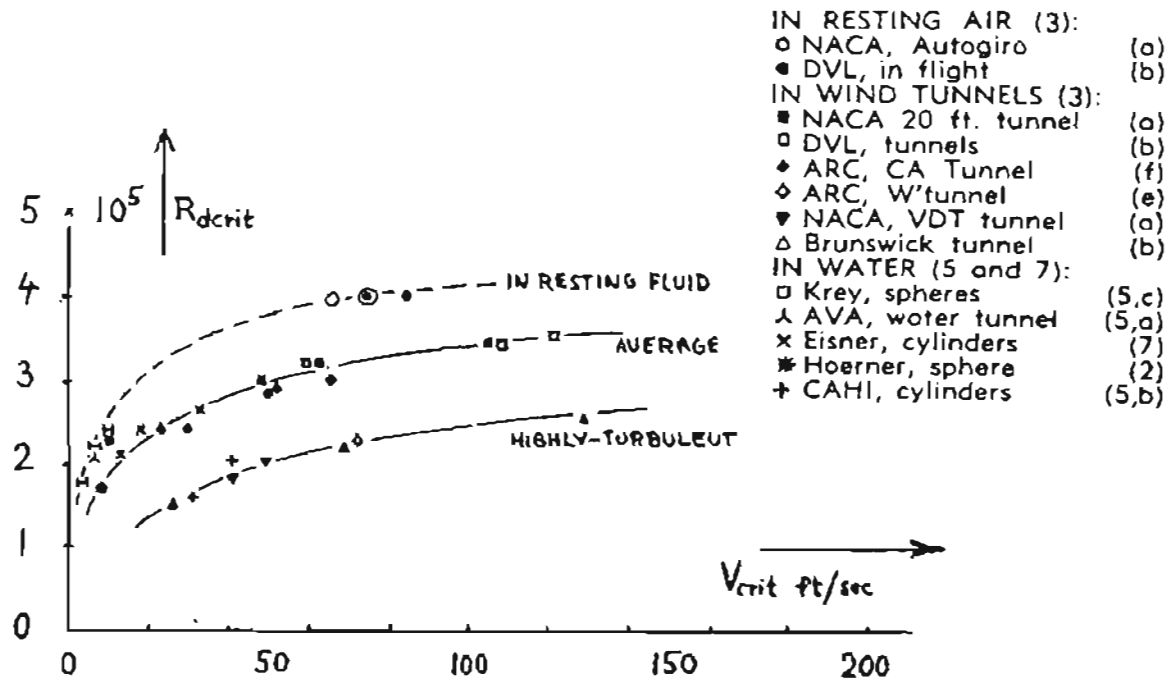


Figure 2.1. 2 Transition Reynolds Number, Hoerner (1965)

This was claimed to be accounted for in the turbulence effect, where turbulence was predominant in experiments in water, whereas the same sphere / cylinder, tested in air, displayed laminar flow up to much higher Reynolds Numbers. The turbulence effect also caused a shift of the drag coefficient plotted against Reynolds Number of the order of 1:2, when measured on the 0012 foil section.

### 2.1.3 Surface Roughness

The influence of surface roughness on turbulent skin friction drag occurs only at critical Reynolds numbers, where the coefficient of roughness is defined according to the grain size. Since the turbine blade surfaces under current research are typically finished with a smooth surface and shape, the effect of surface roughness will be minimised.

### 2.1.4 Pressure Drag

Figure 2.1. 3 shows the influence of the shape of the body profile on the coefficient of pressure drag  $C_D$ . The coefficients shown can be considered to be comparatively constant with regards to the Reynolds Number. The implication of the relationship of the profile

geometry to the coefficient of drag was used in the shape conceptualisation in the initial stages of design.

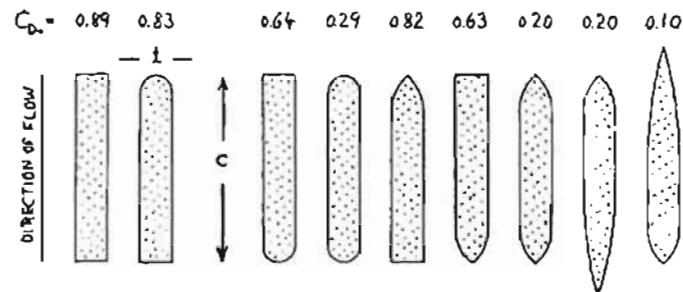


Figure 2.1. 3 Drag of various shapes in 2-D flow towed in water, Hoerner 1965

### 2.1.5 Drag Characteristics in Cavitating Flow

Cavitation is a mechanism whereby vaporisation occurs about microscopic nuclei existent in the flow medium. Vaporisation usually occurs at the vapour pressure, which is a function of the temperature due to the saturation of its volume percentage of air. The existence of cavitation causes a restriction in the speed up to which the flow in water can be expected to be identical to that about a similar body in an air stream. Above a certain critical speed, the mechanism referred to as cavitation becomes evident. Only two characteristics of this mechanism can be predicted: the critical speed and/or pressure at which cavitation starts and the drag of bodies in the final phase of full cavitation.

## 2.2 Airfoil Data for Blade Design

### 2.2.1 Types of Airfoil Section

The inclusion of camber into the mean line allows for greater working loads to be obtained by the blades. The streamlining of the mean line is then a function of;

- a)  $t / c$
- b)  $x_{t/c} / c$
- c) leading edge radius

where  $[ t ]$  is the maximum thickness of the section normal to the camber line,  $[ c ]$  is the airfoil chord and  $x_{t/c}$  is the distance from the leading edge to the point of maximum thickness.



Small leading edge radii produce large local flow accelerations when the airfoil is at workable incidences because of the resultant change in attitude of the profile. The flow that develops downstream of this accelerated flow can be subject to separation.

### 2.2.2 Lift

An increase in the angle of incidence of the blade within the flow increases the flow velocity at any point along the top surface while the opposite is true for the lower surface. Bernoulli's equation implies that these velocity changes give decreasing and increasing static pressures on the upper and lower surfaces respectively. The resultant pressure difference determines the lifting force acting on the airfoil.

The lift coefficient is given by the equation: 
$$C_L = \frac{L}{(1/2)\rho U_0^2 A} \quad (2.2. 1)$$

### 2.2.3 Pitching moment

The locality in which the resultant lift force acts is generally between the 25% and 50% chord positions, depending largely on the amount of camber in the airfoil.

### 2.2.4 Drag

Skin friction and pressure forces are the cause of profile drag. On a blade of finite span, the air tends to flow from the high-pressure region on the lower side around the extreme tip to the low-pressure region on the upper side. This introduces a span-wise velocity component that produces turbulence at the tip of the blade called tip vortex. The momentum loss caused by tip vortex flow is known as the induced drag.

### 2.2.5 Flow Deflection in Cascade Airfoils

An important feature of rotor or stator blade design is the properties of the flow-deflection of a cascade of airfoils. By simple momentum losses the deflection angles can be related to the lift coefficient of the blades. For incompressible, two-dimensional flow, the axial velocity component normal to the cascade must remain constant in order to satisfy continuity. In the Figure 2.2.1, the velocity component parallel to the cascade has been reduced by the deflecting airfoils, this reduction involves a rate of change of momentum which is equal to the force acting on the blades in the parallel plane.

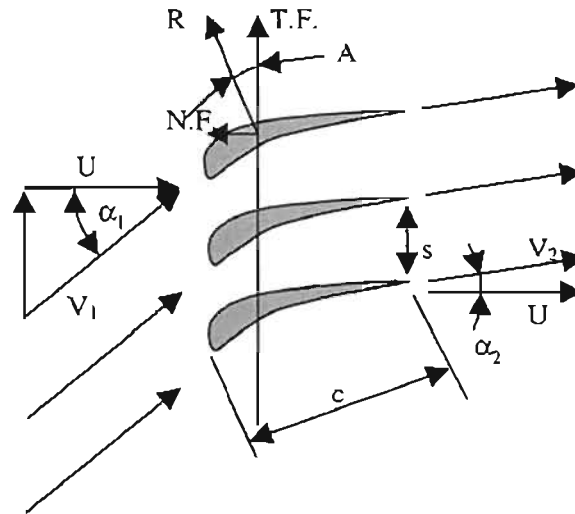


Figure 2.2. 1 Velocity Vector addition

Due to the decrease of the flow velocity from  $V_1$  to  $V_2$ , there is a corresponding increase in the static pressure related by Bernoulli's equation. This pressure produces a force normal to the cascade. Then assuming that there is no loss in total head through the blade row allows for the determination of the normal force [N.F.].

Hence we can arrive at the solutions:

$$T.F. = \rho s U^2 (\tan \alpha_1 - \tan \alpha_2) \quad (2.2. 2)$$

$$N.F. = s(P_1 - P_2) = s(1/2)\rho(V_1^2 - V_2^2) \quad (2.2. 3)$$

$$\text{Then: } \tan A = (N.F./T.F) \quad (2.2. 4)$$

The above assumption that the total head remains constant implies that the fluid is an ideal inviscid fluid and hence there is no drag acting on the airfoils. The force must then be equal to the resultant force and therefore act at right angles to the mean vector. The lift can then be written:

$$L = (1/2)\rho c C_L V_m^2 \quad (2.2. 5)$$

Taking the component of lift parallel to the cascade and equating to T.F.:

$$C_L = 2(s/c)\cos \alpha_m (\tan \alpha_1 - \tan \alpha_2) \quad (2.2. 6)$$

### 2.2.6 Flow Deflection in Fan Blades

A stage of rotor or stator blades is essentially a circular cascade of airfoils. In spite of the fact that the volume of flow deflection will usually vary along the span of the blade, the

conditions at a given radial position can be determined from two-dimensional test data for the particular airfoil section. This independence of a blade section with respect to a neighbouring section of the same blade has long been recognised theoretically and experimentally.

Airfoil characteristics are available in two general classes, isolated or free airfoil data and cascade airfoil data. The first type of data are obtained from wind tunnel tests performed on a single airfoil whilst the second type of data are obtained from tests on airfoil performance in a cascade testing tunnel. This produces two methods by which the design process may be implemented:

isolated airfoil method

cascade airfoil method

The first method utilises lift data in design, whilst the second is based on flow deflection. In terms of this relationship between lift and deflection, the distinction between the two methods is essentially unimportant. Thus it is possible to apply the data of isolated airfoils to the application of cascade airfoils. This will have varying effect on the turbine blades as one looks radially outward, since the blade spacing changes with radius.

### 2.2.7 Isolated Airfoil Data

Figure 2.2. 2 shows an example of the variation in camber for a profile having a maximum  $(t/c)$  ratio of 0.02. The test was performed at a Reynolds number of approximately  $3 \times 10^5$ .

*Variation of Camber: at  $Re \cong 3 \times 10^5$ ,  $(t/c) = 0.02$ .*

As the camber is increased from 2% to 10%, the coefficient of lift  $C_L$  increases by approximately 100%. The increase in lift is accompanied by an increase in the optimum angle of incidence. The reason for this is the angle of incidence being maintained at zero, which produces the minimum of shock losses. As the camber is increased the profile drag increases due to the increase in frontal surface area. This is true for low ( $Re \cong 3 * 10^5$ ) and medium ( $Re \cong 6 * 10^5$ ) Reynolds numbers.

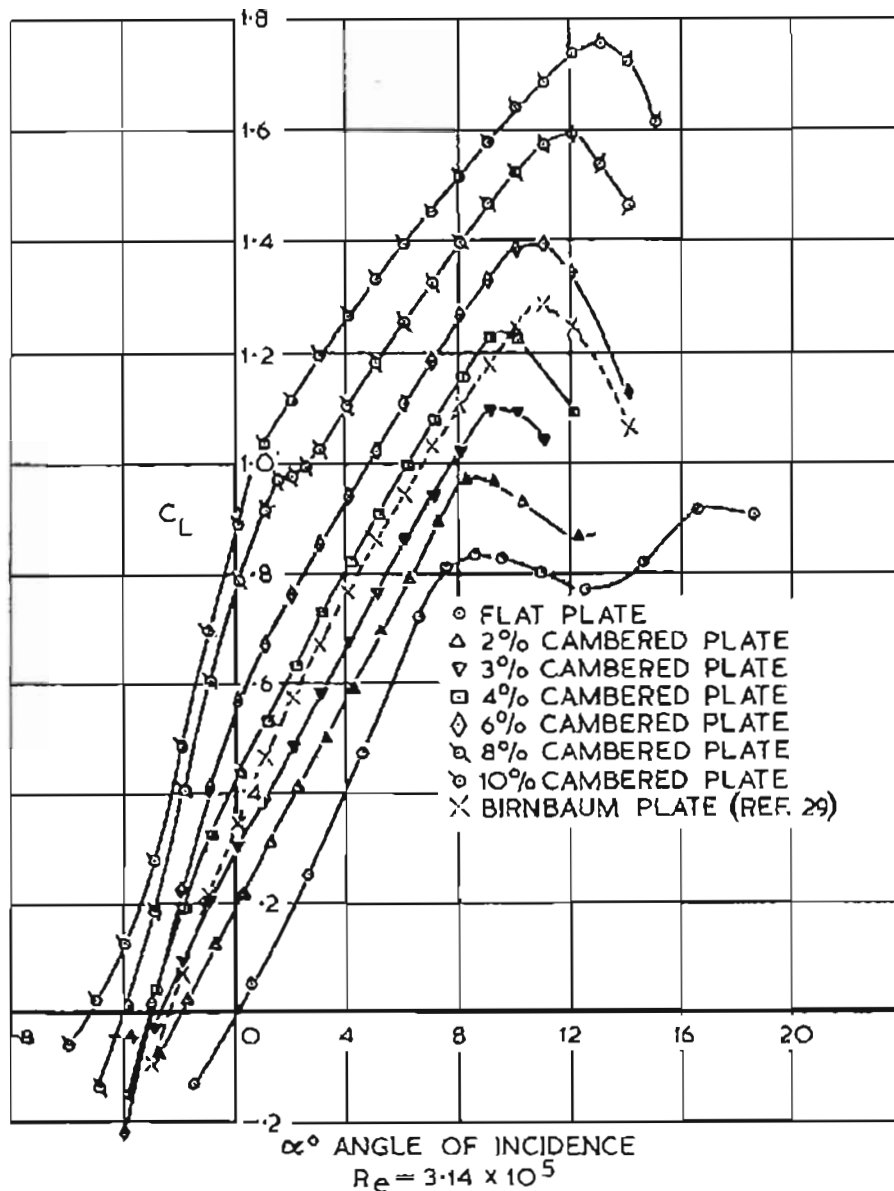


Figure 2.2. 2 Lift characteristics of cambered plates ( $t/c=0.02$ ),  $Re=3 \times 10^5$ , Wallis (1983)

The relationship between these two quantities, the lift and drag coefficients, is the method used to determine the curvature of the camber. The curves of  $C_L / C_{Dp}$  show an overall increase in value as the camber is increased for both of the above-mentioned Reynolds's numbers, for the given thickness distribution.

### 2.2.8 Cascade Airfoil Data

After many tests were performed on airfoils with different mean-line camber and thickness distribution, it was found that a combination of the basic streamline shape,  $C_4$ , with a circular arc camber line produced a very satisfactory blade section. Flow deflections are, within reason, assumed to be independent of the streamlined shape adopted, hence the most important feature of the airfoil is the camber line, seen typically in Figure 2.2. 3.

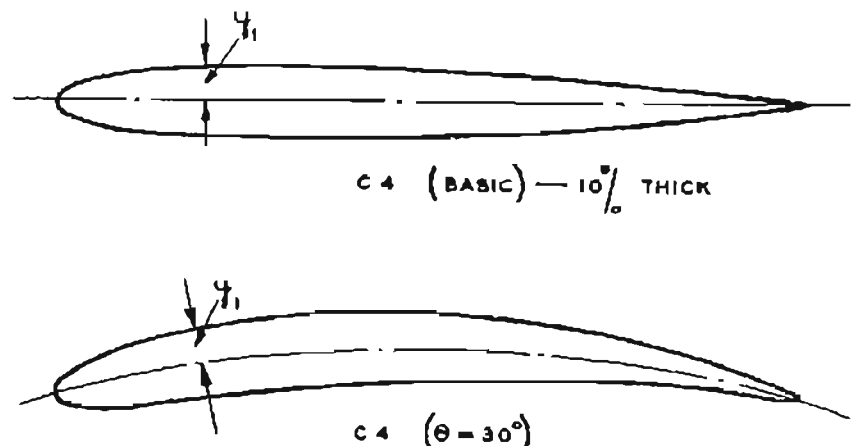


Figure 2.2. 3 Example of the cascade airfoil design method, Wallis (1983)

### 2.2.9 Effect of Reynold's Number on Airfoil Data

Airfoil lift and drag force data are usually presented as functions of the chord Reynold's number. From Figure 2.2. 4 it will be seen that the major effects of Reynold's number are confined to the profiles of higher incidence, where flow separation begins to take place. Furthermore, the separation of the boundary layer on the suction surface increases the frontal area of the profile, causing higher losses. This disproportionately alters the lift / drag relationship.

It is not possible to assume that the lift / drag relationship will yield an entirely accurate fan design Reynold's number since the boundary layer growth on an airfoil is also affected by the surface roughness and free-stream turbulence which cannot be practically accounted for in theory. But the changes in the lift and drag caused by these factors are not sufficient to cause difficulties in blade design difficulties.

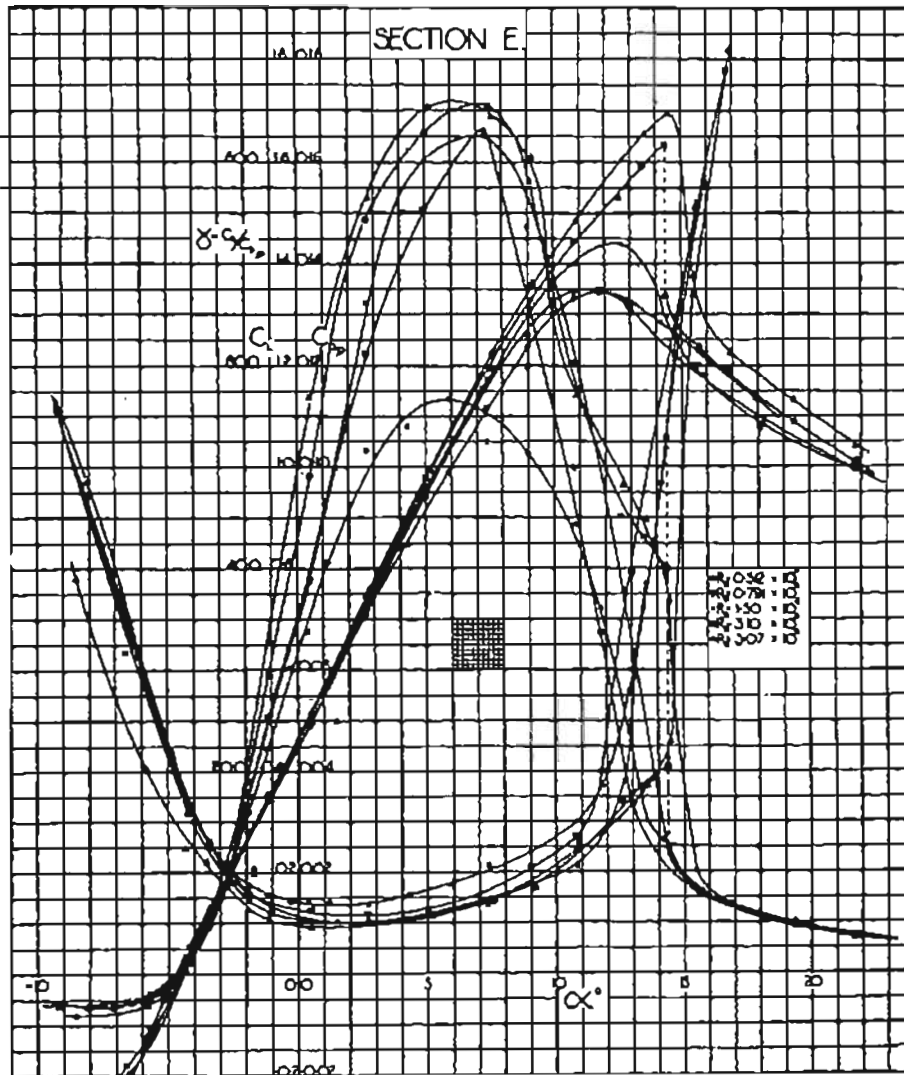


Figure 2.2. 4 Airfoil Characteristics, Wallis (1983)

## 2.3 Fundamentals of Hydraulics

### 2.3.1 Introduction

The development of airfoil blade design for turbines has provided a new method of solution in comparison to that of momentum blade design. For the design in which the passage between the blades is wide when compared with the length of the blade, the airfoil method yields the more accurate results. In fact if the blades are relatively far apart, it is not possible to obtain a solution using the momentum theory method.

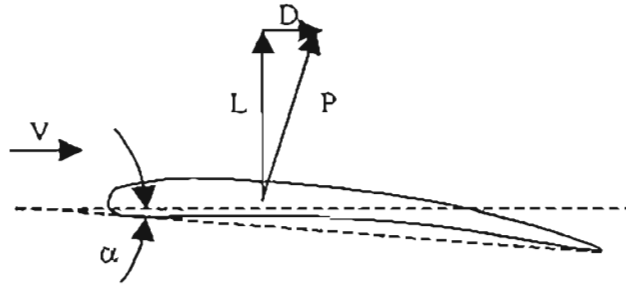


Figure 2.3. 1 Cross Section of Blade

### 2.3.2 The pressure distribution

Most of the lift force can be attributed to the negative pressure on the upper face. The inclination of the chord to the direction of the motion of the airfoil is known as the angle of incidence or the angle of attack. By varying this angle the values of lift and drag are also varied. The position of the centre of pressure of the airfoil is significant in the design process and its point of application is at the resultant force P, which varies with the angle of incidence.

### 2.3.3 Airfoil Characteristics

The primary characteristics of the airfoil are the values of the coefficients  $C_L$ ,  $C_D$  &  $C_p$ . These values all vary with  $\alpha$ , the angle of incidence, and are determined from wind tunnel tests. The lift to drag ratio,  $(L/D)$ , is plotted against  $\alpha$  with the position of the centre of pressure, as a fraction of the chord from the leading edge, and against values of  $C_L$ ,  $C_D$ . The point at which the  $(L/D)$  ratio is a maximum determines the most efficient value of  $\alpha$ . Note that as  $\alpha$  is increased the  $C_p$  moves toward the leading edge. (This may or may not be specific for the particular blade shape)

### 2.3.4 Airfoil blade design methods for turbines

There exists two methods of solving for blade shaping:

Momentum blading:

This is the application of the equation: 
$$\text{Work} = \frac{V_w v}{g} + \frac{V_{w1} v_1}{g} \tag{2.3. 1}$$

Airfoil blading:

This is the application of the equations:  $L = C_L A \rho V^2$ ,  $D = C_D A \rho V^2$ , using these values to find the work required to overcome drag. But in order to apply this method it is necessary to first determine the characteristic curves of the blade.

When the blade design is based on the airfoil theory, the blades are shaped according to a suitable airfoil profile instead of the concave circular section. In certain types of turbines, the airfoil design method is more efficient than the momentum method because of the wider passage between the blades, since the broader passage produces less friction drag.

If there is no interference with the fluid through which it flows, the airfoil will yield maximum lift. Hence the airfoil-designed blades of a turbine must be spaced such that there is no interference between adjacent blades. However, if the blades are spaced too far apart, a portion of the fluid stream may flow freely between them without doing any work, wasting energy. The exact spacing of the blades to satisfy both of these conditions can only be obtained from tests.

Another factor to consider in view of the airfoil design is the effect of the suction on the upper surface of the blade. If this negative pressure becomes too large, cavitation will occur, particularly in water turbines, thus interfering with the fluid stream. This will reduce the force on the blade and its efficiency.

### **2.3.5 Minimum spacing of airfoil blades**

The criterion for the type of blade for a turbine is specified by the pitch-chord ratio of the blades. If the blades are relatively close together, the passage of the fluid follows that of a curved jet and the resultant force on the blade is then determined from the rate of change of momentum of the jet.



If the pitch-chord ratio is large, the path of the fluid between them cannot be assumed to be a curved jet. The blades then tend to act as airfoils in a fluid stream, and the work done on them can be derived from airfoil theory.

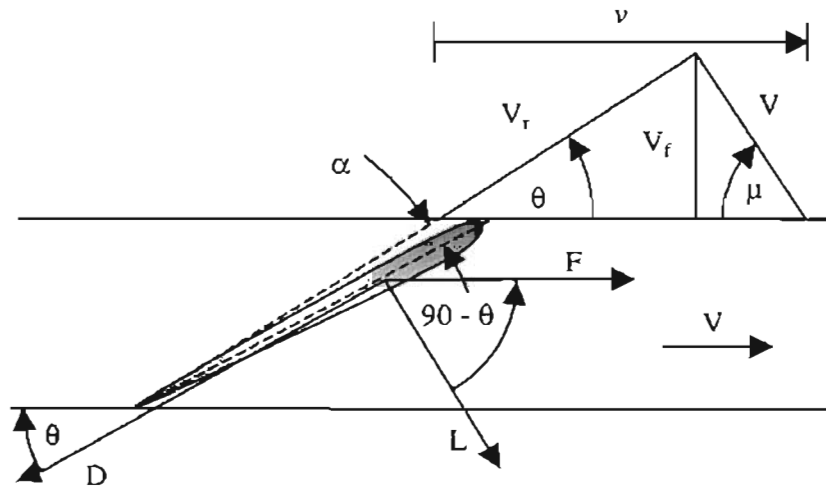


Figure 2.3. 2 Profile Velocities

### 2.3.6 Work done on airfoil blades

The water enters from the guide blade at an angle  $\mu$  and with velocity  $V$ . The airfoil blade is moving at velocity  $U_b$ , generating the relative velocity  $V_r$  with direction  $\theta$ . The airfoil chord must be sloped at an angle of  $\theta - \alpha$  to the direction of the blades' motion, where  $\alpha$  is the best angle of incidence for the airfoil section used.

Let :  $S$  = length of span of airfoil blade [m]

Then:  $A = c * S$  [m<sup>2</sup>] (2.3. 2)

$r$  = mean radius of blade circle

$N$  = total number of blades on the runner

$H$  = total head of water supplied

$U_b$  = mean blade velocity =  $\omega r$

Then :  $L = C_L \rho A V_r^2 / 2$  (2.3. 3)

$D = C_D \rho A V_r^2$  (2.3. 4)

$F = L \sin \theta - D \cos \theta$  (2.3. 5)

= tangential force on the blade

$$W = FvN \quad (2.3. 6)$$

= work done on the turbine per second

$$Q = \text{net axial area of flow} \times V_f = k2\pi rSV_f \quad (2.3. 7)$$

= quantity of water used per second

$$\eta = \frac{FvN}{\omega QH} \quad (2.3. 8)$$

= work done per second / energy supplied per second

= theoretical efficiency of the turbine

where:  $k$  = blade area coefficient

$V_f$  = velocity of flow [m/s]

In designing the blade the values of  $Q$  &  $H$  are known. The rotor and stator radii, speed and angle are chosen from previous experience. Then it is possible to determine:

$$V_f = \frac{Q}{k2\pi rS} \quad (2.3. 9)$$

Using the above value, it is now possible to determine the velocity diagram from which the values  $V_r$  and  $\mu$  can be obtained.

### 2.3.7 Effect of blade pitch on Lift and Drag

It was determined from experiment that the lift coefficient decreases with a decrease in the blade pitch. The drag coefficient also decreases with a decrease in the blade pitch. These phenomena are seen in Figure 2.4.3.

It was also determined that the fluid, passing over the blades, loses velocity and pressure in overcoming the drag. As the values of  $C_L$  &  $C_D$  depend on the pitch to chord ratio of the blade, it is possible to obtain an approximate value of these coefficients from the results of a test on an isolated airfoil. These values can then simply be added together according to the number of blades of the stator and the rotor. However, it must be borne in mind, that these values are dependant on the specific blade shape, and the losses will

vary according to the value of camber, thickness and nose and tail radii. However, typical values are shown in the following figures:

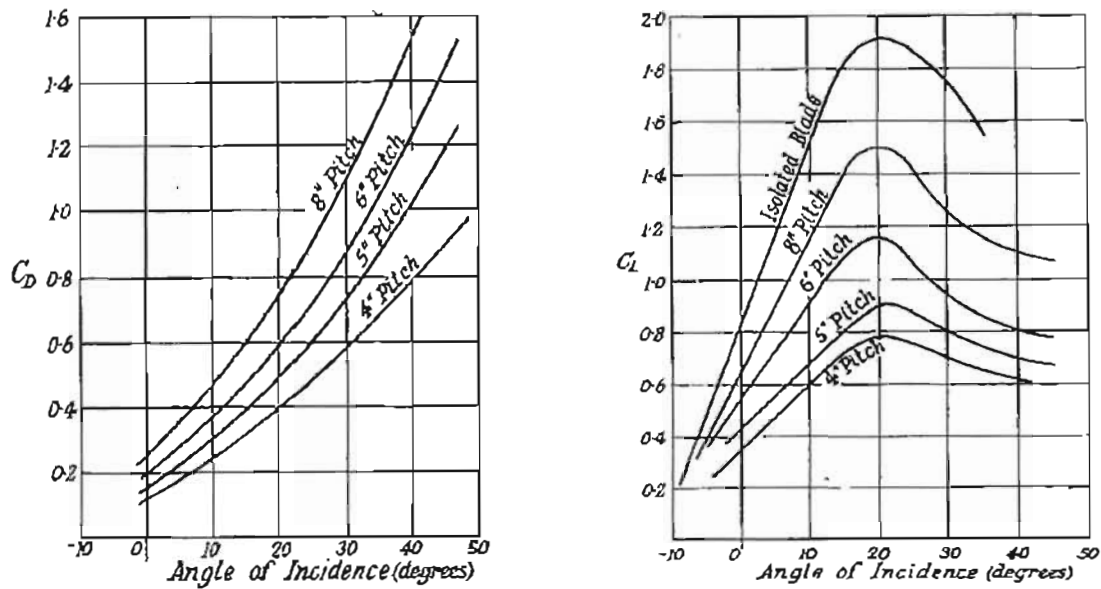


Figure 2.3. 3 Coefficients of drag and lift vs angle of attack, Lewitt (1932)

## 2.4 Axial Flow Turbines

### 2.4.1 Propeller turbines

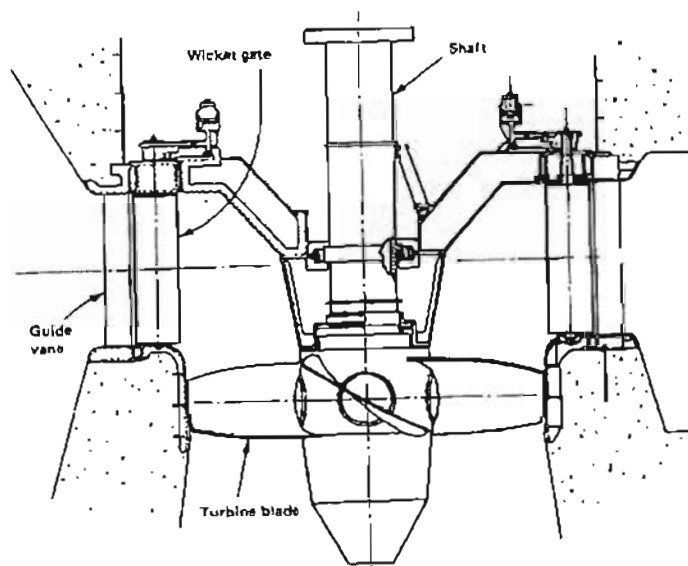


Figure 2.4. 1 Cross-sectional view of propeller turbine, Warnick (1984)

The flow direction for the majority of propeller turbines is axial in nature, typically parallel to the axis of rotation of the turbine shaft. Many of the early developments of axial flow turbines made use of the vertically orientated shaft with the more recent designs utilising the horizontal shaft. There are two characteristics of the axial flow turbine that further divide the family of the design. These are namely the fixed-blade and the adjustable blade turbines (named the Kaplan turbine after Victor Kaplan), the advantage of the adjustable blade being capable of a wider range of efficiency than that of the fixed-blade due its ability to adjust to the variation in flow conditions.

Table 2.4. 1 Turbine Constants, Warnick (1984)

Parameter	Designation	Formula
Speed ratio	-	-
Unit speed	$\omega_{ed}$	$\omega_{ed} = \frac{\omega D}{(g'H)^{0.5}}$
Unit discharge	$Q_{ed}$	$Q_{ed} = \frac{Q}{D^2 (g'H)^{0.5}}$
Discharge coefficient	$Q_{\omega d}$	$Q_{\omega d} = \frac{Q}{\omega D^3}$
Unit torque	$T_{ed}$	$T_{ed} = \frac{T}{\rho' D^3 gH}$
Torque coefficient	$T_{\omega d}$	$T_{\omega d} = \frac{T}{\rho' \omega^2 D^5}$
Energy coefficient	$E_{\omega d}$	$E_{\omega d} = \frac{g'H}{(\omega D)^2}$
Unit power	$P_{ed}$	$P_{ed} = \frac{p}{\rho' D^2 H^{1.5}}$
Power coefficient	$P_{\omega d}$	$P_{\omega d} = \frac{p}{\rho' \omega^3 D^5}$
Specific speed	$\omega_s$	$\omega_s = \frac{\omega Q^{0.5}}{(g'H)^{0.75}}$
Conversion term	$\omega_s$	$\omega_s = \frac{N_s}{435\sqrt{\eta}}$

## 2.4.2 Turbine constants and empirical equations

Each family of turbine has its particular design based on the laws of similarity, which allow the turbine to be designed from standardised curves. These curves are known as the Hill Curves, Warnick (1984), and are based on the non-dimensionalised constants, which define the respective turbine characteristics. These figures are shown in Table 2.4. 1 and once calculated could be applied to determine the practicality of the turbine design. The non-dimensionalised values are based on the more common parameters of head, speed and power output. The Hill curves, Warnick (1984), shown below in Figure 2.4. 2 have as their variables the coefficients of:

$Q_{wd}$  = discharge coefficient;

$E_{wd}$  = energy coefficient;

$P_{wd}$  = power coefficient.

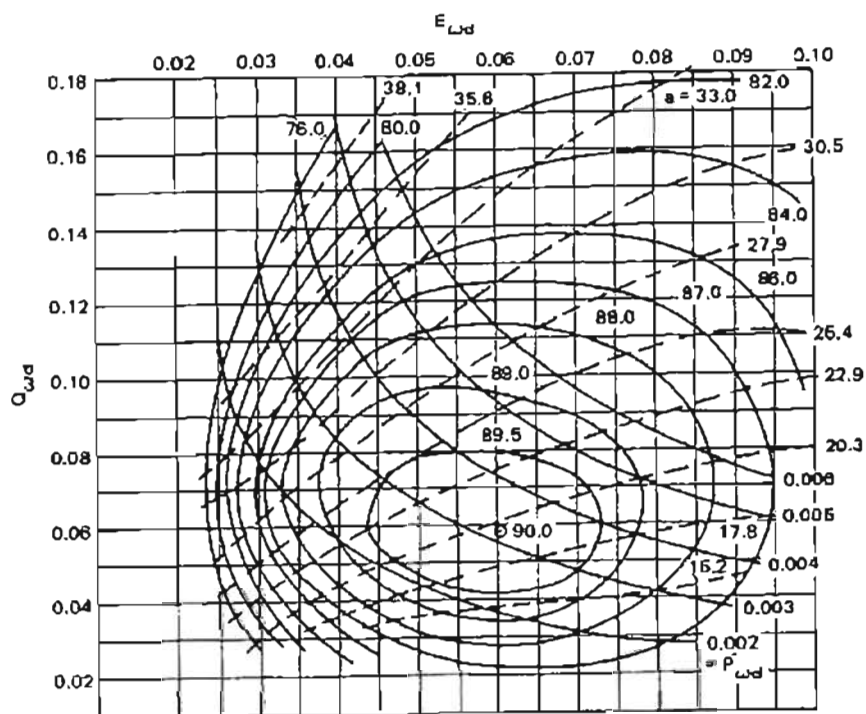


Figure 2.4. 2 Typical turbine Hill Curve, Warnick (1984)

Plotting the discharge coefficient against the energy coefficient yields the contour map of lines of equal power coefficient. Superimposed on these lines are lines of equal turbine efficiency, which correspond to the simultaneous values of  $Q_{wd}$  &  $E_{wd}$ , as well as the

corresponding values of the gate opening,  $\alpha$ . The Hill Curves, Warnick (1984), are developed from extensive testing of turbines and due to the nature of turbine similarity, these values are used to predict prototype performance. For example, it may be pointed out that the energy coefficient,  $E_{ad}$ , is directly proportional to the net head  $H$ , where  $D$  and  $\omega$  are given. Hence it is possible to use the curves in making final design selections from a predetermined performance criterion.

It has been found that there is no precise relation between the model and its prototype when it comes to calculation of the turbine efficiency due to the relative differences in the boundary layer conditions of friction and turbulence effects. To attempt to correct for this, an efficiency step-up equation is normally used, Warnick (1984):

$$\frac{1 - \eta_p}{1 - \eta_m} = \left( \frac{D_m}{D_p} \right)^a \quad (2.4. 1)$$

where:  $\eta_m$  = model turbine efficiency;

$\eta_p$  = prototype turbine efficiency;

$D_m$  = model turbine diameter;

$D_p$  = prototype turbine diameter;

$a$  = set-up coefficient;

Moody (1926) proposed that  $a = 0.2$ . Kovalev (1965) proposes that (2.4. 2), Warnick (1984) be used for predicting the efficiency of prototype turbines from model turbine performance:

$$\eta_p = 1 - \left( 1 - \eta_m \right) \left( \frac{D_m}{D_p} \right)^{m-1} \left( \frac{H_m}{H_p} \right)^{1-0.5n} \quad (2.4. 2)$$

where the coefficients of  $m$  &  $n$  are determined through the relationship to the coefficients used in calculating head losses in the prescribed system.

However, work by Hutton (1954) and Salami (1969) has determined the efficiency in terms of the Reynolds number of the model and prototype for different losses in the system. These losses are typically found in the casing, guide vanes, and the draft tube. Following is the equation given by Hutton and Salami, Warnick (1984):

$$\frac{\eta_p}{\eta_m} = 1 - K \left[ 1 - \left( \frac{R_m}{R_p} \right)^{1/a} \right] \quad (2.4.3)$$

where:  $K$  = a coefficient shown to vary between 0.5 to 0.81

$R_m$  = Reynolds number for the model turbine

$R_p$  = Reynolds number for the prototype turbine

### 2.4.3 Experience Curves

In the initial stages of design, it is often required that the parameters of the turbine speed, size and power output be determined by the synchronous speed and required power of the plant. Extensive experience curves have been developed for this purpose. The specific speed of the turbine is a universal number and has therefore been used as the basic reference number to which other turbine parameters may be related. The most important of these relations is that between the specific speed and the net effective head,  $h$ , since the most prominent design factor is the available head. Figure 2.4. 3 displays the typical grouping of the different turbine families.

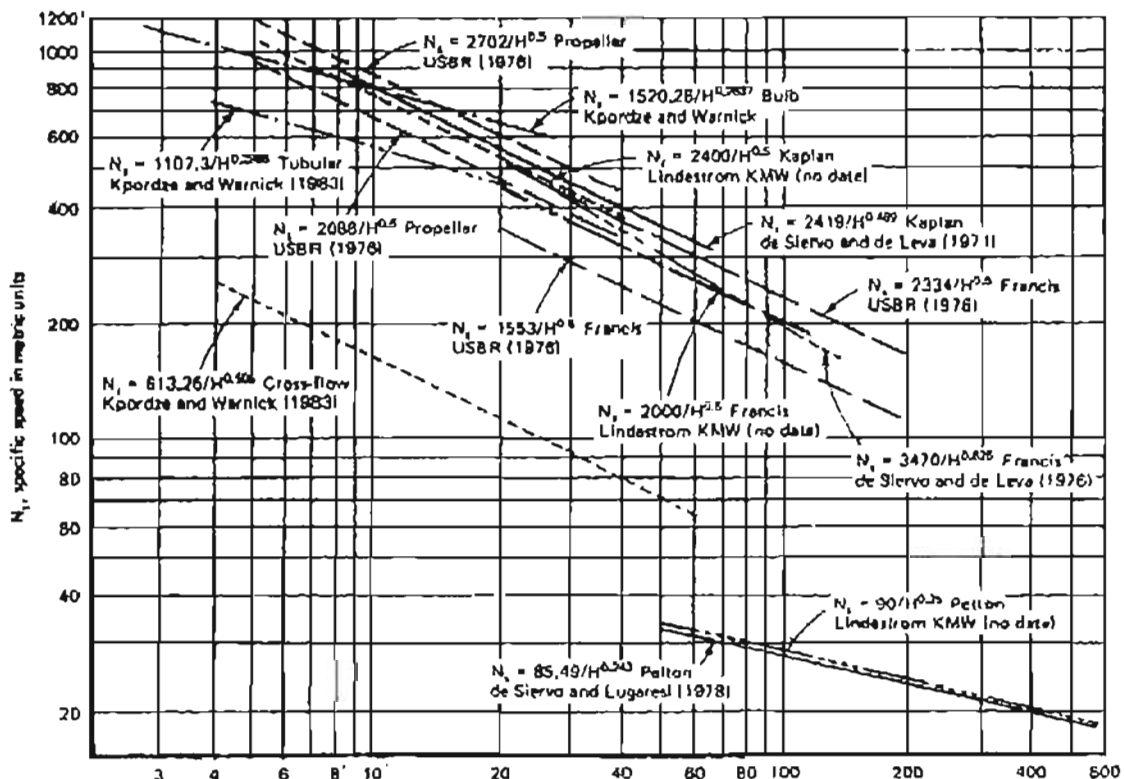


Figure 2.4. 3 Experience curves, Warnick (1984)

It is also useful to determine the type of turbine required as a function of the particular head and required power output, and this representation is given in Figure 2.4. 4.

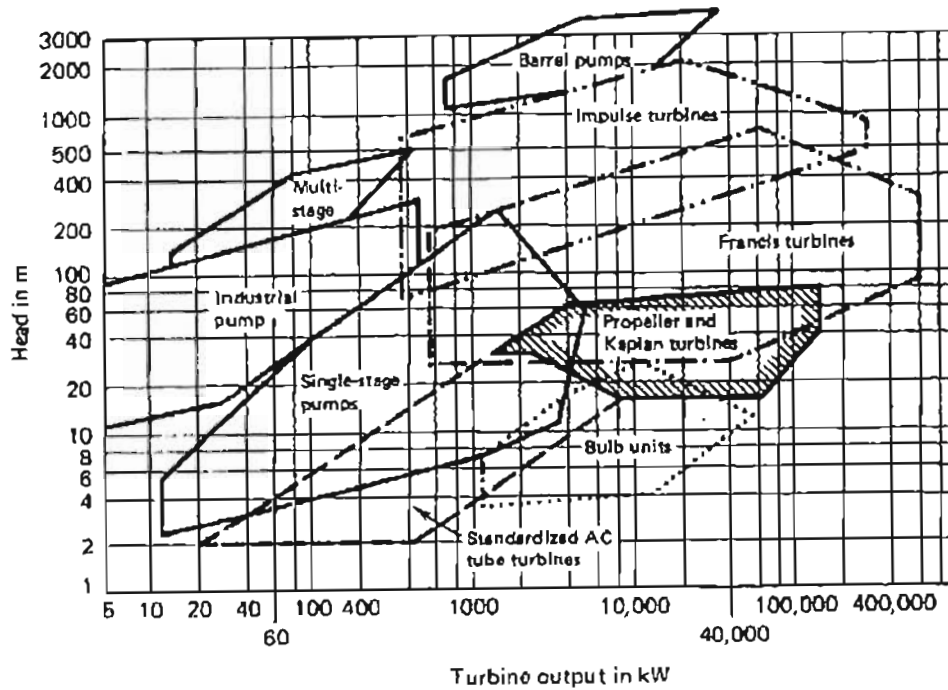


Figure 2.4. 4 Application ranges for conventional hydraulic turbines, Warnick (1984)

#### 2.4.4 Runner Speed

The runner speed is usually determined by the speed of the generator that it is to be driving. Should it be determined that the turbine be connected directly to the generator then the following equation defines the turbine speed:

$$n = \frac{120f}{N_p} \quad (2.4. 4)$$

where:  $n$  = rotational speed [rpm];

$f$  = electrical current frequency, hertz [Hz];

$N_p$  = number of generator poles; multiples of four are recommended.

If there exists a variation in net head less than 10%, it is advised that the next greater synchronous speed be selected. However, if the net head varies by more than 10%, the next lower synchronous speed should be chosen.



### 2.4.5 Runner Diameter

The diameter of the turbine may also be determined from the empirical relationships, the customary relation is to the specific speed of the turbine. deSiervo and deLava(1976) have developed the following equation for the Francis runner, Warnick (1984):

$$D_3 = (26.2 + 0.211N_s) \frac{\sqrt{H}}{n} \quad (2.4.5)$$

where:  $D_3$  = discharge or outlet diameter, m.

and for the propeller turbine for which the design is intended, (1977), Warnick (1984):

$$D_M = (66.76 + 0.136N_s) \frac{\sqrt{H}}{n} \quad (2.4.6)$$

where:  $D_M$  = outer diameter of propeller, m.

### 2.4.6 Turbine efficiency

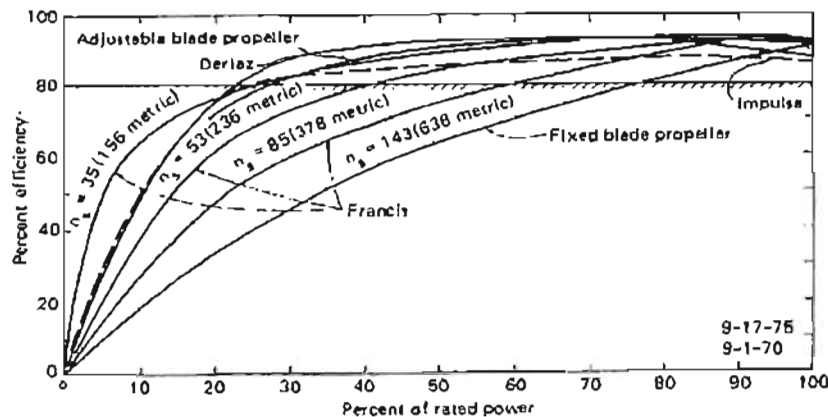


Figure 2.4. 5 Turbine efficiency variation, Warnick (1984)

Figure 2.4. 5 shows the typical variation in turbine efficiencies throughout their typical operating range. The results are in some cases specific to a particular installation and may appear vague, but they are nevertheless beneficial toward making estimates of selection of particular units.

### 2.4.7 Cavitation and Turbine Setting

Cavitation may be defined as: “The formation of voids within a body of moving liquid (or around a body moving in a liquid) when the local pressure is lower than the vapour

pressure and the particles of liquid fail to adhere to the boundaries of the passageway”, Warnick (1984). The inability of the particles to adhere to the surface boundaries is a condition of the low localised vapour pressure, which is insufficient to overcome the force of inertia of the fluid particles as they are accelerated typically about a curved surface. A void thus develops containing the vapour of the liquid. Since the inertia of a particle is a function of the square of velocity and the higher the velocity, the greater is the pressure force required to prevent cavitation, it may be inferred that cavitation is a function of three conditions, namely: high velocity flow, low pressures and abrupt changes in flow direction. The effect cavitation has on the boundary surfaces is to cause pitting, which is the removal of material through the violent collapse of the vapour bubbles so formed through cavitation.

#### **2.4.8 Cavitation Coefficient**

*Plant sigma*, or cavitation coefficient both describe a turbine constant. The derivation of the coefficient equation yields an important understanding of the origins of cavitation and presents the use of the parameter in terms of selection of turbine setting.

The equations that formulate the analysis are those of Bernoulli, head loss and the orifice equation. The typical parameters involved are shown in Figure 2.4. 6.

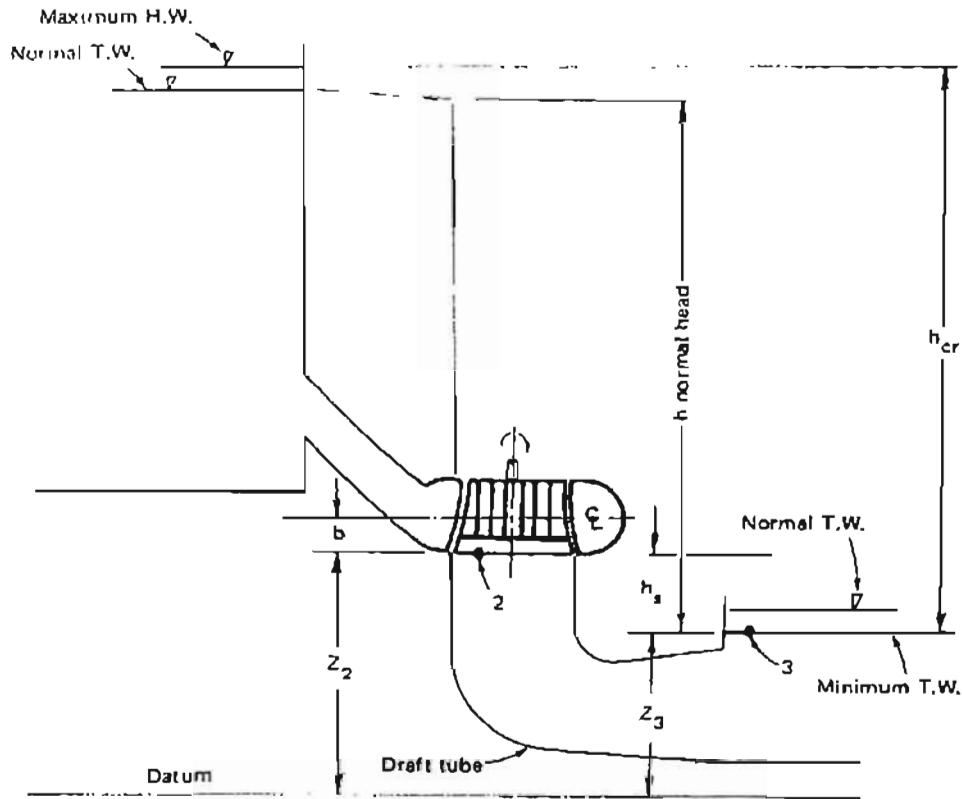


Figure 2.4. 6 Cavitation coefficient parameters, Warnick (1984)

From this diagram and a Bernoulli analysis between points 2 & 3, Eq (2.4.7) is developed:

$$\frac{V_2^2}{2g} + \frac{p_2}{\gamma} + z_2 = \frac{V_3^2}{2g} + \frac{p_3}{\gamma} + z_3 + h_{f_{2-3}} \quad (2.4.7)$$

where:  $\gamma$  = specific weight of water, [ $\text{kgm}^{-3}$ ];

Then writing the equations of continuity for the head loss, the following equations may be developed:

$$V_2 = C\sqrt{2gh} = K_1\sqrt{h} \quad (2.4.8)$$

$$V_3 = \frac{A_2V_2}{A_3} = \frac{A_2K_1\sqrt{h}}{A_3} = K_2\sqrt{h} \quad (2.4.9)$$

$$h_f = \frac{fLV_{2-3}^2}{2dg} = K_3 \frac{\sqrt{h}}{2g} \quad (2.4.10)$$

where:  $h$  = net effective head.

Substituting these values for  $V_2$ ,  $V_3$  and  $h_f$  into Eq (2.4.7) and grouping the results, Warnick (1984):

$$\left[ \frac{K_1^2}{2g} - \frac{K_2^2}{2g} - \frac{K_3}{2g} \right] h = \frac{p_3}{\gamma} - \frac{p_2}{\gamma} + z_3 - z_2 \quad (2.4. 11)$$

The term with all the constants can then be replaced by the cavitation coefficient:

$$\sigma = \frac{K_1^2}{2g} - \frac{K_2^2}{2g} - \frac{K_3}{2g} \quad (2.4. 12)$$

The term  $z_3 - z_2$  is replaced with:

$$h_s = z_3 - z_2 \quad (2.4. 13)$$

and

$$\frac{p_3}{\gamma} = \frac{p_{atm}}{\gamma} = h_a \quad (2.4. 14)$$

and as a limit:

$$\frac{p_2}{\gamma} = \frac{P_{vapour\ pressure}}{\gamma} = h_v \quad (2.4. 15)$$

The resulting convenient equation is:

$$\sigma = \frac{h_a - h_v - h_s}{h} \quad (2.4. 16)$$

where:  $h_s$  = the difference in the minimum tailwater and the cavitation reference point at the outflow of the turbine, [m];

$h_a$  = atmospheric pressure head, [m];

$h_v$  = vapour pressure head as a function of the water temperature, [m].

In practice it should be noted that the term,  $h$ , or net effective head is replaced with the term called critical head,  $h_{cr}$ . Furthermore, the headwater and forebay water levels rise and fall, causing adjustments to the determined values of head and tail water. These variations cause changes in the value of the turbine setting and a degree of compensation is required for this.

Figure 2.4. 7 indicates the uncertainty of the inception of cavitation. The inception of cavitation is usually defined in terms of a loss in power or an increase in the operating noise level. It is also difficult to determine where the cavitation begins, since the vapour bubbles may be swept downstream of their origin before they become noticeable.

Once the level of cavitation has been plotted versus the level of efficiency, the graphs are used to determine what the permissible levels of cavitation for the turbine may be. In most instances, the level of cavitation in the model turbine is of a higher level than that experienced in the prototype.

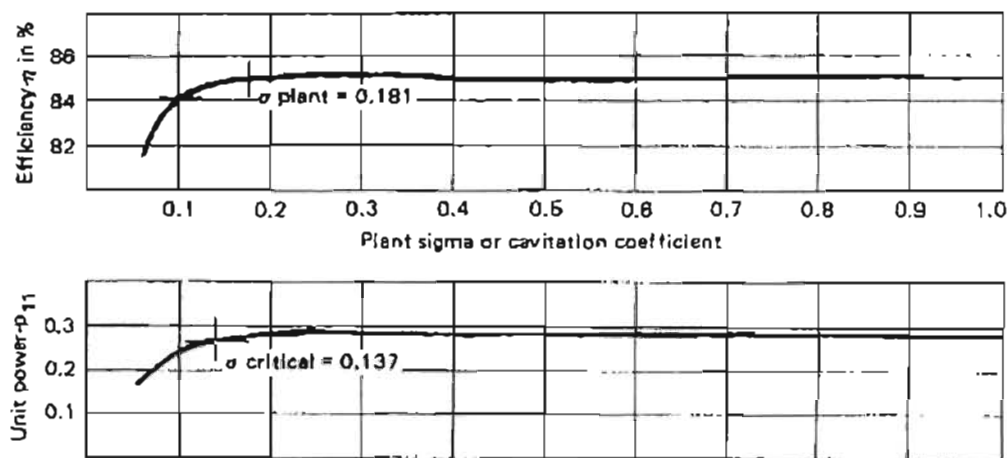


Figure 2.4. 7 Representative cavitation coefficient curves, Warnick (1984)

### 2.4.9 Control of Cavitation

The most successful method of controlling turbine cavitation is through the application of turbine setting, where the runner is positioned at a specific height such that the pressure and velocity of the critical areas do not produce cavitation. The setting of the turbine is however, in some cases, determined by the cost of the project, which is likely to increase rapidly should the turbine setting require that it be placed below the tailwater level.

Another method of controlling turbine cavitation is simply to limit the effect of the pitting damage, such as increasing the thickness of the material in the region of the pitting damage, or using a harder, more resistant material, or finally coating the material with an impact resistant coating.

The control of cavitation may also be achieved indirectly through design, by pre-selecting the speed of the runner. Should the runner diameter be decreased, higher velocities through the turbine will occur and subsequently increase the likelihood of cavitation inception. In order to compensate for the increased likelihood of cavitation, it would be necessary to lower the turbine setting. Hence a balancing of the turbine speed and setting is paramount.

Designing the shape of the turbine passages, from the penstock through to the draft tube and even for the turbine blade passages, can also affect a significant delay in the inception of cavitation.

#### **2.4.10 Selection of the Turbine Setting**

The primary objective of turbine setting is to determine the vertical distance of the critical part of the turbine from the full-load tailwater level. The cavitation coefficient must be referred to particular point on the runner. For the case of the Francis runner, it is customary to choose the bottom of the runner as the water exits the vanes. For the vertical axis propeller turbines, the reference point is the centreline of the blades and for horizontal axis turbines the reference point is near the upper tip of the runner blade.

The manufacturer performs the final selection of the turbine setting in much the same way as the selection of the turbine's size and shape, by using results from model tests. The prediction of the turbine setting then is used as an entry-level approximation. It is nevertheless useful to determine the turbine setting using the homologous nature of turbines and this is achieved from experience curves. As was the case for the determination of the turbine parameters, the setting is defined against the specific speed.

For example, the compilation of the experience curves relates the acceptable level of the cavitation coefficient to the specific speed and uses the homologous nature of turbines that operate under similar hydraulic conditions, to indicate that they will also have similar values of critical runner sigma. Mentioned earlier was the compensation required for the

indeterminate value of the head and tail water levels. Figure 2.4. 8 allows for a 0.3m offset in the turbine setting which is lower than what is required and will therefore allow for a decrease in the potential for cavitation.

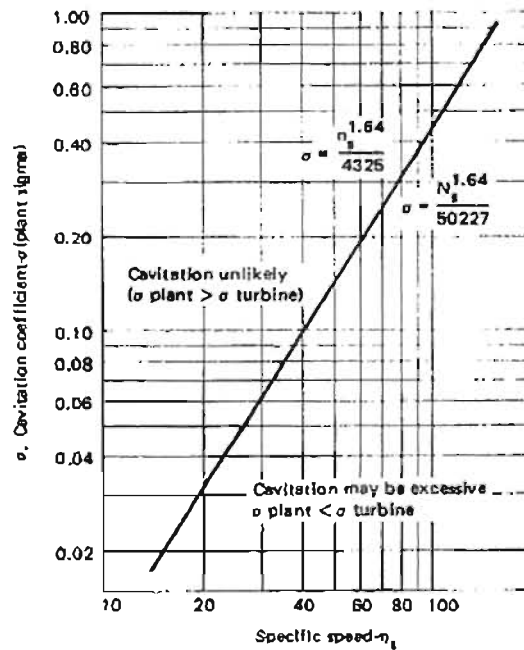


Figure 2.4. 8 Cavitation coefficient limits, Warnick (1984)

Table 2.4. 2 gives an indication of the relative values of  $h_a$  and  $h_v$  as they appear as functions of atmospheric pressure or altitude and of the water temperature.

Altitude (m)	$h_a$ (mm Hg)	$h_a$ (m H <sub>2</sub> O)
0	760.00	10.351
500	715.99	9.751
1,000	674.07	9.180
1,500	634.16	8.637
2,000	596.18	8.120
2,500	560.07	7.628
3,000	525.75	7.160
3,500	493.15	6.716
4,000	462.21	6.295

Water Vapor Pressure			
Temp (°F)	$h_v$ (ft)	Temp (°C)	$h_v$ (m)
40	0.28	5	0.089
50	0.41	10	0.125
60	0.59	15	0.174
70	0.84	20	0.239
80	1.17	25	0.324

Table 2.4. 2 Atmospheric and vapour pressure variation, Warnick (1984)

### 2.4.11 Draft Tubes

Draft tubes are the final component of the turbine and serve the purpose of recovering some of the kinetic energy. An efficiently functional design of draft tube can provide for a recovery of a portion of the velocity head as the water exits the turbine, improving the overall efficiency. The draft tube further utilises the runner discharge head if this is set above the tailwater level.

For the initial design phase, the sketches shown in Figure 2.4. 9 are useful for shaping the relative dimensions and sizing of the spacing of units and for making estimates of the excavation requirements. Diameter  $D_3$  is the discharge diameter of the runner and can be applied to more than one turbine family, however, there are small modifications required for the different types of turbine.

The design of the draft tube for the Kaplan turbine is provided by the work of deSiervo and deLava (1978), Warnick (1984), which provides the following empirical equation for determining the velocity of the water at inlet to the draft tube:

$$V_4 = 8.42 + \frac{250}{N_s} \quad (2.4. 17)$$

where:  $V_4$  = water velocity at the draft tube inlet section, [ $\text{ms}^{-1}$ ];

$N_s$  = turbine specific speed.



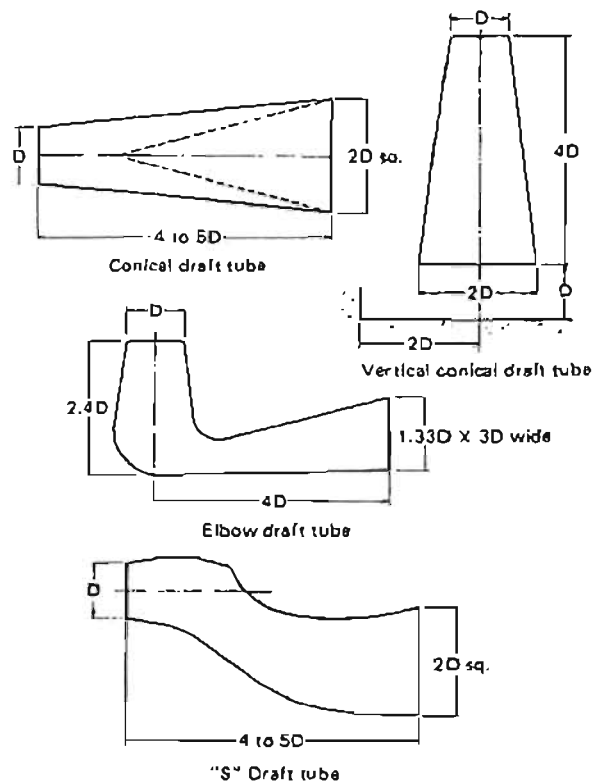


Figure 2.4. 9 Relative dimensions for different types of draft tubes, Warnick (1984)

## 2.5 Diffuser design for small turbines

Technology is available to make efficient turbines of almost any size, but in the past the cost has been prohibitive for small systems. Thus most of the recent work in this area has been devoted to reducing overall system cost rather than improving efficiency. In all sizes, the cost per unit of energy is the deciding factor, but because of different constraints, optimum designs differ. Some of the constraints that should be considered are: available head, flow, flow duration, load and particularly for small systems, any existing construction at the site.

The diffuser is a significant component that must be considered in the overall design of hydropower systems. It is particularly important for low-head systems, where the kinetic energy leaving the turbine is usually a large part of the total available head. Primary design factors include the inlet velocity and the pressure recovery. Other factors include limitations imposed by cavitation and civil construction.

For small systems it is not feasible to conduct extensive test programs in the design of each installation. Where possible, standard units are used, many of which have been tested in full scale. Because of limitations imposed in many applications, standard draft tubes cannot be used. Thus it is important to accurately estimate the diffuser performance and its effects in the complete system.

This means that any design criteria for the existing system are only meant as guidelines and the draft tube design may be adopted to be specific to a particular site as shown in the calculations performed in the design section. In the current research, a draft tube was already in place and was designed for another turbine. The short space between the turbine to be designed and the existing draft tube imply that it will be impossible to develop a draft tube well suited to design conditions. However, the purpose of including design theory is to complete the design criteria for the turbine, should it be required that another turbine be built.

### 2.5.1 Effect of the draft tube on performance

To examine the effect of the draft tube on hydropower system performance, one should begin with the losses of the entire system. The total head at any point in the system is defined as:

$$H_t = \frac{P_s}{\rho g} + \frac{V^2}{2g} + z \quad (2.5. 1)$$

And the static head is given by:

$$H_s = \frac{P_s}{\rho g} + z \quad (2.5. 2)$$

The gross head available to produce work is:

$$H_{t_{gross}} = H_t - H_s \quad (2.5. 3)$$

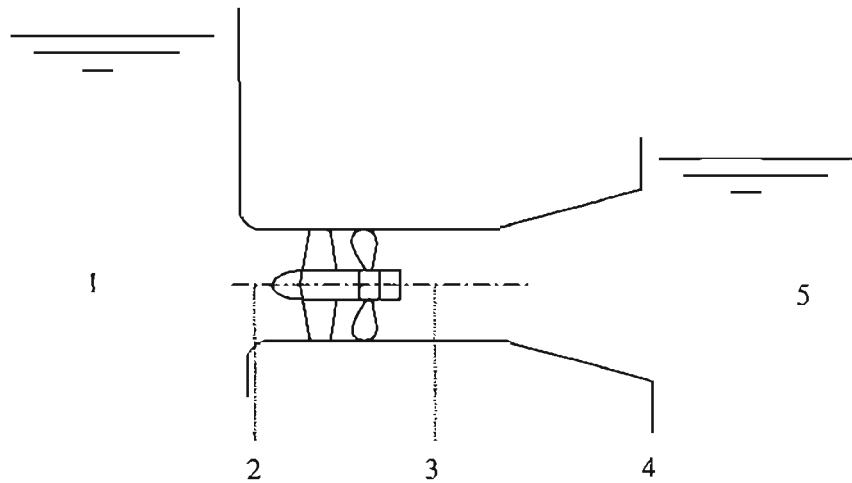


Figure 2.5. 1 Typical turbine system

However, because of losses in the intake, draft tube and exit, the effective head across the turbine is:

$$\Delta H_{i,eff} = H_{i_2} - H_{i_3} \quad (2.5. 4)$$

The turbine efficiency ( total-to-total ) can be defined as:

$$\eta_t = \frac{P_{shaft}}{\rho Q g H_{i,eff}} \quad (2.5. 5)$$

The effective head for efficiency calculations is often defined as the total head across the turbine and the draft tube,  $H_{i_2} - H_{i_4}$ , but this definition does not account for the losses in the draft tube exit. The overall system efficiency ( water-to-wire ) is defined as:

$$\eta_{OA} = \frac{P_{elect}}{\rho Q g \Delta H_{i,gross}} = \eta_t \eta_m \eta_g \frac{\Delta H_{eff}}{\Delta H_{gross}} \quad (2.5. 6)$$

Since the objective is to examine the losses in and at the exit of the draft tube, all other losses are assumed constant. The following values are assumed:

$$\eta_t = 0.90; \quad \eta_g = 0.98; \quad \eta_m = 0.98; \quad H_{i_1} - H_{i_2} = 0$$

The draft tube performance is characterised by the pressure recovery coefficient, based on the mean axial velocity at the inlet to the draft tube:

$$C_p = \frac{P_{s_4} - P_{s_3}}{\rho (V_3^2 / 2)} + \frac{g(z_4 - z_3)}{(V_3^2 / 2)} \quad (2.5. 7)$$

Then the total head loss for the draft tube as a fraction of the gross head is:

$$\frac{H_{13} - H_{15}}{\Delta H_{i, \text{gross}}} = (1 - C_p) \frac{V_3^2}{2g\Delta H_{i, \text{gross}}} \quad (2.5.8)$$

The ratio of the velocity  $V_3$  to the quantity  $\sqrt{2gH_{i, \text{gross}}}$  is a system design parameter and the pressure coefficient is a function of the draft tube geometry.

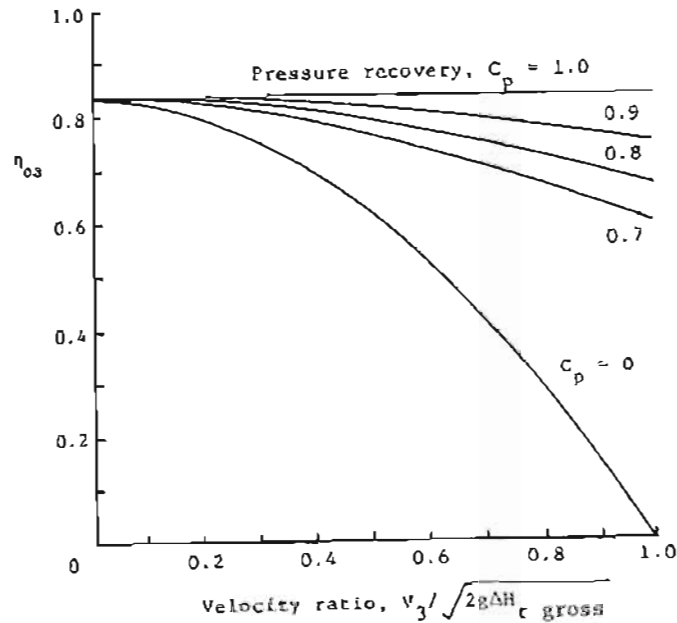


Figure 2.5. 2 Effect of draft tube on performance, Moses (1982)

The effect of these two parameters on overall system efficiency is shown in Figure 2.5. 2, based on the above-assumed component efficiencies.

### 2.5.2 Turbine-Draft tube matching

Neither component should be designed without consideration of the other and the two should be tested together. The turbine efficiency is often defined to include draft-tube losses, so that combination can be optimised. As shown in Figure 2.5. 2 the system performance depends strongly on the velocity  $V_3$  entering the draft tube. Since  $Q = V_3 A_3$  this velocity is also related to the size of the turbine. With very high velocities, the turbine size is small, but draft tube losses are high. For a velocity ratio of 0.7-0.8, which is typical of low head, axial flow turbines, overall efficiency depends strongly on draft

tube performance,  $C_p$ . For high head systems, the velocity is much less relative to the spauling velocity and the draft tube is much less important.

The above arguments are included in the turbine design, but only in an indirect manner and as only part of the selection. Typically, the turbine type and speed selection are based on the specific speed:

$$N_s = \frac{N\sqrt{P}}{\Delta H_t^{5/4}} \quad (2.5.9)$$

The turbine size is then based on the head, flow rate and specific speed. For example, relations such as the following for axial flow turbines have been developed to determine the rotor diameter:

$$D_3 = \frac{7.1}{\sqrt[3]{N_s + 100}} \times \frac{\sqrt{Q}}{\sqrt[3]{\Delta H_t}} \quad (2.5.10)$$

In general then, turbine design for a given head and flow begins with the selection of turbine type, speed and size. Next the vane angles must be determined to extract the correct power at the desired flow and head.

$$\Delta H_t = U_2 C_{\theta_2} - U_3 C_{\theta_3} \quad (2.5.11)$$

The design of the turbine and draft tube must also consider the problem of cavitation, which results from low pressure through the turbine. Since the pressure at each point in the flow field is difficult to predict, turbine design is usually based on experimental correlations such as the following for axial flow turbines:

$$z_i \leq \frac{P_a}{\rho g} - \sigma \Delta H_t \quad (2.5.12)$$

$$\sigma = 0.28 + \frac{1}{660} \left( \frac{N_s}{100} \right)^3 \quad (2.5.13)$$

To minimise turbine diameter, a large value specific speed is required, but in order to avoid cavitation, the specific speed is limited by the turbine elevation and head.

### 2.5.3 Draft tube performance

Within the constraints imposed by the turbine design and system layout, the draft tube must be designed to minimise losses and maximise pressure recovery. Considering the

simple case of a straight conical diffuser, there are only two variables, for which a large amount of experimental data is available, Figure 2.5. 3.

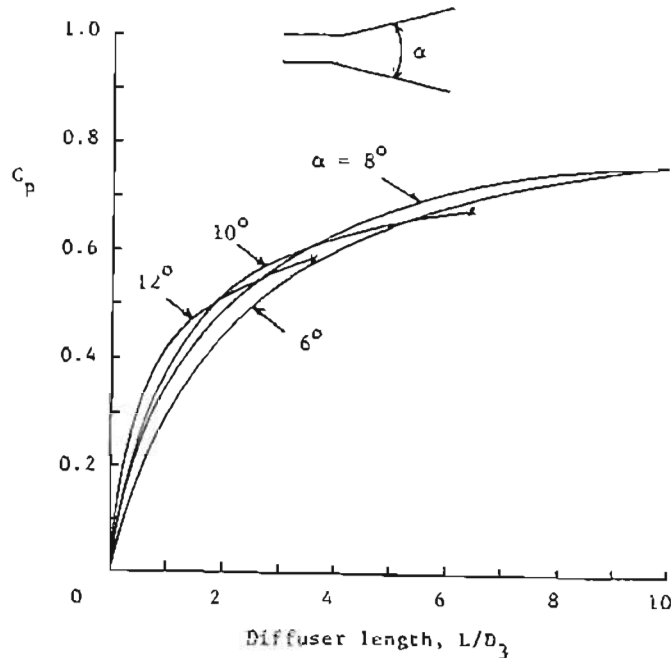


Figure 2.5. 3 Conical diffuser performance, Moses (1982)

As shown, the maximum recovery occurs with a very long diffuser and a small angle. However, the diffuser can be made much shorter with a larger angle without a substantial loss in performance. Typical values for small axial flow turbines are a length/diameter ratio of 4 and a total included angle of  $14^\circ$ - $15^\circ$ .

The maximum recovery is limited by the growth and for large angles separation of the turbulent boundary layer along the diffuser wall. Large amounts of separation, or stall, can lead to large fluctuations in flow and generally should be avoided in draft tubes. However, maximum recovery in plane diffusers usually occurs with small regions of separated flow. Since the exit velocity results in a loss, maximum recovery is optimum for system efficiency, but increases the danger of cavitation.

In addition to length and area ratio, the primary factors that affect diffuser performance are inlet flow conditions and the overall configuration. It is desirable to minimise swirling flow into the draft tube since this kinetic energy results in a loss. Almost all turbines

result in some swirl, particularly at part load conditions. Small amounts of swirl are beneficial to diffuser performance, but large amounts can result in stall or cavitation near the centre of rotation. Non-uniform flow into the draft tube can result from boundary layers on the casing, radial variations in work extracted by the turbine, wakes from vanes and centre-body and wake from a downstream shaft. In well designed turbines the flow is relatively uniform, but wakes from the hub and downstream shaft can each result in a decrease of 2% – 5% in pressure recovery.

In general, a straight conical diffuser is near the optimum configuration, but this design is not always possible. Thus a number of different configurations have been developed as indicated in Figure 2.5. 4.

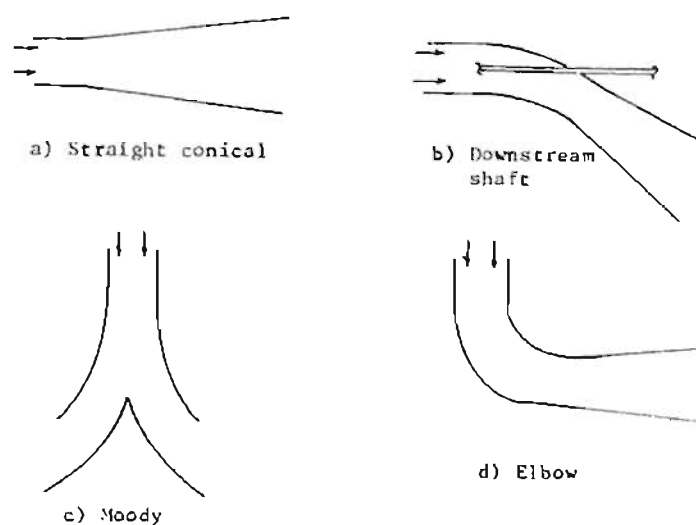


Figure 2.5. 4 Draft tube configurations, Moses (1982)

Since there are many more variables involved and turning of the flow increases the danger of separation, the design of these draft tubes is much more difficult, requiring computational modelling where extensive testing of small scale models is required in order to reduce cost.

## CHAPTER 3 DESIGNING THE TURBINE

### 3.1 Site specific parameters

The site into which the turbine was to be installed had already been prepared. This consisted of a gate valve controlled supply, fed by a channel from the Karkloof river and the exhaust was through a draft tube which dumped the water back into the river. A shed enclosed the entire unit. The turbine will be run from the supply pipe and controlled by the gate valve. The reduction in diameter to suit the supply to the turbine required the development of a nozzle spanning the distance between the turbine and the valve.

The existence of the draft tube posed a similar dimensional problem hence a diffuser was required to match the turbine output diameter to that of the draft tube inlet diameter. It was reasoned that this would cause problems with respect to the flow exiting from the turbine in terms of the pressure recovery capability of the diffuser.

The area required for the installation of a generator, pump or a dynamometer is available at the PTO (power take out) of the turbine shaft. The network of cables and piping is already in existence should it be required that these options be pursued after the testing phase is complete. The feeder pipe, which supplies the pump with water, is also currently available. The parameters of the turbine design had previously been determined by the project supervisor and have only been listed for the purpose of further calculation and for the benefit of the reader.

Turbine parameters:   Nominal bore (gate valve): 610mm  
                              Nominal bore (turbine delivery pipe): 676 mm  
                              Flow velocity (turbine delivery pipe): 2.5 m/s  
                              Pressure (at penstock): 0.1MPa  
                              Power required from the turbine:  $\pm 40$  kW



The first question to consider was then what type of turbine was to be specified for this particular application. Consideration had to be given to the complexity of the turbine, its ability to produce power through large changes in the stream flow rate, the necessity to service the turbine and the frequency at which this must be performed and finally the available pressure head combined with the flow rate. The three types of turbines under consideration are the impulse, Francis and propeller turbines. These different types of turbine are described in Figure 2.4.4 and plotted against the head and output produced by the turbine.

For the values of initial conditions given above, the turbine most suited would be the propeller turbine. Furthermore, the propeller turbine can be simplified to an axial flow turbine, which further simplifies the design and operation. Considering that these turbine installations are aimed at the informal sector, a simplified design will provide an advantage over a design that requires skilled labour and expensive equipment.

The ability of the flow to intercept the rotor blade at relative angles of the order of 60 degrees is justified by the conservation of angular momentum of the flow as it moves from a large annular area at the wicket gates to a smaller annular area at rotor. The increase in the tangential velocity component causes this increase in inlet angle.

If it may be assumed that the inlet angle is 0 degrees then the turning angle may be assumed to equal the outlet angle. In which case the remaining factor to consider, when selecting this turning angle as a parameter for the purely axial flow turbine, is the blade solidity, which affects the design of the blades, i.e. momentum blading versus airfoil blading.

## **3.2 Piping**

### **3.2.1 Supply**

The piping immediately above and below the turbine is shown in **Drawing 1** in Chapter 9 and serves the purpose of directing the water flow from the channel, which removes water from the river, through the gate valve, which is used to control the volume flow

rate supplied to the turbine. The turbine will be designed such that the rotor and stator are placed in a 350 nominal bore diameter, downsized by a 400/350 nominal bore reducer. The purpose of decreasing the diameter of the flow only at the penstock, is to increase the flow velocity whilst the supply, travelling at a lower speed, will incur minimal friction losses. An additional reduction in bore diameter is required between the gate valve, 600 nominal bore, and the large end of the reducer.

### **3.2.2 Penstock**

The penstock is where the potential energy of the flow is converted into kinetic energy through the turbine and is noted as the red item, the reducer, in **Drawing 1**. The total pressure, the sum of the static and dynamic pressures, forces the flow through the stator blades, which induce a tangential velocity component that drives the rotor.

### **3.2.3 Diffuser**

The bend in the pipe seen in **Drawing 1**, shortly after the turbine, does not have positive implications for the flow dynamics but it allows for the protrusion of the shaft from the flow axis such that power may be extracted from the system. The inclusion of the curtain plate, **Drawing 21**, facilitates the change in the direction of the flow and furthermore is able to reduce the effects of swirl from the turbine rotor. The main purpose of the plate is therefore to minimise the curtain effect of the flow, which is to ignore the path of the bend and continue without a change in direction.

The final stage of the piping is the draft tube. The draft tube serves the function of recovering the dynamic flow pressure. The efficiency of the tube will determine the effectiveness with which this is done. The draft tube acts as a diffuser, slowing the flow down to recover the remaining velocity potential in the form of static pressure. The length of the draft tube, determined by turbine setting, will determine the amount of recovery possible, subject to the limitation of the inception of cavitation. The existing draft tube currently on site served as the draft tube for the turbine, regardless of its suitability. However, an additional diffuser will be required to match the bore size of the turbine, 350 nominal bore, to the diameter of the existing diffuser, diameter 560mm. This was expected to induce high losses simply due to the required large change in diameter

over a short length, resulting in an included angle of  $44^\circ$ . The typical set-up of the turbine site and of the manufactured turbine components can be seen in Drawing 1.

### **3.3 Stuffing Box**

#### **3.3.1 Design conditions**

The stuffing box serves the purpose of preventing the flow of water from the main piping out to atmosphere, through the clearance between the shaft and its housing. The flow of fluid will depend on the pressure differential that exists between the pressure of the water in the pipe and the pressure of the surrounding atmosphere. During operation the water pressure is most likely to be below that of the surrounding atmosphere due to the pressure recovery action of the draft tube. Under this condition, the flow will tend to draw air into the piped flow through the stuffing box. In which case it will be necessary to provide the stuffing box with water from the high-pressure side of the turbine to prevent the stuffing drying out and overheating, typically caused by friction. Running a small pipe from the high-pressure flow side of the turbine into the stuffing box easily solves this problem.

However the turbine may be run under a condition where the vacuum pressure is non-existent, such as when the turbine is stalled under overload or when cavitation causes localised low pressure producing vapour and air bubbles in the flow, which nullify the effect of the draft tube by inducing an airlock, i.e. the expanding area is offset by the volume of bubbles. The stuffing box will then prevent excessive leakage of the piped water.

#### **3.3.2 Design Options**

The initial design of the stuffing box considered the use of an En 8 hollow bar welded to the pipe bend where the shaft exits and would serve the dual purpose of being the structure to which the bearing pedestal is secured. The problem with such a design is the rust factor. Steel in direct contact with the water will experience significant rusting and the fact that the housing is also designed to take the thrust of the turbine, failure of the component would disable the turbine completely. Several solutions were considered and are outlined below:

- painting of the inside surface of the stuffing box and shaft housing section will suffice only under conditions where the water contains no contaminants. Since it is river water that shall flow through the turbine, abrasion of the paint will be expected.
- galvanising in preference to painting is a more likely option. The galvanising may however not form a uniform coating on the surface of the inner wall and may prove problematic when aligning the stuffing box. A simple machining process to skim off the high spots would resolve such an issue.
- using a different material that does not rust develops problems with the welding of two dissimilar materials. Cast iron, usually used in conjunction with water will prove to be too brittle in this instance when recalling that it will be required as the platform for the bearing pedestal.
- a simple stainless steel sleeve would solve the problem altogether. Its use allows the stuffing box pipe to be welded to the pipe bend and is stronger than cast iron. Furthermore, it will facilitate the use and servicing of the stuffing and lantern ring.

The selection process reasoning indicates that the best option to pursue is the stainless steel sleeve since it meets all the requirements of the design.

### **3.4 Drive Train**

The speed ratio of the drive train is to be set at 2:1. The drive pulley will have a P.C.D. of 307mm and the driven pulley will have a P.C. D. of 154mm. The drive train must transmit a power of 40kW at a speed of 450~900rpm. These values are used to calculate the necessary shaft diameters and the loading of the bearings 2 & 3 shown in Figure A 7.2.1. Should the drive sprocket be the option of transmitting the power, the resultant additional axial load represented as one third of the axial load was considered, with respect to the minimum required load on the thrust bearing. This should not cause separation of the thrust bearing since, to generate the thrust initially requires that the rotor be running. When the rotor is running, there exists approximately 4.5 times the force in the opposite direction, which pushes the thrust bearing together. Hence separation will not occur due to this thrust.

Once the drive train diameters had been selected, the suppliers were contacted in order to determine what the nearest standard size diameters were in order to avoid the additional costs of custom-made power transmission mechanisms.

### **3.5 Bearing Selection**

#### **3.5.1 Bearing types**

Many different bearing types and configurations were considered, Drawings 21, 22 and 23 in Chapter 9, initially in the light of simple and low maintenance. This could easily have been achieved by using plummer block bearings. Specialised help was sought through bearing companies in the selection of bearing configurations and bearing types. The investigation revealed that it would not be possible to consider a bearing that is normally intended for radial loading because in each case the ratio of axial-to-radial load is specified by the bearing manufacturers as being less than one. However, this was not the case with the load configuration encountered in the turbine and it was necessary to move away from the plummer block bearing type, toward a thrust bearing / radial bearing combination configuration, which would avoid the complications of using angular contact bearings.

Other options such as the hydrodynamic film bearing and standardised housings were also considered. But the hydrodynamic film bearing required a high level of maintenance and a clean environment; conditions not freely available in rural South Africa. The standardised housing could easily have been adapted from the bearing housing manufactured by the pump supplier, but it was completely under-rated in terms of its axial load absorption capacity and was therefore also deemed unsuitable.

#### **3.5.2 Final selection**

The final selection was for a combination of the two bearing types, two square flange bearings and one thrust bearing as seen in Drawing 21 of Chapter 9. Although bearings 2 & 3 are designed for a radial load only, it is possible that they may also take an axial load. This may result if a sliding fit is not obtained on the shaft journal.

Once the size of the bearings had been calculated such that a life of approximately 3 years was obtained, the size of bearing 2 was then increased to suit a 60mm shaft, fitting the dimensional requirements of the pipe bearing pedestal. As a result, the bearing cost increased by 85% which can be argued to be recovered in the reduction in machining cost, the number of bolts to be purchased and from the replacement period extension gained by using a larger bearing. There is also a level of simplification to be gained by choosing two bearings that are alike when re-ordering and purchasing nuts and bolts.

The change in the bearing size allowed the seating plates, seen in **Drawing 13** of Chapter 9, to be excluded but the problem of diaphragm bending of the bearing housing arose. A look at the design of the seat of the bearing revealed that the bearing was seated on raised platforms at each corner, the location of the bolt holes. This meant that the bearing was designed to be seated only on these platforms. However, should the problem arise whereby the bearing housing becomes subjected to diaphragm bending, it is dimensionally possible to include the backing plates without having to change the design of the bearing pedestal or the shaft. The only design change remaining is then to increase the uncompressed length of the pre-load spring by 15mm.

### **3.5.3 Pre-load spring**

Separation of the bearing seats from one another would be very common in thrust bearing use save for one detail, the use of the pre-load spring. An application of a constant force on the bearing seats ensures that they remain together at all times, refer to **Drawing 17** of Chapter 9. This pressure guarantees that the balls within the bearing have sufficient dynamic friction to roll rather than slip, cutting grooves into the seat. Separation can be caused by either gravity or gyroscopic moments separating the two seats. The purpose of the spring is therefore to induce a pre-load on the thrust bearing such that the minimum allowable pressure is maintained at a constant level. The spring will run on the inner race of the radial bearing and on the turbine side of the thrust-bearing bearing face.

## 3.6 Bearing Pedestal

### 3.6.1 Design options

The first design iteration regarding the bearing housing was to use a conventional bearing box supplied by the pump manufacturer, refer to **Drawing 22** of Chapter 9. But after a short research into its axial load capacity, it was quickly determined that the axial load rating of the turbine far exceeded that of the pump. It was then considered feasible to change the bearings, but keep the housing. The bearings were selected as being spherical thrust or angular contact bearings. The design of the housing meant that these bearings would be splash lubricated. Grease lubrication is only feasible for housings that do not have large air gaps within. Grease lubrication under these circumstances is prone to higher levels of contamination. The design of the housing would have allowed it to be bolted to the flange of the stub pipe and the base bolted to the supporting framework.

The benefit of having a custom made bearing pedestal reduces:

- the amount of machining and welding but does not avoid the problem of attaching the pump to the bearing pedestal, which requires further fabrication of a pump mounting frame,
- the potential stress on the welded joint between the stub pipe and the main pipe.

The second solution as advised by an external company was to have a custom housing for the axial thrust bearing separate from the plummer block bearing. The thrust housing would be bolted directly to the stub pipe, which would then support the axial load. The plummer block bearing, bolted to the supporting framework could then absorb the radial load. See **Drawings 22 and 23**.

The main problem with such a design would be the misalignment of the shaft with respect to the plummer block. Locating the framework to which the plummer block is bolted, relative to the stub pipe, thus becomes difficult.

Large quantity production of a custom made axial thrust support bearing housing would decrease the cost of manufacturing the component but for a small number of items it may prove an expensive venture. Due to the simple shape of the bearing housing an equally simple casting process could be used, such as sand casting, which is relatively inexpensive once the die has been made.

Having separate housings for the thrust and plummer block bearings would require that a separate landing be made for the plummer block for the purposes of accurate alignment, which will require complicated design features. Ideally then, it would be most efficient to adopt a pedestal design that would support both radial and axial loads yet allows for the separate bearing requirements of the thrust and radial bearings.

The most simplified design, shown in **Drawing 21**, and which meets all the design criteria, is to have the bearing pedestal made from a single pipe with inserts that serve as the locators / backing plates for two radial and one thrust bearing. The bearing pedestal housing this combination would therefore support both the radial and the axial loads. Since the load is 80% axial – assuming the belts will be used as the method of power transmission – the pipe design may be considered appropriate because of its orientation to support the load in a tensile manner.

### **3.6.2 Final selection**

After much consideration, the design of the bearing pedestal fell in favour of the bearing tube, proving to be a better proposition for the following reasons:

- the material requirements for the design of the framework are at a minimum
- improved loading configurations by means of the axial support
- simplified construction
- provides a protective housing for the bearings
- eliminates the problem of pipe movement when compared to other designs

However, factors counting against the design are:

- construction may be slow due to the necessity to weld and machine at each stage
- the design is bulky and may require handling equipment



It was concluded then that the best design was the bearing tube option.

### **3.7 Main support frame**

The large volume of flow in the main pipe raises the question of movement of the main pipe caused by the reaction to the force needed to changing the flow direction through the 70 degrees. What remains then is to determine whether or not it would be necessary for the framework to incorporate a supporting feature. The best solution would be to design a main frame that would not only benefit the installation but one that would be additionally suited to the pump unit.

Without the main frame and just a support on the end of the pedestal, the only part of the structure preventing movement is that of the bearing pedestal weld join to the main pipe. Any movement would therefore have to be absorbed by the bearing pedestal and the feeder pipe, depending on the magnitude of the relative movement. Expansion joints may be required for the feeder pipe only. The introduction of the main frame would help to minimise any movement, provide a base to which the bearing pedestal can be bolted and a frame that would provide the necessary support for the structure during transport and installation. And with the simple means of welding on lifting lugs, transport and installation become easier.

The objective of the framework would not be for supporting heavy loads during the operation of the turbine because the bearing pedestal will take up the main load of axial thrust. The remaining radial load, approximately 20% of the axial load and caused by the belt drive power take out, will then be supported by the framework. Thus the design of the loading capacity of the framework would be based on the loading of the lifting lugs, the magnitude of which is determined by the mass of the entire turbine unit. However, the final method of selection is based on relative sizing of the frame, which is a function of the size of channel section used in the pipe support beams.

The framework may then be standardised according to the size of the turbine with the primary purpose of facilitating the installation and moving of the turbine. Sizing of the

framework components is therefore at the discretion of the designer, subject to certain limitations.

### 3.8 Rotor and Stator

In designing the blades the first critical stages are revealed by asking certain intuitive questions and deciding which factors will play a predominant role in the design of the turbine and which factors will play a secondary role. The necessity to determine this right from the start is due to the inter-relation of the design conditions as will be seen outlined in the following blade design and selection objectives and furthermore in the chapters to follow.

1) Obtain the lowest drag in terms of the friction, form and pressure drag.

2) Locate the position of the diffuser, nozzle:

What adjustments can be made to the blade shape to obtain the nozzle / diffuser effect without large sacrifices in the shape effect?

3) Optimise the number of blades:

The solidity ratio will determine the effectiveness, lift and drag, of a single blade weighed against the effect of interference of additional blades. This needs to be examined at radial intervals due to the increase in space from hub to tip.

4) Examine blade geometry:

What is an effective blade shape that satisfies the dependence of shape on the design type, for example the airfoil versus momentum theory design?

5) Optimise camber line versus angle of attack:

The camber line and corresponding shape determine the pressure distribution of the foil section, generating the lift and drag vectors. These vectors generate the highest torque when their direction is perpendicular to the axis of the hub.

6) Design condition:

It is possible to design the blade geometry according to an exact set of operating conditions, but it must be expected that the turbine will operate above and below these design conditions. The geometry of the blade must take this into account.

7) Change in drag as a function of the Reynolds Number:

The drag changes as a function of the Reynolds Number as given in many textbooks and a particular example is shown in Figure 3.8. 1. The graph shows a general decline of the drag coefficient  $[C_D]$  as a function of increasing the Reynolds Number.

8) What pressure exerts the highest force when water is the flow medium?

This question has two components since the pressure distribution about any non-symmetrical profile is a function of its camber and the camber affects the direction of the lift and drag vectors which are then divided up into axial and perpendicular components. Hence the camber will determine the direction of these vectors. Once the direction has been ascertained, the thickness distribution about the camber line needs to be determined according to the desired pressure distribution, which establishes the suction and pressure characteristic curves.

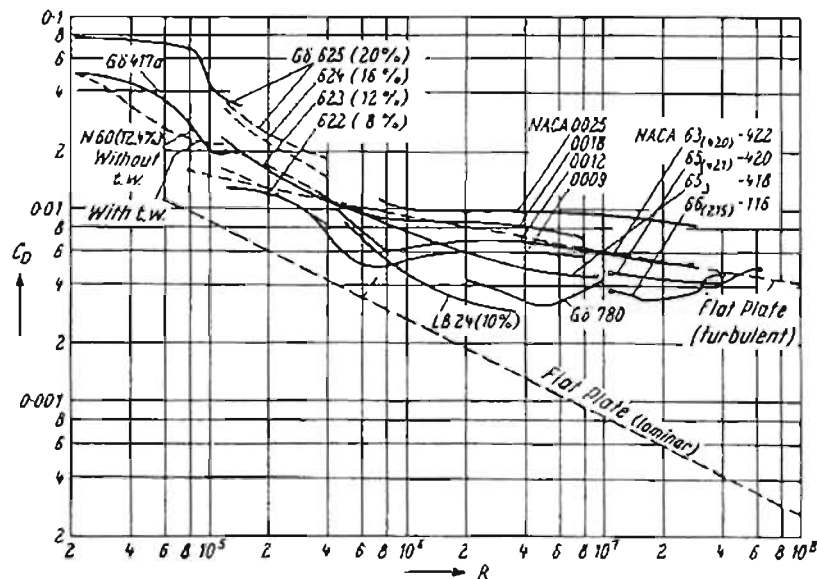


Figure 3.8. 1 Minimum drag coefficient as a function of Reynolds number, Reigels (1961)

9) The blade shape may also be subject to the availability of shape definition:

Many of the existing profiles are defined according to an equation, such as the NACA series and Joukowski profiles, for which much data is available which describes the  $[C_L & C_D]$  characteristics as a function of the angle of attack. For profiles that do not have empirical definitions, it will be necessary to find or develop the xy-coordinate pairs defining the specific blade.

### 3.8.1 Shaping the blade

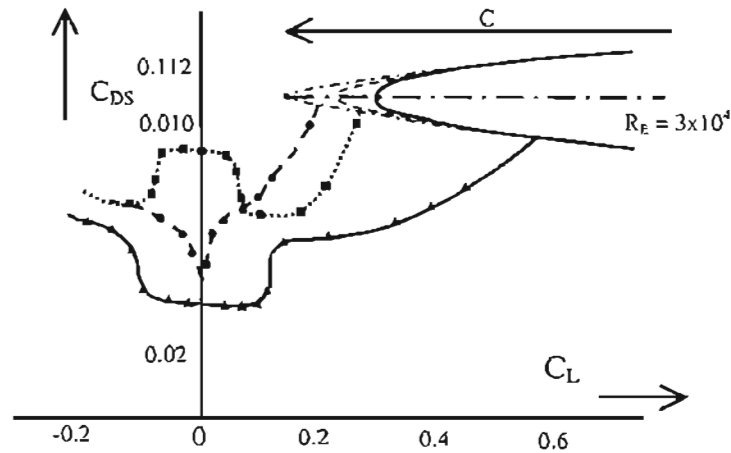


Figure 3.8. 2 Influence of leading edge shape on boundary layer and  $C_D$ , Hoerner (1965)

Figure 3.8. 2 shows that it is most suitable to use a parabolic leading-edge radius since it promotes the stability of the flow as it enters both the stator and rotor blade hubs. Although it does not provide an indication of the equation of the parabola it is expected that it would be dependent on the thickness distribution. It should however be noted that the arms of the parabola are required to tangentially intersect with the thickness distribution as a function of the camber line of the profile.

Changing the radius of curvature of the camber line may therefore be used to cause transition of the flow from laminar to turbulent. However the methodology behind the design is to attempt to ensure that this transition does not occur. This can be promoted in two ways:

- 1) a decrease in the radius of curvature should correspond to a decrease in the Reynolds number
- 2) maintaining a constant radius of curvature of the camber line.

The requirement of changing the Reynolds Number can be executed in two ways. Firstly the velocity can be reduced overall, by a reduction in the pressure differential across the penstock. Alternatively the length over which the fluid flows can be reduced. Both of these variables will reduce the power developed by the turbine blades. The only criteria that can be met, is the constant radius of curvature, which is most easily defined by a

circular arc camber line having a low thickness distribution such that the profile thickness does not deviate far from the circular arc camber line.

The minimum drag can be obtained when defining  $x/c = 50\%$  for conventional profile thickness ratios, beyond which, the pressure and separation drag increase as a function of the wedge angle at the trailing edge. But a trade-off exists between the skin friction and the profile drag. Increasing the length over which the profile is tapered to the trailing edge decreases the wedge angle. The trade-off is then caused by an increased skin friction drag resulting from the length of the profile over which the turbulent boundary layer flows. Turbulence along the afterbody of a laminar profile can therefore be expected to be unavoidable.

### **3.8.2 Defining the pressure distribution**

For the purpose of performance, it was established that the positive pressure gradient should be formed as late as possible on the profile. This would result in the location of the transition of the flow from laminar to turbulent to be far back on the profile, thus reducing the skin friction drag caused by the turbulent flow. Hence the shape of the profile or thickness distribution will be developed to meet this criteria.

The difference in the flow velocity between the upper and lower surface describes the reason for the pressure distribution as a function of the sum of the static and dynamic pressures. If the static pressure is assumed to be constant it means that the total pressure varies proportionally to the velocity. The pressure thus affecting the kinematic viscosity will result in a different point of transition and similarly different points of reattachment, not ignoring however that this mechanism is also a function of the state of the boundary layer.

It is seen from Figure 3.8. 3 that the angle  $\beta_1$  is conserved, allowing the blades to operate at their design lift coefficient at all times. However, a distinct possibility is for stream turbulence in the inlet flow resulting in non-zero incidence for the stator blades. Such an unpredictable characteristic cannot be accounted for in the design except to attempt to make the inlet flow laminar.

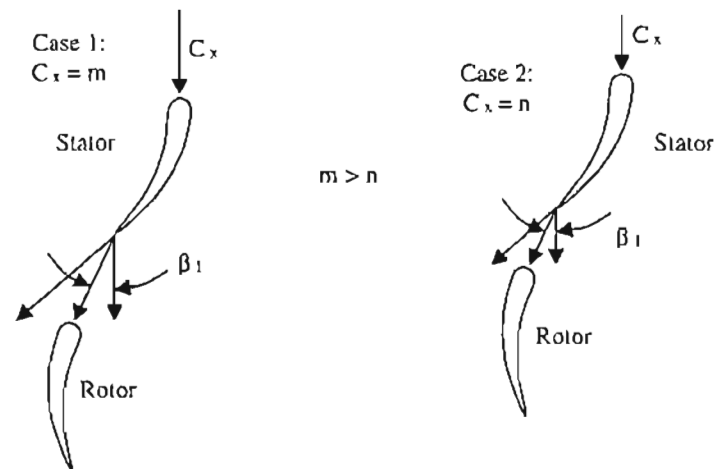


Figure 3.8. 3 Rotor blade angle independent of  $C_x$

### 3.8.3 Location of the transition point

The maximum thickness affects three variables:

- 1) the location of the minimum pressure point;
- 2) the pressure distribution;
- 3) the lift coefficient.

The minimum pressure point should be set as far back as is practically possible, allowing the transition from laminar to turbulent flow to occur as late as possible and hence reduce the friction drag on the profile. Moving the location of the minimum pressure downstream can be achieved by setting the maximum thickness at 40% – 60% chord.

The importance of defining the location of the maximum thickness when considered relative to the  $C_D$  vs.  $C_L$  is far outweighed in comparison to the definition of the pressure gradient. The reason for this is that the turbine is not expected to operate for any significant period of time exactly within its design criteria, because of the unpredictable nature of the supply head, since the supply head is currently drawn from a non-perennial water source.

The location of the transition point is independent of the thickness ratio. Rather, it is defined by the location of the maximum thickness, which influences the pressure distribution. Although the benefits of laminarisation on the pressure distribution are

developed by high percentages of the maximum thickness location  $x/c > 30\%$ , there remains a limitation on the thickness distribution of the profile shape, in the form of the profile drag. This limitation is described above as a function of the dynamic pressure. The effect of which can be defined by the profile drag, which is a summation of the adverse pressure gradient formed at the frontal area and along the afterbody of the profile.

The value of the minimum pressure also affects the transition point. It is expected that a function defined mathematically as “continuous” is the most suitable definition of the desired pressure distribution. “Discontinuities” would be the expected cause of transition. “Smooth” functions therefore can be defined by the combination of the camber and the profile thickness.

#### **3.8.4 Flow conditions**

Accepting that it is not possible to accurately predict the location of the boundary layer separation it will be borne in mind that only the experimental results can give the true indication of the flow condition about the profile. Drag coefficients will also need to be obtained experimentally if they are to be determined accurately, since it is not possible to predict from theoretical analysis the pressure at the rear of the profile yielding the pressure differential, which determines the pressure drag. Hoerner (1965) also makes mention of the fact that the pressure drag is related to the skin friction drag by reasoning that the resistance is a function of the momentum losses incurred by the boundary layer.

It should also be borne in mind that experiments performed in air will have slight differences to the values determined for the same profile in water due to the difference in the medium in which the profile operates. This is due to the fact that air and water have different ratios of inertia and viscosity.

The Reynolds Number is the ratio of the inertial and viscous terms and typically, if the Reynolds Number is small, the viscous terms will dominate and we can ignore the inertial terms. Conversely if the Reynolds number is large, the inertial terms dominate and we can ignore the effects of viscosity.

Considering that water has the comparatively lower kinematic viscosity,  $\nu_{\text{water}} (20\text{ }^{\circ}\text{C}) = 1\text{E-}6\text{ [m}^2\text{/s]}$  and  $\nu_{\text{air}} (20\text{ }^{\circ}\text{C}) = 1.51\text{E-}5\text{ [m}^2\text{/s]}$ , it will be assumed that water will reattach to the surface at a point on the profile further from the point of separation of that of air. The water having its comparatively higher inertial force “damped” by the comparatively lower viscous force means that the momentum of the boundary layer is less “damped” by the viscous effect causing the flow to become turbulent before the flow of air at the same velocity. This is seen in Figure 2.1.2

There are two possible causes of the inception of turbulent flow. The first being the flow pattern caused by the gate valve, where the shape of the resultant orifice would force the boundary layer flow to become turbulent.

Provided that the flow upstream can be made to be laminar, the second cause of turbulence at the headstock can be a result of the velocity of the flow. The flow across the blades would be beyond the region of the critical Reynolds Number ( $Re_{\text{crit}}$ ) since the Reynolds number is in the order of  $10^6$  to  $10^7$  for any point along the blades (both stator and rotor). And coupled with the a non-laminar flow downstream of the turbine due the pipe bend, it is then very likely that the flow will be turbulent.

### **3.9 Draft tube design considerations**

#### **3.9.1 General design**

The increase in area from the draft tube entrance to the exit is required to reduce the exit loss and cannot be obtained in less than the critical length. The reason for this is that the corresponding increase in the taper angle is limited by the increase in the eddy losses that cause cavitation.

It should be noted that for a conical section of draft tube with a total angle of divergence somewhat greater than the ideal for axial flow of approximately  $7^{\circ}$ , an improvement in efficiency is obtained by designing a small swirl component. The best efficiency of a turbine does not occur with axial flow from the runner but with a small swirl component in the same direction as that of the runner.



### 3.9.2 Draft tube bend

Under static conditions, the absolute pressure at runner exit is lower than atmospheric by the water column  $H_s$ , provided that no air is allowed to enter the draft tube. Furthermore, the draft tube must recover as much of the velocity head in the water as it leaves the runner. This recovery takes the form of a further reduction in absolute pressure, which is expressed by:

$$\eta_D (C_2^2/2g) \quad (3.9.1)$$

and is called the dynamic suction head, Brown (1970), where  $\eta_D$  is the coefficient of recovery or efficiency of the draft tube, and  $C_2$  is the  $V_{abs}$  of water as it leaves the runner. The velocity head  $(C_2^2/2g)$  varies in importance according to the specific speed of the turbine. For low specific speeds  $(C_2^2/2g)$  is of the order of 3%-4% of the head  $H$ , whilst it reaches 15% or more for high specific speeds. Hence at high specific speeds, the correct form of the draft tube is required to ensure a good recovery coefficient. The higher the coefficient, the smaller will be the exit losses and the lower can be the value of  $(D_2^3 n/Q)$  which fixes the size of the runner outlet diameter  $D_2$  and thus has a direct bearing on the cost of the turbine.

Losses typically arise from the following:

1. velocity head of the water at discharge from the runner is only partially recovered at the draft tube
2. skin friction in the runner passage
3. eddies at runner blade inlet
4. eddies at the runner blade outlet
5. water leakage past the seals between moving and fixed parts
6. friction losses in the bearings and shaft gland
7. friction losses in the spiral casing, guide apparatus and draft tube

Of the losses mentioned above, the first two are directly dependent on the size of the runner. The following two can be very small with correct inlet angles and blade shapes. All others arise from causes outside the runner. The runner must be designed so as to

obtain a minimum sum of losses 1 and 2 and this is the basis upon which the size of the runner is fixed.

Adopting small absolute velocities at the discharge, for which a large exit diameter  $D_2$  is necessary, reduces the losses of 1. However, an increase in  $D_2$  entails a correspondingly large area of the blades and smaller exit angles, increased skin friction and relative velocities caused by high peripheral speeds. Hence a balance is sought between friction losses and recovery of the velocity head, attained when suitable exit angles are chosen. And practice indicates that this is so when the value of  $(D_2^3 n / Q)$  lies between 85 and 115, depending on the finish of the blades and the efficiency of the draft tube. This ratio is applicable to all reaction turbines. It will be noted that the expression is independent of the head and is consequently independent of the specific speed.

In order to prevent cavitation, the turbine must not be placed higher above tailwater level than is permitted by the relation, Brown (1970):

$$H_s \leq H_b - \sigma_c H \quad (3.9. 2)$$

As  $\sigma_c$  depends partly on the dynamic suction head, a reduction in the diameter  $D_2$ , leads to the lowering of the turbine and deeper excavation, or to a lesser overall efficiency of the machine resulting from a smaller efficiency  $\eta_D$ . The recovery of the velocity head can only be obtained by a gradual increase in the cross-sectional area of the draft tube resulting in a gradual reduction of the velocity. An increase in the cross-sectional area that is too rapid, leads to dead water, back flows and generally poor  $\eta_D$ . The increase must be such as to permit irregularities of flows to even out, which leads to the general rule that any two sections of areas  $[A_1 \text{ \& } A_2]$  separated by the distance  $[l]$ , must satisfy the expression, Brown (1970):

$$0.12l(\sqrt{F_2} - \sqrt{F_1}) < 0.2l \quad (3.9. 3)$$

On a straight cone of circular cross-section, this relation leads to the angle  $[\delta]$  formed by the generatrix of the cone and the centreline being  $4^\circ < \delta < 8^\circ$ , Brown (1970). This relation applies generally to sections of the draft tube that are in a straight line.

For small-size vertical-shaft turbines the simplest form of draft tube is in a straight cone, discharging sufficiently low under the tailwater level to maintain an ample seal against air. This simple arrangement is not possible with horizontal-shaft turbines where a bend must be inserted almost immediately after the runner exit. This bend leads to poor recovery of the velocity head  $(C_2^2/2g)$  because of the necessity for placing it close to the runner in order to minimise the space required by it in the power house. Furthermore, the bend leads to non-symmetric flow at the runner exit causing poor turbine efficiency.

The flow of water in the draft tube is much more at regular loads near [ Q ] than at part gate opening, where water is discharged with a considerable rotational component of the velocity. This leads to irregular flow at the bend of the draft tube.

### 3.9.3 Choice of speed and setting

The requirements that a turbine shall operate frequently at low loads and yet have only shallow excavation for the draft tube are in conflict. A high-specific-speed turbine with dimensions smaller than normal, with a high cavitation factor, would meet the first requirement, but it would not satisfy the second because a deep setting is required to give the requisite section head. The existing turbine has been shown to have a runner diameter smaller than normal, by the Hill Curves, Warnick (1984). Applying the above information implies that the turbine may be subject to high cavitation although calculations of  $H_s$  using:

$$\sigma = \frac{H_a - H_v - H_s}{H} \tag{3.9. 4}$$

would imply that  $H_s$  may be made greater than the normal relationship.  $H_s$  as given by  $H_s = 4D$ , Brown (1970), but still maintaining a value of  $\sigma$  as given in Figure 3.9. 1 above the critical cavitation factor.

The requirement that best efficiency should be achieved close to or at full load with a turbine of normal specific speed, will lead to the use of a design of runner best suited to a higher head and one which will also be appreciably larger than for normal design. The

full output is required over a range of head varying by more than  $\pm 5\%$  from the design head. The turbine dimensions will increase as the head variation increases.

Where the head water level is almost constant and variations in nett head of less than 10% are created by fluctuations of the tail water level such as occur during floods, full output can generally be obtained without departure from the normal design, other than a small increase in the maximum runaway speed.

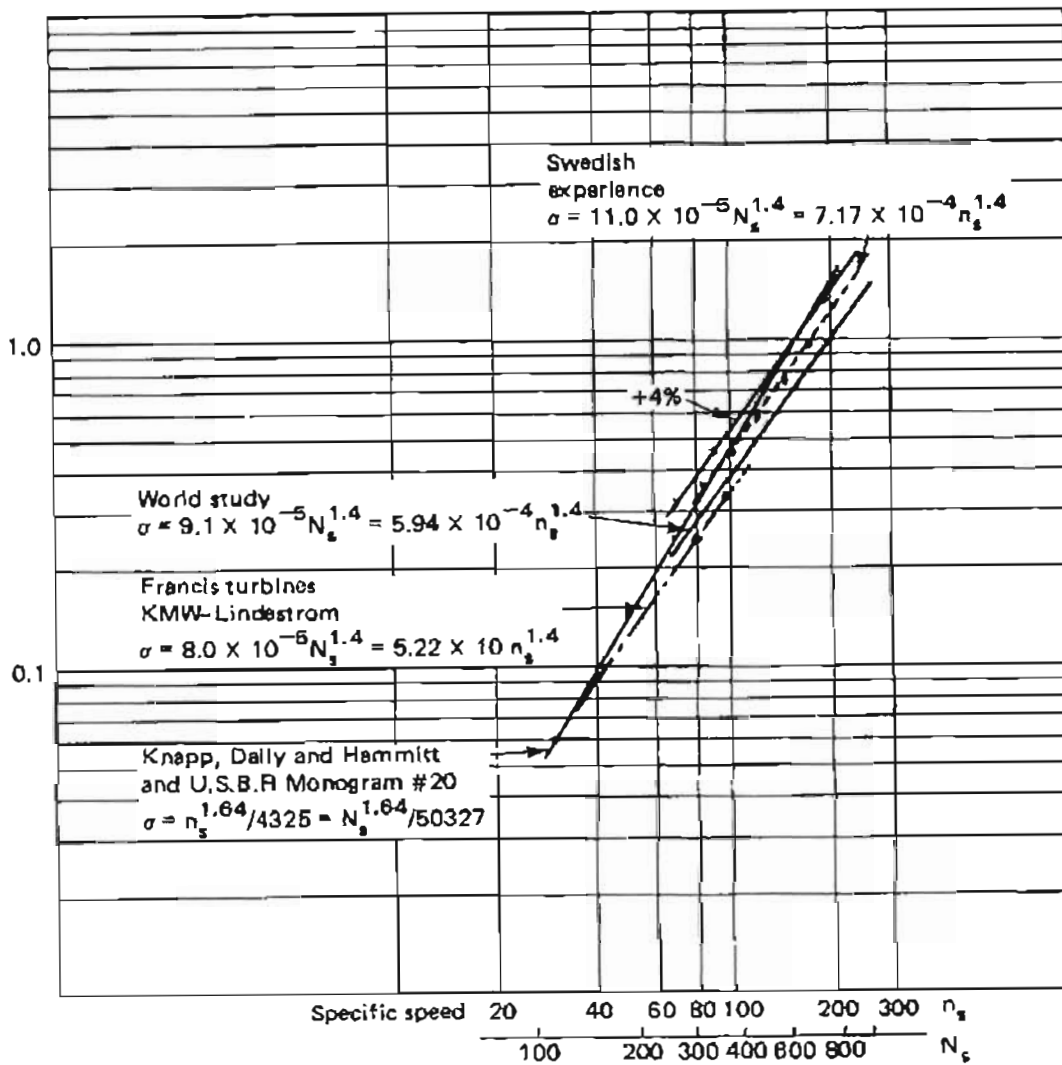


Figure 3.9. 1 Comparison of experience curves for cavitation coefficient, Warnick (1984)

The best efficiency will not be obtained at full load primarily due to the existence of the incorrect runner diameter. Point 1. of the turbine losses also implies that the turbine will be suited to a lower head as was calculated using the Hill Curves, Warnick (1984). Point

2. implies that the turbine dimensions are smaller than normal, meaning that the turbine is suited to operate over a very small head range. Also having a relatively high specific speed, resulting primarily from the rpm, means that the turbine will not experience favourable efficiencies over a range of heads.

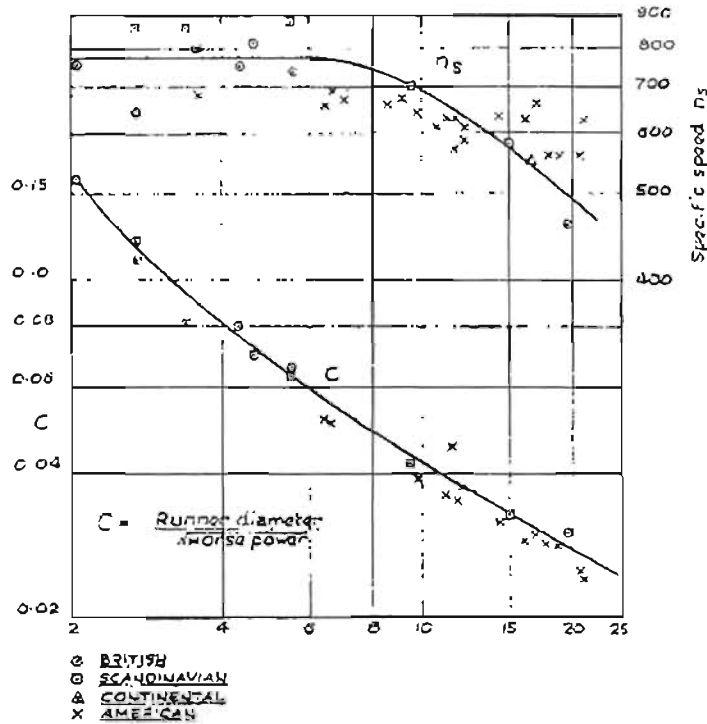


Figure 3.9. 2 Curves of specific speed, head and runner diameter (propeller turbines), Brown (1970)

The difference between preliminary estimates and the final design will be small in most cases, but may be appreciable where unusual requirements must be met. Figure 3.9. 2 gives the specific speed and a constant plotted against head for propeller turbines, Brown (1970).

$$C = \frac{\text{runner } \phi}{\sqrt{\text{horse power}}} \qquad n_s = \frac{n\sqrt{N}}{H^{5/4}} \qquad (3.9. 5)$$

The specific speed varies considerably between different designs for small variations in runner diameter. The estimation of the latter is therefore less liable to inaccuracies than the specific speed.

The head for which full load output is required is used for reading off the constants. It is assumed that this head also corresponds to that at which the best efficiency is required. If these two heads are not the same, an adjustment to the speed as found from the upper curve must be made. For example if full output is required at 25m but best efficiency at 28m, then the speed is increased in the ratio of the square root of the heads.

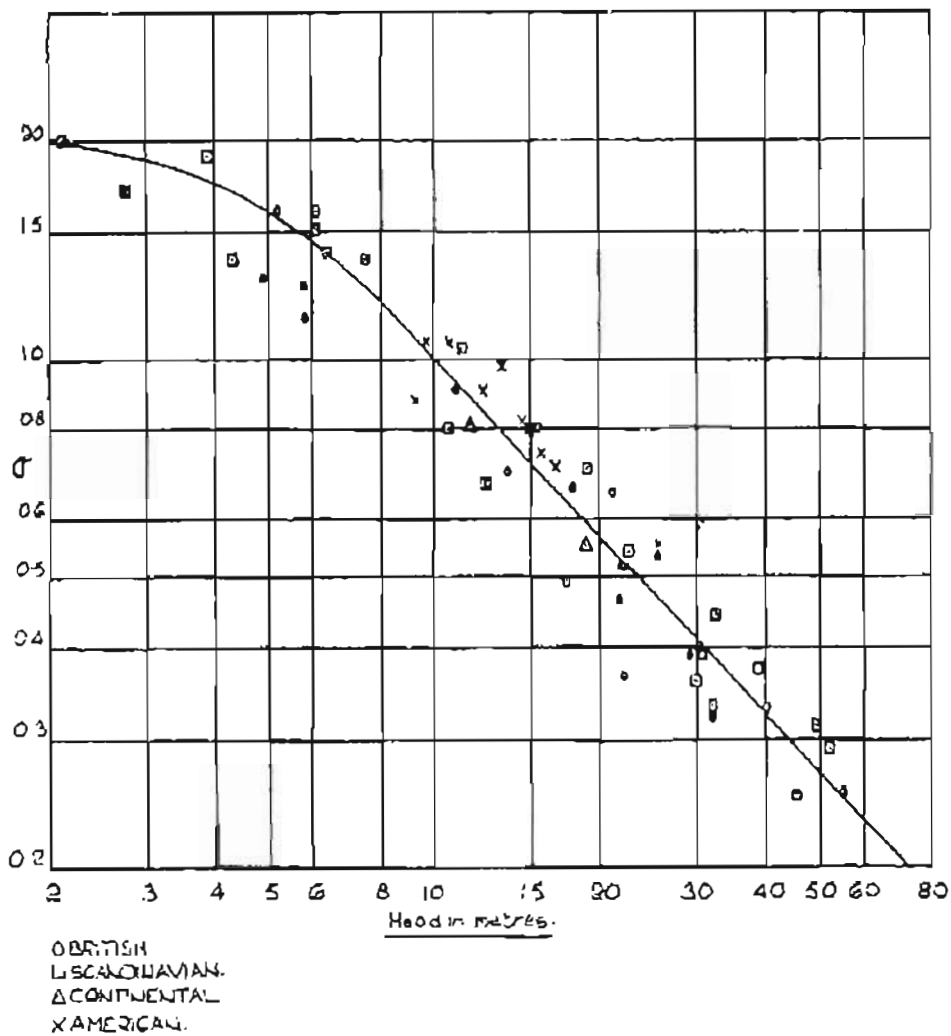


Figure 3.9. 3 Cavitation factor and operating head for Kaplan turbines (for propeller turbines reduce by 8%), Brown (1970)

In most cases, the distance  $H_s$  is a negative quantity and the runner is below tail water level, low-head being a general exception. Figure 3.9. 3 gives the curves of cavitation

factor plotted against head. The suction head,  $H_s$ , is then estimated as follows, Brown (1970):

$$H_s = H_B - (\sigma H + H_v + H_l) \quad (3.9. 6)$$

where:  $H_B$  = barometric pressure at runner elevation

$H_v$  = vapour pressure of water

$H_l$  = height of runner blade leading edge above runner centre line  
 = 0.5D for horizontal shaft units

Applying the above equation with a value of  $\sigma$  obtained from Figure 3.9. 3:

$$\sigma_{10m} = 1.0; \quad \sigma_{12m} = 0.9; \quad \sigma_{14m} = 0.77.$$

$$H_s + \sigma(H_{in} + H_s) = H_B - H_v - H_l$$

$$H_s(\sigma + 1) = H_B - H_v - H_l - \sigma H_{in}$$

$$H_s = \frac{H_B - H_v - H_l - \sigma H_{in}}{(\sigma + 1)}$$

$$= \frac{9.180 - 0.324 - 0.5 \times 0.33656 - \sigma \times 10}{\sigma + 1}$$

$$= \frac{8.688 - 10\sigma}{\sigma + 1}$$

- Therefore:
- 1)  $H_{s10} = -0.656m$
  - 2)  $H_{s12} = -0.164m$
  - 3)  $H_{s14} = 0.558m$

### Hydraulic similarity

A turbine can be operated over a range of heads and speeds, but for each head, there is only one speed at which it has the best efficiency. For a well designed turbine, this speed corresponds to the conditions of smooth entry of water into the revolving runner and to a maximum of losses throughout. Setting the runner speed to 735rpm and defining the blades accordingly will ensure smooth entry of the flow to the runner blades. The problem thereafter lies in the losses and cavitation.

If  $H$  is identified as the head and  $n$  as the rpm, generating velocities  $v$ . If the same turbine is operated at head  $H$ , the direction of the velocities is conserved for the new speed  $n'$ . As

the total energy available has changed from  $H \Rightarrow H'$ , the squares of all the velocities and the friction losses alter in the ratio of the heads. Hydraulic similarity then exists when:

$$\frac{C}{C'} = \frac{W}{W'} = \frac{U}{U'} = \sqrt{\frac{H}{H'}}$$

$$\frac{n}{n'} = \frac{Q}{Q'} = \sqrt{\frac{H}{H'}}$$

$$\frac{P}{P'} = \frac{HQ}{H'Q'} = \frac{H\sqrt{H}}{H'\sqrt{H'}}$$

Which implies that  $\eta_H = \eta_{H'}$  due to the similarity of the losses and congruent angles. If two turbines are considered to be geometrically similar and have runners of diameters  $D$  &  $D^*$  respectively, corresponding dimensions are in the ratio:

$$D/D^*$$

If it is then assumed that the two turbines operate under identical heads, at a certain pair of speeds  $n$  and  $n'$ , the corresponding velocities  $C$  and  $C'$ ,  $W$  and  $W'$  and  $U$  and  $U'$  form identical patterns in direction and magnitude. Because:

$$U = \frac{\pi D n}{60} = U^* = \frac{\pi D^* n^*}{60}$$

the speeds of revolution are in the inverse ratio of the diameters:

$$\frac{n}{n^*} = \frac{D^*}{D}$$

And the discharges are proportional to the areas of the passages, and therefore, in the ratio:

$$\frac{Q}{Q^*} = \left(\frac{D}{D^*}\right)^2 \quad \text{and} \quad \frac{P}{P^*} = \frac{QH}{Q^*H^*} = \left(\frac{D}{D^*}\right)^2$$

### Choice of turbine

The head under which the turbine will operate gives the first indication of the selection of the turbine. Should the head indicate more than one type of turbine, a further selection according to  $n_s$  can be made. The total power to be installed must be known and the number of machines then chosen by economic consideration of load factor, extent of water storage, cost of power house and convenience of operation and maintenance. Once



the output per machine has been decided, information must be obtained concerning suitable speeds for which the generator can be constructed economically.

From this data, specific speed is calculated.

$$n_s = \frac{\text{rpm} \sqrt{P}}{H^{5/4}} \tag{3.9. 7}$$

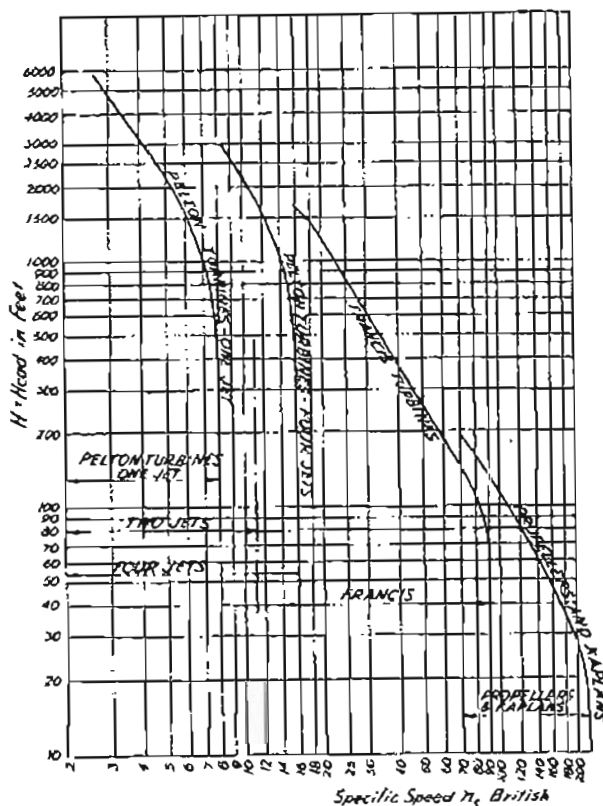


Figure 3.9. 4 Limits of head for various specific speeds, Brown (1970)

The appropriate specific speed is indicated in Figure 3.9. 4, which shows the upper limit of head for each particular turbine family. Should the head exceed this permissible limit, a lower speed or lower output must be adopted to reduce the value of  $n_s$ . When selecting between two potential machines, a wider knowledge of the advantages and disadvantages of each machine is necessary, especially with respect to efficiency when running at part load. This is shown in Figure 3.9. 5.

The purpose of the existing turbine is to pump water at a constant rate. And since the supply head and flow rate are expected to remain constant due to the supply head being piped from a river at a higher elevation, large variations in the loading are not expected. This allows for the design of the turbine to be aimed at the full load capacity with little design allowance for the part load conditions. Such an application is well suited to the propeller turbine also seen in Figure 3.9. 5.

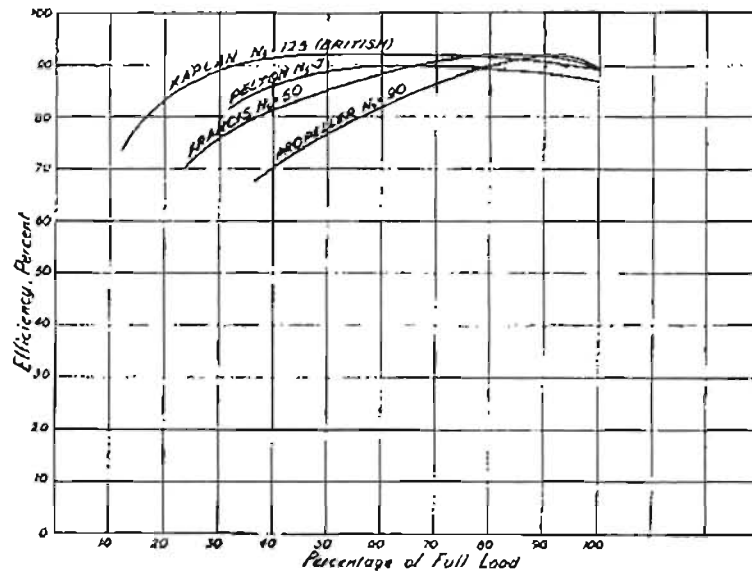


Figure 3.9. 5 Efficiencies at various loads, Brown (1970)

Apart from statistical information from existing turbine installations, the limitations to  $n_s$  fall under various headings:

Mechanical strength: Any one type of turbine of given  $n_s$  is subject to stresses that are proportional to the head under which it operates. In deciding on the use of a given  $n_s$  for a head higher than that of the prototype, the designer faces new problems of mechanical strength. Solving this by increasing thickness results in departure from true geometrical similarity and may affect performance.

Best maximum efficiency: Experience shows that each type of turbine has a narrower best maximum efficiency than generally shown in Figure 3.9. 5. The very large values of  $n_s$  attainable with Kaplan turbines depends on high recovery in the draft tube of the

velocity head and extremely high specific speeds are attainable only at some sacrifice in efficiency.

Reynolds number: It provides a basis for comparing machines according to the nature of the flow through them. When they are geometrically similar but are of different sizes, as defined by the diameter  $D$  and operate under various heads, which affect the velocity  $[v]$  of the water at any given point. Since  $v \propto \sqrt{H}$ , one and the same runner operates at increasing Reynolds Number as the head increases, maintaining hydraulic similarity. For one and the same head, turbines of identical  $n_s$  of typically larger diameter may be required to work at higher Reynolds Number's and may then show unexpected vibrations that could cause eddies.

Setting: In order to ensure satisfactory operation reaction turbines of given  $n_s$  require a lower setting of the turbine in relation to the tailwater level when the head  $[H]$  increases. This may result in such deep excavation that the cost of it may well absorb any saving in the machines arising from a higher speed. Also vibrations at part load due to the phenomenon shown in Figure 3.9. 6 become more severe due to the higher energy rejected into the draft tube.

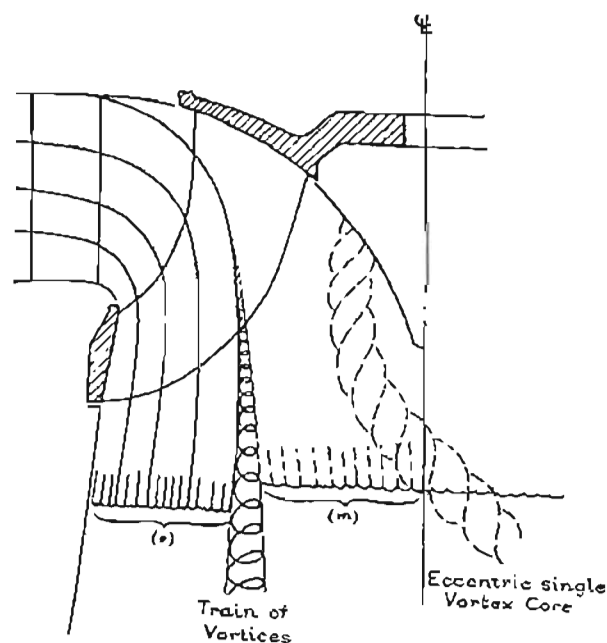


Figure 3.9. 6 Typical flow in runner and draft tube at part-gate, Brown (1970)

Turbine setting and Cavitation

Any turbine that is geometrically similar and operates under similar hydraulic conditions has the same value of  $\sigma_c$ . With a different design or proportions  $\sigma_c$  will generally be different. As can be expected, the specific speed had a great influence on the initial  $\sigma$ , as may be seen in the following considerations:

The exit diameter of all reaction turbines is related to the speed by, Brown (1970):

$$\frac{D_2^3 n}{Q^2} \cong const. \tag{3.9. 8}$$

From this it is possible to calculate the dynamic suction, Brown (1970):

$$\eta_D \frac{C_2^2}{2gh} \cong 3.6 \times 10^{-4} (n_s)^{4/3} \tag{3.9. 9}$$

Figure 3.9. 7 shows the function of  $n_s$ . From experimental data, safe values of the depression at the back of the vane are given by the relationship, Brown (1970):

$$\frac{kW_2^2}{2gH} \cong 4.0 \times 10^{-6} (n_s)^{7/3} \tag{3.9. 10}$$

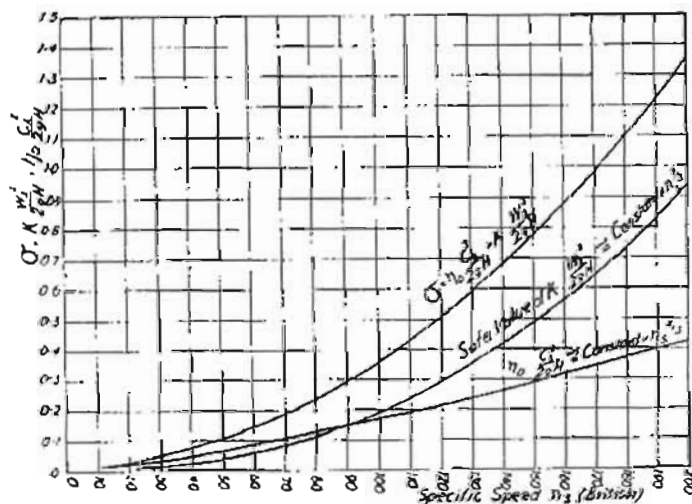


Figure 3.9. 7  $\sigma$  as a function of specific speed ( $N_s$ ) , Brown (1970)

Values of the quantity have been shown in Figure 3.9. 7 in order to give the curve of permissible  $\sigma$ . It can be seen how rapidly  $\sigma$  increases with  $n_s$ , and thus correspondingly its importance at large specific speeds.

It must be remembered that the coefficient  $[k]$  depends to a great extent upon each particular design of turbine, namely the specific loading on the runner blades, their curvatures and the ratio of chord to pitch. The curve of  $\sigma$  in Figure 3.9. 7 represents actual installation values for the lowest tailwater level with some small margin of safety over the critical sigma  $[\sigma_{cr}]$ , as determined from model tests. By plotting the efficiency, discharge and output under unit head at constant speed, against  $((H_B - H_S)/H)$ , the point of discontinuity is made apparent.

#### 3.9.4 Selection of the turbine setting

As has been discussed, determining the turbine setting is based primarily on defining the plant sigma and choosing the vertical distance from the minimum, full load tailwater level to the critical part of the runner, which differs for the orientation of the turbine. The  $[\sigma]$  should be referred to some specific point on the runner and may have  $[K_s]$  assigned as an elevation position in some literature. For horizontal axis turbines, a point near the tip of the runner blade is used because the pitting damage is typically a function of time and the most critical position is only exposed instantaneously during each revolution.

In spite of the availability of these theoretical results, the final turbine selection should rather be based on model test results. Since these are not available for the turbine, the estimates made will be assumed suitable for operation, but with the expectation of a necessity to change the draft tube parameters, such as the length and final diameter.

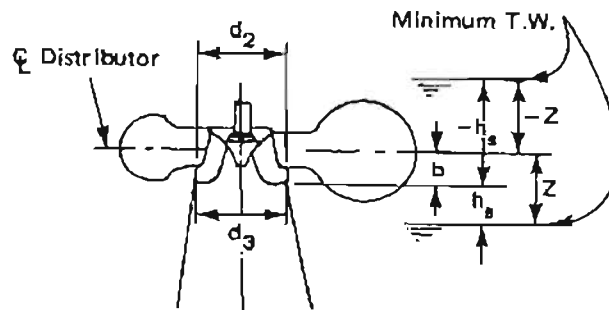
The curve shown in Figure 2.4.8 relates the acceptable plant sigma to the specific speed and thus using the homologous nature of turbines to indicate that turbines having geometrically similar design and operating under similar hydraulic conditions will have the same value of sigma. This experience curve has been plotted to place the turbine 0.3m lower than the elevation at which the cavitation damage occurs and loss of performance has approached unacceptable values. This so provides a limited margin of safety to allow for variation in the atmospheric pressure and minor variations in the runner characteristics.

Considering Eq.(3.9. 4), it is possible to proceed with the determination of the turbine setting elevation. However, another experience curve is necessary to relate the turbine setting elevation,  $H_s$  to the centreline of the turbine distributor. Using the definition of  $h_s$  as shown in Figure 3.9. 8 and the following equations, Warnick (1984):

$$h_s = h_b - \sigma h_{cr} \quad (3.9. 11)$$

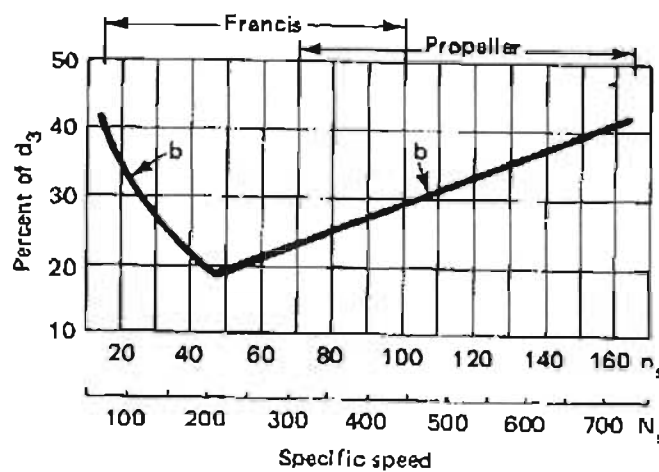
$$z = h_s + b \quad (3.9. 12)$$

$$h_b = h_o - h_v \quad (3.9. 13)$$



- $h_{cr}$  = Critical head in ft or m
- $h_s$  = Distance from  $d_2$  to minimum T.W. in ft or m
- $h_b = h_o - \sigma h_{cr}$  ft or m
- $Z$  =  $\phi$  distributor to minimum T.W. ft or m
- $Z = h_s + b$  = Total draft head
- $d_2$  = Least diameter through shroud in ft or m
- $d_3$  = Discharge diameter of runner in ft or m
- $b$  = Distance from  $d_2$  to  $\phi$  of distributor in ft or in m

(a)



(b)

Figure 3.9. 8 Experience curve for recommending total draft head, Warnick (1984)

### 3.9.5 Manufacturing procedures

One company provides a useful approach for preliminary planning which is more a rule of thumb approach; that the submergence of the unit centreline, Warnick (1984) should be:

$$z = -kD \quad (3.9. 14)$$

The manufacturing companies' all caution that the final design and the decision for setting elevation, together with the assignment for an admissible value of sigma,  $\sigma_{adm}$ , should be carried out by the manufacturer because the manufacturer must be responsible for the guarantee for cavitation performance.

The common design procedure at yet another company is to choose a setting lower by a safety margin according to the estimate of, Warnick (1984):

$$|\Delta H_s| = \Delta \sigma H \quad (3.9. 15)$$

This mathematical check is made in addition to the determination of  $H_s$  according to the inception of cavitation indicated by model tests. Such a precaution is to ensure that the prototype turbine will be largely cavitation free. The safety margin  $|\Delta H_s|$  is chosen to compensate for uncertainty resulting from inaccuracies in manufacturing. The amount of  $|\Delta H_s|$  is chosen with consideration of the turbine speed and the rated and operating heads. The company recommended that a value of  $\Delta \sigma = 0.1$  for low specific speed turbines and a  $\Delta \sigma = 0.2$  for high specific speed turbines be used.

Applying the information as given in turbine setting:

$$\sigma = \frac{H_a - H_v - H_s}{H}$$

where:  $H_a = 10.351$  at 0m altitude; 9.180 at 1000m altitude

$H_v = 0.174\text{m}$  at 15°C; 0.239m at 20°C; 0.324m at 25°C

$$H = H_{net} = \frac{P_s}{\rho g} + \frac{V_1^2}{2g} + H_s - \frac{V_E^2}{2g} = 10 + H_s - \frac{V_E^2}{2g}$$

$$V_E = \frac{Q}{A}$$

$$A = \frac{\pi}{4} D_4^2$$

$$D_4 = D_3 + 2 \times H_s \times \tan\left(\frac{\alpha}{2}\right)$$

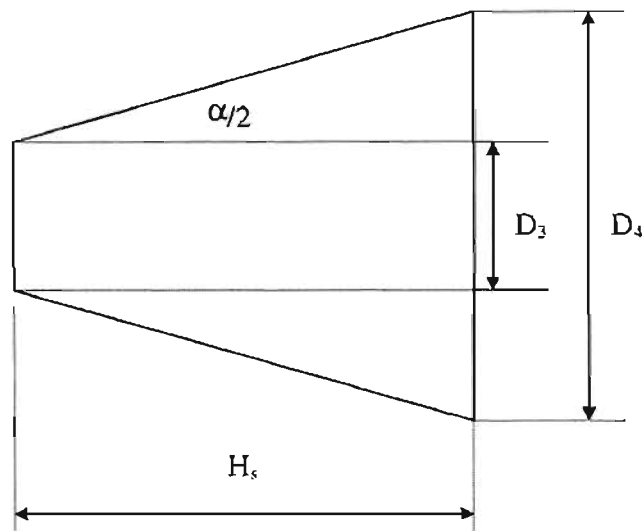


Figure 3.9. 9 Diffuser design

The value of  $\sigma$  so determined is then limited by the plant sigma as given in Figure 3.9. 1:

$$N_s = \frac{N\sqrt{P}}{H_{net}^{5/4}} = \frac{735\sqrt{40}}{11^{5/4}} = 232$$

The graph of  $\sigma$  versus  $N_s$  is then reviewed and it is found that  $\sigma$  does not go below 0.7. This graph is misleading in the sense that the value of  $\sigma$  does not apply as it would for length  $H_s$ , but rather it applies at the turbine outlet / draft tube inlet at the corresponding value of  $H_s$ .  $H_s$  was then increased to 2m and the process repeated until such time that  $\sigma \approx 0.1866$ , its limiting value for a turbine of  $N_s = 232$ . The final value of  $H_s$  was 5.8, with an associated  $\sigma$  of 0.1934.



This causes a corresponding change in  $H_{net}$  and hence the available hydraulic power becomes:

$$P = Q\Delta P = \dot{m}gH_{NETT} = 0.5 \times 9810 \times 15.8 = 77.5 \text{ kW}$$

And recalculating the specific speed where  $\eta_{OA} = 0.855$ :

$$N_s = \frac{735 \sqrt{77.5 \times 0.855}}{15.8^{3/4}} = 190$$

For a specific speed of  $N_s = 190$ , the corresponding limiting  $\sigma = 0.108$  and the true  $\sigma$  is:

$$\sigma = 9.1 \times 10^{-5} \times N_s^{1.4} = 0.1409$$

Hence the cavitation parameter remains within acceptable limits. Applying the "safety factor", Warnick (1984), and assuming a low specific speed:

$$|\Delta H_s| = \Delta \sigma H \quad \Rightarrow \quad \Delta H_s = 1.58$$

And  $H_s$  is reduced by 1.58 to 4.22m, which implies that the final  $H_{net} = 14.22\text{m}$

Reapplying the Hill Curves, Warnick (1984), from Figure 2.4.2:

$$P_{\omega} = \frac{P}{\rho \omega^3 D^5} = 0.0032 \quad E_{\omega} = \frac{gH}{(\omega D)^2} = 0.06 \quad Q_{\omega} = \frac{Q}{\omega D^3} = 0.058$$

with  $H$  fixed at 14.22m and  $D$  fixed at 0.33656m the angular rotation is given by:

$$\omega = \sqrt{\frac{gH}{E_{\omega} D^2}} = \sqrt{\frac{9.81 \times 14.22}{0.06 \times 0.33656^2}} = 143.3 \text{ rads}^{-1}$$

for the most efficient use of energy for the energy coefficient.

For the calculation of the power coefficient, the most efficient angular velocity would be:

$$P = Q\Delta P = \dot{m}gH_{NETT} = 0.5 \times 9810 \times 14.22 = 69.75 \text{ kW}$$

$$\omega = \sqrt[3]{\frac{P}{\rho P_{\omega} D^5}} = \sqrt[3]{\frac{69749}{1000 \times 0.0032 \times 0.33656^5}} = 171.54 \text{ rads}^{-1}$$

And for the flow coefficient, the most efficient angular velocity is:

$$\omega = \frac{Q}{Q_{\omega} D^3} = \frac{0.5}{0.058 \times 0.33656^3} = 226.1 \text{ rads}^{-1}$$

Any angular velocity exceeding  $735\text{rpm} \equiv 77\text{rads}^{-1}$  is typically too high when compared to the conventionally designed turbine and it is likely that cavitation may develop due to the high rotor exit velocities. Typical examples of Kaplan turbines show rotational speeds in the region of  $173\text{rpm}$ , which is much lower than that determined for the propeller turbine.

**Table 3.1: Typical turbine parameters**

	Head [m]	Power [kW]	$\varnothing_{\text{run}}$ [m]	$Q$ [ $\text{m}^3\text{s}^{-1}$ ]	$\omega(P_{\text{ax}})$ [ $\text{rads}^{-1}$ ]	$\omega(Q_{\text{ax}})$ [ $\text{rads}^{-1}$ ]	$\omega(E_{\text{ax}})$ [ $\text{rads}^{-1}$ ]
1	10	200	0.560	2.3	70.87	225.8	72.2
2	7	1500	2	25	24	53.9	16.9
3	5	450	1.4	10	29	62	20
4	6	150	0.710	2.9	63	139	44

**Table 3.2: Typical Kaplan turbine values**

	Power [MW]	Head [m]	Speed [rpm]	Max. $\varnothing_{\text{runner}}$ [m]	$P_{\text{ax}}$
1	20.9	37.5	214.3	3.25	0.005
2	3.16	5.35	125	3.6	0.0023
3	18	16.15	125	4.88	0.0029
4	5.6	21.0	250	2.44	0.0036
5	26	29.25	166.7	4.29	0.0034
6	31.5	30.5	166.7	4.35	0.003

From Table 3.1 and Table 3.2 it is possible to determine that the smaller diameter turbines have the higher angular velocities and higher heads. Hence it can be assumed that the power is obtained from high velocities within the stator and rotor for the smaller turbines and power for the larger turbines is obtained from the volumetric flow. Typically then, the design of the smaller turbine would be according to the power and energy coefficients and the design of the larger diameter turbines would focus more on the flow coefficient efficiency.

## 3.10 Manufacturing the master patterns

### 3.10.1 Defining the blade

The manufacture of the master blade pattern began with a turbine blade generating program which calculated the points on the surface of the blade from several initial condition parameters related to the size of the piping and headstock and the flow rate and pressure difference across the turbine. The points were then converted for use by the manufacturer.

The first potential manufacturing process that could be used to develop the blades is that of CNC machining. It was first proposed that the cutting tool path would have to run the length of the blade since the increment length along the blade is larger than that for the chord-wise increments. The ridges generated by the chord-wise increments should ideally run parallel to the fluid flow direction and avoid causing a turbulent boundary layer as would be promoted by the span-wise ridges. However, due to the required narrow radius of the ball-nose cutter, too many extra would be required to cut the blade.

This would increase both data entry and machining time. The surface that is finished by span-wise milling will therefore require a finishing process to minimise the ridging and resultant turbulent boundary layer formation. After exhaustive research into the feasibility of machining the turbine blades using a three axis TNC Maho milling machine, it was concluded that it was not possible. The machine was not sufficiently versatile to cut in three-dimensional space due to the limitation on the number of controlled axes.

Another manufacturing option was considered which involved the spark erosion process. This typically requires a “profile” at the top and bottom of the billet from which the object is to be cut. These points are then joined by a straight line, the wire, which is then capable of tracing the independent patterns on the two separate surfaces. The problem with this process is the straight line joining the two profiles. Furthermore, the joining of the two points needed to be within a certain angle limit and a quick manipulation of the

program results revealed that this criteria was not met either. This was not true of the curvature of the blade caused by the twist of the profiles about the 30% stacking point. The process would have caused gross error in the shape of the blade.

### **3.10.2 Profile fabrication**

The program output format of the co-ordinates was then changed to suit a number of planes in the z-axis, the spacing of which was determined by the thickness of the supawood which was in turn determined from the degree of resolution required to produce accurate results. The resolution proved to be a function of the radius of the profile, each [x y] point was dependant upon a z value, and the angle of the blade relative to the axis of rotation. This would be the equivalent of converting from cylindrical co-ordinates to Cartesian co-ordinates. High resolution was obtained by using a combination of linear interpolation and projection. It was endeavoured to use points that were as close together as possible to perform the interpolation since the points were on a curve defined by the twist of the blade and were therefore not linearly related.

The profiles were then placed next to each other with a constant spacing on a single sheet. The profiles would then be cut out of the single piece of supawood with a second cut, producing the blocks containing the profiles. The reason for this is that the design would allow the profiles to be stacked one on top of the other using the sizing of the profile blocks to locate the [x y] co-ordinates of the blade.

The problem with this method is that it provided the artisan with a negative of the master pattern, which did not prove to be conducive to the remaining stages of production. It was decided that it would be more appropriate to develop a positive master pattern from which the wax patterns could be developed. A major problem encountered in this decision was in the stacking of the profile patterns. Each pattern had to be located with respect to a single point on the profile and it became the task of the artisan to accurately align each profile with the angle associated with its z-displacement. Once this had been achieved, the profiles were glued together.

### 3.10.3 Producing a master pattern

The stage to follow covered the finalisation of the master blade pattern. This began with filling the gaps of the profiles with body filler. Once it had dried, the body filler and some of the profile were sanded down to get a master pattern shaped as closely as possible to the computer generated model. These patterns were then prepared for the production of the wax patterns, adding a dovetail, reservoir and sprues for the wax moulding process.

Once the blade shape had been completed it was necessary to determine what method was going to be used to attach the blades to the central hub. The initial consideration was to use dove-tailed slots that would slide into the hub for both the rotor and the stator. Two problems experienced with this design method were the limitation of space on the inner radius of the hub caused by the width of the dovetail and the second problem being the resultant lack of rigidity for the stator blades. The solution to these problems was a combination of reducing the size of the dovetail to allow a greater cross-sectional area between the dovetail slots on the hub and adding a “support ring” on the outer radius of the blades.

Further points that are necessary to take into consideration when defining the size of the dovetail slots:

- The space limitation on the hub was partially solved by swapping the roles of the “hub ring” and “outer ring”
- The space limitation at the hub needed to be compared to the tangential displacement of the blade camber to check interference
- It was not required for a limitation to be placed on the blades to prevent displacement in an upstream direction. Although the force was not purely axial, it did not cause the blades to move. However, a taper will be required for streamlining and will thus be used in a dual purpose as a preventative measure for the purpose of fluid flow.

The steps to follow were for the development of the wax patterns and required that two separate moulds were made for the rotor and stator blades master patterns. These moulds were fabricated from silicon rubber, by pouring fluid silicon into a coffer dam containing

firstly the rotor and then the stator blade and then allowing it to dry. The rubber was matched to the temperature tolerance of the wax that was to be used for moulding. The wax was then heated in a separate container and poured into the cavity. A sufficient number of waxes for both the rotor and stator were made plus two additional blades of each, in case of mistakes.

#### **3.10.4 The blades**

Once having made the wax patterns, the decision as to how they were going to be converted from waxes to moulds was investigated. The options that were available included sending the wax patterns out for production, developing the patterns into water or alcohol based shell-type investment, or to find another investment that required less in terms of time and cost. Eventually, the decision made was based on cost and the remaining option was to purchase jewellery investment due to the reduced units of capacity in which it was sold relative to the amount required. The details of the investment process are included in the appendix under manufacturing procedure for additional information.

The casting process was then attempted. It was initially intended that the blades be cast by an external company, but due to cost limitations, the blades were to be cast in house. The first casting operation made use of the conduction furnaces, neither of which were large enough to heat both the casting and the crucible containing the bronze billets. Hence two furnaces were used to heat the crucible and the casting, which was more suitable considering that they required different heating cycles.

The heating cycle of the castings in order to remove the wax is provided in the appendix, but the period extended over some 10 hours in order to get the castings up to the pouring temperature. Considering that it took the furnace approximately the same time to heat to its maximum temperature, the process could not have been achieved much more quickly

Due to overshoot error on the controller, the furnace exceeded its temperature tolerance and burnt out. The furnace that was run in parallel was not capable of the required

maximum temperature and it was intended to be used for pre-heating the crucible. The entire operation being dependent on the main furnace was then abandoned when it failed.

The remaining option was to utilise the induction furnace. Before the operation was accepted, some concern was expressed as to the potential capacity of the furnace, since it only provided for small volumes. However the induction furnace promised to have a higher performance in terms of speed of heating. Another potential problem area of the induction furnace is that it does not have an automated controller. Any control process would have to be done manually and the castings require that they be heated slowly to prevent temperature cracks. There is also the risk of the fluid solidifying on contact with the surface should the castings not be heated to the correct temperature. This solidification could adversely affect the surface tolerance of the blades and cause problems with the flow dynamics.

## CHAPTER 4

### PROGRAMMING FOR BLADE DESIGN

#### 4.1 The governing equations

The program for developing the blade angles for the rotor and stator is based on the free vortex design. The program firstly determines the diameters that would yield constant areas per segment for a predetermined number of segments, then the blade velocity at the mid-span of each. Once the tangential component of the absolute velocity of each segment through the stator had been determined, it was possible to determine the relevant blade angles, as shown in Figure 4. 1.

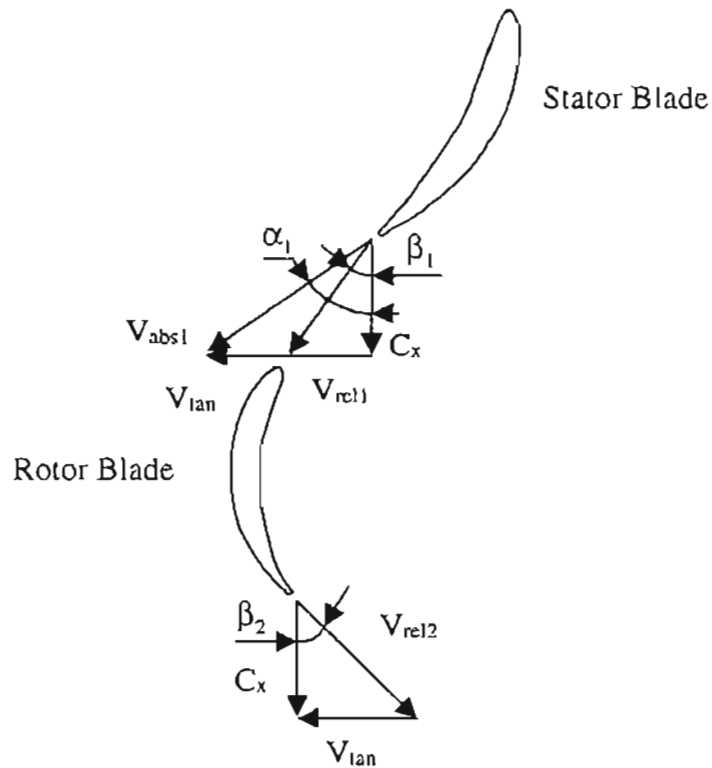


Figure 4. 1 Velocity triangles

The equations used to set up the blade angles and velocity distributions are shown below:

$$\text{Free vortex: } qr = \text{const.} \quad (4. 1)$$

$$\text{Power: } P = \rho A_{\text{each}} C_x U_b \Delta C_w \quad (4. 2)$$



$$\text{Angles:} \quad \alpha_1 = a \tan\left(\frac{C_{w_1}}{C_x}\right) \quad (4.3)$$

$$\beta_1 = a \tan\left(\frac{C_{w_1} - U_b}{C_x}\right) \quad (4.4)$$

$$\beta_2 = a \tan\left(\frac{U_b}{C_x}\right) \quad (4.5)$$

$$\text{Velocities:} \quad C_{w_1} = C_x \tan(\alpha_1) \quad (4.6)$$

$$U_b = \frac{\pi d \text{ rpm}}{60} \quad (4.7)$$

$$\text{Assume:} \quad C_{w_2} = 0$$

It is necessary at this point to remind the reader that segmenting the blade requires that each calculation that is performed for the forthcoming blade shape design will need to be applied to each section. Such design characteristics are easily accounted for in software that works with matrices.

Once the blade angles have been determined they are then used to generate the required camber of the profile. At this point, it is necessary to consider the design of the blade shape.

#### 4.2 Program structure

The aim of the program was to produce outputs of graphs and text files from which the blade shape may be taken. The outputs were to be derived directly from the initial conditions taken from an existing river, such as values of pressure head, volumetric flow rate and flow rate. However, some knowledge of turbines is required to convert these conditions into turbine related dimensions.

The next problem was to define the length of the stator chord as a function of the stator outlet angle,  $\alpha_1$ , and the axial chord, which in the final analysis was taken as a constant

value. Recall that the stator outlet angle remains a function of the radius of the mid-span of the segment.

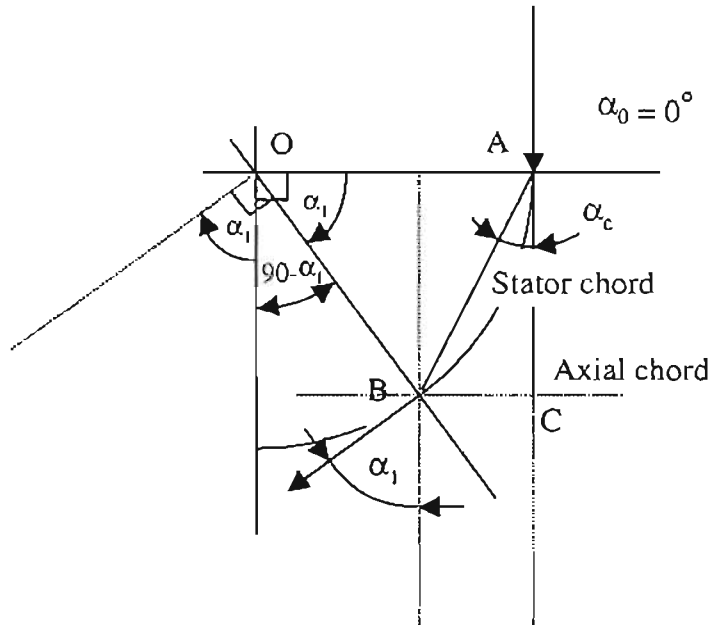


Figure 4. 2 Determining the stator arc length from the inlet and outlet angles

$$180 = 90 + \frac{\alpha}{2} + \angle OAB = 90 + \frac{\alpha}{2} + (90 - \alpha)$$

$$\angle OAC = 90 = \angle OAB + \alpha_c$$

$$\alpha_c = 90 - \angle OAB = 90 - \left(90 - \frac{\alpha}{2}\right) = \frac{\alpha}{2}$$

This now allows for the calculation of the angle at which the stator chord will be positioned, and knowing that the chord length is set at a constant length, the profile shape of the blade may follow. It is also necessary to stack the blade profiles about a certain point and this will be 30% of the arc length. The 30% value is typical of hydrodynamic flow about a profile, since the stacking point is typically aligned with the pitching moment of the profile to reduce the stress on the blade caused by the moment.

This process is repeated below for the rotor blade design, also with the pre-determined chord length. However, the process is slightly more complicated by the value of the entrant angle,  $V_1$ , not being equal to zero. The calculation of the chord was then divided up into two vectors as shown in Figure 4. 3, the angles  $\beta_1$  and  $\beta_2$  determined from the inlet angles. The calculation for determining the value of the 30% stacking point as mentioned for the stator was also performed for the rotor.

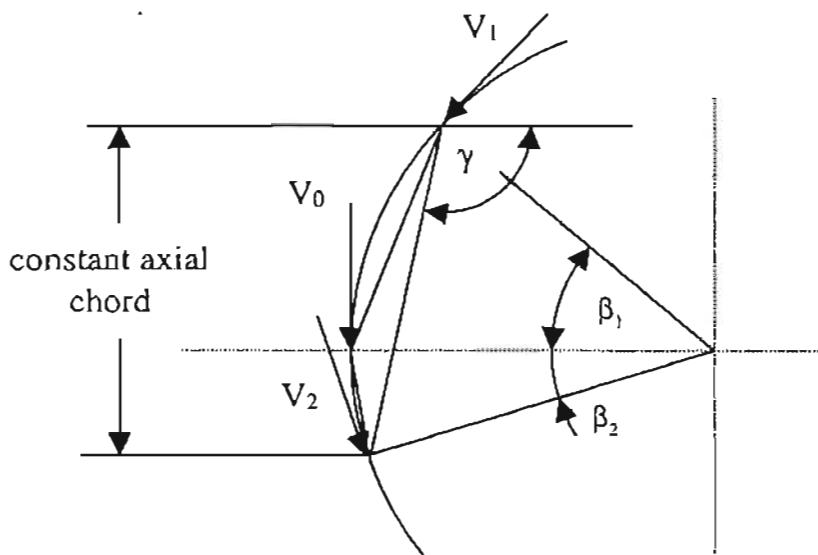


**Figure 4. 3 Determining the rotor arc length from the inlet and outlet angles**

The section of program for the blade design was adjusted from being simply dependent on the chord length to being a constant. The reason for this was that the blade was becoming increasingly thicker at the tip in comparison to the hub because of the dependency of the profile thickness on the chord radius. The chord radius is a function of the turning angle of the blade, which decreases with increasing radius for a free vortex design.

The two variables that effect the design in this instance are the dependency of the thickness on the axial chord and whether  $(t/c)$  is a function of the chord. The examples shown below express the difference in the solidity for the different cases:

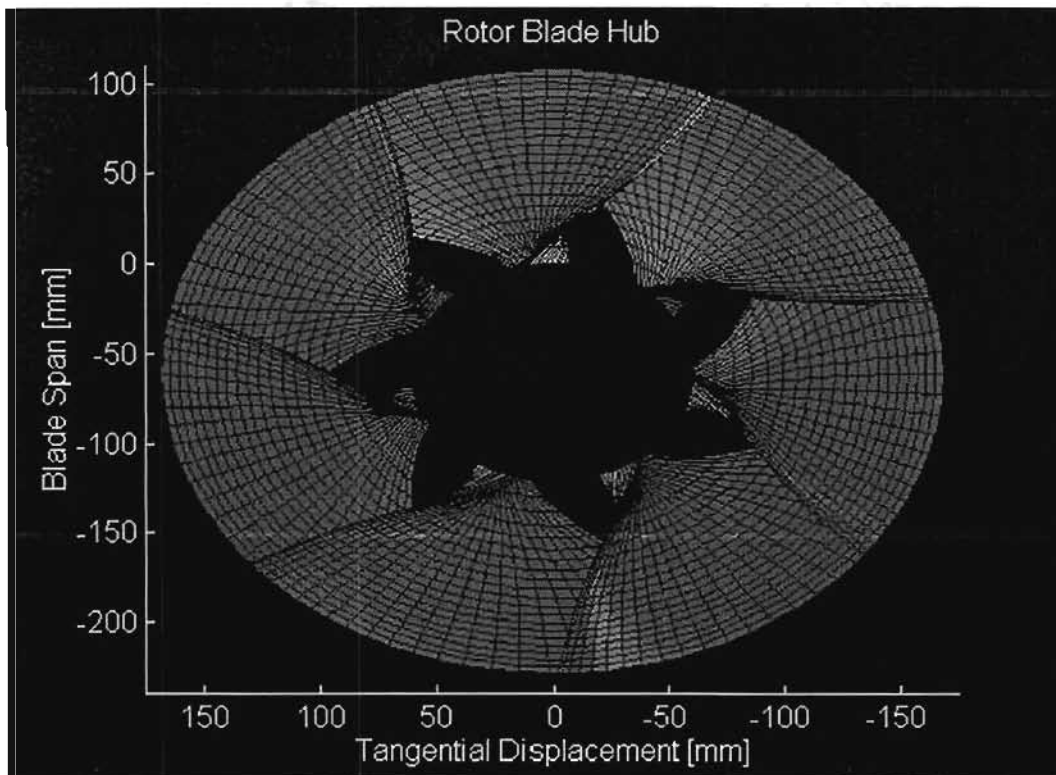


**Figure 4. 4 Rotor Hub for case 1**

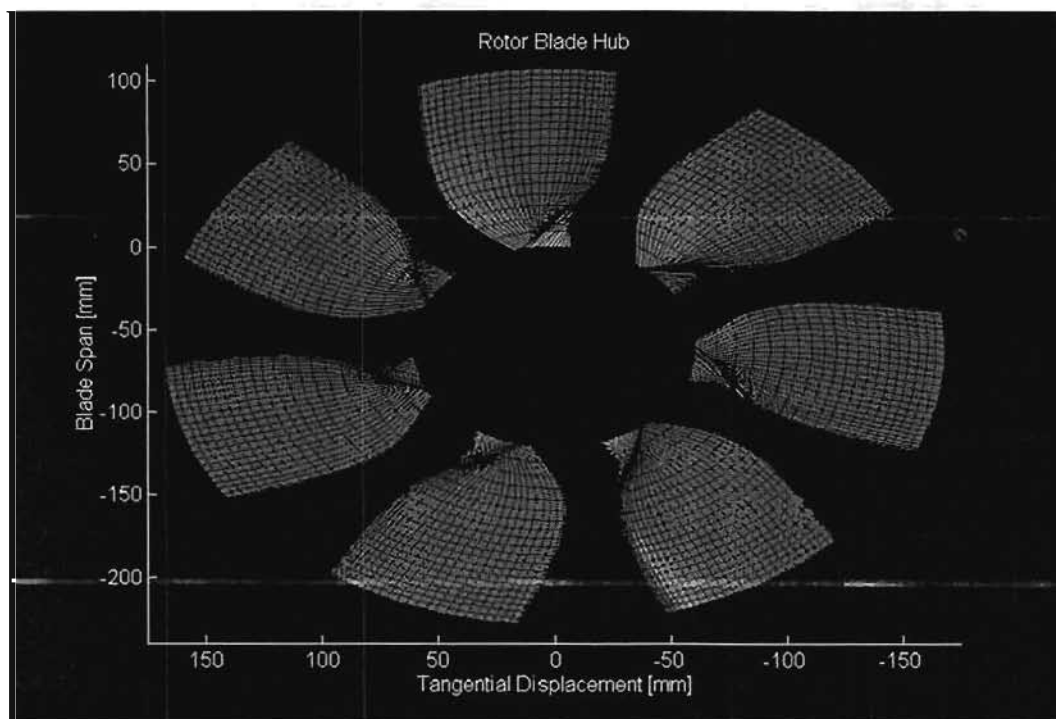


**Figure 4. 5 Rotor hub for case 2**

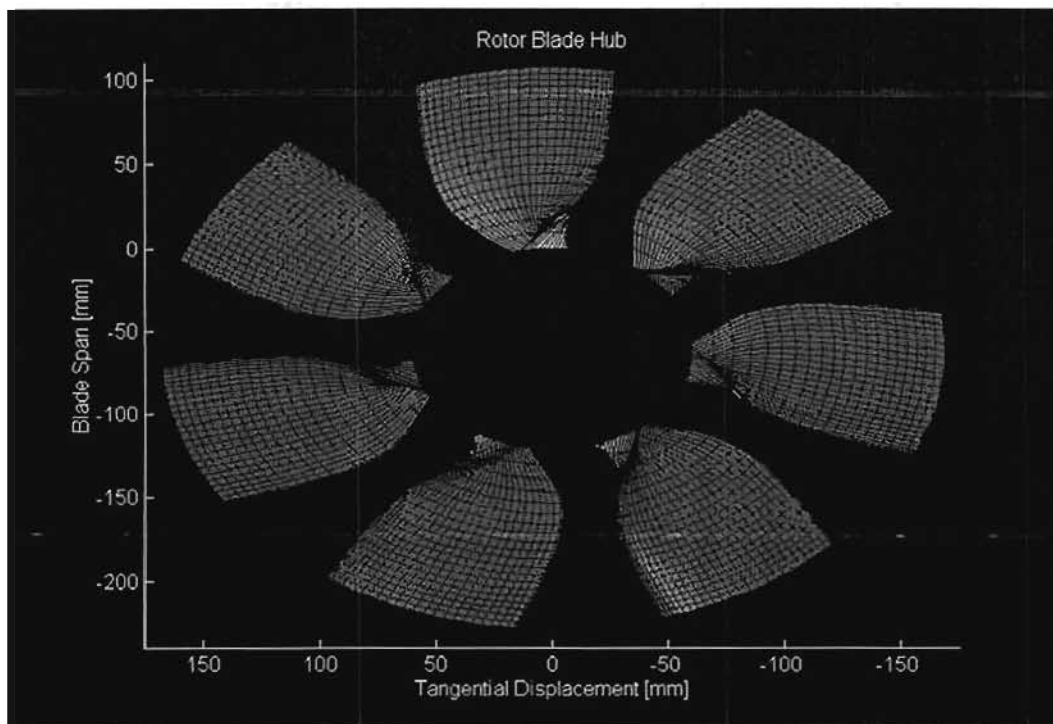


**Figure 4. 6 Rotor hub for case 3**

\* Note that the number of blades shown is not an indication of the number of blades used in either the stator or rotor. The number was chosen simply to display the difference in the solidities of the various designs.

- 1) variable chord  
 $t / c = t / c$  ( arc radius )  
 @ 1115 rpm,  $C_x = 7.142 \text{ ms}^{-1}$ ,  $\alpha_{01} = 60^\circ$
- 2) constant chord  
 $t / c = t / c$  ( arc radius )  
 @ 1115 rpm,  $C_x = 7.142 \text{ ms}^{-1}$ ,  $\alpha_{01} = 60^\circ$
- 3) constant chord  
 $t / c = t / c$  ( chord )  
 @ 1115 rpm,  $C_x = 7.142 \text{ ms}^{-1}$ ,  $\alpha_{01} = 60^\circ$

There is no significant visible difference in the blade shape between cases 2 and 3, but there is a small difference in the thickness of the blade affecting the profile performance.

The final selection of setting the chord length to a constant and having the profile thickness as a function of this chord rather than that of the arc length was determined more from a practical materials design theory in preference to fluid dynamic theory. Although the latter remains satisfied since the importance of small variations in the maximum thickness are not considered to have an effect on the performance as significant as the radius of the circular arc for example.

### 4.3 Profile Selection

Once the circular arcs for each segment had been generated, it was necessary to find a profile shape that most suited the purpose of hydrodynamics. Research into the most suitable profile shape revealed that the maximum thickness of the profile was to be at 40% of the chord. A search for a collection of profiles on the Internet and in books was then initiated. It was not expected that it would be possible to find a collection of profiles that would suit the exact purpose of the turbine blades, because each shape was a function of a variable segment radius. The default option was then to select a profile that most closely matched the requirements and then to form it to match the inlet and outlet angles established in the first programming segment. An option that would prove to be the most universal in its selection was the symmetrical profile.

Once the profile had been selected from a collection of profiles downloaded from an internet site, <http://aerolab>, it had to be multiplied by a length vector to suit the length of the circular arc because each arc had a different length and it was necessary to conserve the length of the chord.

The velocity distribution of each segment according to a free vortex distribution meant that the circular arc length increased with an increase in the radius of the segment from the hub. Once the unitary length profile had been multiplied by the circular arc length, the thickness of the profile increased with an increase in radius from the hub. This is poor design from a structural viewpoint and was expected to lead to failure.

The solution was to multiply the profile shape by a pre-determined length, such that the thickness distribution did not remain constant, rather the value of the maximum thickness

was retained as the constant. This yielded a blade shape that had a constant maximum thickness along its length. The rounded edge is likely to be the cause of boundary layer separation at the tail, and may cause flow turbulence for the rotor blades, which typically results in inefficiency.

Furthermore, it was necessary to modify the tail of the profile for the purpose of machining or manufacture. The tapered edge of the tail was decidedly too thin to be machinable and it was proposed that it would just fold during the machining process. However, should the blades be cast, the thin edge may be a target area for air bubbles during casting and such a thin taper would bend during service. The tail of the profile was therefore rounded off to a suitable radius.

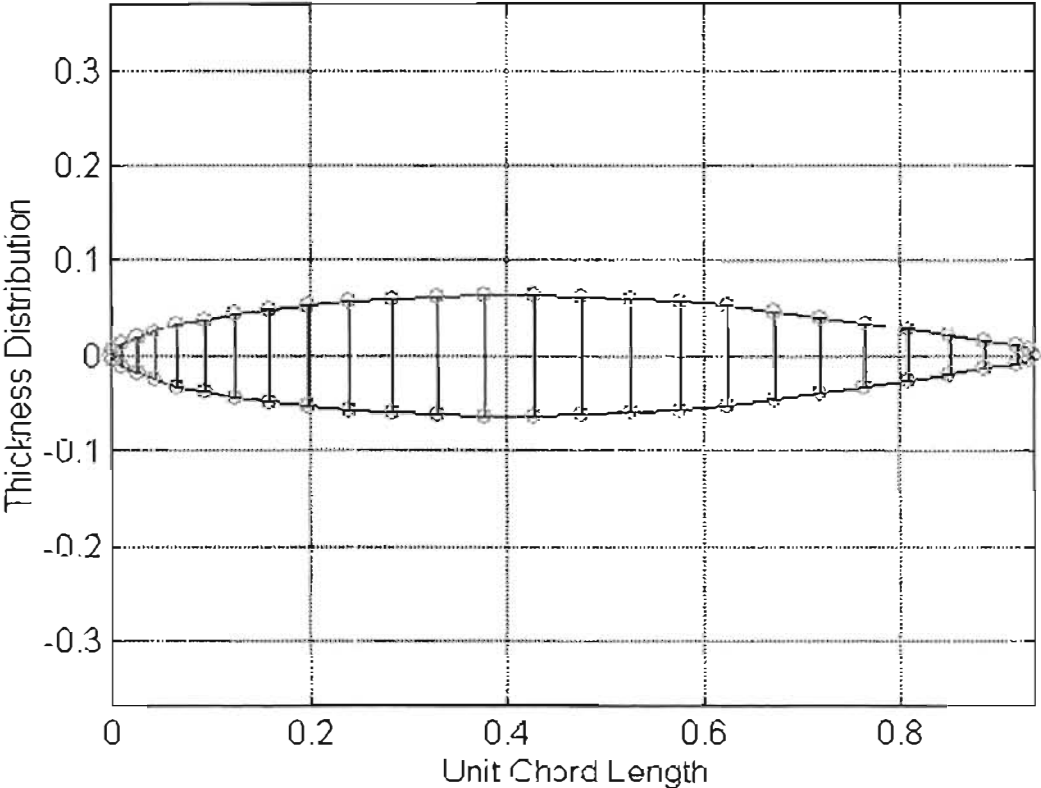


Figure 4. 7 The ribbing of the symmetric profile

Figure 4. 7 illustrates the initial blade from which the profile was adapted. This blade shape includes the changes that had been made to the original shape for the purpose of rounding the tail. The objective that followed was to “bend” the profile to the circular established by the segment of the program which defines the flow angles. This involved both translation and rotation of each of the ribs shown in Figure 4. 8.

#### 4.4 Geometric Representation

Firstly the rib was set at an angle matching the angle of the chord as determined by the flow angle calculations, then the centre point of the rib was translated from the chord to the circular arc, as shown in Figure 4. 8. Once  $\beta$  was known, it was possible to determine the location of point B. The angle was then used to determine the values of  $\Delta x$  and  $\Delta y$ , which allowed the final locations of the profile points to be calculated. Thus the profile with a circular arc radius was developed.

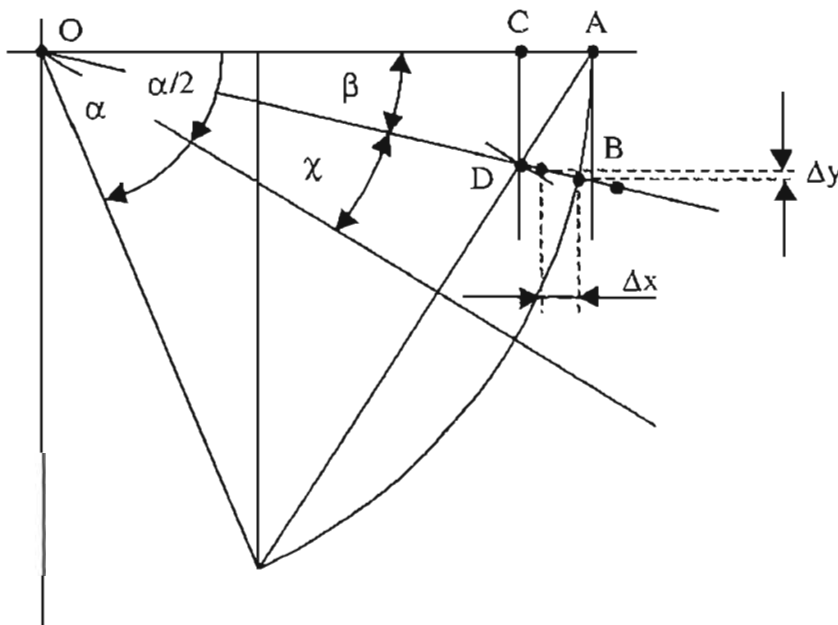


Figure 4. 8 Translation and rotation of ribbed joints for stator blade

A similar principle was applied to the calculation of the translation and rotation of the ribbed points for the rotor blade although it was somewhat more complicated by the necessity to divide the chord vector into two segments. Figure 4. 9 shows the diagram from which the equations were derived.



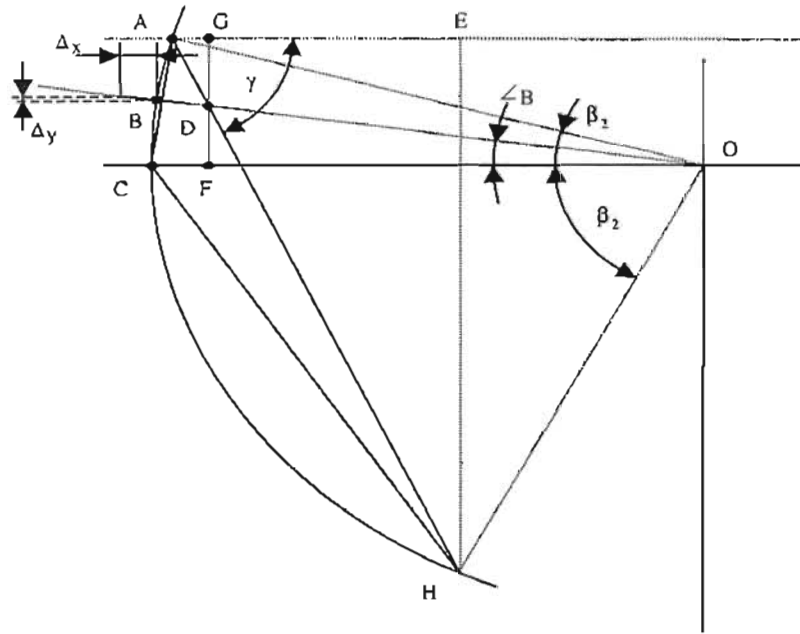


Figure 4. 9 Translation and rotation of the rotor ribbed points

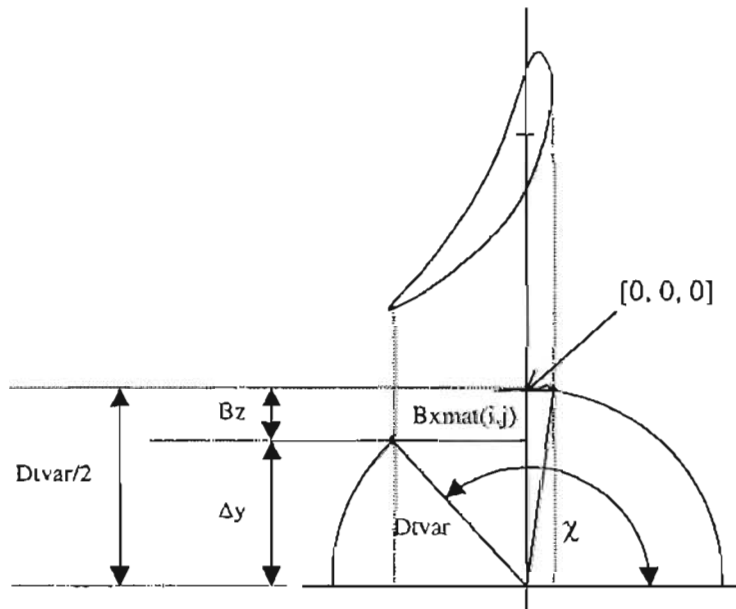


Figure 4. 10 Changing the plane of the ribbed points

The points developed thus far have only been defined in the z-plane with respect to their segment heights. The profiles do not have any radius fitting them to the radius at which

the segment is situated. Due to the wrap effect of the radius, the x and z-values of the profile will be shifted and the blade shape altered. Figure 4. 10 shows the development of the diagram governing the equations which define the angle and magnitude of the required wrap.

Once the blade had been converted from the stacking of flat z-planes to the curve of the radius of the respective segment, the profile was placed on the hub. The purpose of doing this was to determine the required number of blades from solidity. Once the blades had been stacked around the hub, it was easy to determine how many were required. Further programming was required to develop the blade pattern at the different angular increments.

Once the blades had been stacked about the hub and the solidity determined, the manufacturing process of the blades could begin. It was first necessary to ascertain what manufacturing process was going to be used for the production of the blades. Once the choice had fallen in favour of the lost wax process, further programming was required. The program was developed to produce points that would be suitable for the z-planes associated with the stacking of 12mm thick supawood.

These points had to be projected or interpolated from the radial stacking points of the existing blade pattern, the preferred method yielding the higher accuracy. Due to the twist of the profile along the length of the stack, the blade curvature was not a linear function, which reduced the accuracy of the linear interpolation and projection. The acuteness of the blade shape was therefore dependent on the level of shaping workmanship once it came to the production of the master pattern.

The results of the linear interpolation and project program were then required in a format compatible with the *.dwg* or *.dxf* file formats. Once the points of each profile had been entered into computer they were joined using a spline function and stacked alongside each other, as they would be cut from a section of supawood. Once the profiles had been cut, they were set up for the development of the master blade patterns.

## CHAPTER 5

### EXPERIMENTAL RESULTS

#### 5.1 Experimental apparatus

The experimental apparatus that has been used in taking measurements from the turbine is a dynamometer and a computer. The dynamometer was used to load the turbine and crosscheck the results with those obtained on the computer. The computer results were generated by a strain gauge on the PTO shaft attached to the dynamometer, which fed values to a data acquisition card. The results were sent through a multiplier, verified by calibration and checked for linearity. These results produced the values for torque. The sampling frequency for rpm was analogue, since it allowed the sampling to be performed in real time rather than digital, which would have required averages over a period of sampling time. Readings of pressure were measured by 6 static pressure gauges.

The turbine itself was made in house with each critical part being fabricated within the workshop. Accessories such as gaskets, packing or bearings were purchased through external companies, and only the casting of the turbine blades was outsourced, this being after a number of attempts at casting the blades inhouse. The installation site was set up by a previous project and so all that was required over and above the standardised turbine was a nozzle and a diffuser. These were made up to match the size of the outlet from the supply gate valve to the reducer and to match the size of the turbine outlet to the existing diffuser respectively.

#### 5.2 Objectives

The objectives of the experiment will be to:

1. Determine the efficiency of the turbine
  - firstly at its predicted optimum operating range of 1115 rpm
  - secondly through a range of rpm
2. To determine the power output of the turbine:
  - the maximum
  - the variation of power output with rpm

3. The supply flow rate will also be varied and measurements of efficiency determined
4. The cavitation parameter will have to be carefully analysed due to the difference in the correct design and the existing design of the draft tube. This effect will have large implications on the efficiency and the level of interpretation of this effect may determine the level of precision and accuracy of the design.
5. Both hydraulic and mechanical efficiency must be calculated.

Each of these processes will have to take into account the volume flow rate of the water through the turbine. These measurements will be taken in the form of differential pressure measurements within the nozzle, which is the supply pipe to the turbine. The temperature of the water will also have to be taken into account since it affects the vapour pressure of the water, which is critical to the cavitation limit.

### **5.3 Experimental procedure**

#### **5.3.1 Methods of water flow measurement**

Several methods are available for determining the velocity of the flow and the one that was selected for this experiment was the differential head method. The method requires that pressure measurements be taken at two or more points in the flow. A simple application of Bernoulli's equation and an inclusion of various friction loss equations then yields the velocity of the flow. Then knowing the exact dimensions of the pipe within which the water flows, it is possible to determine the flow rate.

#### **5.3.2 Obtaining results**

Labels 1-5 shown in Figure 5.3.1 represent the points at which the static pressure gauges are placed and point 6 is the location of the PTO shaft. The pressure gauge readings at points 2 and 3 are entered into the Bernoulli equation and used to calculate the velocities of the flow at points 2 and 3.

Friction loss calculations are made for the losses in the concrete supply pipe, the gate valve and the tapered steel tube using the values of velocity calculated from Bernoulli and the solution is repeated until convergent. Pressure readings 2-3 are preferred for the

calculation, since the readings between gauges 1-2 and are likely to be less accurate since there is interference in the flow caused by the spade of the gate valve at point 1, resulting in turbulent flow. This characteristic is shown graphically in Figure 5.3.2.

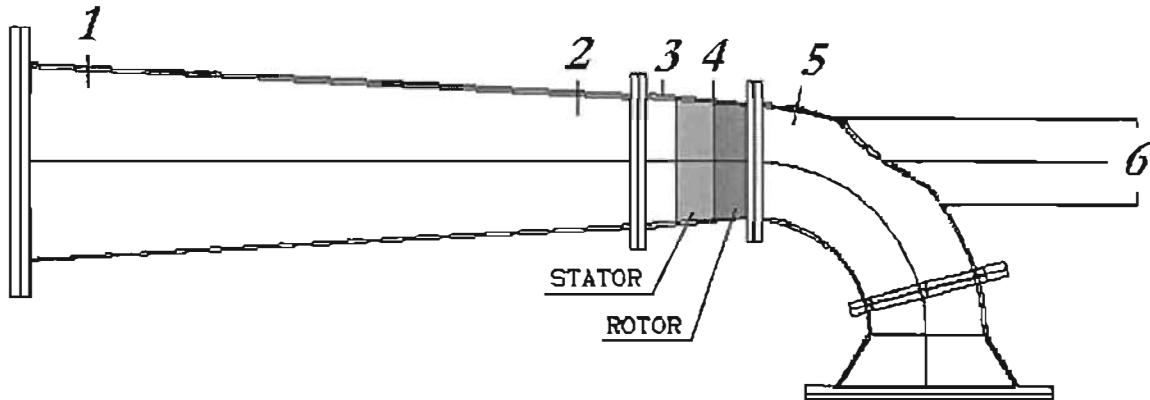


Figure 5.3. 1 Location of pressure gauges and stages

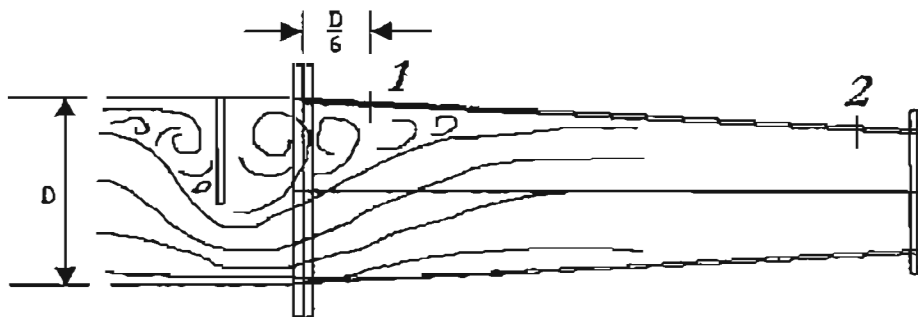


Figure 5.3. 2 Turbulent flow characteristics

Figure 5.3.2 shows the typical streamlines expected for the flow about the gate valve spade. Pressure gauge 1 is located approximately  $1/3D$  downstream of the gate valve and will experience the highest proportion of the unstable and buffeting flow caused by the partially open gate valve. The localised partial vacuum caused by the turbulent flow will give a characteristically lower pressure at 1, when compared to the pressure at 2 as the turbulence reduces as it progresses downstream. Therefore, until such time as the gate valve is in the fully open position, it is not feasible to take the pressure readings at gauge 1 for the purpose of determining the mass flow rate.

Even though the turbulence would still exist downstream at pressure gauges 2 and 3 it would still be more laminarised than the flow closer to the gate valve and measured at pressure gauge 1. Therefore, the option of using the pressure readings from gauges 2-3 would prove more accurate. The pipe diameters at which these gauges are located are known and hence it is possible to use Bernoulli's equation and the conservation of mass equation to determine the mass flow rate.

A dynamometer was used to take readings of torque and rpm. The readings for the torque curves were divided up according to the free running rpm of the turbine into increments of 200rpm up to 1000rpm and then a higher resolution of increments of 50rpm thereafter up to 1300rpm, since this was the critical design region. Thereafter, the dynamometer was limited to a maximum rpm rating of 1300rpm. It was decided that the maximum operating rpm of the dynamometer would be the pivotal point about which the gate valve would be opened to allow additional flow through thereafter.

Due to an rpm limit on the dynamometer, the method of testing for no-load speeds above 1300rpm was adopted as follows. By adjusting the gate valve under no-load conditions, sufficient flow was allowed through the turbine such that the speed reached the rpm limit of the dynamometer. Thereafter, a load was applied to the turbine until its peak power output, causing a resultant reduction in the rpm. At this stage, the gate valve was then opened further until the rpm limit of the dynamometer was reached again. The process was repeated until the gate valve was opened fully and the peak power and torque of the turbine had been measured under the condition of a fully opened gate valve.

The rpm measured at stall condition as referred to in the tables of experimental results below and the chapters that follow therefore has the meaning of the rpm measured at the maximum torque and does not refer to the rpm measured at the maximum power output of the turbine. This will be seen in the figures of torque and power, where the power initially increases with increasing rpm, peaks and then decreases with increasing rpm in the shape of an inverted parabola. And the torque continues to increase in a closely

proportional relationship with the rpm. It is at the stage of the measurement of the maximum torque, that the rpm is measured and recorded as the rpm at stall condition.

#### 5.4 Experimental results

The following test results were taken from the axial flow turbine test site.

**Table 5.1: Test Results – Test 1 on the 30/11/2000**

Shaft power kW	Stall Speed rpm	P1 kPa	P2 kPa	P3 kPa	P4 kPa	P5 kPa	Pressure Coefficient	Hnett m
@ stall rpm						Load		
0	21.1	0	0	0	0	-0	-1.516	4.307
0.7	89.3	0	0	0	0	-0	-1.435	4.431
2.8	203.5	0	0	0	0	-0	-1.092	4.594
6.1	246.4	0	8	2	0	-15	0.420	4.986
11.3	309.4	7	18	9	4	-20	0.594	5.857
12.5	317	10	20	12	5	-20	0.548	6.184
14.3	343.7	12	23	15	6	-20	0.516	6.506
16.5	381	15	25	17	10	-22	0.591	6.740
19.7	429.1	20	30	25	13	-22	0.527	7.486
20.5	430.8	25	35	28	15	-22	0.497	7.793
22.5	442.5	30	39	30	20	-22	0.448	8.012

Figure 5.4.1 shows the plots of the pressure distribution curves generated by the turbine during loading. P<sub>1</sub> shows the effect of the localised reduction in pressure caused by the turbulence resulting from the gate valve spade. P<sub>2</sub> shows the highest pressure curve since P<sub>3</sub> is downstream of P<sub>2</sub> and being located in a nozzle would show a rise in velocity with a corresponding decrease in pressure. Similarly for P<sub>4</sub>, which would see a further reduction in pressure due to the work output from the turbine rotor. P<sub>5</sub> represents the decreasing vacuum pressure caused by larger volumes of mass flow, as the gate valve is opened to allow more water through.

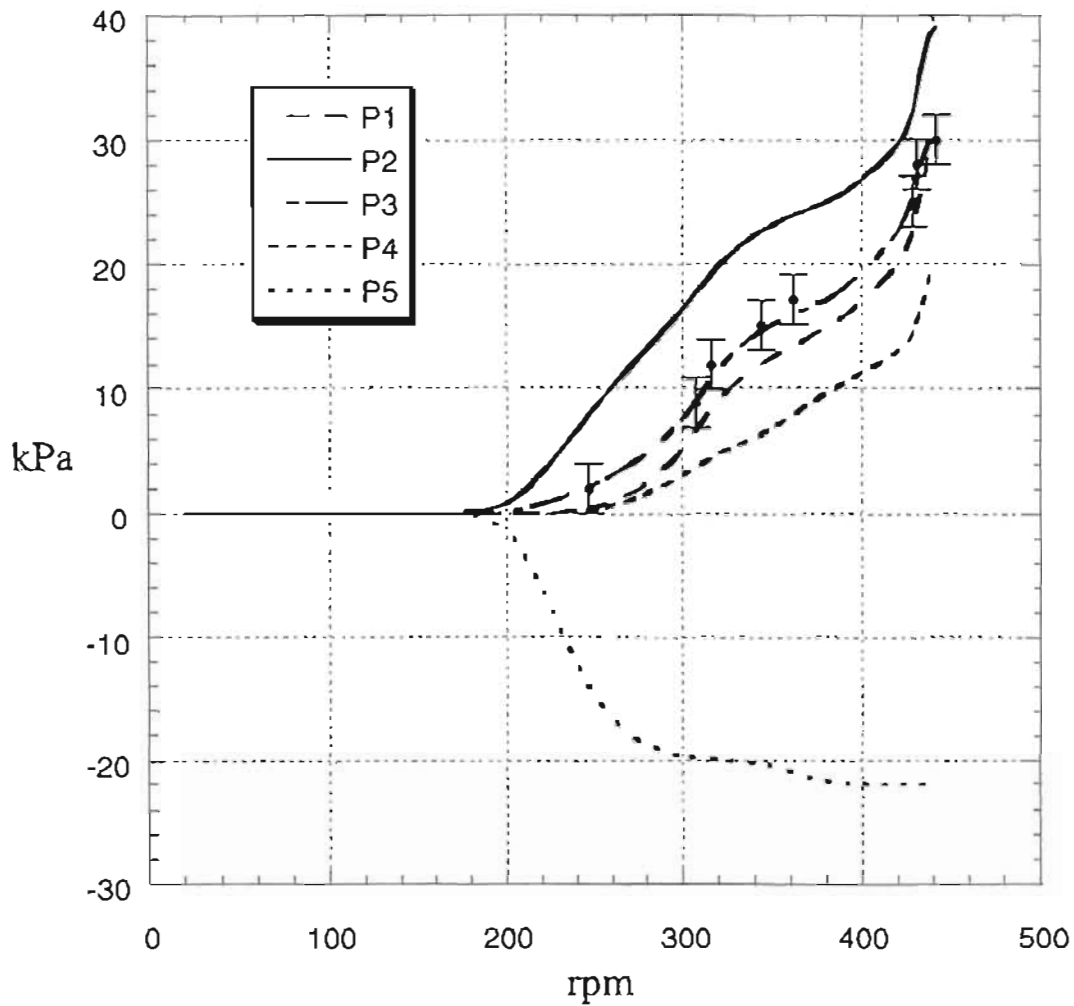


Figure 5.4.1 Pressure vs Stall rpm Test 1

The period between the first and second test included heavy rainfall and some settling of the draft tube piping occurred, marginally offsetting the alignment of the flanges joining the turbine diffuser and the draft tube pipe. The resultant air leak in the draft tube therefore caused a regulating effect on the vacuum pressure, resulting in the pressure leveling off as seen in Figure 5.4.2.



**Table 5.2: Test results - Test 2 on the 14/12/2000**

Shaft power	Stall Speed	P1	P2	P3	P4	P5	Pressure	Hnett
kW	rpm	kPa	kPa	kPa	kPa	kPa	Coefficient	m
@ stall rpm						Load		
0.130	49	0	0	0	0		-1.595	4.306
0.609	66	0	0	0	0		-1.459	4.431
2.382	134	0	0	0	0		-1.090	4.594
5.114	188	0	0	0	0		-0.784	4.801
9.554	245	10	20	12	5	-20	0.614	6.125
11.474	275	11	20	14	5	-20	0.572	6.361
13.364	303	13	25	18	10	-20	0.536	6.769
14.500	310	18	28	19	10	-20	0.504	6.913
16.347	327	20	30	21	12	-20	0.464	7.141
17.973	335	25	34	28	20	-20	0.401	7.793
22.238	413	28	35	30	20	-20	0.403	8.012
44.4	757	65	55	45	25	-28	0.890	9.890

Figure 5.4.2 shows the plots of the pressure distribution curves generated by the turbine during loading for the second test carried out on the turbine. The pressure distribution curves are similar to those for the first test except for the leveling off of the pressure values around 400rpm, which is expected to be a result of the air leak affecting the vacuum pressure on the downstream side of the turbine.

The general trend of the increase in pressure  $P_1$ - $P_4$  in Figure 5.4.1 and Figure 5.4.2 indicates the increase in the static pressure, which corresponds to an increase in mass flow rate. This is also reflected in the lower negative pressure  $P_5$ , which measures the vacuum pressure of the draft tube. The larger volume of water, as the turbine piping fills to capacity, has a larger mass, which in turn increases the vacuum pressure through the draft tube. The increasing gradient of  $P_1$ - $P_4$  shows the increase in the static pressure caused by increasing the load on the turbine.

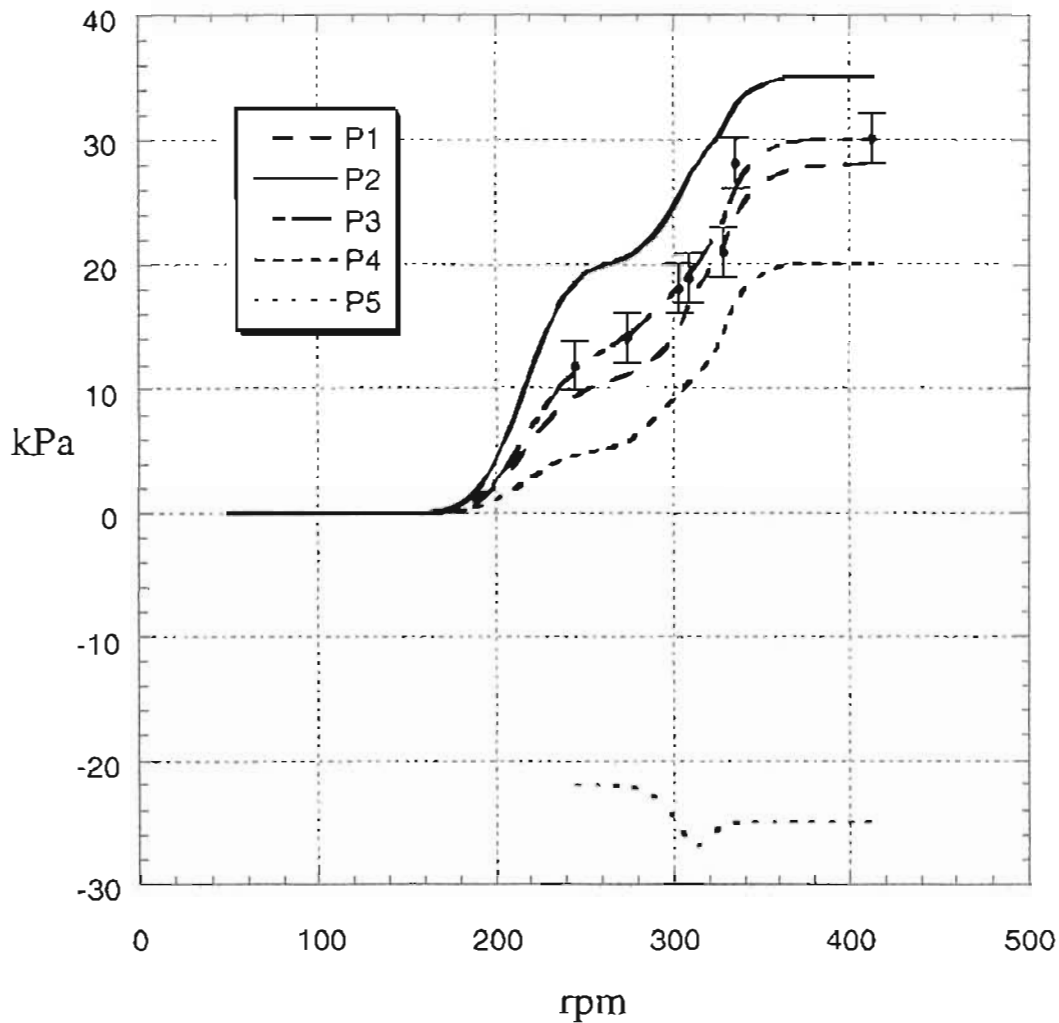


Figure 5.4.2 Pressure vs Stall rpm – Test 2

Figure 5.4.3 and Figure 5.4.4 showing the torque and power versus rpm curves were taken in real time, using a strain gauge attached to the shaft linking the dynamometer to the turbine. The plots show the points that were measured as well as the best-fit trend lines, which are typically a 2<sup>nd</sup> or 3<sup>rd</sup> order polynomials. The torque curves show a typically linear relationship to the rpm and are spaced by setting the no-load rpm condition by adjusting the gate valve opening.

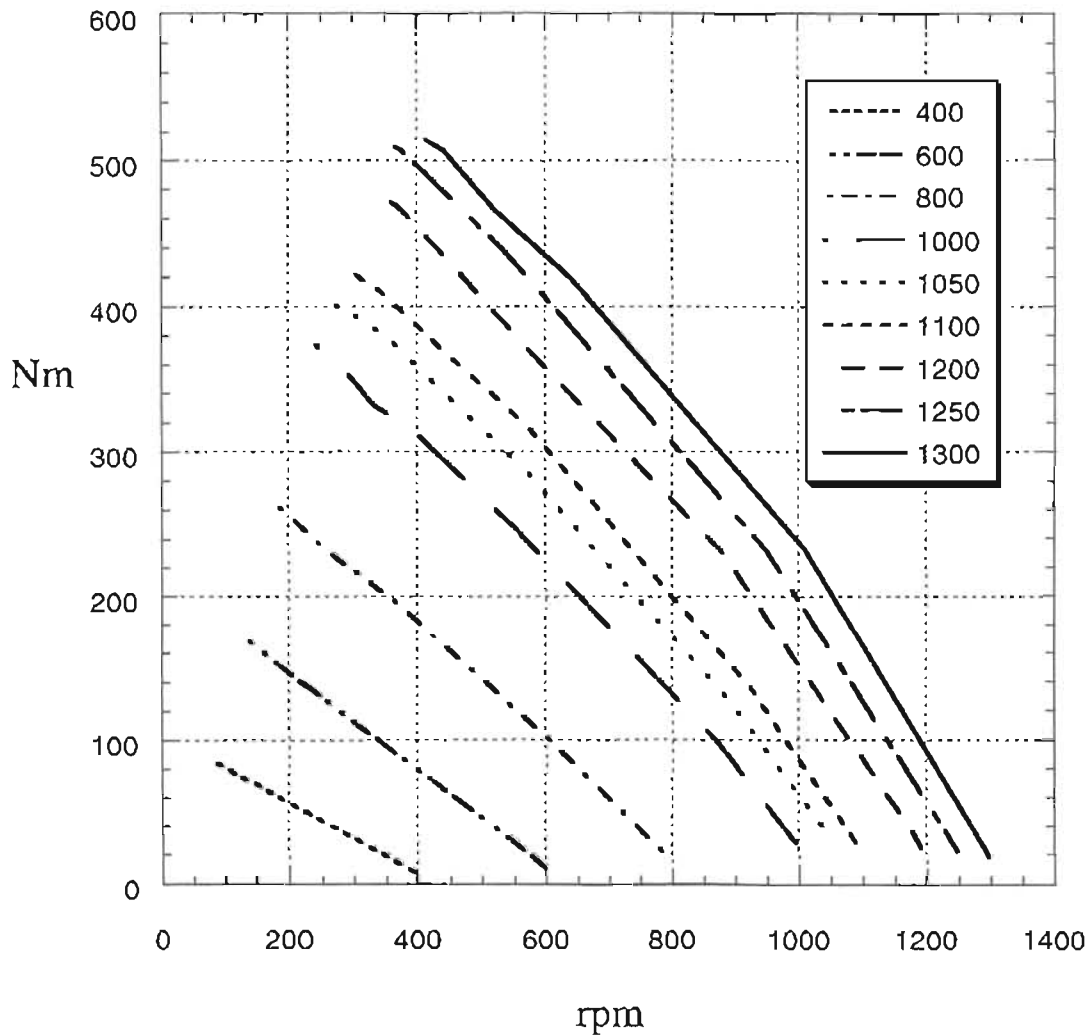


Figure 5.4.3 Torque Curves Test 2: Range 400 – 1300rpm

The power curves shown in Figure 5.4.4 expose an excellent progression of the maximum power output with an increase in the rpm up to the maximum power output, which tapers off with increasing rpm. The decrease in the power output after the peak shows the limitations induced on the performance of the turbine due to the limit on mass flow rate by the initial setting of the gate valve. Further restrictions are incurred by cavitation in the boundary layers on the blades and in the draft tube. This phenomenon is observed again in Figure 5.4.11 showing power versus efficiency.

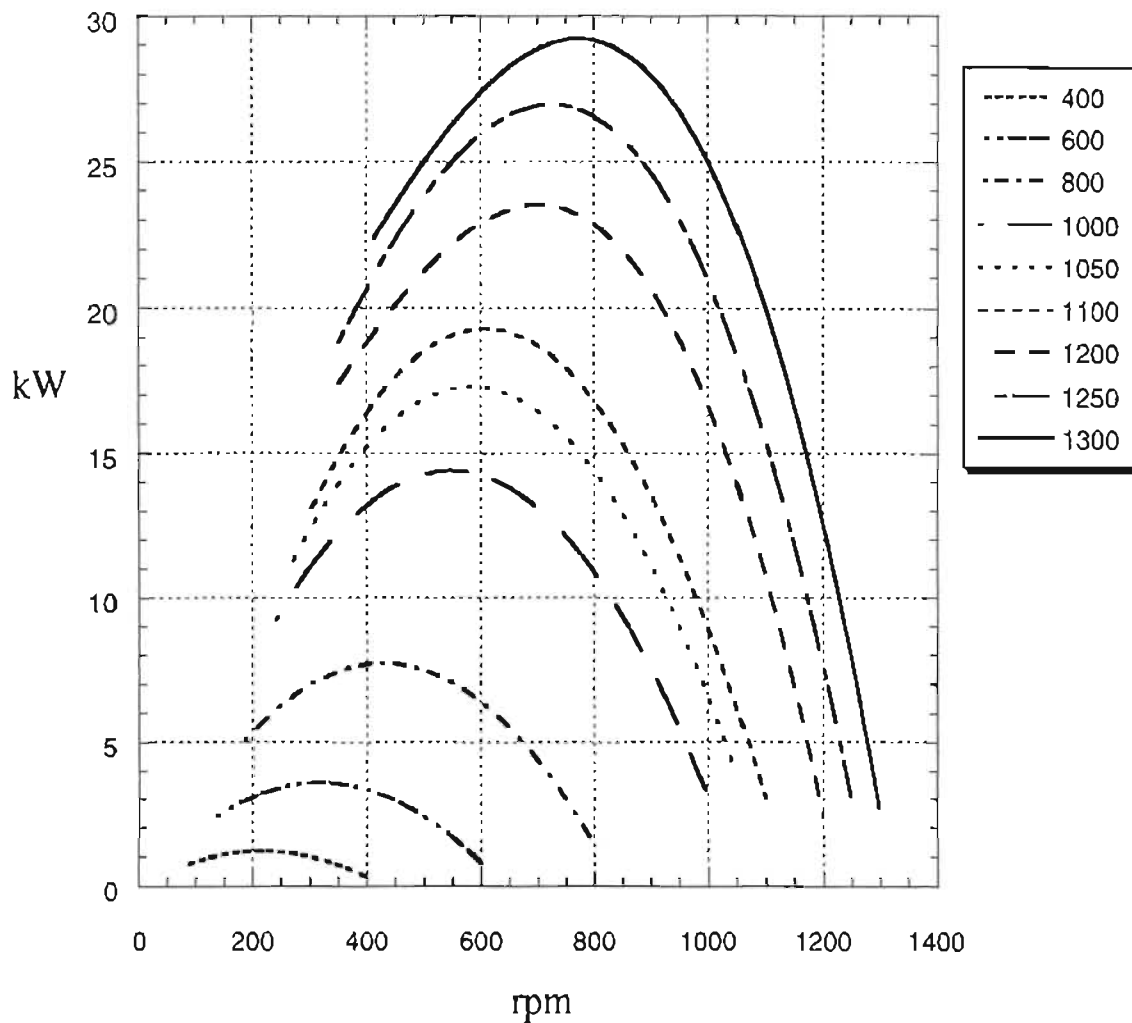


Figure 5.4.4 Power Curves Test 2: Range 400 – 1300rpm

The first equation that is required to analyse the above results is that of Bernoulli, governing the summation of the static and dynamic pressure heads. Since it may be assumed that  $P_1 - P_6$  are all set at the same height, the respective component of Bernoulli's equation, typically the potential energy, may be excluded. However, the losses for a section of tapered pipe and those for a gate valve should not be neglected. The various areas of losses are mentioned as follows:

- 1) Pressure losses through the gate valve, as the flow is converted from potential energy into kinetic energy at narrow gate valve openings. This is typically a function of the measure of the gate valve opening. Characteristic results are available from which the curve of the loss coefficient may be extracted.
- 2) Turbulent losses through the nozzle and following into the turbine. These can simply be measured by the frictional losses within a pipe.
- 3) It has been well researched that the ideal flow condition through the turbine is laminar and flow that is turbulent tends to cause losses due to early separation from the blade surface, negatively affecting the pressure distribution. This tends to be more of a problem for airfoil blading, used in the design of the turbine under examination, when compared to momentum blading.
- 4) At smaller gate valve openings, the turbine will not be “flooded” and neither will the diffuser. The net result is very low draft tube efficiencies, since it is not possible to utilise the negative pressure of the draft tube due to the air cavity. Furthermore, the turbine itself will not be flooded, where only the lower half of the blades would receive water. This makes measurement of any results literally impossible until such time as the draft tube is flooded. It is therefore determined that the results which show that the draft tube is not completely flooded, typically when there pressure readings are zero, will be ignored.
- 5) Losses from blade tip clearance. This would occur in both the stator and the rotor and is caused by excessive clearances between the blade tips and the outer wall. In these areas, the flow does not conform to the designed free vortex pattern and therefore does not produce any work.
- 6) Losses caused by the shaft of the turbine restricting the flow on the outlet, resulting in turbulence in the draft tube and thus reducing its efficiency. However, these losses may be sufficiently small to neglect.
- 7) Losses caused by the draft tube are expected to account for the first or second highest value of loss compared to that of the gate valve losses. The reason for this is that the draft tube efficiency affects the overall head of the turbine, which is directly proportional to the power. The design of the draft tube shape, cross-section and setting has a large bearing on the cavitation coefficient. This is

typically what is used to define the efficiency of the draft tube, which is then cross-checked against the Bernoulli equation.

- 8) Losses caused by the friction of the bearings; namely the two radial bearings, the single thrust bearing and the rubber bush supporting the shaft overhang and additional friction losses due to the stuffing box packing running on the surface of the shaft
- 9) Furthermore, when taking measurements, the PTO shaft and dynamometer incur their own losses, but these do not form part of the losses of the system since the voltage gain on the strain gauge is adjusted during calibration to read the exact measurements to within 1Nm of torque. It is further assumed that drift is negligible and the measurements are repeatable.

### 5.5 Precautions for the analysis

- A mechanical efficiency of  $\eta_{\text{mech}} = 0.95$  was assumed to take into account the friction losses in the two radial bearings, the single thrust bearing and the rubber bearing supporting the shaft within the stator hub.
- The radial pressure distribution resulting from the swirl caused by the stator blade angles significantly affects the static pressure reading taken by gauge 4 and similarly at 5 as well. One of the criteria for good design stipulates that the tangential velocity after the rotor will equal zero. However, this design condition will be suited only to the optimum design condition due to the blade angles being fixed and therefore any condition other than the optimum, will see  $C_{w2} \neq 0$ . A pressure gradient exists to counteract the acceleration of a body of mass caused by the centrifugal forces inherent in the flow from the stator blades. The effect of this pressure distribution is to cause an increased pressure at the tip diameter of the blades.
- In an attempt to account for this distribution, the author has developed the pressure distribution as a function of radius from a knowledge of the rpm and change in tangential velocity with respect to radius. These values have been developed in conjunction with the annular rings of equal area as determined by the free vortex design. Hence, when taking pressure readings and applying them

within the analysis, it was necessary to match the readings with the respective velocities.

- The resolution of the pressure gauges was another source of error and these error bars are shown on the graphs of the gauge readings to show the degree of expected inaccuracy.
- The values of losses through the gate valve cannot be assumed to be constant throughout the full operating range of the turbine since the gate valve acts like a nozzle for the initial stages of the gate valve opening, which requires a different analysis of the losses. This characteristic is due to the condition that the flow recovers to “flooded pipe” conditions only after the flow has travelled a length of  $n$  diameters and the sudden contraction analysis is no longer suitable. It was therefore determined to develop a graph of the loss coefficient for the variation in value according to the degree of valve opening.
- It must also be borne in mind that small differences will be found in the loss coefficient factor between tests and various diameters of gate valve. Generalisation of these results may therefore incur small errors.
- The volume of the blades occupying the annular area of the stator and rotor must also be deducted.

## 5.6 Analysis of the results

The raw data were analysed as follows:

Firstly, the velocity at point 3 – that is just before the stator, was calculated as shown below, by taking a streamline from the entrance to the supply pipe through to point 3, as a function of the pressure at 3 and the losses incurred before 3, such as the friction losses in the concrete and steel pipe and the “turbulence friction losses” through the gate valve. The values of the losses through the gate valve were extracted from typical test results taken from various values of gate valve opening.

$$\frac{P_{s_0}}{\rho g} + \frac{V_0^2}{2g} + z_0 = \frac{P_{s_3}}{\rho g} + \frac{V_3^2}{2g} + z_3 + h_{f_{0-1}} + h_{f_{0-1}} + h_{f_{1-3}}$$

$$h_{friction} = \frac{4fIU^2}{2Dg}$$

$$h_{f_{v,i,v_i}} = k \frac{V_{ave}^2}{2g}$$

$$\Rightarrow V_3 = \sqrt{2g \left( \frac{0 - P_{s_3}}{\rho g} - \left( z_3 + h_{f_{0-1}} + h_{f_{(s_1)}} + h_{f_{1-3}} \right) \right)}$$

$$\text{Mass flow rate} = \rho V_2 A_2 = \rho V_3 A_3$$

$$\Rightarrow V_2 = V_3 \frac{A_3}{A_2}$$

Note: the calculation of  $h_f$  and  $V_3$  are interdependent and require simultaneous calculation to the point of conversion. Since this was not possible to determine in a typical spreadsheet, the columns were written out separately as the completion of the loop to solve the equation by convergence. Determination of the values of friction loss through the concrete and steel pipes required a calculation of the Reynolds number to allow the friction factor to be determined. Since these values are dependant on the velocity of the flow for which they are determined, the minimum and maximum values were taken and the range of friction factors attained. The average value was then used as a constant throughout the range of mass flow rate.

Following after this calculation was the determination of the values for  $V_2$ . Once the values for  $V_3$  had been calculated, there were then two methods by which the value of  $V_2$  may be calculated, these were through continuity or solving for  $V_2$  in the same way in which  $V_3$  was solved. The difference between the two values was then an indication of the authenticity of the gauge readings and their respective calibration and lead to some insight as to the reason for some results, such as the losses across the rotor being negative.

In Figure 5.4.5 and Figure 5.4.6 the plot of velocity versus rpm shows a general increase in velocity. This is based on the experimental procedure as discussed earlier. The experiment was initialised by the no-load rpm being set and then a load applied to the turbine. The pressure measurements were taken once the turbine reached stall condition.



Therefore the increase in the velocity was a result of the increased mass flow rate, which was determined by setting the gate valve aperture, rather than the load on the turbine.

The readings taken from pressure gauge  $P_2$  are irregular and indicate the turbulent effects of the gate valve on the downstream flow. The location of the pressure gauge at the top of the nozzle would also contribute to the irregular readings because it is the highest point immediately ahead of the turbine, which means it is subjected to the highest risk of cavitation. It is also the point along the streamline that is subjected to the highest acceleration as the flow enters the bend.

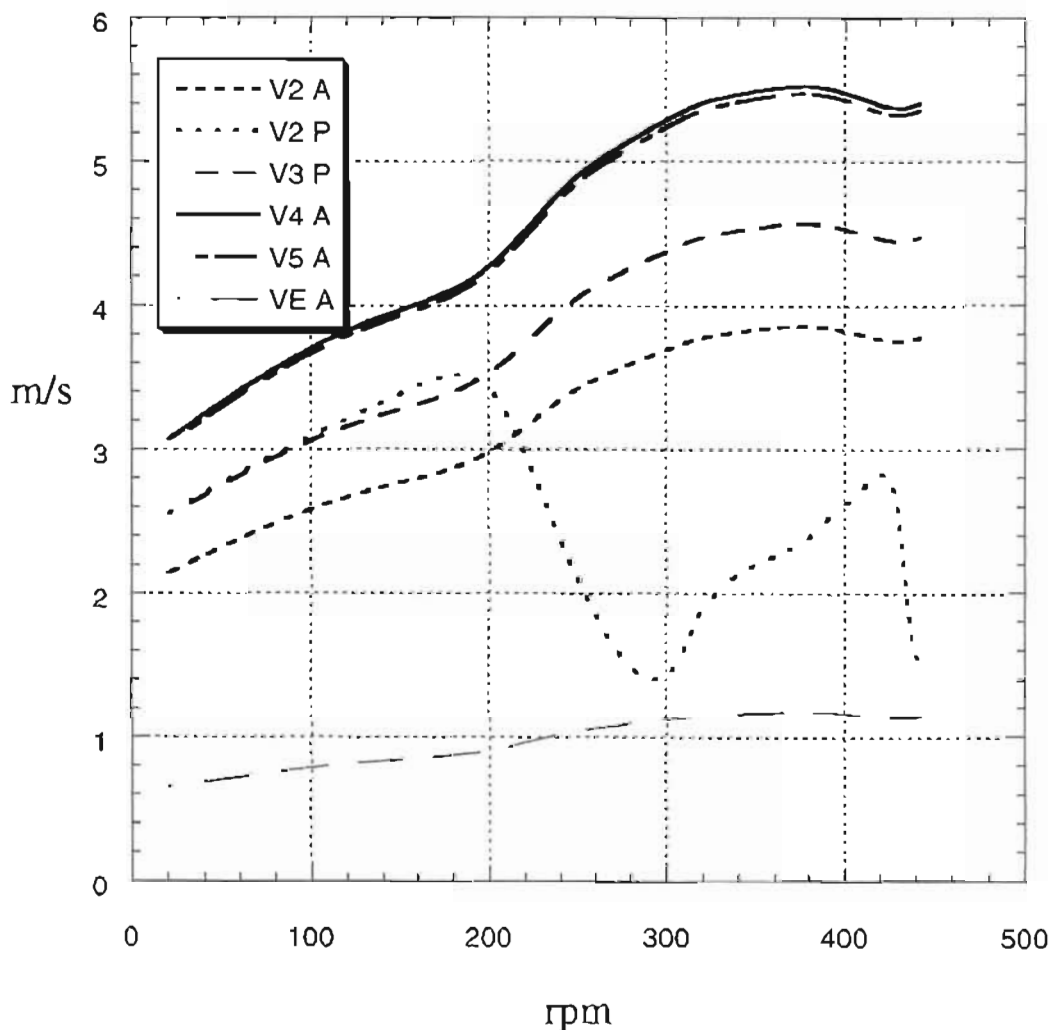


Figure 5.4.5 Velocity at Stage 2: Exhaust – Test 1

In Figure 5.4.5 and Figure 5.4.6, trend lines for  $V_4$ ,  $V_5$  and  $V_E$  have been excluded since the values are calculated on the basis of continuity from the velocity calculations from  $V_3$ . Therefore the only curve that has had a trend line fitted is  $V_{3\text{gauge}}$ , which represents the curve that is determined directly from the measured results from the pressure gauge and not through calculation using Bernoulli or the conservation of mass.

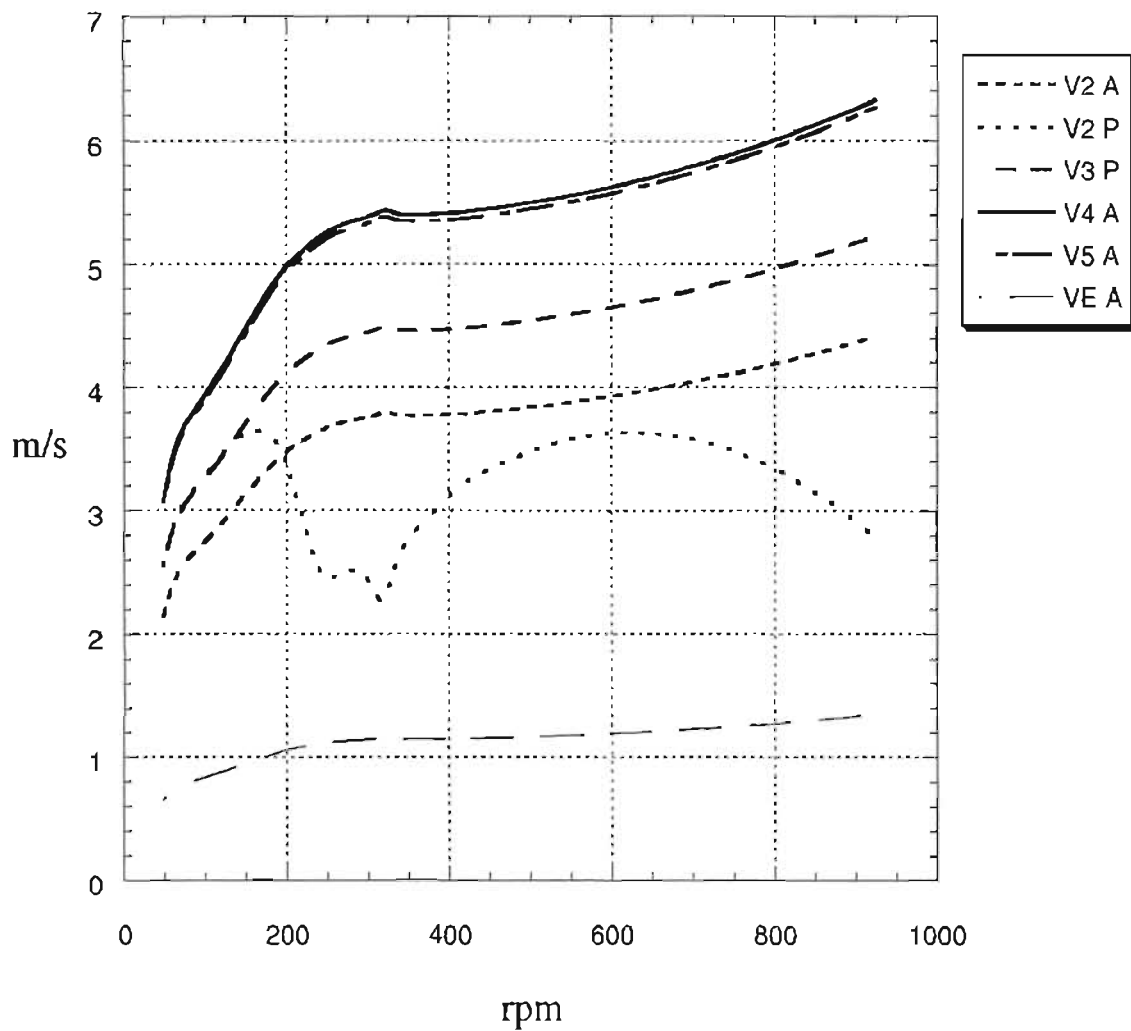


Figure 5.4.6 Velocity at Stage 2: Exhaust – Test 2

Following on from these results, the values of the stator, rotor and draft tube losses were calculated. This was performed using the raw data values of the pressure readings along with the values of velocity calculated from continuity for the stator and rotor. These values were found to be very sensitive to the cross-sectional area.

To calculate the draft tube efficiency, the loss coefficient was multiplied by the velocity head, which gave the value of the draft tube loss and was compared to the values calculated according to Bernoulli.

$$C_p = \frac{0 - P_{s_3}}{\rho(V_3^2/2)} + \frac{g(z_6 - z_5)}{(V_3^2/2)}$$

where: 0 = atmospheric pressure or 0 gauge pressure

$z_6$  = height of draft tube exhaust modified to the location of the leakage

$$\frac{P_{s_4}}{\rho g} + \frac{V_4^2}{2g} + z_4 = \frac{P_{s_5}}{\rho g} + \frac{V_5^2}{2g} + z_5 + h_{f_{4-5}} + \frac{U_{b1} \Delta C_w}{g}$$

As a means to crosschecking the results, the friction losses of the piping before the turbine were summed with  $H_{NETT}$  and the result expected to sum to the total pressure head. These results were impressively close, not varying by more than 1%. When considering the potential inaccuracy of the pressure gauge readings and the potential inaccuracy in assuming an extrapolation for the values of the gate valve loss coefficient, these values are considered acceptable. Another method of crosschecking, was to sum the losses with the total pressure at point 3.

As a separate check to the expected losses across the gate valve at partial valve opening, the valve was assumed to act as a nozzle, in which case, the flow upstream of the valve was assumed static relative to the flow downstream of the valve. This allowed an estimation of the velocity through the valve. The velocity corresponded well to the velocity calculated from the mass flow, which takes into account the losses through the valve.

The losses before the turbine headstock are a summation of the:

1. head loss due to friction in the concrete supply pipe
2. head loss corresponding to the gate valve opening fraction
3. head loss in the steel nozzle

The trend in the sum of these losses is characteristically decreasing since the losses in the concrete pipe and steel nozzle are negligible in comparison to that caused by the gate valve. Hence the trend of the losses will most closely follow the trend of the losses introduced by the gate valve, Figure 5.4.7. The trend of the gate valve losses is shown to decrease exponentially with an increase in the opening fraction, Figure 5.4. 12.

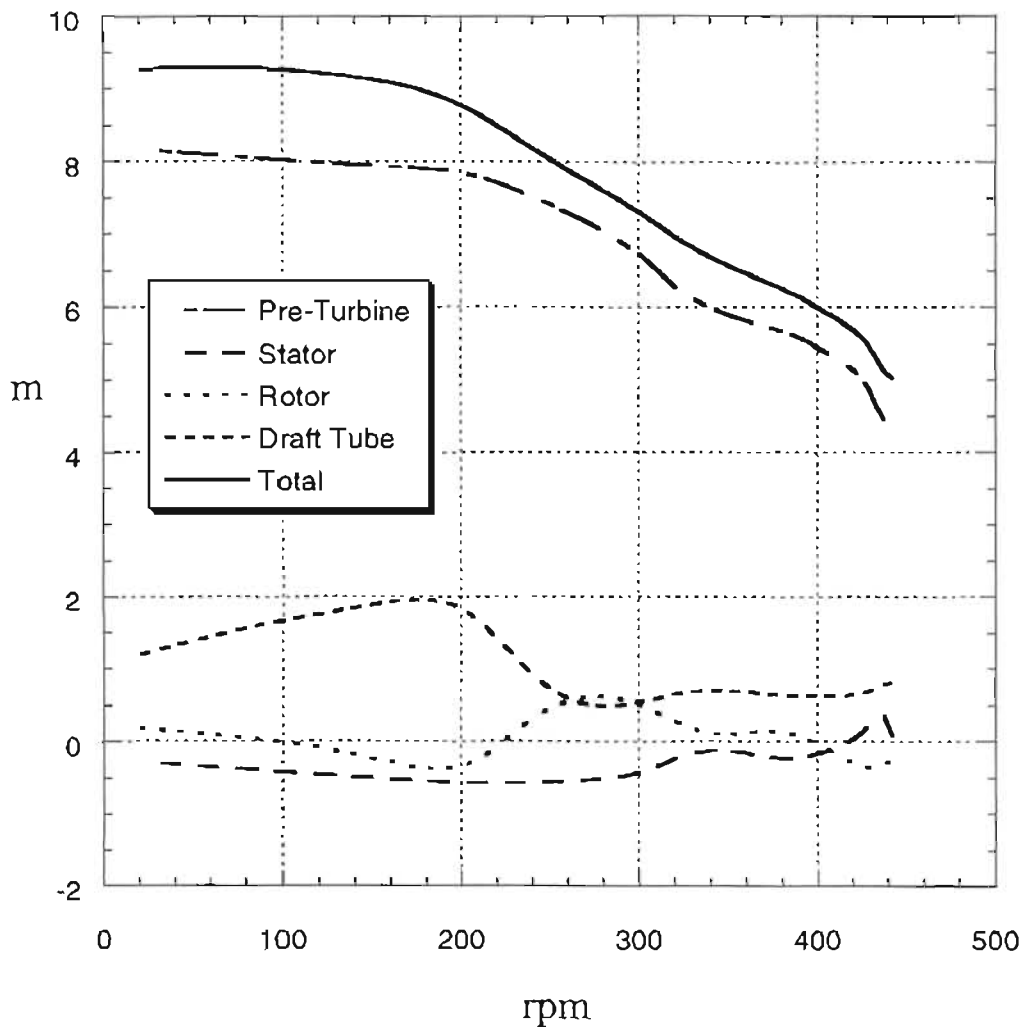


Figure 5.4.7 Turbine Blade Losses – Test 1

The losses across the rotor, Figure 5.4.7 and stator, Figure 5.4.8, remain a function of the turbulence levels associated with the gate valve opening fraction. The initial peak in these values is most likely to be a result of the gate valve losses. The gradual increase in the

stator losses can be associated with the increase in the mass flow rate as determined by the experimental procedure.

The rise and fall of the losses in the rotor may be caused by the inefficiency associated with the incorrect inlet angle as the blades rotate below their design rpm. As the mass flow increases, the velocity increases and causes the inlet angle of the fluid to swing toward the designed inlet angle of the rotor blade and promote an improvement in the efficiency.

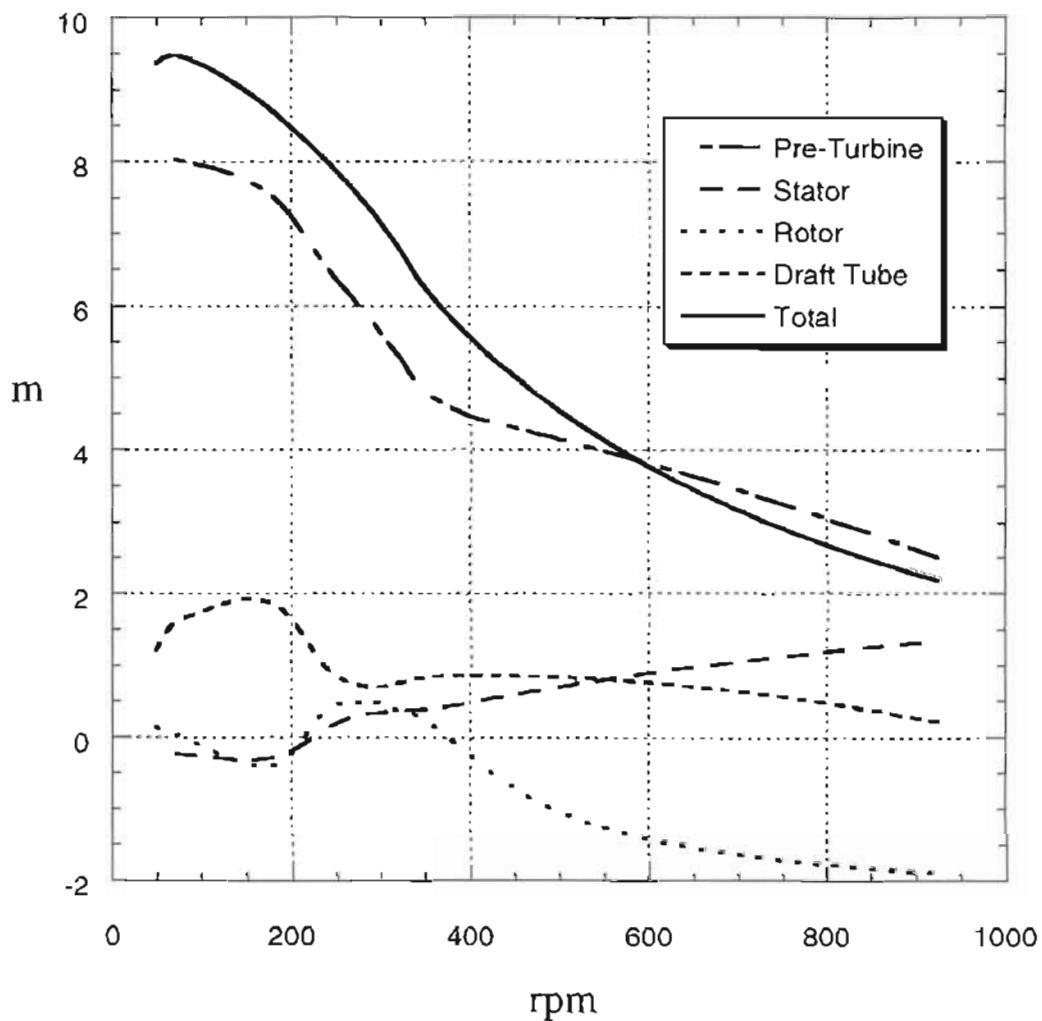


Figure 5.4.8 Turbine Blade Losses – Test 2

The rise and fall of the draft tube losses are a function of a slight leak in the joint between two flanges along the draft tube. However, the more dominant effect on the losses is the condition of the draft tube not being completely filled during the initial stages of testing where the gate valve is only opened a small fraction at lower rpm.

Figure 5.4.9 shows the mass flow rate measured for both Test 1 and Test 2. Test 2 shows the efficiency curve right up to 930rpm, whereas Test 1 only shows the test up to 450 rpm. The reason is that the test condition for Test 1 did not include running the turbine up to full load stall condition. Results are again determined according to the readings from the pressure gauges, which introduced an error due to the limitations of resolution.

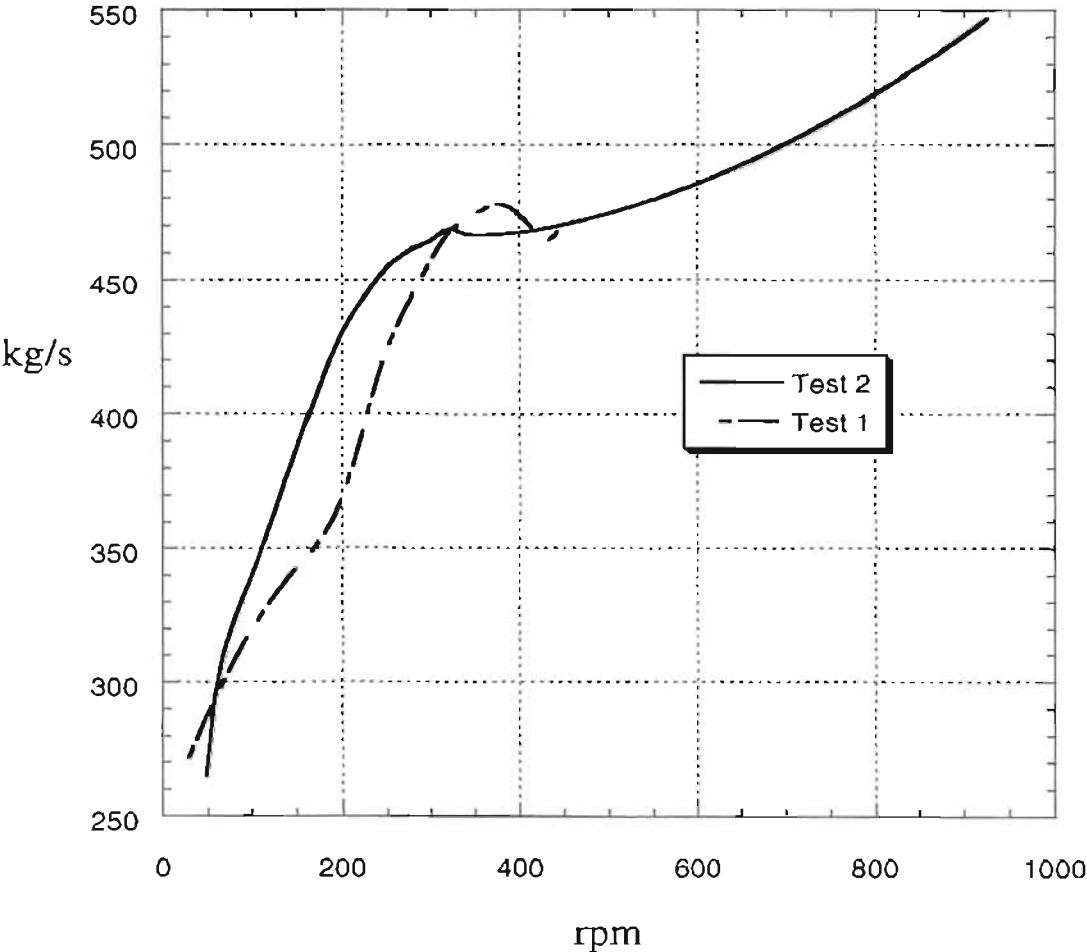


Figure 5.4. 9 Mass Flow Rate

The calculation of  $\Delta C_w$  was determined using the mechanical efficiency as follows:

$$\eta_{mech} = \frac{P_{shaft}}{\dot{m}U_b\Delta C_w}$$

Since the power at the shaft is known and the mechanical efficiency is assumed to be 95%, mass flow rate is calculated from the determination of  $V_3$  and  $U_b$  is measured directly through the dynamometer.

These values of  $\Delta C_w$  are then substituted into the hydraulic efficiency as follows:

$$\eta_{hyd} = \frac{\dot{m}U_b\Delta C_w}{Q\rho gH_{t,g}}$$

once the value of  $H_{NETT}$  had been determined from the following equation:

$$H_{NETT} = \frac{P_{o_2}}{\rho g} + \frac{V_3^2}{2g} + z_6 - \frac{V_E^2}{2g}$$

with  $V_E$  being determined simply from continuity.

The following efficiency is the total-to-total, or overall efficiency and represents the power conversion capability of the turbine, once the losses external to the turbine blade operation have been deducted.

$$\eta_{oa} = \eta_{hyd} \times \eta_{mech} = \frac{\dot{m}U_b\Delta C_w}{Q\rho gH_{t,g}} \frac{P_{shaft}}{\dot{m}U_b\Delta C_w} = \frac{P_{shaft}}{Q\rho gH_{t,g}}$$

Figure 5.4.10 is a reflection of the efficiency of both the gate valve and the turbine. The initial low gradient of efficiency reflects the high losses caused by low gate valve opening fractions. As the rpm is increased, which corresponds to an increase in the mass flow rate for the experiment, the effect of the gate valve losses fade and the efficiency curve of the turbine is exposed.

The end of the efficiency curve corresponds to the maximum power output at stall condition. Due to a limitation on the dynamometer of the no-load rpm, it was not possible to develop the efficiency curve beyond what is shown.

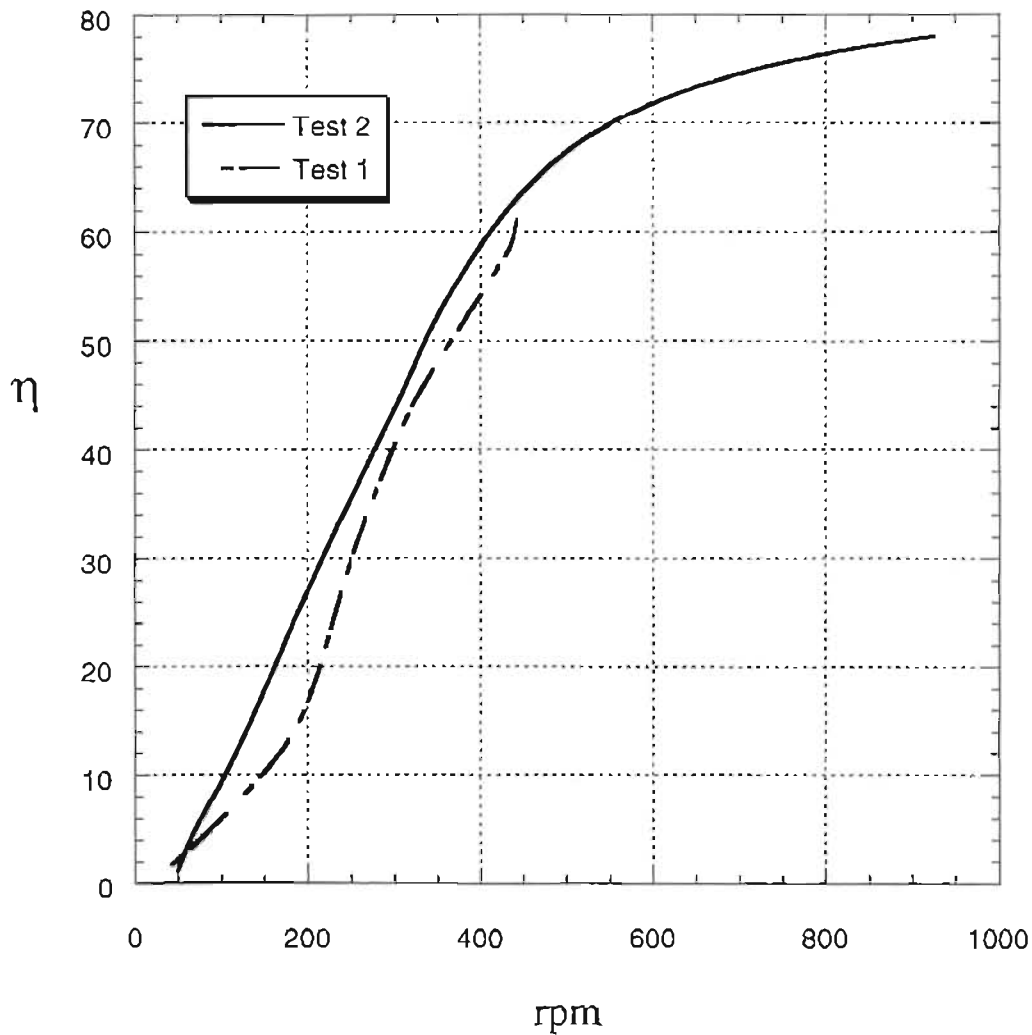


Figure 5.4. 10 Hydraulic Efficiency

Figure 5.4.11 shows the plot of the power versus the efficiency and indicates a very steady increase in the efficiency with power output. It is expected that this curve would be more linear without the effect of the gate valve as discussed in Figure 5.4.10 and the effect of the narrow gap between the draft tube flanges as discussed in Figure 5.4.7 and Figure 5.4.8.



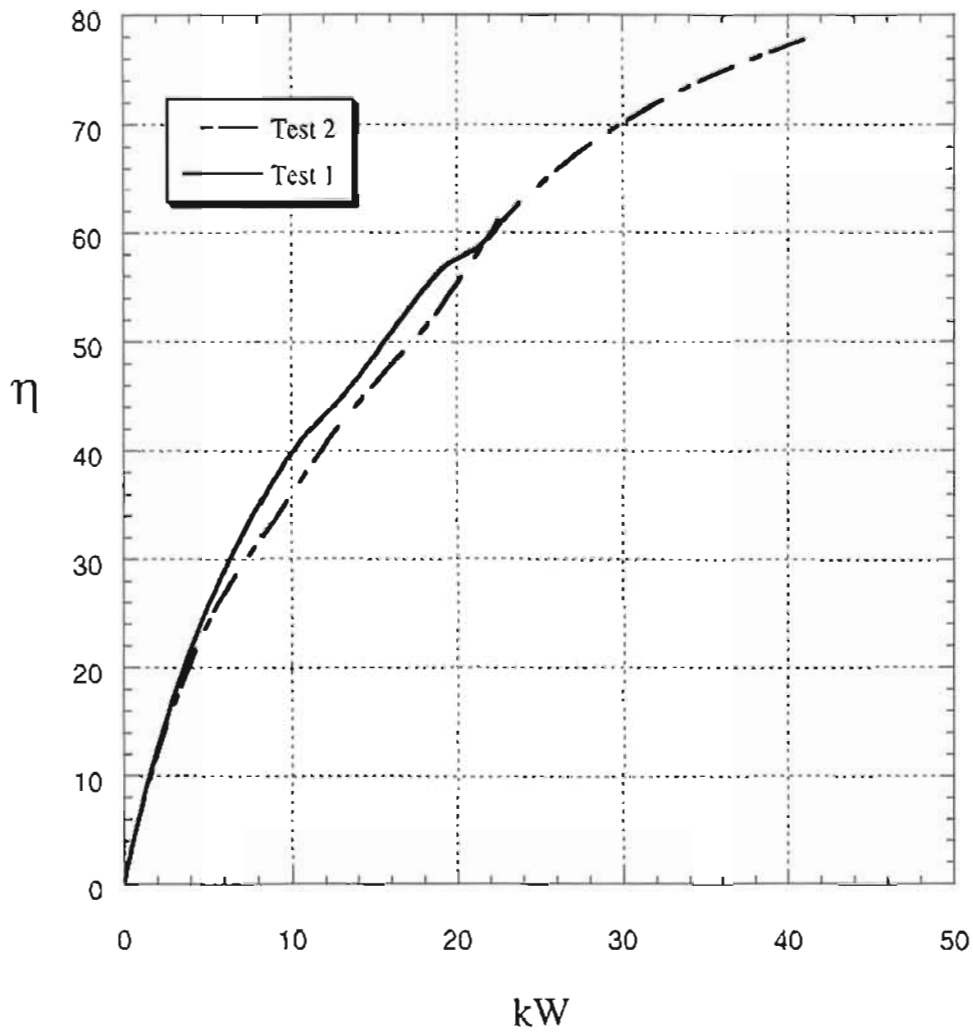


Figure 5.4. 11 Power versus Efficiency

Figure 5.4.12 shows the plot of the gate valve loss factor used to determine the value of the losses as a function of the valve opening fraction and the velocity of the flow through the valve. The calculation of this figure was tied in with the calculation of the friction losses through the piping and was repeated until convergence of the velocity of flow was reached.

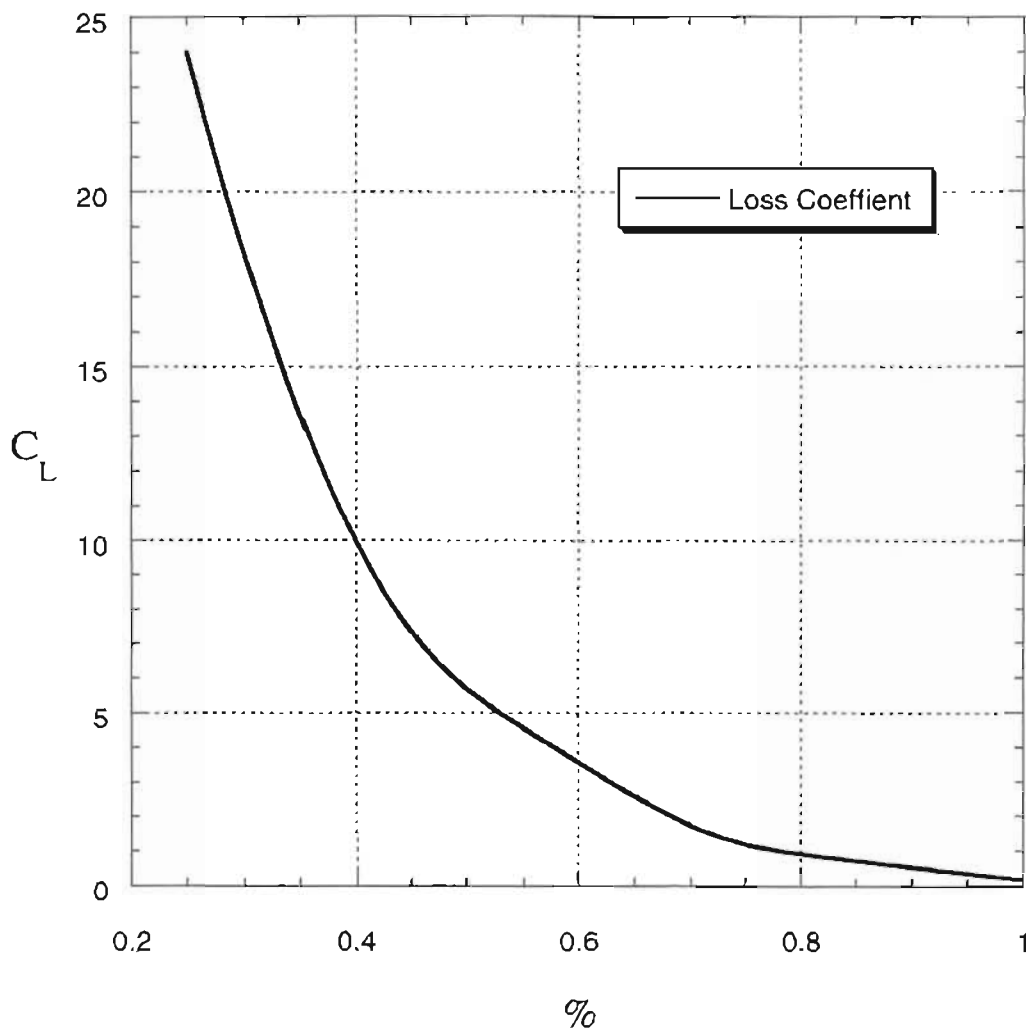


Figure 5.4. 12 Gate Valve Loss Factors

## CHAPTER 6

### CONCLUSIONS AND RECOMMENDATIONS

#### 6.1 Conclusions about the design

According to Figure 2.4.4 the category into which the turbine falls, when rated by head and power, is in the bulb units category but within close proximity to the category of conventional Kaplan and propeller turbines.

It is expected that this relation of values may be more appropriate than those shown by the Hill Curves, Warnick (1984), due to the difference in the rating of the turbine, assuming that these values are more suited to larger diameters of turbine with higher ratings.

The rating of the Hill curves, Warnick (1984), is as follows:

$$P_{\omega d} = \frac{P}{\rho \omega^3 D^5} = \frac{41400}{1000 \left( 925 \frac{\pi}{60} \right)^3 0.336^5} = 0.0851$$

$$Q_{\omega d} = \frac{Q}{\omega D^3} = \frac{0.54673}{\left( 925 \frac{\pi}{60} \right) 0.336^3} = 0.298$$

$$E_{\omega d} = \frac{gH_{NETT}}{(\omega D)^2} = \frac{9.81 \times 9.89}{\left( \left( 925 \frac{\pi}{60} \right) 0.336 \right)^2} = 0.3364$$

The above real values do not feature at all in the regions of peak operating efficiency shown in Figure 2.4.2. This means that the turbine does not operate anywhere within its peak design efficiency range. The power, flow rate and energy coefficients can all be improved by an increase in both the rpm and the runner diameter. This deduction from the results is correct since this phenomenon was discussed during the design phase in Chapter 7.7.4.

It was expected that the efficiency of the turbine would suffer largely under the efficiency of the draft tube. Chapter 2.4.11 discusses the dimensioning of suitable, characteristic designs for draft tubes. Unfortunately, this area in particular has not been implemented due to the existence of the current draft tube installation.

It would seem that the airfoil design of turbine blading is better due to the close approximation of the measured efficiency to the design efficiency, in spite of the uncharacteristic sources of losses for typical turbine design. It shows that airfoil blading has a more efficient pressure distribution capacity than that of the typical momentum design.

## **6.2 Conclusion: Experimental Results**

The experimental results exposed the concern that existed over the location of the pressure gauges. The opening fraction of the gate valve played a dominant role in the condition of the flow for smaller mass flow rates and consequently affected the overall efficiency. The general trends of the results followed the theoretical predictions. The pressures upstream of the turbine increased steadily with an increase in the mass flow rate and the negative draft tube pressure also decreased steadily. Unfortunately the effect of the leak between two of the draft tube flanges, caused a governing effect on the negative pressure and resulted in some shortcoming in the power produced by the turbine. The profiled design of the turbine rotor and stator blades gave smooth curves for the power and torque curves as well as for the hydraulic efficiency and power curves.

The results show the importance of the need for laminar flow through the turbine and for an effective draft tube design. The flow pattern caused by the gate valve was typically buffeting and unstable and the leak in the draft tube resulted in a lower pressure drop across the turbine and therefore a lower power output. The losses across the turbine are minimal in comparison to the pre-turbine losses and indicate a successful design.

It was not possible to assume that the turbine was flooded at all times during the course of the testing phase. The reason for this is the limit that the gate valve placed on the flow

rate, tending to act as a pressure regulator. The large losses induced by the orifice of the valve had very large and very negative effects on the performance of the turbine, to such a degree, that it was determined that the first four readings, which were yielding 0 kPa pressure readings would be ignored for the purpose of analysis. This was plausible when considering the additional exaggeration of the error caused by the pressure valves being placed at the top of the piping, rather than on the side where a more accurate reading may be obtained, by the reasoning of averaging.

Furthermore, the readings from pressure gauge 2 show large inconsistencies, seen in Figure 5.4.6, when compared with the expected results obtained from continuity from the reading of gauge 3. This effect was expected and the reason for it explained in Figure 5.3.2.

The difference in the losses of the draft tube, when compared to the typical losses seen in conventional designs, may be accounted for by the fact that a significant leakage existed in the piping system just after the first diffuser expansion, shown in **Drawing 1**. The cause of this leakage was a misalignment of the diffuser flange with the draft tube flange. The two potential causes of such an error, were settling of the draft tube, which may have occurred due to previous flooding conditions, or a misalignment introduced during welding of the flange to the diffuser. This may have occurred in spite of the flange being spot welded in situ.

An expected direct result of this leakage is to incur the action of a pressure regulator. As the mass flow through the turbine increases, the vacuum caused by the draft tube also increases and therefore draws more air into the flow than for lower flow rates. It is expected that this action is the reason for the consistent readings taken from gauge No. 5. Due to the consistency of the readings, it was suspected that the gauge itself was in error and it was therefore calibrated, with the results showing the gauge to be accurate.

The value of the gate valve opening-fraction had a large effect on the overall efficiency of the turbine with the losses introduced by the valve being the highest source of losses in

the system. For this reason, it was attempted to back-calculate the value of the gate valve opening by making it an intrinsic part of the determination of the velocity calculated according to the Bernoulli analysis. This required an expression of the mass flow rate as well as the respective area as functions of the valve loss coefficient, as shown below.

If the area of the orifice may be expressed by the equation:

$$A_{gv} = \frac{\pi}{4} 0.61^2 - 2 \left( \frac{\pi}{4} 0.61^2 \times \frac{2\theta}{2\pi} - \frac{1}{2} \left( \frac{D}{2} \cos \theta \right) \left( \frac{D}{2} \sin \theta \right) \right)$$

where:

$$\theta = a \cos \frac{x}{D}$$

and:  $x$  = displacement of the gate valve spade

$D$  = diameter of fully opened orifice

and:

$$x = \frac{\ln \frac{127}{k}}{6.3782}$$

where:  $k$  = valve loss coefficient, Massey (1968)

such that:  $A_{gv} = f(k)$  and  $V_{gv} = f(k)$

The problem with such an approach is that the dependence of the flow rate on the initial estimate of the value of  $k$  does not converge. Rather, the value of  $k$  converges as  $x$  tends to zero and no longer provides a useful insight into the trending value of  $k$ .

The final approach to the determination of the value of  $k$  was to halve the maximum opening area of the valve in parallel with the values of power, which correlate closely with increments in rpm, which is intimately linked to the mass flow rate. Then, the area opening was divided up according to the number of increments of the free running speed. These extracted values of valve opening were then used to determine the values of  $k$ .

If the effect of the gate valve is to reduce the efficiency of the turbine and similarly for the draft tube, then it is expected that the shape of the power vs efficiency curve shown in Figure 5.4.11 will be influenced by these two additional factors. As seen by the

exponential shape of the curve in Figure 5.4.12, showing the loss coefficient of the valve as a function of the valve opening, the expected effect of the valve efficiency on the overall efficiency would be to factor the losses by exponentially decreasing the reduction of efficiency for larger mass flow rates.

Two of the final loss calculations for the rotor are calculated to be negative. These negative values have been approved by virtue of the reasoning that the errors in the pressure gauge readings caused by the low resolution as well as the rapid fluctuation of the gauge needle will cause the recorded readings to be incorrect by a factor of +/- 2kPa. The relative magnitude of these factors are shown in the error bars added to the readings taken from pressure gauge 3 as shown in Figure 5.4.1 and Figure 5.4.2. In addition, the mass flow rate has been based on the reading of pressure gauge 3, which implies that any errors in the reading of pressure gauge 3 is carried through to the comparison of the other readings.

Due to a leak being discovered in the pipeline after the rotor, between the wide-angle diffuser and the exhaust diffuser, the following reasoning was applied to the analysis of the results:

Let:  $P_6$  = atmospheric pressure at the location of the leak in the pipe

$P_7$  = the pressure at the exhaust dump side of the exhaust diffuser, then:

$$\frac{P_{s_5}}{\rho g} + \frac{V_5^2}{2g} + z_5 = \frac{P_{s_6}}{\rho g} + \frac{V_6^2}{2g} + z_6 + h_{f_{5-6}}$$

$$\frac{P_{s_6}}{\rho g} + \frac{V_6^2}{2g} + z_6 = \frac{P_{s_7}}{\rho g} + \frac{V_7^2}{2g} + z_7 + h_{f_{6-7}}$$

Assuming that  $z_5$  is the reference plane and that  $P_6$  is at atmospheric pressure, then:

$$\frac{V_6^2}{2g} + z_6 = \frac{V_7^2}{2g} + z_7 + h_{f_{6-7}} \quad \text{and}$$

$$\frac{P_{s_5}}{\rho g} + \frac{V_5^2}{2g} + z_5 = \frac{V_7^2}{2g} + z_7 + h_{f_{6-7}} + h_{f_{5-6}}$$

However, if it cannot be assumed that  $P_6 = 0$ , then the analysis is as follows:

$$\frac{P_{s_5}}{\rho g} + \frac{V_5^2}{2g} + z_5 = \frac{P_{s_6}}{\rho g} + \frac{V_6^2}{2g} + z_6 + h_{f_{5-6}}$$

$$\frac{P_{s_6}}{\rho g} + \frac{V_6^2}{2g} + z_6 = \frac{P_{s_7}}{\rho g} + \frac{V_7^2}{2g} + z_7 + h_{f_{6-7}}$$

$$\frac{P_{s_5}}{\rho g} + \frac{V_5^2}{2g} + z_5 = \frac{V_7^2}{2g} + z_7 + h_{f_{6-7}} + h_{f_{5-6}}$$

This implies that the determination of  $H_{NETT}$  will be the same for the case of the leak in the pipe, as that for the case where there is no leak in the pipe.

However, the leak in the pipe does have an effect on the draft tube efficiency. A Bernoulli analysis from 5-6 reveals the typical values of the draft tube losses and is compared against the value of the losses taken from the pressure coefficient, with differences ranging from 0.03m to 0.5m head.

The test results of torque and rpm reveal a fluctuation at the stall point. The overshoot is expected to be generated by the momentum of the water causing higher axial velocities than what would be attainable at equilibrium. Once the momentum is lost, the pressure builds up and a slight decrease in power is seen to occur off the maximum overshoot. This is typical of the problems associated with the governing of the turbine.

### 6.3 Recommendations

The turbine performance can be improved simply by minimising the losses. This can be achieved through a number of ways, discussed in the following paragraphs.

Further filtering of the water – such as making the grid at the entrance to the inlet pipe of a slightly finer mesh. Although this will tend to begin to limit the flow when the amount of debris builds up on the grid, it is much easier to keep clean when compared to having to repair damages to the turbine itself, even if the comparison is purely on an accessibility level and ignoring the effort of repairing damages to the turbine itself.



Laminar flow characteristics could be beneficial, not only to the operation of the turbine itself, but also to the reduction of the losses due to friction. A filter grid is needed to improve the laminarization of the flow entering the nozzle, at the expense of a small pressure drop, but would not be able to cause the flow to be entirely laminar due additionally to the velocity of the flow causing high Reynolds numbers and falling into the region of turbulent flow.

An unexpectedly high amount of heating of the thrust bearing occurred during the operation of the turbine. Due to the damage that can be caused in this instance, where the heating causes the grease to carbonize and no longer provide sufficient lubrication, it is necessary to provide cooling. This can quite easily be provided by including a water jacket around the thrust bearing, supplied in a manner similar to that of the cooling water for the stuffing box. A pipe tapped from the high-pressure side of the flow, directed through the water jacket and returned to the low-pressure side.

Balancing of the turbine rotor may further eliminate vibration within the system. Vibration noise tends to initiate premature turbulence, if the flow Reynolds number is near the laminar to turbulent transition. Thus balancing of the turbine, may not only help reduce the amount of mechanical work lost, but also the amount of friction losses, when comparing turbulent and laminar friction losses.

Optimising the design of the draft tube, as discussed in Chapter 2.4.11 and following, would further increase the efficiency of the turbine, since the power is proportional to the head. Optimisation of the draft tube design is covered in the aforementioned chapter.

Being able to restrict the flow within the draft tube during partial gate valve opening to ensure that the turbine remain “flooded” during the full range of its potential operating conditions, would increase the efficiency. When the turbine is not flooded, the presence of an air gap implies that not all the blades are producing work at any given point in time.

The turbine should also be disassembled periodically to check for debris restricting the flow, to check the stuffing box packing and the bearings should be replaced as recommended in the bearing design chapter.

Eliminating the leak found in the draft tube pipeline would change the power output, since it would raise the level of the vacuum caused by the exhaust water although such a high vacuum may cause cavitation due to localised low pressure gradients which will result in a decrease in efficiency.

The location of the high-pressure feeder pipe should be in such a position that it is capable of supplying the stuffing box with water even when the level of the water is not at its peak, for example when the turbine is run at lower volumetric flow rates.

Likewise for the pressure gauges, but this applies more to the flooding of the gauge itself, where it is necessary to bleed the air from the gauge. Although it should also be borne in mind that there is much debris and sand that flows with the water in spite of the gate upstream of the pipe inlet which filters larger debris. Should any of this enter the pressure gauge, it is bound to cause failure. It is therefore recommended that the gauges be placed halfway up the side of the pipe.

The final results of Figure 5.4.11 show an overlay of the valve, turbine and draft tube efficiencies. It is believed that a higher overall efficiency may be attained if the leak in the draft tube as well as the draft tube itself were modified to suit the ideal case as discussed in previous sections.

Finally, the governing of the turbine is the method of smoothing the power output such that the rpm may be set at 50Hz with minimal variations in power. This is necessary in terms of the power driven components supplied by the turbine. For this particular turbine, with its characteristically high torque at fairly low rpm, gearing to achieve the required 50Hz should prove to be a very productive task. However, as mentioned in the introduction, it was not required that this topic be researched.

**CHAPTER 7**  
**APPENDIX**

**7.1 Curtain plate**

Since the curtain plate, drawing 10, is to be welded on both edges, the plate has been analysed according to that of a beam of unit length clamped at both ends with a uniform load distribution as shown in Figure A7.1. 1 below:

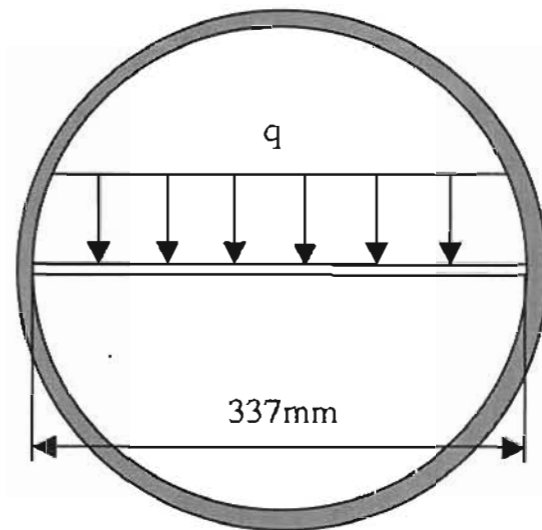


**Figure A7.1. 1 Uniform load distribution along curtain plate**

$$\text{at } x=0 : v=0, V = \frac{qL}{2}, v'=0$$

$$\text{at } x=L : v=0, V = \frac{qL}{2}, v'=0$$

$$Eiv'''' = q \tag{7.1. 1}$$

$$Eiv''' = -V = qx + c_1 \tag{7.1. 2}$$

$$Eiv'' = -M = \frac{qx^2}{2} + c_1x + c_2 \tag{7.1. 3}$$

$$Eiv' = \frac{qx^3}{6} + c_1 \frac{x^2}{2} + c_2x + c_3 \tag{7.1. 4}$$

$$Eiv = \frac{qx^4}{24} + c_1 \frac{x^3}{6} + c_2 \frac{x^2}{2} + c_3x + c_4 \tag{7.1. 5}$$

From Eq (7.1. 4) at  $x=0$   $v'=0 \Rightarrow c_3=0$

from Eq (7.1. 5) at  $x=0$   $v=0 \Rightarrow c_4=0$

$$\text{from Eq (7.1. 2) } -\frac{qL}{2} = 0q + c_1 \Rightarrow c_1 = -\frac{qL}{2}$$

$$\text{Substituting into Eq (7.1. 5) at } x=L: 0 = \frac{qx^4}{24} + c_1 \frac{x^3}{6} + c_2 \frac{x^2}{2} \Rightarrow c_2 = \frac{qL^2}{12}$$

Maximum moment:

$$M = -\frac{qx^2}{2} + \frac{qLx}{2} - \frac{qL^2}{12} \quad (7.1. 6)$$

$$\frac{dM}{dx} = 0 = -qx + \frac{qL}{2} \Rightarrow x = \frac{L}{2}$$

$$M_{(x=L/2)} = \frac{qL^2}{24} \quad \text{and at } x=0: M_{(x=0)} = \frac{qL^2}{12}$$

Maximum shear force:

$$V = \frac{q}{2}(L - 2x) \quad (7.1. 7)$$

$$V_{(x=0)} = \frac{q}{2}L$$

For flow that is turned through  $90^\circ$  and having velocities normal to the flow areas, the momentum equation can be written as follows:

$$\sum \vec{F} = \sum_{CS} (\rho \vec{U} Q) \quad (7.1. 8)$$

Then the force of the fluid on the pipe as it undergoes a change in flow direction is:

$$\begin{aligned} F &= \rho V_{IN} A \bar{U} + \rho V_{OUT} A \bar{U} = 2m\bar{U} \\ &= 2 \times 600 \times 7 \\ &= 8400N \end{aligned}$$

Since the curtain plate is situated along the bend's axis and only subtends  $45^\circ$ , the force acting on the curtain plate can be expected to be  $\frac{1}{4}$  of that acting on the pipe. The plate only effects half of the turning angle of the pipe and half of the fluid volume.

$$q = \frac{8400}{4 \times 410} = 5.12 \text{ N/mm}$$

where: 410mm is the length of the plate; see Drawing 10

Therefore:  $M_{\max} = 48.5 \text{ Nm}$

$V_{\max} = 1050 \text{ N}$

Using an En 57 carbon steel:  $S_u = 850 \text{ MPa}$  &  $S_y = 680 \text{ MPa}$

$$\sigma_s = \sigma_b = \text{S.W.L.} = 1/3 S_u = 283.3 \text{ MPa}$$

$$\sigma_{\text{bending}} = \frac{My}{I} = \frac{6M}{bd^2} \Rightarrow d = \sqrt{\frac{6M}{\sigma_b b}} \quad (7.1.9)$$

$$= 3.19 \text{ mm}$$

$$\sigma_{\text{shear}} = \frac{F}{A} \Rightarrow d = \frac{F}{\sigma_s b} \quad (7.1.10)$$

$$= 9 \text{ mm}$$

say 10mm plate thickness

where: b is the plate width which is the length 406 under the shear loading condition

A 10mm thickness was chosen since it is a standard plate size and satisfies both moment and shear force criteria.

## 7.2 Bearing Design

The design of the bearing life is based on a thrust bearing life of 3 years, which translates into:  $3 \times 365 \times 24 = 26\,280$  hours

$$26\,280 \text{ hrs} \Rightarrow f_h = 3.74 \quad [f_h = \text{time factor}] \quad (7.2.1)$$

$$n = 450 \text{ rpm} \Rightarrow f_n = 0.42 \quad [f_n = \text{speed factor}] \quad (7.2.2)$$

$$C = \frac{f_h}{f_n} P = 224\,400 \text{ N} \quad (7.2.3)$$

where: P = bearing load = 25 200N [value of  $F_{\text{running}}$  as determined in 7.6 Shaft Design].  
[Note the bearing load has not been modified by X&Y factors since these factors are not applicable for thrust bearings.]

Single direction thrust bearing: selected bearing # NSK 53413U

$C_a = 234\ 000\text{N}$

I.D. = 65mm

Abutment diameter = 110mm

O.D. = 140mm

Washer aligning seat diameter = 145mm

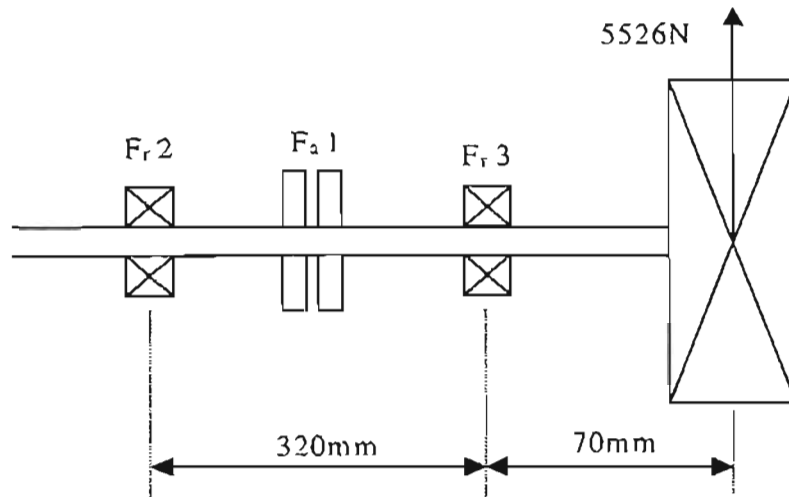


Figure A7.2. 1 Bearing / Pulley configuration

- The value of 320mm is set by the distance between the radial bearing mounting plates but the value of 70mm is set assuming that the chain drive sprocket is set out 26mm from the backing plate of bearing Fr3.
- Due to the difference in magnitude of the bearing loads it is advisable to alternate the bearings when servicing the pump.

Table 7. 1 Design equations, NSK (1970)

Bearing #2	Bearing #3
$(-1)(70)(5526) + (1)(320)(F_{r2}) = 0$ $\Rightarrow F_{r2} = 1209\text{N}$	$(1)(320)(F_{r3}) + (-1)(390)(5526) = 0$ $\Rightarrow F_{r3} = 6735\text{N}$
$f_h = \frac{f_n C}{P} = \frac{0.42 \times 52500}{1209}$ $= 18.24$	$f_h = \frac{f_n C}{P} = \frac{0.42 \times 52500}{6735}$ $= 3.274$
Bearing will run for the life of the pump	$L = 500 \times 3.274^3 = 2 \text{ years}$

It is desired that the bearing, which absorbs radial loading and facilitates the locating of the shaft, be as close as possible to the thrust bearing, for the benefit of the thrust bearing. Bearing selection was based on the necessity to have bearings 2&3 the same to satisfy the dimensional constraints of the system, once the loading had been determined.

The size of the square flange bearing is very well suited to the bearing pedestal design feature in that it allows for the bolt holes of the seating plate to correspond to the bolt holes of the welded plate. This means it is not necessary to attach the bearing to an intermediate plate and then attach this plate to the welded plate. The bearing may be bolted directly to the welded plate. The benefit of doing this is to reduce the number of bolt holes and the machining thereof, and to avoid the necessity for additional plates. This was most practical from a dimensional viewpoint which means that the plates need only be included if diaphragm bending occurs. Having bearings 2&3, the two radial bearings of the same size, allows for; all three of the bearings to be drawn out of the pedestal, interchangeability of bearings 2&3 and simplifies ordering of the bearings. Hence the final bearing selection is for (2 of): square flange bearing #CUCF212+C+CE

where: L = 173mm

$\Rightarrow R2 = (143^2 + 143^2)^2 + (175 - 143)$	Distance across the corners
= 234.23	
J = 143mm	Distance between hole centres
$\Rightarrow \text{P.C.D.} = (143^2 + 143^2)^2$	
= 202.23mm	
A <sub>3</sub> = 68.7mm	Width
C <sub>r</sub> = 52 500N	Radial load rating

Drawings 12 and 16 show the bearing tube and thrust bearing housing respectively.

### 7.3 Pre-load spring

The magnitude of the required spring force is determined by the equation, NSK (1977):

$$F_{a \min} = \frac{C_{oa}}{100} \left( \frac{n}{N_{\max}} \right)^2 = \frac{495000}{100} \left( \frac{450}{1100} \right)^2 \quad (7.3. 1)$$

$$= 830N$$

$$F_{a\min} = \left( \frac{C_{oa}}{1000} \right) = 495 N$$

Therefore use the larger value: 830N

where:  $F_{a\min}$  = minimum axial load (N)

$C_{oa}$  = Basic static load rating (N)

$N_{\max}$  = limiting speed (rpm)

It is noted that this force does not exceed the maximum permissible axial force of the square flange bearing. The calculations of thrust bearing design have not been revised to include the additional loading since it accounts for only 3% of the final load and 0.4% of the Basic Load Rating.

Radial limitations:    spring I.D. = 60mm;            O.D. = 75mm  
                              => maximum spring thickness = 7.5mm  
                              maximum allowable compressed length = 48mm  
                              minimum force at compressed state = 830N

**NOTE: the spring is required to be cone shaped at an angle of 20 degrees included in its compressed state. This can be seen in drawing 17.**

Selecting a spring wire diameter of 7.5mm:

$$C = D/d = 60/7.5 = 8$$

The nomogram for close helical springs yields:             $k_w = 1.182$

$$\tau = \frac{8PD}{\pi d^3} k_w = \frac{8 \times 830 \times 60}{\pi \times 7.5^3} \times 1.182 \quad (7.3.2)$$

$$= 355.3 MPa$$

where:  $\tau$  = max. Shear stress in wire

P = applied load

D = mean diameter of spring;            d = wire diameter

$k_w$  = Wahl's factor

This value was checked as correct against the nomogram value of 362MPa, and hence this value of stress is acceptable.



## 7.4 Bearing pedestal design

The nearest fitting pipe diameter that suits the bearing size – including wall thickness, bolt holes and castellation – is the 250mm nominal bore. A large wall thickness is selected to minimise bending and ensure a rigid structure for plate welding. The bearing pedestal is shown in **Drawing 12**.

### 7.4.1 Design of the diaphragm plates

Plate #1:

Seating plate - distance between flat surfaces: 177mm

castellation O.D. = 238mm

M16 bolts at P.C.D. of 202.24mm

plate thickness = 80mm

castellation steps to set at 45° intervals with bolt hole centres at 90° intervals beginning at 0° at top dead centre

thickness selected on basis of the thickness necessary to house the bearing and provide a shoulder for the thrust bearing

Welded plate - O.D. = 254.46mm (pipe I.D. = 254.46mm)

Distance between flat surfaces = 177mm

castellation O.D. = 238mm

thickness = 25mm

To avoid increasing costs it is advisable to use the dropout from the cutting of the welded plate for the seating plate, if abuse of the square flange bearings proves that these plates are necessary. This should then be done for all three of the plates.

Plate #2&3:

Seating plate - castellation dimensions are set by plate #1 and used for plates 2&3 to simplify manufacturing processes.

plate thickness adapted to the pipe wall thickness to 15mm for both seating plate and welded plate

M16 bolts at P.C.D 202.23mm

**Note:** when welding the seating plates into the pipe, the plates must be orientated the same as the thrust bearing plate. This facilitates the ease of access to the mounting bolts through the windows;

and ensure that the grease nipple faces directly out the window for ease of access.

#### 7.4.2 Calculating the stress of the plate supporting the thrust bearing

Due to the castellated shape of the annular plate, each castellation is considered as a cantilever beam with the following dimensions:

width = 80mm

depth = 25mm

length = 38.73mm

load length = 26.1mm

load magnitude = 6 300N

(applied load = 25 200/4N)

$$\sigma_s = \frac{F}{A} = \frac{6300}{80 \times 25} = 3.15 \text{ MPa} \quad (7.4.1)$$

$$\sigma_m = \frac{6M}{bd^2} = \frac{6 \times 6300 \times 26.1}{80 \times 25^2} = 19.73 \text{ MPa} \quad (7.4.2)$$

$$\sigma = \sigma_s + \sigma_m = 3.15 + 19.73$$

$$= 22.88 \text{ Mpa}$$

=> therefore cantilever failure will not occur

Such a low stress is suitable, even for a plain carbon steel such as En8, since it leads to a high rigidity for backing plate #1 and this is desirable for the safety of bearings 2&3 as discussed under bearing selection. Backing plate thicknesses for bearings 2&3 were similarly selected, i.e. primarily due to rigidity and uniformity of heat dissipation during welding.

The axial loading is in one direction only and hence the bolts serve only to centralise the bearing. For an M8 bolt with  $S_y = 200 \text{ Mpa}$  (a relatively low stress) a shear force - equivalent to a radial force- of 10kN could be supported. This amounts to 40kN for the four bolts used, a load which will not be encountered. Thus the final selection of bolt will adequately support the load; also investigated in the bearing selection section.

## 7.5 Drive Train Shaft Design

Initially the option of using belts for the power transmission was considered. The method by which this was done is outlined below. In knowing the speeds and the power to transmit one may select a suitable belt tension that corresponds to the manufacturers specifications for  $\alpha$ ,  $\beta$  or  $\gamma$  type belts. Professional advice was obtained for the final selection and this yielded a final cost of R2136 for one 500mm, one 250mm diameter pulley and 4 SPC belts. The proposition was re-evaluated for power transmission by chain. This seemed more viable since chains are more suited to low speed, high torque applications.

Assume the following:

drive sprocket diameter = 307mm

driven pulley diameter = 154mm

triplex chain P.C. = 25.4mm

$$\text{Chain velocity: } v = \frac{N\omega P.D.}{60000} = \frac{38 \times 450 \times 25.4}{60000} = 7.239 \text{ m/s} \quad (7.5.1)$$

where: N = # teeth

$$\text{Chain pull: } T = \frac{1000P}{v} = \frac{1000 \times 40}{7.239} = 5525.6 \text{ N} \quad (7.5.2)$$

where: P = power in kW (safety factor incl.)

The resultant cost analysis showed that the chain option was R312 more expensive than the belt option but; did not require a belt tensioner, avoided slip problems, required no additional fabrication and had a longer life than the belts. Hence power transmission by chain was selected in the initial design phases. However in later design stages, it was independently determined that the rotational speed of the turbine was to be increased to 1100rpm. At this speed, the chain option ran the risk of severe chain slap and it was

elected to opt for the belt drive, should the driven component require an increase in speed, or simply a direct flexible coupling, were the driven component to run at the same rpm. For example a water pump.

Shaft diameter at the pulley:

$$d = \left[ \frac{32RF}{\pi} \sqrt{\left( \frac{k_t M}{S_e} \right)^2 + \left( \frac{k_{ts} Mt}{S_y} \right)^2} \right]^{1/3} \quad (7.5.3)$$

$$= \left[ \frac{32 \times 2}{\pi} \sqrt{\left( \frac{1.8 \times 5525 \times 26}{425} \right)^2 + \left( \frac{1.4 \times 850000}{680} \right)^2} \right]^{1/3}$$

$$= 33.54 \text{mm}$$

where:  $k_t$  = bending factor

$k_{ts}$  = torque factor

These calculations show that a shaft diameter of, say 35mm, would adequately support the load.

## 7.6 Shaft Design

The shaft material is chosen as En 57 steel with parameters:  $S_u = 850 \text{Mpa}$ ,  $S_y = 680 \text{Mpa}$ , BHN = 246

$$\text{shaft load: } F_{ax} = PA = 0.1 \frac{\pi}{4} 400^2$$

$$= 12.6 \text{kN}$$

$$\text{at } F_{\text{running}} = 2 \times F_{\text{theory}} = 2 \times 12.6 = 25.2 \text{kN}$$

where:  $F_{ax}$  = axial compressive force

$P$  = static pressure

$A$  = area

Torque:

$$P = \omega T \quad \Rightarrow T = \frac{P}{2\pi \frac{n}{60}} = \frac{60 \times 40000}{2\pi 450}$$

$$= 850 \text{Nm}$$

Chain pull = 5525.625N [as calculated in section 7.5 Drive train shaft design]

Using the residual stress method to solve for the shaft stress for static loads:

$$\text{Torsional stress: } \tau = \frac{16M_t}{\pi d^3} \quad (7.6.1)$$

where:  $M_t$  = torque

$$\text{Tensile stress: } \sigma = \frac{F}{A} \quad (7.6.2)$$

where:  $F$  = axial force

$A$  = tensile stress area

$$\text{Bending stress: } \sigma = \frac{32M}{\pi d^3} \quad (7.6.3)$$

where:  $M$  = bending moment

For a shaft diameter of 50mm:

$$\begin{aligned} S_n = S_n = C_l C_s C_d C_t C_m &= 2 \times 850 \times 1 \times 0.73 \times 0.927 \times 1 \times 0.897 \times 1 \\ &= 258 \text{MPa} \end{aligned} \quad (7.6.4)$$

where:  $S_n$  = stress at  $10^6$  cycles

$S_n$  = ultimate tensile strength

Constants are for factors of: load, surface finish, size, temperature, reliability and miscellaneous respectively

$$\begin{aligned} \tau &= \frac{16 \times 850 \times 1000}{\pi 50^3} K_f \\ &= 51.95 \text{MPa} \end{aligned}$$

where:  $K_f$  = torsion factor = 1.5

$$\begin{aligned} \sigma_a &= \frac{25200}{\frac{\pi}{4} 50^2} K_f \\ &= 25.7 \text{MPa} \end{aligned}$$

where:  $K_f$  = axial load factor = 2

$$\begin{aligned} \sigma_b &= \frac{32 \times 5525.6 \times 26}{\pi 50^3} K_f \\ &= 23.4 \text{MPa} \end{aligned}$$

where:  $K_f$  = bending factor = 2

$$\sigma_m = \frac{\sigma_{ax}}{2} \pm \frac{\sqrt{\sigma_{ax}^2 + 4\tau^2}}{2} = \frac{-25.67}{2} \pm \frac{\sqrt{-25.67^2 + 4 \times 51.95^2}}{2} \quad (7.6.5)$$

$$= 40.7 \text{ MPa}$$

$$\sigma_b = \sigma_{alt} = 72.04 \text{ MPa}$$

$$R.F. = \frac{S_a}{\sigma_{alt} + \sigma_m \frac{S_a}{S_u}} = \frac{258}{72.04 + 40.68 \frac{258}{850}} \quad (7.6.6)$$

$$= 3.06$$

where:  $S_a$  = stress at  $10^6$  cycles

Minimum shaft diameter at the rotor:

$$d = \left[ \frac{32RF}{\pi} \sqrt{\left( \frac{k_t M}{S_e} \right)^2 + \left( \frac{k_{ts} M t}{S_y} \right)^2} \right]^{1/3} \quad (7.6.7)$$

$$= \left[ \frac{32 \times 2}{\pi} \sqrt{\left( \frac{1.8 \times 0}{425} \right)^2 + \left( \frac{1.4 \times 850000}{680} \right)^2} \right]^{1/3}$$

$$= 32.91 \text{ mm}$$

These calculations show that a shaft diameter of 50mm would adequately support the load. Bearing sizes require larger shaft diameters (60-65mm) and the resultant steps in the shaft cause high stress concentrations due to the changes in the shaft diameters, which can be reduced simply by selecting the largest possible fillet radii. This is possible at all radii except for the fillet radius at the thrust bearing which is specified as less than or equal to 2mm.

The final shaft dimensions are shown in **Drawing 3**.

## 7.7 Rotor and Stator design

### 7.7.1 Determining the axial flow velocity

The design of the turbine blades does not begin or end in a single place, rather it is a process of continuous refinement whereby the initial conditions are used as the starting block and the designer is faced with the decisions of what design factors are going to take preference. The design theory that follows may therefore, in some cases, be repeated, but with a minor or major change to a single design criteria. Drawings of the stator and rotor blades are shown in **Drawing 5** and **7** respectively.

The first stage of the design determines the area in which the blades will operate. This is pre-determined by the limitations set by the project supervisor for the pipe diameter and the required size of the nosecone.

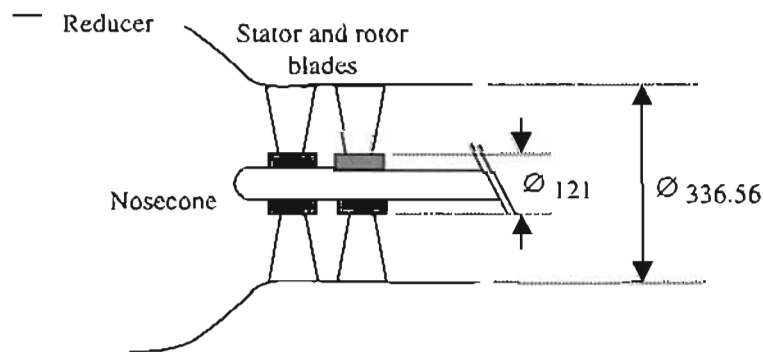


**Figure A7.7. 1 Limitations on the diameter**

$$\text{Annular area: } A_0 = A_1 - A_2 = \frac{\pi}{4} (D_1^2 - D_2^2) = 77\,465 \text{ mm}^2$$

from this value, the blade area is subtracted:

$$\begin{aligned} \text{blade area} &= \text{height} \times \text{width at thickest point} \times \# \text{ of blades} \\ &= 107.78 \times 12.2 \times 7 = 9\,204 \text{ mm}^2 \end{aligned}$$

therefore: annular area = 68 261 mm<sup>2</sup>.

The area of the blade is determined from an initial guess based on the initial blade shape determined from the program. This is also based on a first estimation. Once the annular area has been determined, the value of the axial flow is calculated:

$C_x$  in the main pipe =  $2.5\text{ms}^{-1}$

$$\rho_1 A_1 C_{x_1} = \rho_2 A_2 C_{x_2} \quad (7.7. 1)$$

$$C_{x_2} = C_{x_1} \frac{A_1}{A_2} = 2.5 \frac{\frac{\pi}{4} 400^2}{68261} = 4.60$$

Were it now assumed that 1 extra blade was used, bringing the number of blades to a total of 8, as well as assuming the following constants:

$$C_x = 8\text{ms}^{-1}, 735 \text{ rpm and } \alpha_{01} = 60^\circ;$$

$$P = Q \Delta P = (\rho A C_x) U_b \Delta C_w$$

$$(40\,000 / 8) = 1000 (77\,465\text{E-}6 / 8) \times 8 \times U_b \times (13.9 - 0)$$

$$U_b = 5000 / 1073.4 = 4.658\text{ms}^{-1}$$

which translates into: 735 rpm AT  $\alpha_{01} = 60^\circ$

$$1273 \text{ rpm AT } \alpha_{01} = 45^\circ$$

Applying Bernoulli's equation across the inlet to the outlet shown in Figure A7.7. 2:

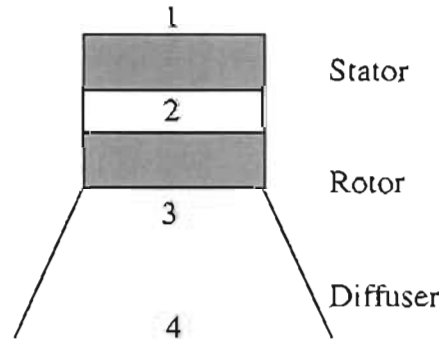


Figure A7.7. 2 Stages of turbine

$$\frac{P_{s_1}}{\rho g} + \frac{C_{x_1}^2}{2g} + z_1 = \frac{P_{s_3}}{\rho g} + \frac{C_{x_3}^2}{2g} + z_3 + h_{f_{1-3}} + \frac{U_b C_w}{g} \quad (7.7. 2)$$

$$h_f = \frac{4fLu^2}{2dg} \quad (7.7. 3)$$

$$U_b = \frac{40000}{1000 \times 0.0774651 C_x \Delta C_w} \quad \text{from Eq (7.7. 1)}$$



$$\frac{U_b C_w}{g} = \frac{40000}{77.4651gC_x} \quad \text{from Eq (7.7. 1) and Eq (7.7. 2)}$$

$$10 + \frac{C_{x1}^2}{2g} = 2 + \frac{C_{x3}^2}{2g} + h_{f12} + h_{f1-3} + \frac{40000}{77.4651gC_{x2-3}}$$

recall that:

$$C_{x1} = 2.5 \text{ms}^{-1} \text{ at } A_1 = (\pi/4)(0.400)^2$$

$$C_{x3} = ? \text{ ms}^{-1} \text{ at } A_3 = (\pi/4)(0.33656)^2$$

$$C_{x2-3} = ? \text{ ms}^{-1} \text{ at } A_{2-3} = (\pi/4)(0.33656^2 - 0.121^2) - 8 \times 1315/1000^2$$

These values can then be determined from continuity of the mass flow:

$$\dot{m} = \rho A C_x \quad \rho = \text{const.}$$

$$\text{Thus: } A_1 C_{x1} = A_3 C_{x3} \Rightarrow C_{x3} = C_{x1} (A_1 / A_3) = 3.531 \text{ms}^{-1}$$

$$A_1 C_{x1} = A_{2-3} C_{x2-3} \Rightarrow C_{x2-3} = C_{x1} (A_1 / A_{2-3}) = 4.692 \text{ms}^{-1}$$

These results do not include the effects of friction losses and can therefore only be taken as estimates.

If it were to be assumed that  $C_x$  is constant throughout each stage then the equation becomes:

$$10 + \frac{C_{x1}^2}{2g} = 2 + \frac{C_{x1}^2}{2g} + 0.8 + 1.2 + \frac{52.636}{C_{x1}} \quad (7.7. 4)$$

$$C_{x1} = 8.773 \text{ms}^{-1}$$

### 7.7.2 Determining the solidity

The current design of blading has 0 incidence. The reason for this is that the stator blades are not required to generate lift, only to change the direction of the fluid flow. Since the only two forces operating on the blade are turning of the flow and drag, it is possible to optimise drag such that it is at a minimum. The drag is seen to increase both above and below the optimal lift coefficient caused by flow around the leading edge and the corresponding momentum loss in the boundary layer. This means that the drag is a minimum at the optimum lift coefficient. Hoerner (1965) describes the optimum lift coefficient as being:

$$C_{l_{opt}} = (10 \rightarrow 12) \frac{f}{c} \quad (7.7.5)$$

for fluid flow which intercepts the nose smoothly. Then relating the flow as a function of  $[\alpha]$ , Hoerner (1965):

$$Cl = 2\pi \sin(\alpha + 0.5\gamma) \quad (7.7.6)$$

where:  $\alpha$  = angle of attack and

$\gamma$  = angle of the trailing edge against the chord line of the arc

Thus solving for  $\alpha$ :

$$\alpha = a \sin\left(\frac{10 \rightarrow 12 f/c}{2\pi}\right) - 0.5\gamma \quad (7.7.7)$$

It should be noted at this point that the  $f/c$  ratio may differ even though both  $f$  and  $c$  vary as a function of the radial location along the blade because the circular arc radius changes with the radius of the blade – or the blade aspect.

Applying the values from the program directly to Eq (7.7. 7):

$$\alpha = a \sin\left(\frac{10 \rightarrow 12 f/c}{2\pi}\right) - 0.5\left(\frac{\text{alpha}(i)}{2}\right) \quad (7.7.8)$$

which yields the required values of  $\alpha$ . These values, whether positive or negative would be the values added to the angles of incidence of the blade, essentially creating an offset to account for the flow deviation, for the purpose of optimum lift.

Due to the magnitude of the flow deviations, it was assumed that they were negligibly small and the following applied:

$$\sigma = \frac{2 \sin \theta}{\psi_z \cos \gamma} \left( \frac{\cos \alpha_1}{\cos \alpha_2} \right) \quad (7.7.9)$$

where:  $\sigma$  = chord to pitch ratio

$\theta$  = blade element deflection

$\alpha_1$  = inlet angle ( assuming flow deviation = 0 )

$\alpha_2 =$  outlet angle ( assuming flow deviation = 0 )

$\gamma =$  stagger angle

$\psi_z =$  Zweifel loading coefficient = 0.8 for minimum loss

Since Eq (7.7.9) is defined for cascade geometry, [ g ] is typically measured in the plane. When applied to a rotor hub, the measurement would be taken according to an arc length.

### 7.7.3 Characteristics of the diffuser

The object of the diffuser is to create a negative pressure gradient at 3, see Figure A7.7. 2, and hence increase the pressure difference from 1-3, which results in an increase in the work output. The typical Bernoulli equation is:

$$\frac{P_{s_3}}{\rho g} + \frac{V_3^2}{2g} + z_3 = \frac{P_{s_4}}{\rho g} + \frac{V_4^2}{2g} + z_4 + h_{3-4} \quad (7.7. 10)$$

where:  $z_3 = 1.5$

$z_4 = 0$

$P_{s_4}/\rho g = 0$

The function of the draft tube being to reconvert the kinetic energy into a flow energy, is achieved by a gradual expansion of the flow cross-section. Applying Bernoulli between the two ends of the draft tube shows that the action of the tube reduces the pressure at the draft tube inlet to below atmospheric. Thus increasing the effective head across the runner to the difference in elevation between head and tail water, less the losses. Hence from Eq (7.7.10):

$$\frac{P_{s_3}}{\rho g} = \text{losses} - \frac{V_3^2}{2g} - z_3 + \frac{V_4^2}{2g} \quad (7.7. 11)$$

$z_3$  becomes defined by cavitation criteria. The value of  $z_3$  determines the pressure at 3 and hence the cavitation index.

The minimum pressure in a pump or turbine generally occurs along the convex side of the blades or near the low pressure side of the impeller. If [ e ] is the point of minimum

pressure, the energy equation applied between [ e ] and the downstream liquid surface can be written as:

$$\frac{P_c}{\rho g} + \frac{V_c^2}{2g} + z_s = \frac{P_a}{\rho g} + 0 + 0 + h_L \quad (7.7. 12)$$

where:  $P_a$  = atmospheric pressure

$P_c$  = absolute pressure at cavitation,  $P_c = P_v$

$P_v$  = vapour pressure

$$\sigma' = \frac{V_c^2}{2gH} = \frac{P_a - P_v - \rho g z_s + \rho g h_L}{\rho g H} \quad (7.7. 13)$$

= ratio of available energy at [ e ] to the total energy across the unit.

$\sigma' = \sigma_{crit}$  for design phase, where  $\sigma_{crit}$  is determined from test data on a model turbine of homologous series and assume that  $h_f$  is defined by Eq (7.7. 3).

The worst case of cavitation occurs when the pressure recovery through the diffuser is at a minimum. This phenomenon is caused by the combination of the conversion of kinetic energy into potential energy and the associated losses. Analysis of Eq (7.7. 11) shows that losses should be at a minimum in order to reduce  $P_3$  to its lowest possible value.

For very small angles the diffuser is excessively long and most of the head loss is due to the wall shear stress as in fully developed flow. For moderate or large angles, the flow separates from the walls and the losses are mainly due to a dissipation of the kinetic energy of the jet leaving the small diameter pipe. As with many minor loss situations, it is not the viscous effects that directly cause the losses. Rather, it is the dissipation of kinetic energy as the fluid decelerates inefficiently. The loss may be quite different if the contraction or expansion is gradual.

There is an optimal angle (  $\theta = 8^\circ$  for the case shown ) for which the loss coefficient is a minimum. The relatively small angle for the minimum  $k_L$  results in a long diffuser. The conditions illustrated in Figure A7.7. 3 represent the typical results only, and the real flow through a diffuser may also be dependant on:

- 1)  $A_2 / A_1$  ratio
- 2) Specific details of the geometry
- 3) Reynolds number

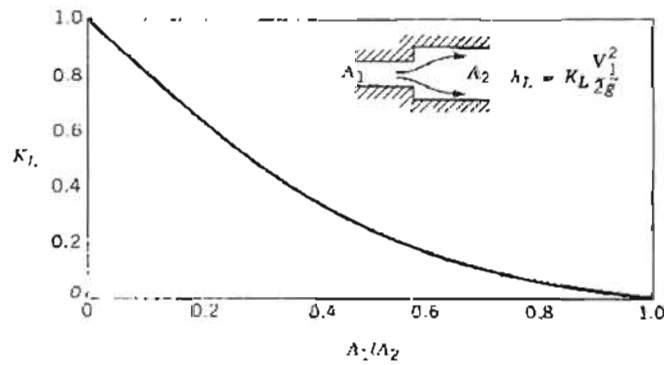


Figure A7.7. 3 Loss coefficient for a sudden expansion, Munson (1990)

#### 7.7.4 Design considerations

Geometric similitude is required to use scaled models in designing turbo machines as well as geometrically similar velocity diagrams. At entry to and exit from the impeller, viscous effects must unfortunately be neglected as it is generally impossible to satisfy the two aforementioned conditions and have equal Reynolds Number in the model and prototype. Two geometrically similar units, having similar velocity vector diagrams are homologous and they will also have geometrically similar streamlines.

The following analysis uses the Hill Curves, Warnick (1984), from Figure 2.4.2 to develop the relationship between the values of flow [  $Q_{wd}$  ], energy [  $E_{wd}$  ] and power [  $P_{wd}$  ] coefficients. It was firstly determined that the turbine would operate in the region of 90% efficiency and this yielded a range of the values for the coefficients:

$$@ \eta_{oa} = 89.9\% : \quad Q_{wd} = \begin{matrix} 0.08 \\ 0.04 \end{matrix} \quad E_{wd} = \begin{matrix} 0.073 \\ 0.043 \end{matrix} \quad P_{wd} \begin{matrix} 0.0045 \\ 0.002 \end{matrix}$$

with:  $H = 12\text{m}$ ;  $D = 0.33656\text{m}$  and  $P = 40\text{kW}$

Since the values of head, diameter and power have been pre-set by the location of the turbine site, what remains is to determine a suitable operating speed. Looking firstly at the energy coefficient:

$$\omega D = \sqrt{\frac{gH}{E_{\omega d}}} \Rightarrow rpm = \sqrt{\frac{gH}{E_{\omega d}} \frac{60}{2\pi D}} = \begin{vmatrix} 1139 \\ 1485 \end{vmatrix} \quad (7.7. 14)$$

Then considering the power coefficient:

$$P_{\omega d} = \frac{P}{\rho \omega^3 D^5} \Rightarrow rpm = \sqrt[3]{\frac{P}{P_{\omega d} \rho D^5} \frac{60}{2\pi}} = \begin{vmatrix} 1215 \\ 1592 \end{vmatrix} \quad (7.7. 15)$$

And finally the flow coefficient:

$$Q_{\omega d} = \frac{Q}{\omega D^3} \Rightarrow rpm = \frac{Q}{Q_{\omega d} D^3} \frac{60}{2\pi} = \begin{vmatrix} 1565 \\ 3131 \end{vmatrix} \quad (7.7. 16)$$

Each of these coefficients yield a different value for the rpm, which shows that it will not be possible to satisfy the peak performance efficiency for each coefficient. Rather, it should be understood that a trade-off will exist between the coefficients and it is up to the designer to determine which coefficient will take preference in the design. If these values are then cross-checked with the typical mechanical and hydraulic efficiencies and turning angle where:  $P = 40\text{kW}$ ;  $H = 12\text{m}$ ;  $D_0 = 0.33656\text{m}$ ;  $D_i = 0.121\text{m}$

with the number of blades = 8

which implies a total blade area of  $0.0105\text{m}^2$

$\eta_{\text{hyd}} = 0.9$ ;  $\eta_{\text{mech}} = 0.95$ ;  $\alpha = 70^\circ$ .

$$\eta_{ca} = \eta_{\text{hyd}} \times \eta_{\text{mech}} = 0.9 \times 0.95 = \frac{\dot{m} U_b \Delta V_\theta}{Q \Delta P} \frac{40000}{\dot{m} U_b \Delta V_\theta}$$

$$\Rightarrow Q \Delta P = Q \gamma H = Q \times 9810 \times 12 = \frac{40000}{0.855}$$

$$\Rightarrow Q = 0.3974 \text{m}^3 \text{s}^{-1}$$

The velocity can then be simply calculated from:

$$C_x = \frac{Q}{A} = \frac{0.3974}{\frac{\pi}{4} (0.33656^2 - 0.121^2) + 0.0105} = 4.517 \text{ms}^{-1}$$

$$\Delta V_\theta = C_{w_2} - C_{w_1} = C_{w_2} = C_x \tan(70^\circ) = 12.41 \text{ms}^{-1}$$

$$\dot{m} U_b \Delta V_\theta = \frac{40000}{0.95} \Rightarrow U_b = \frac{40000}{0.95 \times 397.4 \times 12.41} = 8.538 \text{ms}^{-1}$$

$$U_b = \frac{\pi D_1 rpm}{60} \quad \Rightarrow \quad rpm = \frac{60 \times 8.538}{\pi \times 0.121} = 1347.6$$

This check has shown that the value of rpm falls within the range of both the energy and power coefficients and the value of rpm can be assumed to be within this range.

If the design were to be approached from a best efficiency ratio, the design would proceed as follows at 90% efficiency:

$$Q_{\omega d} = 0.058; \quad E_{\omega d} = 0.06; \quad P_{\omega d} = 0.0032$$

And assuming: P = 40kW and D = 0.33656m

$$\omega = \sqrt[3]{\frac{P}{\rho D^5 P_{\omega d}}} \Rightarrow rpm = \frac{60}{2\pi} \sqrt[3]{\frac{40000}{1000 \times 0.33656^5 \times 0.0032}} = 1361 rpm$$

$$\text{optimal } H = \frac{E_{\omega d} \omega^2 D^2}{g} = \frac{0.06 \times 142.517^2 \times 0.33656^2}{9.81} = 14.07 m$$

$$\text{optimal } Q = Q_{\omega d} \omega D^3 = 0.058 \times 142.517 \times 0.33656^3 = 0.315 m^3 s^{-1}$$

This means that the diameter of the turbine is a problem when attempting to design from a best-efficiency point of view. And since the diameter has already been set, it is necessary to consider the design from a different perspective. In order to determine the correct diameter when given only the power and the flow rate, the flow and power coefficients were combined to yield the following result:

$$Q_{\omega d} = \frac{Q}{\omega D^3} \quad \Rightarrow \quad \omega = \frac{Q}{Q_{\omega d} D^3}$$

and substituting this into the power coefficient:

$$P_{\omega d} = \frac{P}{\rho \omega^3 D^5} = \frac{P}{\rho \left( \frac{Q}{Q_{\omega d} D^3} \right)^3 D^5}$$

to solve for:

$$D = \sqrt[3]{\frac{P_{\omega d} \rho Q^3}{P Q_{\omega d}^3}} = \sqrt[3]{\frac{0.0032 \times 1000 \times 0.5^3}{40000 \times 0.058^3}} = 0.4758 m$$

which is the typical value of the runner diameter for the optimal power and flow coefficients. Considering that the existing diameter is 0.33656m, the optimal design of the larger diameter allows for more flow through the penstock and the potentially lower values governing the velocity triangles will lead to lower friction losses seen in the boundary layer flow. The larger diameter would also allow for a lower rpm, which would reduce the probability of cavitation occurring.

However, the option of maintaining the flow rate at  $0.5\text{m}^3\text{s}^{-1}$ , where the diameter is fixed at 0.33656m and assuming a rotational speed of 735 rpm – a speed assumed from typical values of similar turbines – then it is found that:

$$Q_{opt} = 0.0193$$

And checking this value against the Hill Curves, Warnick (1984), it is seen that an efficiency of 87% can still be attained. However, to remain within this range, the head should be within the limits of:

$$E_{opt} = \begin{cases} 0.095 \\ 0.03 \end{cases} \Rightarrow H = \begin{cases} 6.498\text{m} \\ 2.052\text{m} \end{cases}$$

and the power must correspondingly exist within:

$$P_{opt} = \begin{cases} 0.007 \\ 0.001 \end{cases} \Rightarrow P = \begin{cases} 13.783\text{kW} \\ 1.969\text{kW} \end{cases}$$

However, it is possible to develop higher power and apply higher heads, but with the efficiency declining to approximately  $\eta_{oa} = 70\%$ .

As discussed in section 3.9.2, the following equation, Brown (1970) tends to yield the best results with minimum losses:

$$\frac{D_2^3 n}{Q} = 85...115 \tag{7.7. 17}$$

in conjunction with the values:

$$D_2 = 0.33656; n = 735\text{rpm}; \Rightarrow Q_{85} = 0.3297 \\ Q_{115} = 0.2436 \text{ m}^3\text{s}^{-1}$$



And substituted into:

$$P = Q\Delta P = 0.3597 \times 9810 \times 10 = 32.373 \text{ kW}$$

According to the Hill Curves, Warnick (1984):

$$P_{wd} = \frac{P}{\rho \omega^3 D^5} = \frac{32373}{1000 \times \left( \frac{2\pi}{60} 735 \right)^3 \times 0.33656^5} = 0.0164 \quad (7.7.18)$$

This power coefficient corresponds to an overall efficiency of approximately 80%.

If  $D_2$  were fixed at a diameter of 0.33656m and  $Q$  were fixed at  $0.5 \text{ m}^3 \text{ s}^{-1}$ :

$$n_{85} = 1114.8 \text{ rpm}$$

$$n_{115} = 1508 \text{ rpm}$$

Whereby:

$$P = Q\Delta P = Q\gamma H = 0.5 \times 9810 \times 10 \times 0.9 = 44.145 \text{ kW}$$

$$P_{wd} = \frac{P}{\rho \omega^3 D^5} = \frac{44145}{1000 \times \left( \frac{2\pi}{60} 1115 \right)^3 \times 0.33656^5} = 0.00642$$

This power coefficient corresponds to a maximum overall efficiency of approximately 88%. Repeating the above step:

$$P = Q\Delta P = Q\gamma H = 0.5 \times 9810 \times 10 \times 0.88 = 43.164 \text{ kW} \quad (7.7.19)$$

$$P_{wd} = \frac{P}{\rho \omega^3 D^5} = \frac{43164}{1000 \times \left( \frac{2\pi}{60} 1115 \right)^3 \times 0.33656^5} = 0.0063$$

$$\begin{aligned} \text{But: } P = Q\Delta P &= \dot{m} U_b \Delta C_w \eta_{oa} = \dot{m} U_b (C_{w_2} - C_{w_1}) \eta_{oa} \\ &= 500 \times (\pi \times 0.121 \times 1115 / 60) (C_x \tan(\alpha)) \times 0.88 \end{aligned}$$

$$\text{where: } C_x = Q / A = 0.5 / (\pi/4)(0.33656^2 - 0.121^2) \times 0.9 = 7.172 \text{ ms}^{-1}$$

$$\alpha = \arctan \left( \frac{P_s 0.88}{\dot{m} U_b C_x} \right) = 59.6^\circ$$

The error with such a design is that the runner speed is too high. Typical propeller turbines run in the region of 200 – 300rpm, although this may be increased; for smaller turbines in the microhydro turbine category, and furthermore should the diameter be reduced to below standard efficient diameters. The turning angle is within the typical angle of 67°. It is not likely to result in localised cavitation at the trailing edge of the inlet guide vanes, which would reduce flow area and momentum and result in a loss in power.

The problem with such high runner speeds is that the off-design running conditions cause high losses due to incoherence of the blade angle with the flow angle. As shown in Figure 2.4.5, the efficiency can decrease by as much as 20% for a 30% decrease in the rated power. These losses are caused by shock loading of the runner blade increasing the likelihood of cavitation on the runner blade leading edge, particularly at the tip diameter. The corresponding flow and energy coefficients are:

$$Q_{\omega d} = \frac{Q}{\omega D^3} = \frac{0.5}{\left(\frac{2\pi}{60} \times 1115\right) 0.33656^3} = 0.1123 \quad (7.7. 20)$$

$$E_{\omega d} = \frac{gH}{(\omega D)^2} = \frac{9.81 \times 10}{\left(\frac{2\pi}{60} \times 1115 \times 0.33656\right)^2} = 0.0635 \quad (7.7. 21)$$

The flow and energy coefficients show potential maximum efficiencies of 88% and 89.5% respectively. According to the relation given by deSiervo and deLava, Warnick (1984), the diameter of the runner is given by:

$$\begin{aligned} D_M &= \left(66.76 + 0.136N_v\right) \frac{\sqrt{H}}{n} \quad (7.7. 22) \\ &= \left(66.76 + 0.136 \frac{1115\sqrt{49.05}}{10^{5/4}}\right) \frac{\sqrt{10}}{1115} \\ &= 0.3588\text{m} \end{aligned}$$

The diameter as determined from the power and flow coefficients at maximum efficiency is given by:

$$D = \sqrt[4]{\frac{P_{axl} \rho Q^3}{P Q_{axl}^3}} = \sqrt[4]{\frac{0.0032 \times 1000 \times 0.5^3}{43164 \times 0.058^3}} = 0.4668m \quad (7.7. 23)$$

Hence according to the above relations, the diameter is incorrectly proportioned to the flow rate and required power output. Should this diameter have been used, the runner speed would operate at a more conventional value as given by:

$$\omega = \sqrt[3]{\frac{P}{\rho P_{axl} D^5}} = \sqrt[3]{\frac{43164}{1000 \times 0.0032 \times 0.4668^5}} = 809rpm \quad (7.7. 24)$$

This value of speed is shown to be suitable for the relationship of power and flow rate as well as the head of 10m. This combination of values should yield an overall efficiency of 90%.

The Hill Curves, Warnick (1984) have been developed according to hydroelectric schemes that are typically greater than 1000kW. Due to the difference in the Reynolds Number's between model and prototype, the model turbine tends to have a lower efficiency than the prototype. However, in real situations it is found that no precise equality exists between the model and prototype with regard to the efficiency primarily due to the differences in boundary layer friction and turbulence effects. The following equation, Warnick (1984) attempts to give some relation:

$$\frac{\eta_p}{\eta_m} = 1 - K \left[ 1 - \left( \frac{R_m}{R_p} \right)^{1/\alpha} \right] \quad (7.7. 25)$$

where: K = a coefficient shown to vary from 0.5 to 0.81

$R_m$  = Reynolds Number for the model turbine

$R_p$  = Reynolds Number for the prototype turbine

Figure A7.7. 4 shows the difference between a model and a full size turbine. To a limited extent this relationship can be extended to two turbines of hydraulic similarity, such as

the model turbine and the prototype. The turbine under design construction is thus considered as a model turbine having a lower efficiency than that rated by the turbine of hydraulic similitude as is given by the Hill Curves, Warnick (1984).

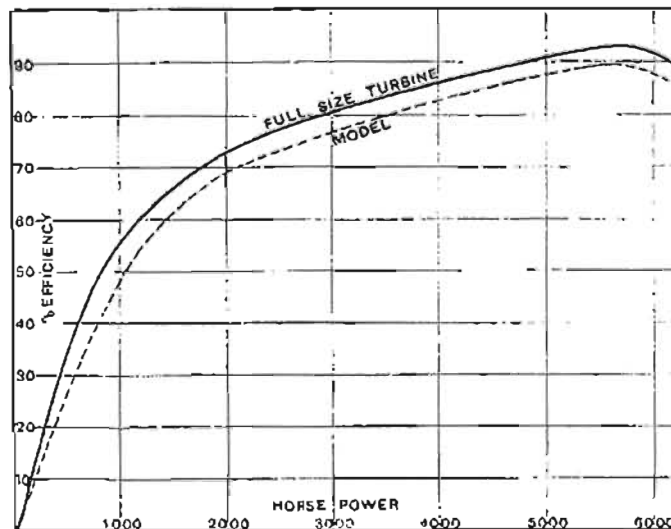


Figure A7.7. 4 Efficiency curves of Francis turbine developing 6000hp at 116rpm, with a head of 49ft, Gibson (1922)

Once the preliminary design of the hub and blades has been set, the design needs to be reviewed with respect to the design of the diffuser. The diffuser or draft tube cannot be considered or designed separately to the turbine. This is particularly important for low head systems, where the kinetic energy leaving the turbine is usually a large part of the total head available. Since the cavitation parameter is defined as the ratio of static to dynamic suction head, the turbine design and setting are determined by observing the pressure and velocity at the critical areas. Because the turning of the inlet guide vanes is below the standard turning angle it will be assumed that the reduction in pressure is minimal, having resulted from the friction losses related to the Reynolds Number across the blades.

The first method of turbine setting is according to the specific speed  $N_s$ , as is the turbine capacity selection. Applying the fact that turbines of similar homologous series have similar geometric designs and hydraulic conditions, it is suffice to say that they shall have similar plant sigmas. The curves shown in Figure 2.4.8 have been plotted 0.3m below the value at which cavitation damage occurs allowing for a reasonable safety margin, as

allowance for variation in atmospheric pressure and changes in head and/or tail water elevation.

Using the equation, Warnick (1984):

$$\sigma = \frac{h_a - h_v - h_s}{h} \quad (7.7. 26)$$

where:  $h_a$  = atmospheric pressure head

$h_v$  = vapour pressure head

$h_s$  = difference in elevation

$h = H_{\text{net}}$

$\sigma$  = cavitation coefficient

However, another experience curve is necessary to relate the turbine setting elevation,  $h_s$ , to the centreline of the turbine distributor or in the case of the horizontal axis turbines, to the point at the top of the turbine runner, i.e.  $b = \frac{1}{2} D_0$ .

The equations that follow were derived from Figure 3.9.8:

$$h_b = h_a - h_v = 9.180m - 0.324m = 8.856m \quad (7.7. 27)$$

$$h_s = h_b - \sigma h_{cr} = 8.856 - \left( \frac{411^{1.64}}{50227} \right) 10 = 5.003m \quad (7.7. 28)$$

$$z = h_s + b = 5.003m + \frac{1}{2} 0.33656 = 5.172m \quad (7.7. 29)$$

Diffusers designed at  $8^\circ$  in preference to  $12^\circ$  are typically smaller turbines having higher inlet velocities into the diffuser and hence requiring a higher pressure recovery or a longer diffuser.

Another method given by a turbine manufacturer as a general rule of thumb; the submergence of the centreline should be:

$$z = -kD \quad (7.7. 30)$$

where:  $z$  = total suction head

$$k = 0.5 \text{ at } 10\text{m } H_{\text{net}}$$

$$= 1.0 \text{ at } 30\text{m } H_{\text{net}}$$

$D$  = runner diameter

From Eq (7.7.33) above,  $h_{\text{cr}} = h_{\text{cr}}(h_s)$  and  $N_s = N_s(h_s)$ , hence the equation is recalculated to convergence:

$$P = Q\gamma H = 0.5 \times 9810 \times 15.172 \times 0.88 = 65488W$$

$$h_s = 8.856 - \frac{\left( \frac{1115\sqrt{65.488}}{15.172^{3/4}} \right)}{50227} 15.172 = 5.343m$$

repeating the above equations for the increased power available caused by the increase in head:

$$P = Q\gamma H = 0.5 \times 9810 \times 15.343 \times 0.88 = 66226W$$

$$h_s = 5.35246m \quad \Rightarrow \text{convergence}$$

The exact value of convergence turns out to be:

$$h_s = 5.353m$$

The new value of the pressure differential across the penstock needs to be checked against the critical design condition, which is the limit of the load on the thrust bearing:

$$P = \frac{F}{A} = \frac{0.1MPa \times \frac{\pi}{4} \times 400^2}{\frac{\pi}{4} 336.56^2} = 0.1197MPa$$

which translates into 11.97m head.

This pressure may still be marginally exceeded since the selection of the thrust bearing is based on  $F_{\text{running}} = 2 \times F_{\text{theoretical}}$  and increasing the head to 15.4m will still maintain the rated thrust bearing capabilities within the design limit. But, the closer the head is to the safety factor design limit, the more likely the design is to fail upon overload of the system such as may occur with water hammer. Water hammer is associated with the controlling or governing of the turbine which is outside the author's scope of research, but which remains a consideration of the design criteria.

The limitation of the power is then checked against the ability to take power out of the flow:

$$P = \dot{m} U_b \Delta C_w = 500 \times \left( \frac{\pi \times 0.121 \times 1115}{60} \right) \times \{7.172 \tan(\alpha)\} \quad (7.7.31)$$

$$P = Q \gamma H \eta_{ns} = 0.5 \times 9810 \times 15.353 \times 0.88 = 66270W \quad (7.7.32)$$

$$\Rightarrow \alpha = 69.08^\circ$$

This value of  $\alpha$  remains within the typical values of the angle of the absolute velocity exiting from the inlet guide vanes and is therefore acceptable. Hence the maximum power available at  $Q=0.5\text{m}^3\text{s}^{-1}$  and 10m supply head is given by Eq (7.7.24).

A common procedure of another company is to chose a setting lower than  $h_s$  by a safety margin given by:

$$|\Delta h_s| = \Delta \sigma |H| \quad (7.7.33)$$

where:  $\Delta \sigma = 0.1$  for low specific speed turbines

$= 0.2$  for high specific speed turbines

$$\Rightarrow |\Delta h_s| = 0.2 \times |15.353| = 3.0706m$$

This change in  $h_s$  is to account for the inaccuracies in manufacturing. Hence the final value of  $H_{net}$  is:

$$H_{net} = 15.353 - 3.0706 = 12.2824m$$

### 7.7.5 Determining a suitable rotor speed

The increase in area of the draft tube needs to occur below a certain rate, to avoid boundary layer separation and hence eddy losses occurring within the tube. This results in an irrecoverable head loss in the draft tube. However, it is necessary to attain the maximum pressure recovery so as to gain a higher  $H_{net}$  from the dynamic suction head. According to Brown (1970); "The best efficiency of a Kaplan or propeller turbine does

not occur with axial flow from the runner, but with a small swirl component in the same direction as the runner.”

The recovery of the dynamic suction head contributes to the overall head in the form of:

$$\eta_D \frac{V_2^2}{2g}$$

where  $\eta_D$  is the coefficient of recovery of the efficiency of the draft tube.

	K	2	5	10	15	20	30	40	50	60	70	80	90
Circular Pipe	K	.20	.13	.18	.27	.43	.75	.91	1.05	1.12	1.12	1.10	1.07
Rect. pipe (with one pair of parallel sides)	K	-	.31	.18	.29	.48	.90	1.10	-	-	-	-	-

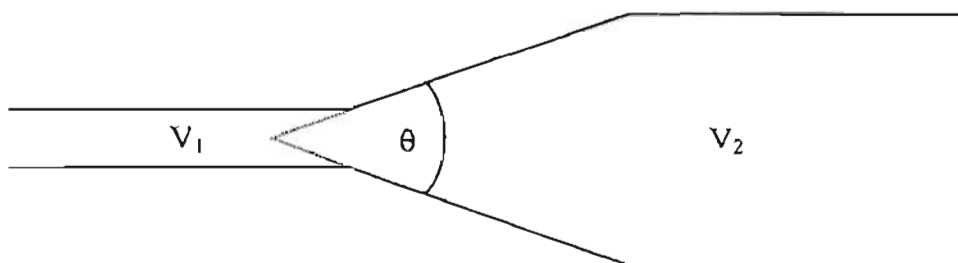


Figure A7.7. 5 Graduating the reduction in velocity, Gibson (1922)

Consider Figure A7.7. 5, the losses are at a minimum when [ k ] is at a minimum and the change in  $V_1$  and  $V_2$  tends to 0. Even though the losses  $\Rightarrow 0$  as  $V_1$  and  $V_2 \Rightarrow 0$ , the highest pressure recovery occurs as  $V_2 \Rightarrow 0$  and hence the efficiency of the draft tube is used to minimise the losses. This occurs as  $k \Rightarrow 0$  and is found to occur between  $5^\circ$  and  $10^\circ$ . Text supporting the minimum of [ k ] points out that this angle is typically  $8^\circ$ .

The correct form of the draft tube is more important for turbines having high specific speeds, since the dynamic suction head becomes an increased percentage of the overall pressure. The types of losses in a turbine are generated by:

- 1) partial recovery of the discharge velocity pressure head
- 2) skin friction across the runner blades



- 3) eddies at the runner blade inlet and outlet
- 4) water leakage past seals, and runner blade tip
- 5) friction losses in the bearings and shaft gland
- 6) friction losses in the penstock, reducer and draft tube

Only the first two losses are directly dependant on the runner, which must then be designed to obtain a minimum sum of the losses. The losses of 1)  $\Rightarrow 0$  as the absolute velocity at the runner exit decreases, which is achieved by having a large exit diameter. However, increasing the exit diameter results in an increase in blade area and decreases the exit angles resulting in high skin friction losses and relative velocities.

“The best compromise is reached when suitable exit angles are chosen, and practise indicates that this is so when the value of  $D_2^3 n / Q$  lies between the values 85 and 115, depending on the finish of the blades and the efficiency of the draft tube.” Brown (1970) Since the flow rate [  $Q$  ] and diameter [  $D_2$  ] have already been set by the available flow rate at the site and the partial fabrication of the reducer, pipe bend and bearing housing respectively, it remains then to determine the runner rpm. In practise, the runner rpm and [  $Q$  ] should be set, with diameter  $D_2$  being the independent variable, but in this case runner rpm is taken as the dependant variable. From Eq (7.7. 17):

$$n_{85} = \frac{85 \times Q}{D_2^3} = 1115 \text{ and}$$

$$n_{115} = \frac{115 \times Q}{D_2^3} = 1508$$

where:  $D_2$  = runner diameter [m] = 0.33656;

$Q$  = flow rate [ $\text{m}^3 \text{s}^{-1}$ ] = 0.5;

It was determined to select the lowest possible rpm since high velocities through the runner cause high friction losses and may result in cavitation, since cavitation is a function of the static and dynamic pressures.

Using Hill Curves, Warnick (1984) to attempt to arrive at a similar ratio as that given above by using the governing equations: Eq (7.7. 17) and Eq (7.7. 20).

$$Q_{ad} @ 89.5\% \left| \begin{array}{l} @ n_{ss} 0.08 \\ @ n_{115} 0.042 \end{array} \right.$$

$$\frac{\omega D^3}{Q} = \left| \begin{array}{l} 23.8 \\ 12.5 \end{array} \right. \times \frac{60}{2\pi} \Rightarrow \left| \begin{array}{l} 227.4 \\ 119.4 \end{array} \right.$$

The higher values obtained by the Hill Curves, Warnick (1984), show higher ratios of diameter  $D_2$  to flow rate  $Q$  for a fixed rpm. Where a large diameter exists, with a low flow rate, the power is based primarily on the static pressure head, rather than on high axial velocities within the inlet guide vanes and runner. Examples from Table 3.3 show that the average head is 18.33m for many of the examples, which have close to the optimum power coefficient. It will be assumed that the ratio of  $D_2^3 n / Q = [85, 115]$  is more suited to the application of low head, high flow rate for which the power is derived from high axial velocities through the blades. This is the application of the turbine to be designed and the design method will not be adjusted.

#### 7.7.6 Cavitation

It should be noted that as the head water or forebay water level rises and the tailwater lowers, a difference in the operating and design heads develops. This condition has to be accounted for in the design of the turbine setting.

The occurrence of cavitation and its inception is usually associated with an increase in noise vibration and loss of performance of the turbine. It is difficult to determine where the cavitation starts because the vapour bubbles may grow rapidly and be washed downstream where they collapse and cause damage through pitting. It is not unusual to study and interpret cavitation by modelling and then relate the plant sigma to the loss in efficiency and power or to turbine coefficients such as unit power or unit discharge. In testing models, the usual coefficients against which plots of cavitation are developed, are:

- 1) turbine efficiency
- 2) power output
- 3) unit discharge

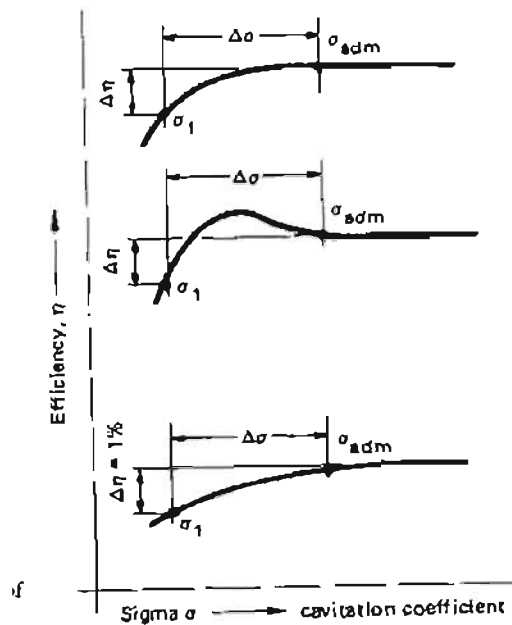


Figure A7.7. 6 Various shapes of cavitation coefficient curves, , Warnick (1984)

Criteria are developed from these plots that are used to develop turbine setting heights and to identify allowable values of the plant sigma [  $\sigma$  ]. Figure A7.7. 6 illustrates the curves which characterise the different graphs associated with turbine testing. Indicated, is the method by which the allowable plant sigma is determined by setting an admissible change in sigma that must be added to the critical sigma [  $\sigma_{cr}$  ], which is typically the cavitation coefficient where the efficiency has decreased by 1%.

In most instances, the variation in the plant sigma gives a greater change in the turbine efficiency for tests on models than that which occurs in the prototype units. Hence the cavitation identified in the model tests will usually be greater than what can occur in homologous prototype units.

### 7.7.6.1 Control of cavitation

There are several ways of controlling cavitation. The most effective being the control of the setting of the runner so that the pressure and velocity at the critical areas in the system do not allow for excessive cavitation to occur. The turbine setting is not simply a function

of dimensions, but may include an element of economics as it is important to consider the design costs of how high above or far below the tailwater to set the turbine. The costs are incurred when attempting excavations or concrete pylons in order to accommodate the turbine dynamics. In some cases, it has been economically viable to allow some cavitation, using a material more resistant to cavitation pitting, or to repair the damage in preference to selecting the correct setting.

Machines of typically high specific speed are limited to low heads because of cavitation but it can be prevented by keeping the turbine setting within the limit of  $H_s$  as given by:

$$H_s \leq H_B - \sigma_c H \quad (7.7. 34)$$

where:  $H_B$  = height of barometric water column;

$\sigma_c$  = critical sigma;

$H$  = head

Because  $\sigma_c$  is dependent on the dynamic suction head, a decrease in the runner diameter must correspond to a lowering of the turbine setting due to the increase in the draft tube inlet velocity causing higher losses and reducing the pressure recovery.

In some cases, the blades themselves are coated with a resistant layer to prevent corrosion of the blades, or fins are added to the turbine blade tip to reduce the velocity causing cavitation. Furthermore, a thin layer of hydrogen could also be used to stop pitting.

An indirect design compensation can be applied by the selection of the runner speed. An increase in the speed of the runner results in smaller diameters and a corresponding increase in the velocities through the turbine stator and rotor, which may however cause an increase in cavitation potential. In order to compensate for this, it will be necessary to set the turbine lower with respect to the tailwater. Thus determining the correct turbine setting is an important and complex problem relating to several levels of design and operation.

This point is particularly important when considering that an analysis, applying the existing design variables of  $P = 40\text{kW}$ ,  $Q = 0.5\text{m}^3\text{s}^{-1}$  and  $D_0 = 0.33656\text{m}$ , showed that  $D_0$  was too small when compared to the values coherent with high efficiency turbines. This is likely to increase the potential for cavitation due to the high water velocities in the runner. Since at this stage in the design when much of the turbine has already been designed and manufactured, it is not possible to change the power, flow rate or tip diameter. The only remaining design parameter is the turbine setting or the choice of  $h_s$ , where  $h_s$  = the difference between the minimum tailwater and the cavitation reference point of the outflow from the turbine.

Due to the inconsistency of the diameter in relation to the power and flow rate as given by the Hill Curves, Warnick (1984), it will be expected that the design of the draft tube will also follow a non-standardised construction. This is expected to entail a shorter draft tube and since large angles induce high losses, much of the velocity potential leaving the draft tube will be irrecoverable. Standard construction of the draft tube is shown in Figure 2.4.9. The values which would normally be applied are  $D = 0.33656$ ,  $2D = 0.67312$  and  $4D = 1.34624\text{m}$ , in comparison to the standardised values of  $D = 0.4758$ ,  $2D = 0.9516$  and  $4D = 1.9032$ .

The pressure recovery in the draft tube can occur gradually, i.e. a gradual increase in cross-sectional area, otherwise a poor  $\eta_D$  develops due to the dead water and back flows, such as separation and eddies. The cross-sectional increase such that the flow irregularities have minimal effect must satisfy the general rule of:

$$0.12l \langle \sqrt{A_1} - \sqrt{A_2} \langle 0.2l \tag{7.7.35}$$

Applying this to a simple conical shape of circular cross-section with included angle  $\delta$ , the relationship develops as follows:

$$4^\circ \langle \delta \langle 8^\circ \tag{7.7.36}$$

For the turbine with a horizontal axis shaft, a bend is required immediately after the turbine causing poor recovery of the velocity head and further constricting the angle  $\delta$ .

The bend also causes non-symmetric flow at the runner exit further reducing turbine efficiency.

Applying the information shown in Figure 3.9.2, the head at full load output is used in selecting the value of the constant C. Hence for an initial guess, using the supply head of H = 10m:

$$P = \left( \frac{0.33656}{0.042} \right)^2 \times 0.7457 \times 0.88 = 42.138kW \quad (7.7. 37)$$

$$C = 0.042 = \frac{D_2}{\sqrt{h.p.}} = \frac{0.33656}{\sqrt{\frac{1}{0.7457} \times P \times \frac{1}{0.88}}} \quad (7.7. 38)$$

The corresponding  $n_s$  at 10m head is 690:

$$690 = \frac{N\sqrt{P}}{H^{5/4}} \quad \Rightarrow \quad N = 1632\text{rpm} \quad (7.7. 39)$$

The values obtained herewith have been used as a check against the values first obtained. It is thus assumed that the initial values are correct and they shall be used for the design.

Figure 3.9.3 gives the values of cavitation versus head. Using this graph, the value of  $H_s$  is determined as follows:

$$H_r = H_B - (\sigma H + H_v + H_1) \quad (7.7. 40)$$

where:  $\sigma$  = cavitation coefficient

$H_B$  = barometric pressure at runner elevation [m]

$H$  = net head [m]

$H_v$  = vapour pressure of water [m]

$H_1 = 0.5D$  for horizontal shaft units.

Applying the above equation with the values of  $\sigma$  obtained from Figure 3.9.3:

$$\sigma_{10m} = 1.0; \quad \sigma_{12m} = 0.9 \text{ and } \sigma_{14m} = 0.77$$

$$\Rightarrow \quad H_s = 9.810 - (\sigma(10) + 0.324 + 0.5(0.33656)) = 9.310 - 10\sigma$$

If it is assumed that H is not a function of  $H_s$  then:

$$H_s = 9.310 - 10(1.0) = -0.690\text{m}$$

And if it is assumed that H is a function of  $H_s$ , whereby  $\sigma$  is also a function of  $H_s$  then:

$$\text{at } H_s \approx 4: \quad H_s = 9.310 - 14 \times 0.77 = 1.61\text{m}$$

From practical application, it has been shown that each turbine has a narrower best maximum efficiency than generally shown in Figure 3.9.5. The very large values of  $n_s$  attainable with Kaplan and propeller turbines depends on high recovery in the draft tube of the velocity head and extremely high specific speeds are attainable only with some sacrifice in efficiency.

The exit diameter of all reaction turbines is related to the speed by:

$$D_2^3/Q = \text{constant}$$

and from this it is possible to calculate:

$$\eta_D \frac{C_2^2}{2gH} \cong 3.6 \times 10^{-4} (n_s)^{4/3} = \text{dynamic suction} \quad (7.7. 41)$$

Figure 3.9.7 shows the function of  $n_s$ . From experimental data, safe values of  $\frac{kW_2^2}{2gH}$  follow the law:

$$\frac{kW_2^2}{2gH} \cong 4.0 \times 10^{-6} (n_s)^{7/3} = \text{depression at back of vane} \quad (7.7. 42)$$

And values of this quantity have been shown in order to give the curve of permissible  $\sigma$ . It can be seen how rapidly  $\sigma$  increases with  $n_s$ , and thus correspondingly its importance at high specific speeds. [ k ] is dependant on the type of turbine and its design, since it is dependant on the specific loading of the runner blades, their curvatures and the ratio of chord to pitch. Applying the above information to solve for the expected draft tube efficiency from Eq(7.7. 41):

$$\eta_D \cong \frac{2 \times 32.174 \times 30}{(7.172 \times 3)^2} 3.6 \times 10^{-4} \left( \frac{1115 \sqrt{43.164/0.7457}}{30^{3/4}} \right)^{4/3} \cong 73\%$$

Calculating the value of the draft tube efficiency including the calculated value of  $h_s$  in the head:

$$\eta_D \cong \frac{2 \times 32.174 \times (12.3 \times 3)}{(7.172 \times 3)^2} 3.6 \times 10^{-4} \left( \frac{1115 \sqrt{43.164/0.7457}}{(12.3 \times 3)^{5/4}} \right)^{4/3} \cong 59\%$$

Hence the draft tube efficiency will be highest at the 12.3m head.

The efficiency was then recalculated using the largest possible value of  $h_s = 5.352\text{m}$ :

$$\eta_D \cong \frac{2 \times 32.174 \times (15.352 \times 3)}{(7.172 \times 3)^2} 3.6 \times 10^{-4} \left( \frac{1115 \sqrt{0.5 \times 9.81 \times 15.352/0.7457}}{(15.352 \times 3)^{5/4}} \right)^{4/3} \cong 74\%$$

The values determined in the draft tube efficiency calculations are all possible when looking at the hydraulic power, Eq (7.7. 31), since the values of axial velocity and inlet guide vane angle are all within the limits. It remains however that the cavitation parameter remain below its allowable limit and hence the draft tube will be set at 2.3m with an expected recovery coefficient of 98%. For the purposes of testing the design the effects of lengthening the draft tube, to its full, calculated length of 5.352m, should be measured. However, it must be borne in mind that the mechanical design of the turbine components are limited to a maximum of 26kN of axial thrust, which translates into:

$$P = \frac{F}{A} = \frac{26000}{\frac{\pi}{4} \times 0.33656^2} = 0.2923 \text{MPa}$$

or equivalently 29.23m head.

Since it is unlikely that the axial thrust will be exceeded because the calculations of the cavitation parameter show that cavitation will occur at approximately half this value, the limitation on head is then assumed to come from the radial bearings:

$$P = 0.5 \times 9810 \times 15.352 = 75.302 \text{kW}$$

From the calculations for the chain pull yielding the associated radial load:

Chain velocity:



$$v = \frac{NnPC}{60000} = \frac{38 \times 1115 \times 25.4}{60000} = 17.93 \text{ms}^{-1} \quad (7.7. 43)$$

Chain pull:

$$T = \frac{P}{v} = \frac{75302}{17.93} = 4200 \text{N} \quad (7.7. 44)$$

This value of radial load is lower than the previously calculated value of 5.526kN and hence the radial loading of the bearings will not be exceeded. Since the loading of both the axial and radial bearings shall not be exceeded, it remains only to check the loading of the shaft:

$$\begin{aligned} d &= \left[ \frac{32RF}{\pi} \sqrt{\left( \frac{k_t M}{Se} \right)^2 + \left( \frac{k_{ts} Ml}{Sy} \right)^2} \right]^{1/3} \\ &= \left[ \frac{32 \times 2}{\pi} \sqrt{\left( \frac{1.8 \times 4200 \times 26}{425} \right)^2 + \left( \frac{1.4 \times 645032}{680} \right)^2} \right]^{1/3} \\ &= 30.6 \text{mm} \end{aligned}$$

The shaft diameter is also smaller than the current rated diameter and will therefore not be subject to failure. Since the shaft is designed to 26kN  $\approx$  30m head, it will most definitely not fail should the head be increased to 15.352m.

It remains hereafter to check the limit on the rotational speed of the bearings, since thrust bearings are particularly susceptible to speed limitations. The thrust bearing is limited to 1100rpm in grease and 1700rpm in oil and of the radial bearings, the limitations are shown in the following calculations.

$$\begin{aligned} 3 \text{years} &\equiv 26280 \text{hrs} \\ &= 500 f_h^2 \\ f_h &= 3.746 \\ &= f_n \frac{C}{P} \end{aligned}$$

where:  $C = 52\,500N$

$$P = \frac{390 \times 4200}{320} = 5120N$$

$$f_n = (0.03n)^{-1/3}$$

$$\Rightarrow n = 684\text{rpm}$$

Hence the limiting speed for a 3year bearing life is 684rpm. However, if the bearing is to be run at the calculated velocity of 1115rpm, then expected life of the bearings is:

$$f_n = (0.03)^{-1/3} = 0.310$$

$$f_h = f_n \frac{C}{P} = 3.183$$

$$L_h = 500f_h^3 = 16\,118.3\text{hrs} \equiv 1\text{year and } 10\text{ months}$$

Hence the only design factor that needs to be taken into consideration when increasing the power to 75.3kW, is the decrease in the bearing life of the radial bearings, from 3 years to just short of 2 years.

## 7.8 Programming for blade development

### 7.8.1 Stator and rotor blade geometry

This file determines the blade geometry's for both the stator and rotor blades, from the initial conditions taken from a specific site. This is achieved per segment by firstly dividing the blade into an equal number of areas.

### 7.8.2 Plotting the camber line

This file uses the values calculated on the previous file to generate the [x y] co-ordinates of the circular arc camber line. The program is defined for circular arc profiles only.

### 7.8.3 Circular arc hub and tip caps

The purpose of having such a file is to cap both the top and bottom of the blades. The reason for doing this was to initialise the programming of the blade shape for the CNC machining process. One design problem that was not overcome due to a change in plan

was to erase the area common to both the cap and the hub and tip profile. The necessity to do this was based on the machining process cutting around the profile at the hub and tip, and not between its caps.

#### **7.8.4 Defining the solidity**

Before the file containing the [x y] data points for the profile could be used, it was necessary to change the size of the trailing edge radius. This was to be implemented primarily to suit the necessity of machining the thin edge. The rounding of the radius was not implemented without the consideration of the fluid flow dynamics surrounding the trailing edge. The radius was determined according to a suitable profile thickness, which when rounded, remained tangent to the circular arc joining the two sides of the profile.

#### **7.8.5 Developing the projected and interpolated points**

This file defines the [x y] co-ordinates in single z-planes by means of projection and interpolation. However, it does need to be run in parts, because some points are interpolated and some points are projected. The mathematics of which are dependant on the "layers" in the immediate vicinity

#### **7.8.6 Plotting the figures**

This file plots all the figures produced by the program, from simple velocity vector diagrams to 3-D plots of the blade shapes.

#### **7.8.7 Designing the diffuser**

The purpose of this file is to determine the length of the diffuser as a function of the losses, rotor exit velocity and pressure.

## 7.9 Manufacturing Procedure

### 7.9.1 Job schedule task list

The following is a manufacturing procedure that covers the fabrication of the turbine. It is a list of the components involved in the building of the turbine and does not include the procedures required for fabrication for the individual components. The list is typically aimed at the artisan who produces the components with the purpose of providing a list of tasks for building the water turbine.

- 1) Reducer
  - welding of flanges ( 2 of )
  - weld in pressure gauges
- 2) Elbow
  - cut 74° angle
  - bore stuffing box housing hole
  - welding of flanges ( 2 of ) to occur after welding of stuffing box and before welding of the bearing housing
  - weld in the curtain plate
- 3) Machine shaft according to drawing 3
- 4) Manufacture the spider to be used to determine the approximate centrality once having checked the “trueness” of the shaft.
- 5) Stuffing box housing
  - cut involute
  - weld flange
  - Weld the stuffing box housing to the elbow using the spider
- \* The shaft length must be long enough to enable the alignment of the stuffing box housing during welding.
- \* A hole for the water bleeder nipple is required in the side of the stuffing box housing. It is necessary from a manufacturing viewpoint to machine this hole before the bearing housing is welded to the elbow.
- 6) Stuffing box
  - weld stainless washer into sleeve
  - weld on flange
  - cut lubrication holes

- machine lantern ring: this will have to be to non-standard sizes since the diameter of the shaft is not suited to existing sizes. A simple interpolation between the standard sizes yields a sufficiently accurate result
- 6) Bearing housing
  - cut involute
  - cut windows
  - mark and drill the castellated plates for the pillow blocks
  - align castellated plates and weld into housing using the correct spacers
  - weld onto elbow
  - weld on flange for belt-guard mounting
- 7) Take out the parts which are detachable and send the skeleton out to be galvanised
- 8) Thrust bearing housing - develop according to drawing 16
- 9) Cut rotor hub - develop according to drawing 6
- 10) Cut stator hub - develop according to drawing 4
- 11) Develop blades
  - write program
  - convert results to 2D and outsource for cutting of profiles
  - stack profiles to make master pattern
  - place into a coffer dam and pour in silicon
  - cut the master pattern out and make (11+2) stator waxes and (10+2) rotor waxes
  - form waxes into a tree for centrifugal casting
  - place into another coffer dam and pour investment
  - melt wax out (at 150°C for 3hrs and at 250°C for 1hr)
  - place cold investment into centrifuge
  - pour bronze with centrifuge rotating at  $\pm 100$ rpm
  - clean blades and prepare for assembly with the respective hubs

It was initially considered that the dimensions of the profile hub would be projected onto the inner wall of the reducer. There was a minor problem with the variation in the tolerance between the blade tip and the reducer, amounting to a 1.6% variation. In

preference to producing another “washer” that would act as a fill, it was decided that the blades would be made to suit the shape of the ellipse.

- 12a) Additional
  - weld flanges to nozzle
  - weld in pressure gauge mounts
- 12b)
  - weld elbow cut-off to diffuser
  - weld flanges to diffuser outlet and the inlet to the intermediate piece

13) Assemble components and test on site

14) Assemble the entire turbine, fitting: shaft, bearings, pulley for drive shaft and the stuffing box with packing, lantern ring and squeezer.

15) Develop the main frame onto which the pump system is to be mounted according to drawing 9

16) Mount the pump

17) Mount the pulley

18) Insert the rotor and stator

At this point, the water turbine should thus be complete for testing and running.

### 7.10 Inventory

- 1) Flanges: 400 ( 2 of ); 350( 6 of ) & 250 ( 1 of ) N/B [SABS 1123 T600/3]
- 2) Reducer: 400-350 [Sched. STD] ( 1 of )
- 3) Elbow: 350N/B, 90°, long radius Sched. STD ( 1 of )
- 4) Curtain plate: 410×340×10 ( 1 of )
- 5) Shaft: En 57, 1.6m×70mm diameter ( 1 of )  
thrust collar En 8, O.D. 110, I.D. 60, t 20 ( 1 of )
- 6) Stator: blade billets 170×100×30 ( 11 of )  
nose cone O.D. 125, I.D. 60, length 120 ( 1 of )  
rubber bearing O.D. 75, I.D. 50, length 100 ( 1 of )
- 7) Rotor: blade billets 170×100×60 ( 10 of )  
hub O.D. 125, I.D. 80, length 100 ( 1 of )  
taper lock and key O.D. 85.5, I.D. 50 ( 1 of each )



The above mentioned nuts and bolts were purchased from Boltfix, but the following were purchased from SA fastners:

M24×100 bolts with nuts ( 16 of )

and washers (32 of)

M18×100 bolts with nuts ( 12 of )

and washers ( 24 of )

14) If it were preferred that the PTO is operated using a pulley system rather than chains, then the following should be ordered:

- pulleys ( 2 off )      315×3SPC
- taper lock ( 2 off )    35×35×55
- belt ( 3 off )          SPC22×2000

This is assuming a service factor of 1.3 with a centre to centre distance of 505mm; a key-way size of 16×4.3×88.9



## CHAPTER 8

### REFERENCES

- Barrows, H.K.: 1943, *Water Power Engineering*, 3<sup>rd</sup> edition, McGraw-Hill, New York.
- Brown, G.: 1970, *Hydro-electric Engineering Practice*, Vol 2, Blackie and Son, London.
- Gibson, A.H.: 1922, *Hydroelectric Engineering*, Blackie, Glasgow.
- Goodman, L.J., Hawkins, J.N. and Love, R.N.: 1981, *Small Hydroelectric Projects For Rural Development: Planning and Management*, Pergamon, New York.
- Hoerner, Dr. S.F.: 1965, *Fluid-Dynamic Drag*, Brick Town, New Jersey.
- Janna, W.S.: 1973, *Introduction to Fluid Mechanics*, 3<sup>rd</sup> edition, Van Nostrand Reinhold, London.
- Karrasik, I.J.: 1989, *Centrifugal Pump Clinic*, 2<sup>nd</sup> edition, Dekker, New York.
- Karrasik, I.J., Krutzsch, W.C., Fraser, W.H. and Messina, J.P.: 1986, *Pump Handbook*, McGraw-Hill, New York.
- Lewitt, E.H.: 1932, *Hydraulics*, Pitman, London.
- Massey, B.S.: 1968, *Mechanics of Fluids*, 6<sup>th</sup> edition, D van Nostrand, London.
- Moniton, L., le Nir, M. and Roux, J.: 1984, *Micro Hydroelectric Power Stations*, Wiley, Place of Publication.
- Moses, H.L. and Siegel, R.P.: 1982, Small Hydro Power Fluid Machinery, *Diffuser Design Considerations For Small Hydroturbines*, Vol 1, 152.
- Munson, B.R., Young, D.F. and Okiishi, T.H.: 1990, *Fundamentals of Fluid Mechanics*, John Wiley and Sons, London.
- Pollock, F.: 1980, *Pump Users Handbook*, 2<sup>nd</sup> edition, Gulf, Houston Texas.
- Rattan, S.S.: 1988, *A Textbook of Fluid Machines*, Khanna, Delhi.
- Rejgels, Dr. F.W.: 1961, *Aerofoil Sections*, Butterworths, London.
- S.A. Pump Manufactures Association: 1991, *Pumps Principles and Practice*, 2<sup>nd</sup> edition, K Myles and Associates, Northcliff, Tvl.
- Streeter, V.L., Bedford, K.W. and Wiley, E.B.: 1985, *Fluid Mechanics*, 9<sup>th</sup> edition, McGraw Hill, Tokyo.
- NSK: 1977, The NSK Rolling Bearing Catalogue, 1101a, NSK, Japan.
- Wallis, R.A.: 1983, *Axial Flow Fans and Ducts*, Wiley, London.
- Warnick, C.C.: 1984, *Hydropower Engineering*, Prentice Hall, New Jersey.

<http://aerolab.virtualave.net/airfoil/index.html>

<http://aeroserver.aero.usyd.edu.au/aero/contents.html>

<http://amber.aae.uiuc.edu/~m-selig/profoil.html>

<http://curricula.mit.edu/~2006/Textbook/Nodes/>

[http://members.tripod.com/~Andrei\\_C/Aerofoil/Aerofoil.html](http://members.tripod.com/~Andrei_C/Aerofoil/Aerofoil.html)

<http://www.desktopaero.com/appliedaero/appliedaero.html>

<http://www.electricityforum.com/et/nov97/gehydro.html>

<http://www.geocities.com/CapeCanaveral/Hanger/2524/nvfoilen.html>

<http://www.itc.nl/~klunne/hydro/>

[http://www.itri.loyola.edu/rp/10\\_01.htm](http://www.itri.loyola.edu/rp/10_01.htm)

<http://www.sorel-tracey.gq.ca/~sabourin/publications/airh96-2/airh96-2.htm>

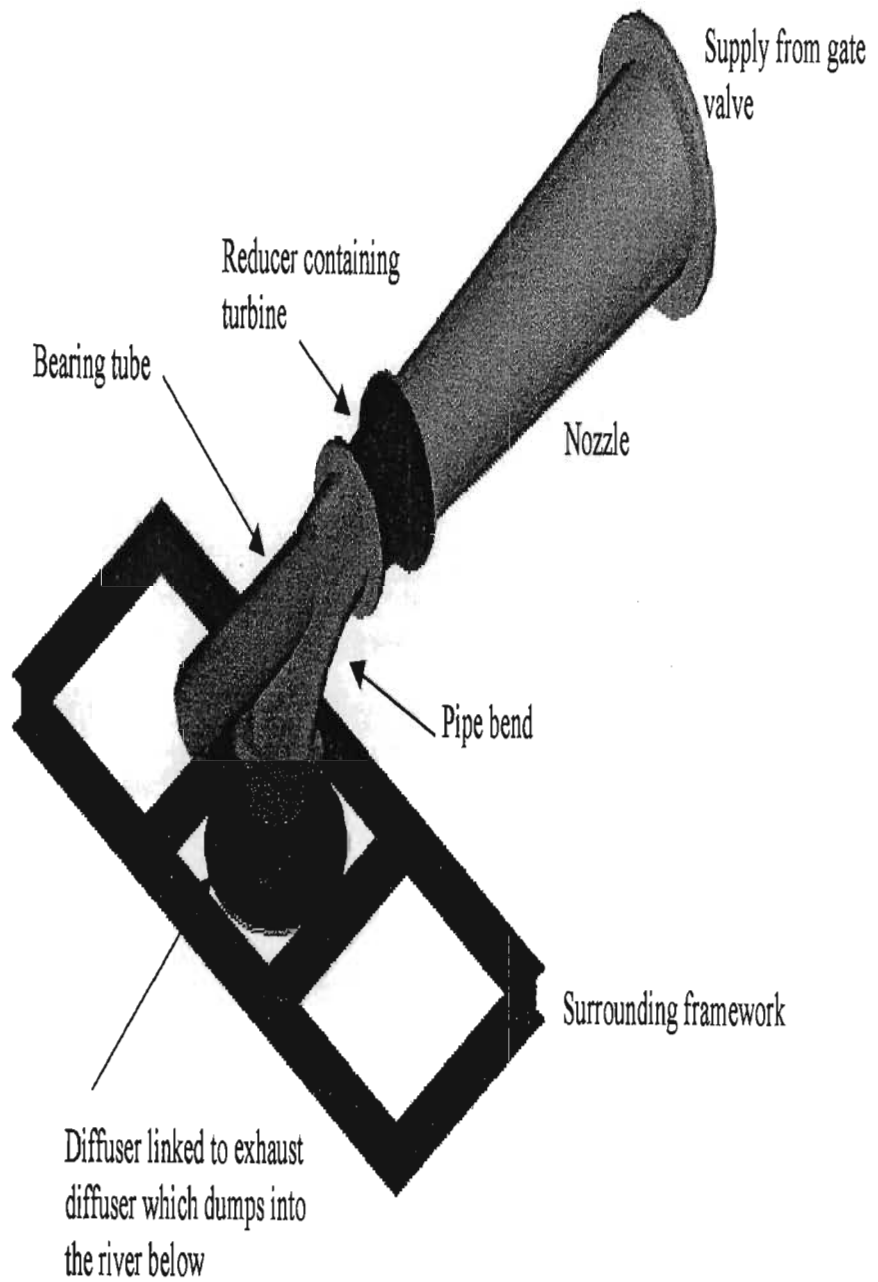
<http://www.twsu.edu/library/aveng/aerospace.html#AA>

## CHAPTER 9

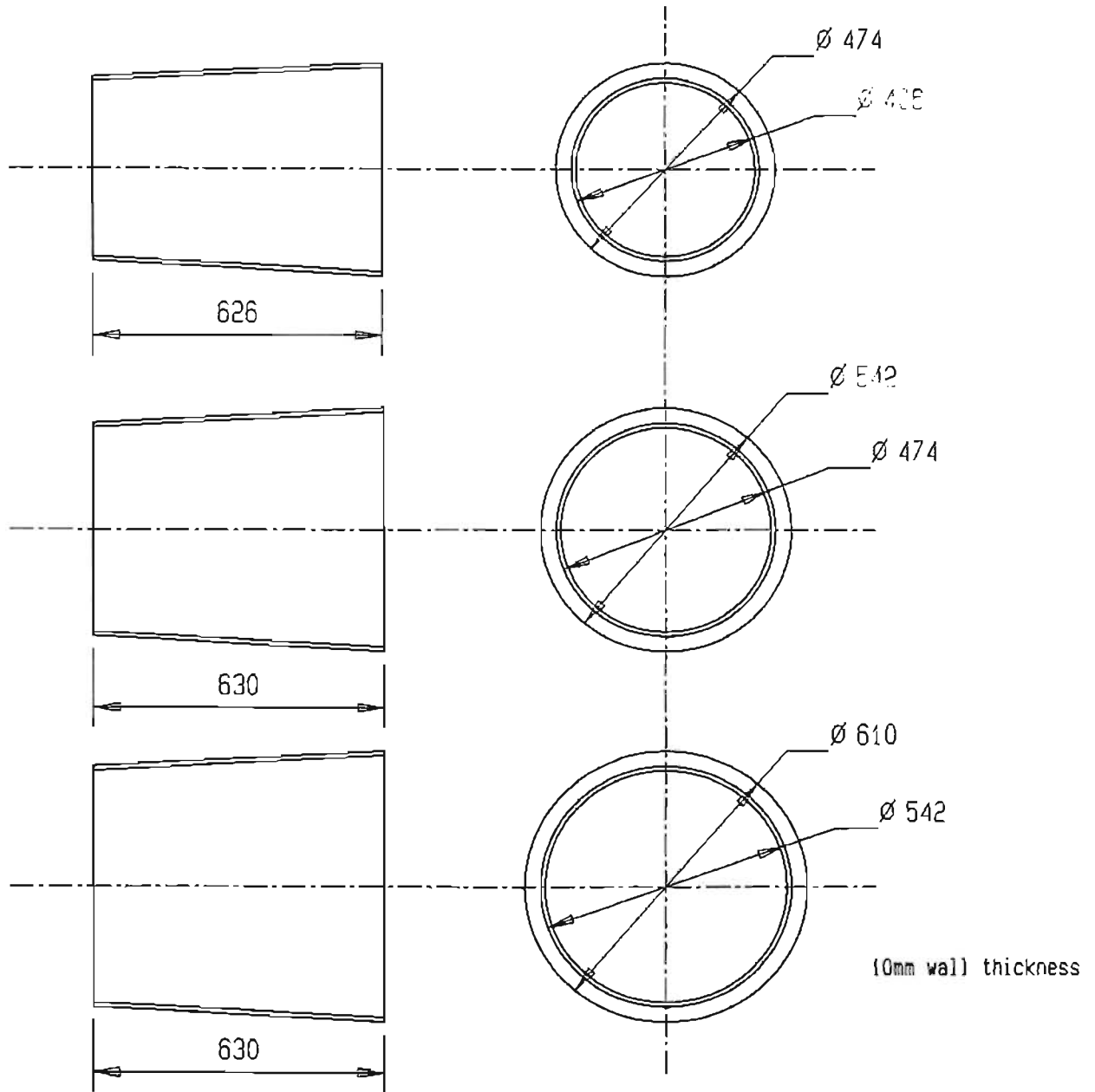
### DRAWINGS

#### Index:

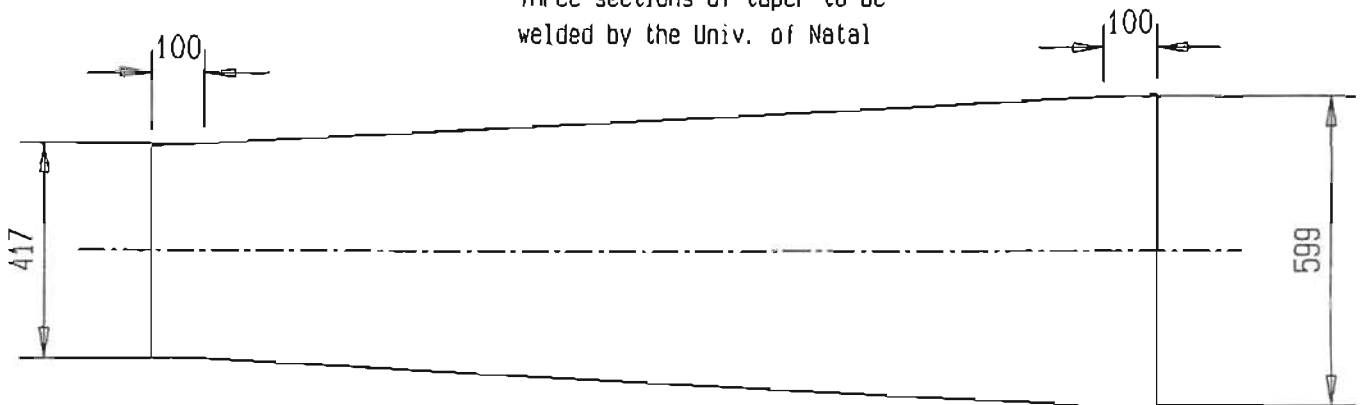
1. Turbine in operating environment
2. Nozzle
3. Drive Shaft
4. Stator nose cone
5. Stator mounting
6. Rotor hub
7. Rotor mounting
8. Pressure gauge mountings
9. Main support framework
10. Curtain plate
11. Bend fabrication
12. Bearing pedestal
13. Castellated plate
14. Stuffing box (cylinder and flange)
15. Stuffing box housing
16. Thrust bearing housing
17. Thrust bearing pre-load spring system
18. Diffuser
19. Diffuser flange
20. Stator with housing
21. Whole assembly
22. Standard bearing assembly (pump bearing)
23. Standard bearing assembly (custom bearing housing)
24. Interpolated dimensioned lantern ring and slinger ring
25. PTO bush cut to match shaft of PTO



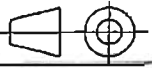
UNIVERSITY OF NATAL School of Mechanical Engineering		REV.	DATE	CHECKED	SCALE	UNITS : mm	PROJECT	No. 1
	Draftsperson				ESTIMATED MANUFACT. TIME:	STUDENT J HANDELHOFF	MSC THESIS	
	Technician					SUPERVISOR PROF. GDJ SMITH	TITLE	
	W'Shop Manager						TURBINE IN OP. ENVIRON.	



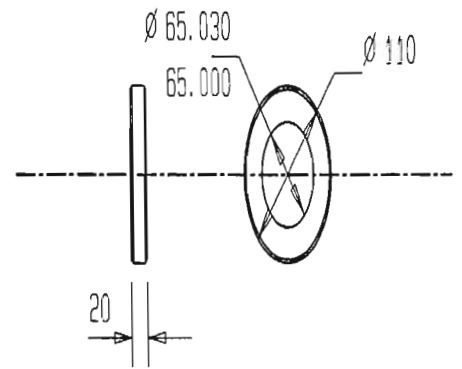
Three sections of taper to be welded by the Univ. of Natal



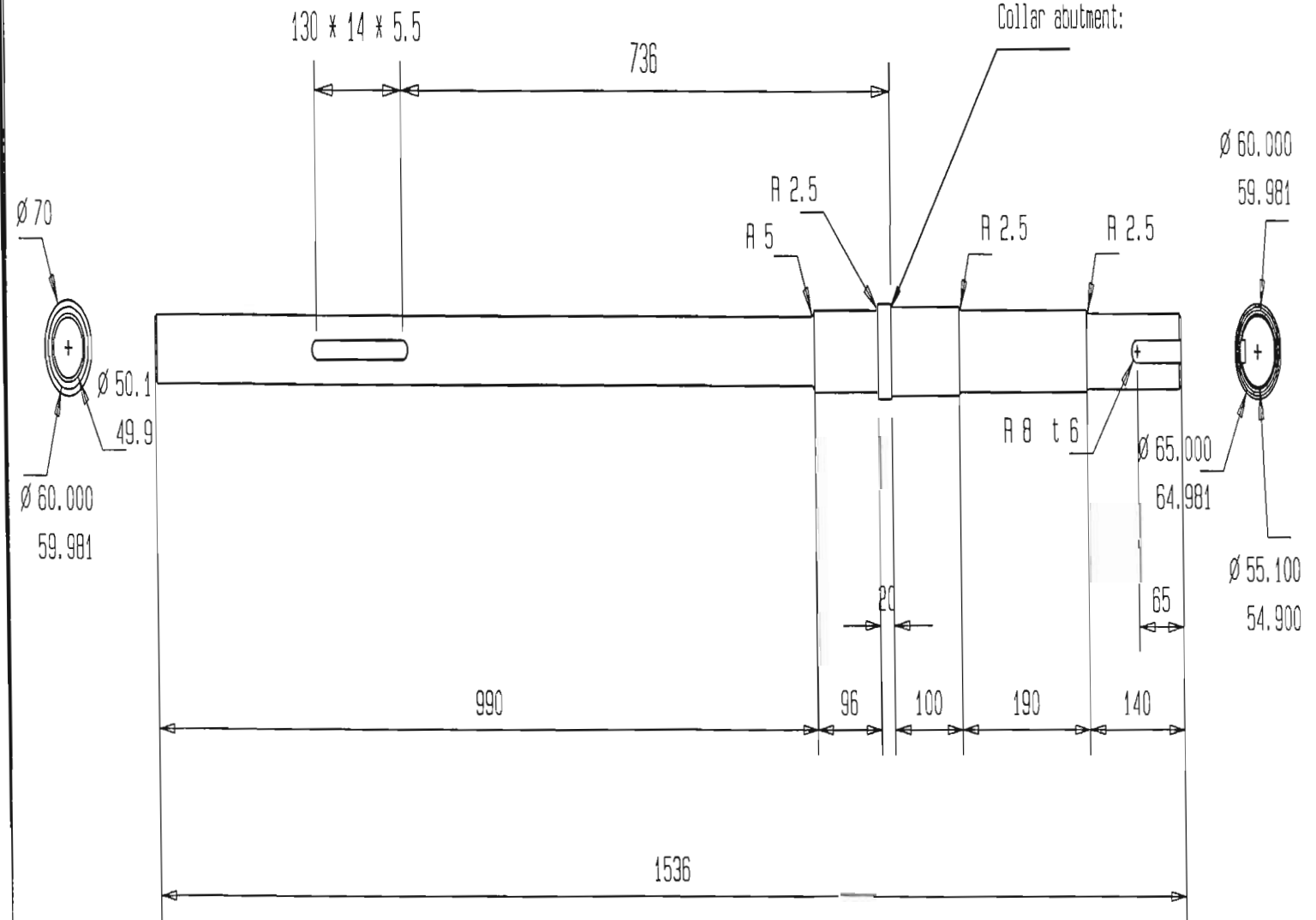
Pressure gauge lugs to be offset at 100mm either side


<b>UNIVERSITY OF NATAL</b>		<b>PROJECT</b>		No. 2	<b>TITLE</b>	
School of Mechanical Engineering		MSC THESIS			NOZZLE	
	<b>REV.</b>	<b>DATE</b>	<b>CHECKED</b>	<b>SCALE</b> 1 : 15		<b>UNITS</b> : mm
Draftsperson				<b>ESTIMATED MANUFACT. TIME:</b>		
Technician						
W'Shop Manager				<b>STUDENT</b>	J RANDELHOFF	
				<b>SUPERVISOR</b>	PROF. GOJ SMITH	

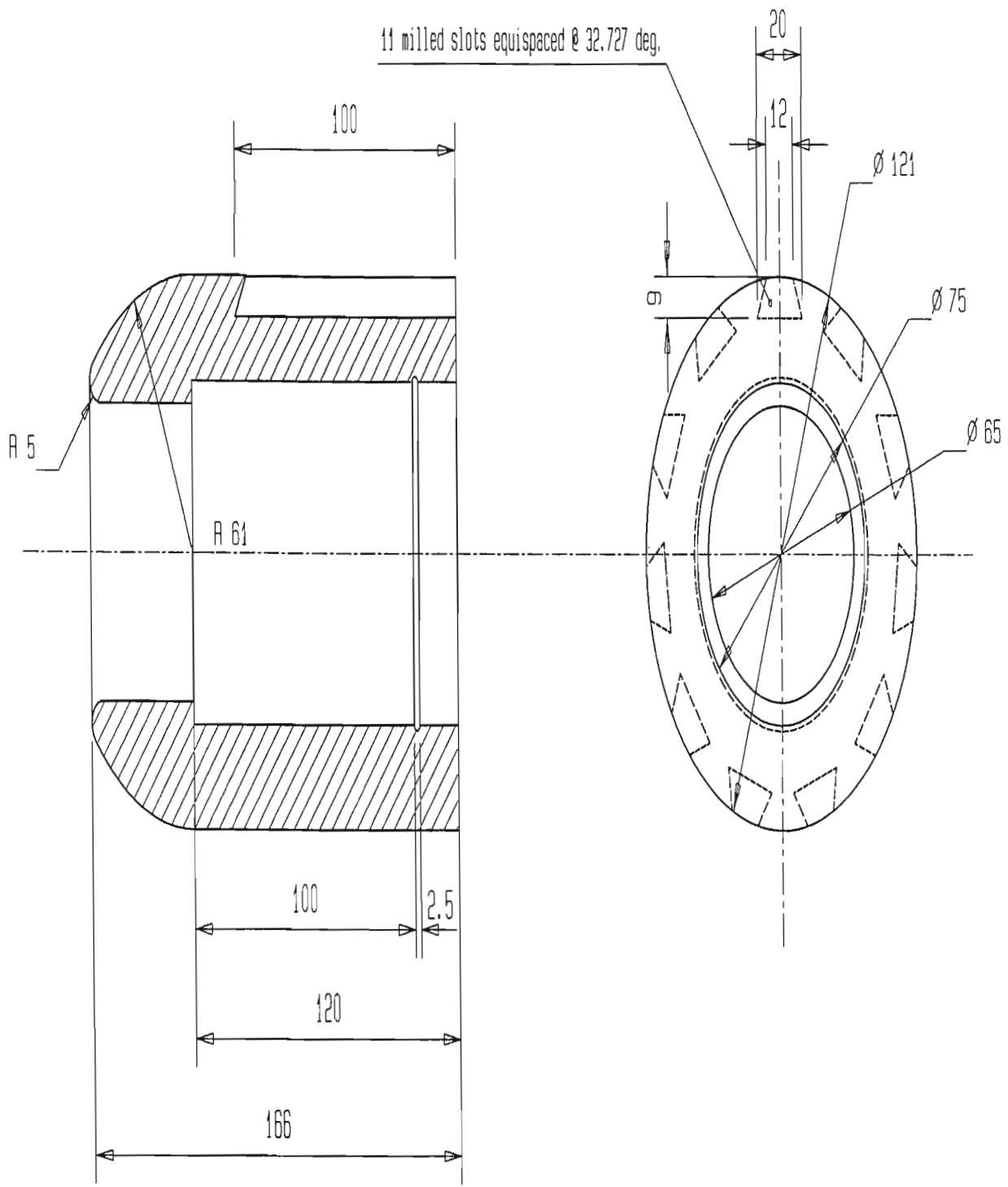
Thrust bearing support collar:



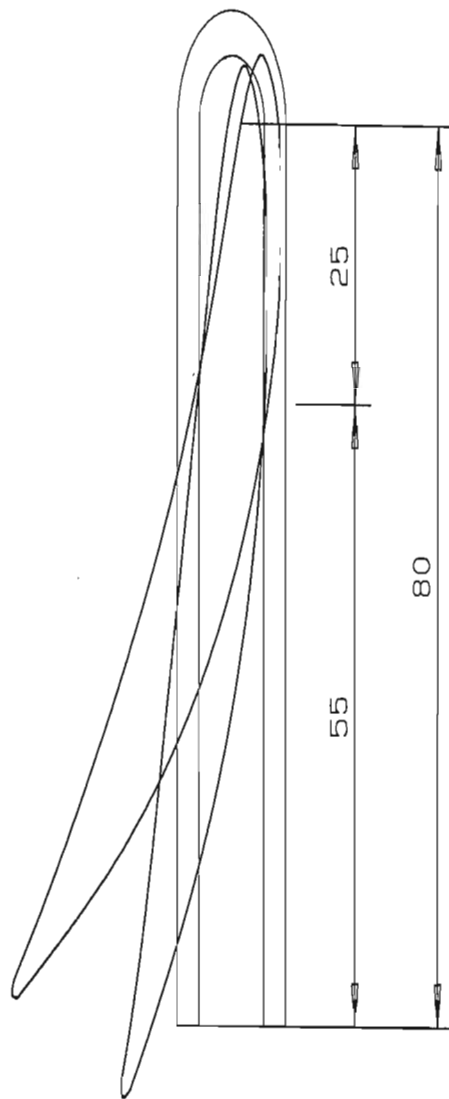
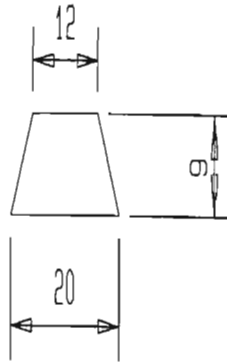
Collar abutment:



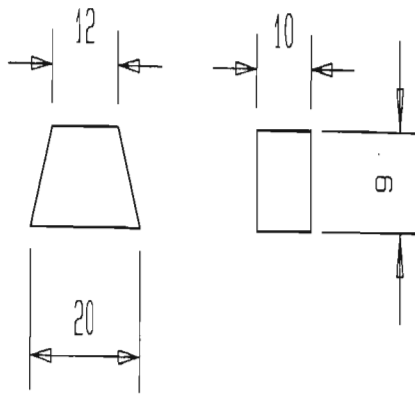
UNIVERSITY OF NATAL School of Mechanical Engineering	REV.	DATE	CHECKED	SCALE 1 : 7	UNITS : mm	PROJECT	No.
				ESTIMATED MANUFACT. TIME:	STUDENT	MSC THESIS	3
					J RANDELHOFF	TITLE	
				SUPERVISOR	DRIVE SHAFT EN57		
				PROF. GOJ SMITH			



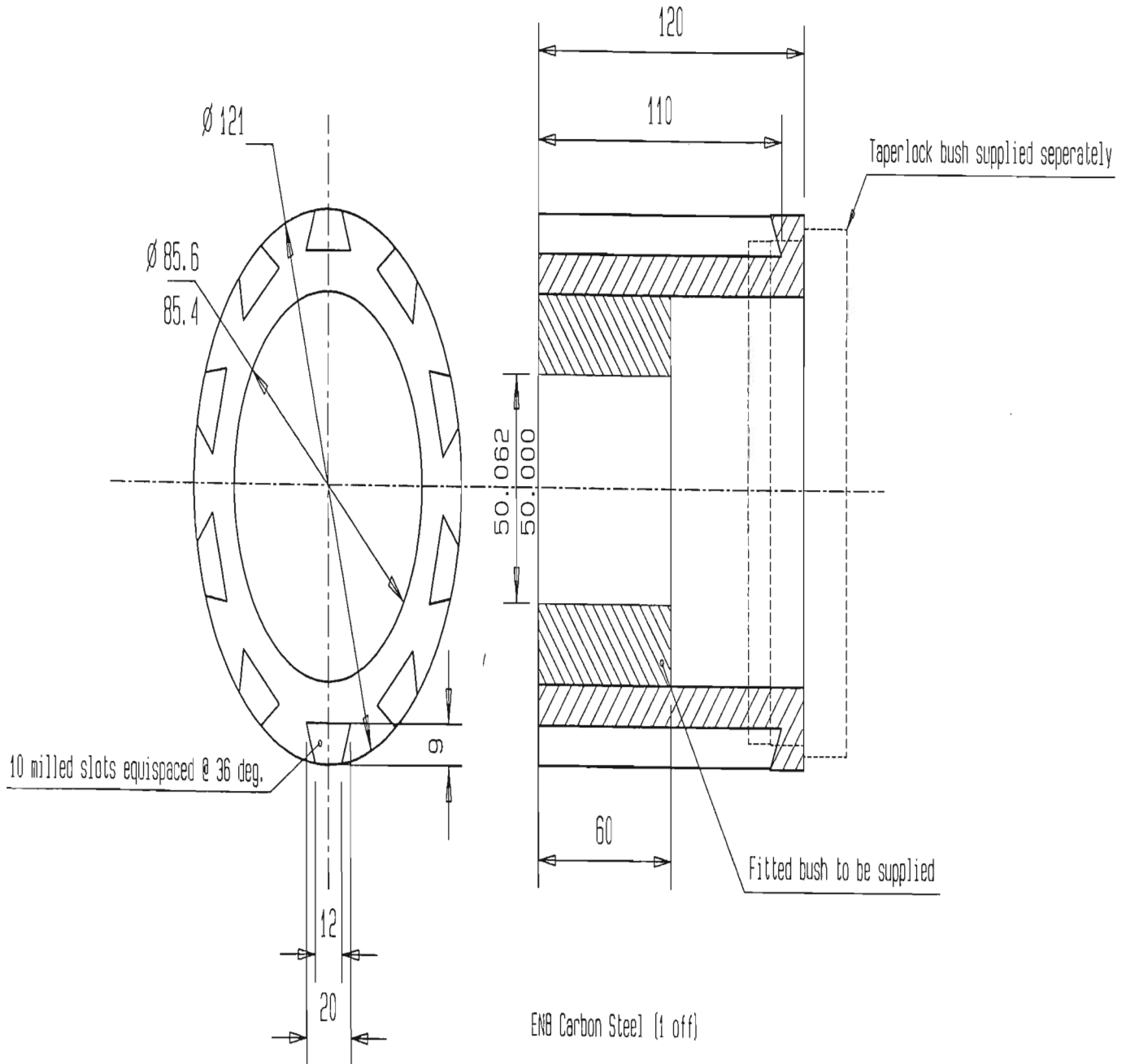
<b>UNIVERSITY OF NATAL</b> School of Mechanical Engineering		REV.	DATE	CHECKED	SCALE 1 : 2	UNITS : mm	PROJECT	No.
	Draftsperson				ESTIMATED MANUFACT. TIME:	STUDENT J HANDELHOFF	MSC THESIS	4
	Technician					SUPERVISOR PROF GOJ SMITH	TITLE STATOR NOSE CONE	
	W'Shop Manager							



UNIVERSITY OF NATAL School of Mechanical Engineering		REV.	DATE	CHECKED	SCALE 1 : 1	UNITS : mm	PROJECT	No.
	Draftsperson				ESTIMATED MANUFACT. TIME:	STUDENT J RANDELHOFF	MSC THESIS	5
	Technician					SUPERVISOR PROF. GOJ SMITH	TITLE	
	W'Shop Manager						STATOR MOUNTING	

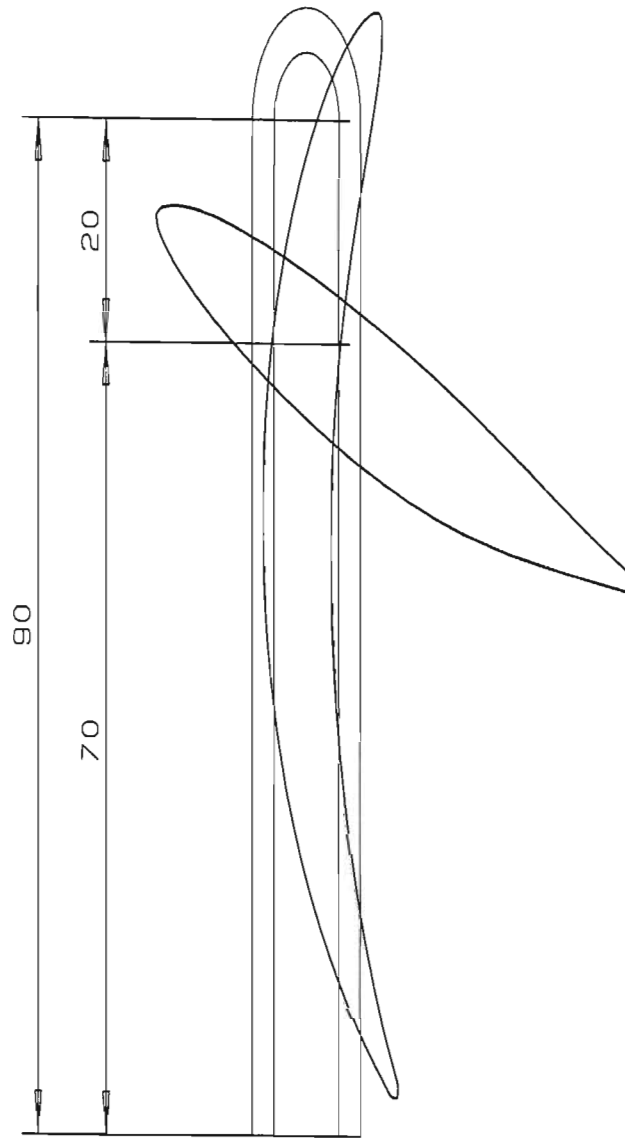
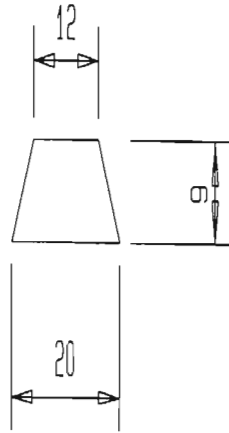


Dovetail slot plug  
Scale 1:1



UNIVERSITY OF NATAL School of Mechanical Engineering	REV.	DATE	CHECKED	SCALE 1 : 2	UNITS : mm	PROJECT	No.
	Draftsperson			ESTIMATED MANUFACT. TIME:	STUDENT J. RANDELHOFF	MSC THESIS	6
	Technician					TITLE	ROTOR HUB
	W'Shop Manager			SUPERVISOR PROF. GDJ SMITH			

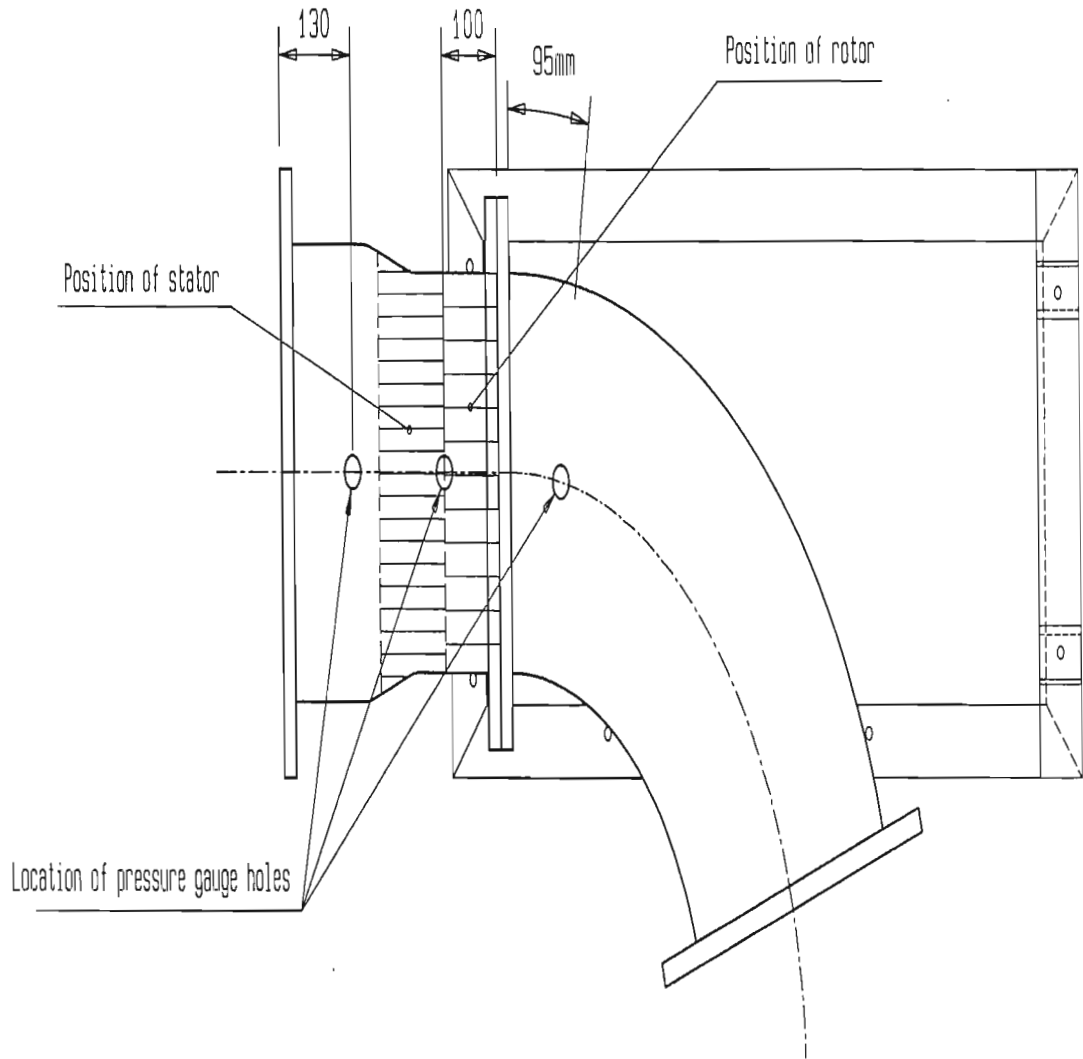
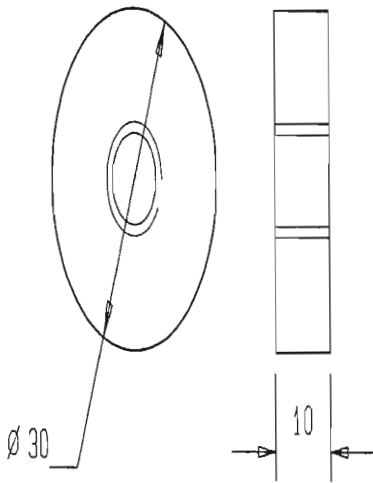




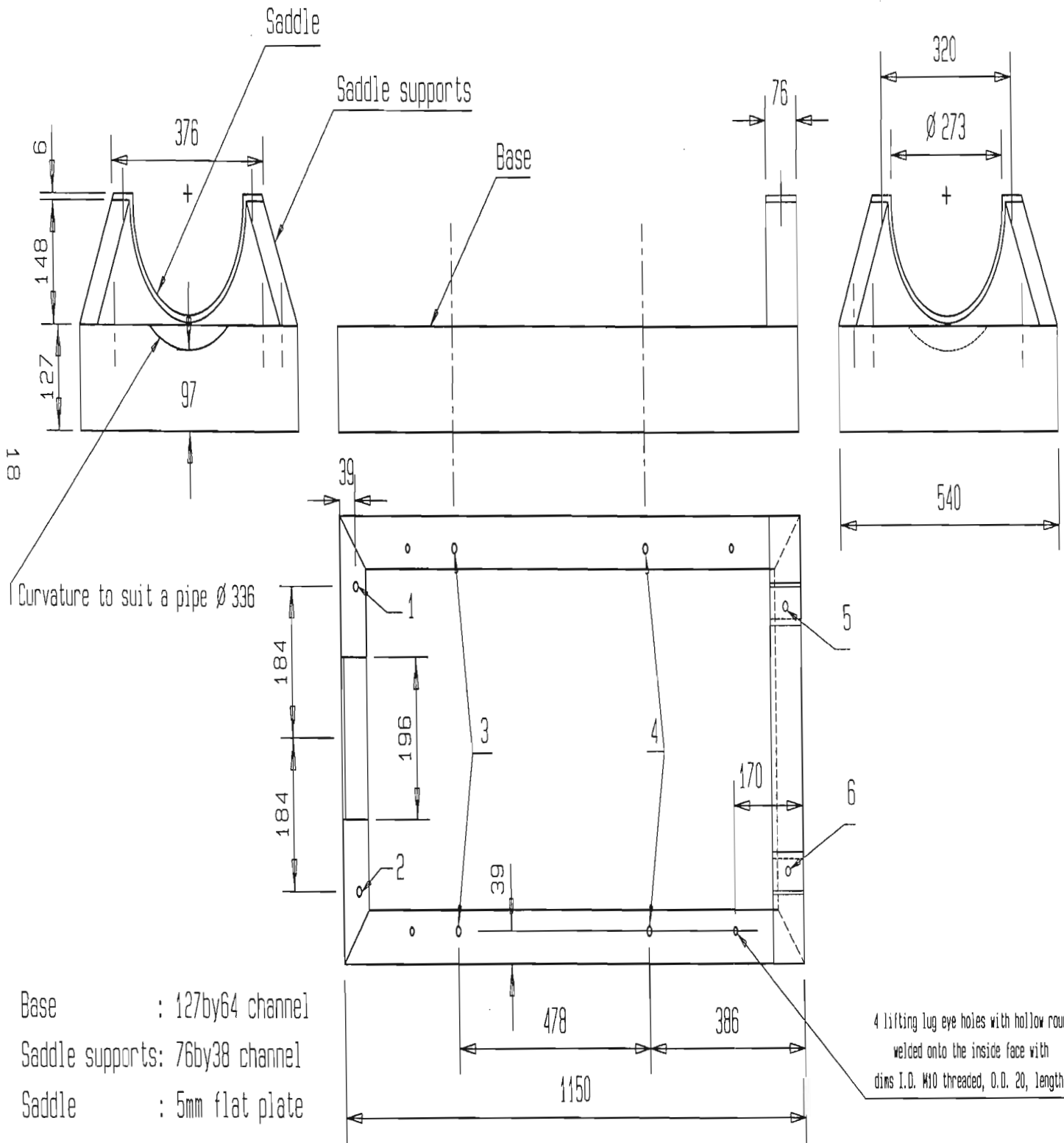
<b>UNIVERSITY OF NATAL</b> School of Mechanical Engineering		<b>REV.</b>	<b>DATE</b>	<b>CHECKED</b>	<b>SCALE 1:1</b>	<b>UNITS : mm</b>	<b>PROJECT</b>	<b>No.</b>
	Draftsperson				<b>ESTIMATED          MANUFACT.          TIME:</b>	<b>STUDENT          J. RANDELHOFF</b>	MSC THESIS	7
	Technician						<b>TITLE</b>	
	W'Shop Manager						ROTOR MOUNTING	
							<b>SUPERVISOR          PROF. GOJ SMITH</b>	

Hole to suit BSP 1/4" thread  
of pressure gauge

Scale 1:1



<b>UNIVERSITY OF NATAL</b>  School of Mechanical Engineering		REV.	DATE	CHECKED	SCALE 1 : 10	UNITS : mm	PROJECT	No.
	Draftsperson				ESTIMATED MANUFACT. TIME:	STUDENT J HANDELHOFF	MSC THESIS	8
	Technician					SUPERVISOR PROF. GDJ SMITH	TITLE	
	W'Shop Manager				P/GAUGE MOUNTINGS			



Curvature to suit a pipe  $\varnothing 336$

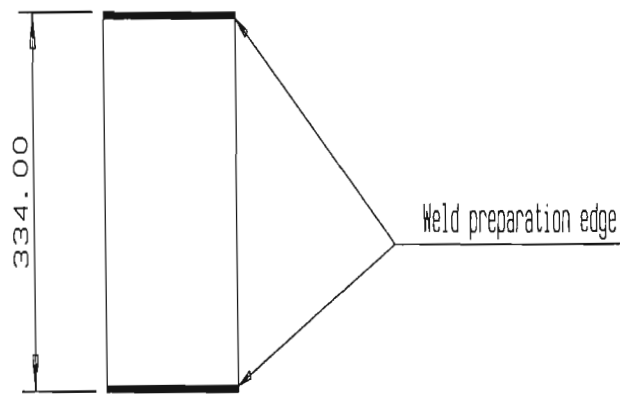
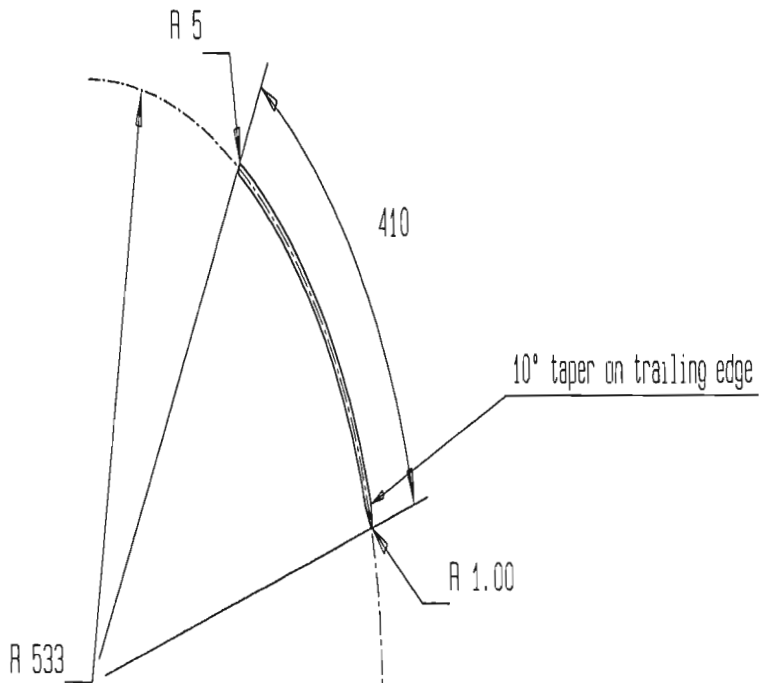
- Base : 127by64 channel
- Saddle supports: 76by38 channel
- Saddle : 5mm flat plate

4 lifting lug eye holes with hollow round welded onto the inside face with dims I.D. M10 threaded, O.D. 20, length 20.

U-bolt clearance holes marked 1-6 with  $\varnothing 11$  should be marked with the complete turbine placed upon the frame since small dimensional errors may have resulted during fabrication.

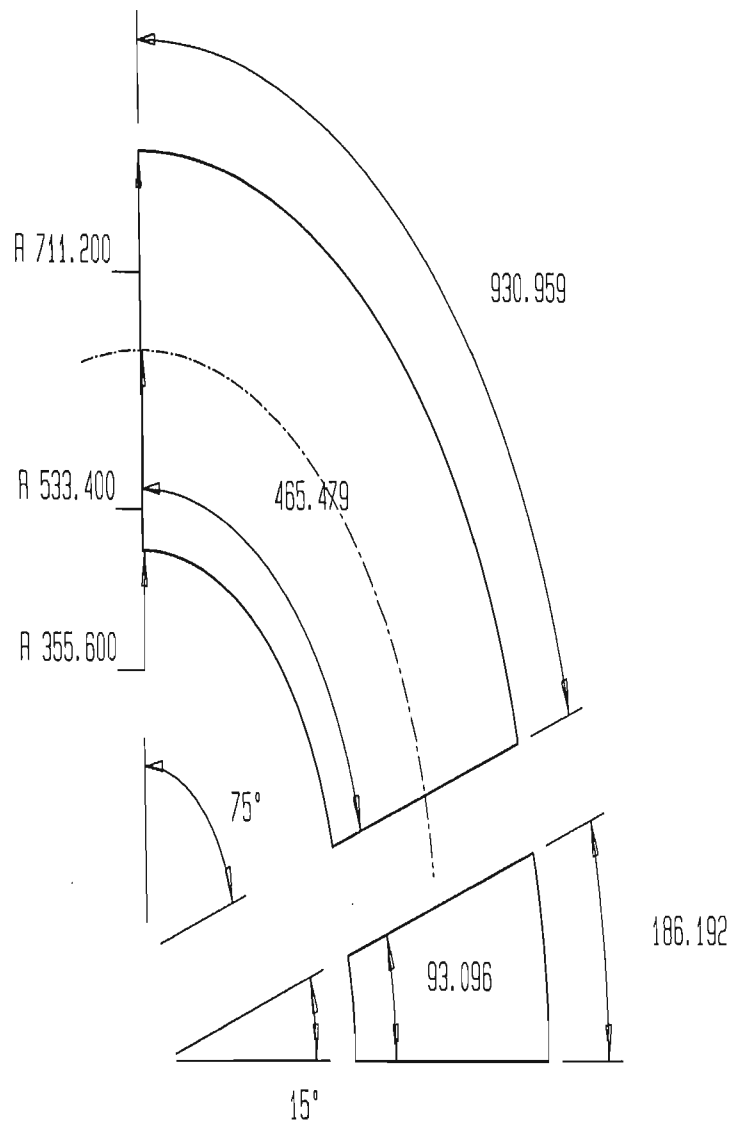
UNIVERSITY OF NATAL School of Mechanical Engineering	REV.	DATE	CHECKED	SCALE 1:10	UNITS: mm	PROJECT	No.
	Draftsperson			ESTIMATED MANUFACT. TIME:	STUDENT J. RANDELHOFF	MSC THESIS	9
	Technician					TITLE	FRAMEWORK
	W'Shop Manager			SUPERVISOR PROF. GOJ SMITH			





A flat plate of dimensions 410 \* 340 \* 10 is to be cut and formed as shown

UNIVERSITY OF NATAL School of Mechanical Engineering		REV.	DATE	CHECKED	SCALE 1 : 10	UNITS : mm	PROJECT MSC THESIS	No. 10
	Draftsperson				ESTIMATED MANUFACT. TIME:	STUDENT J RANDELHOFF	TITLE CURTAIN PLATE	
	Technician							
W'Shop Manager								



UNIVERSITY OF NATAL

Draftsperson

Technician

W'Shop Manager

REV.	DATE	CHECKED

SCALE 1 : 10

ESTIMATED  
MANUFACT.  
TIME:

UNITS : mm

STUDENT  
J RANDELHOFF

SUPERVISOR  
PROF. GOJ SMITH

PROJECT

MSC THESIS

TITLE

BEND FABRICATION

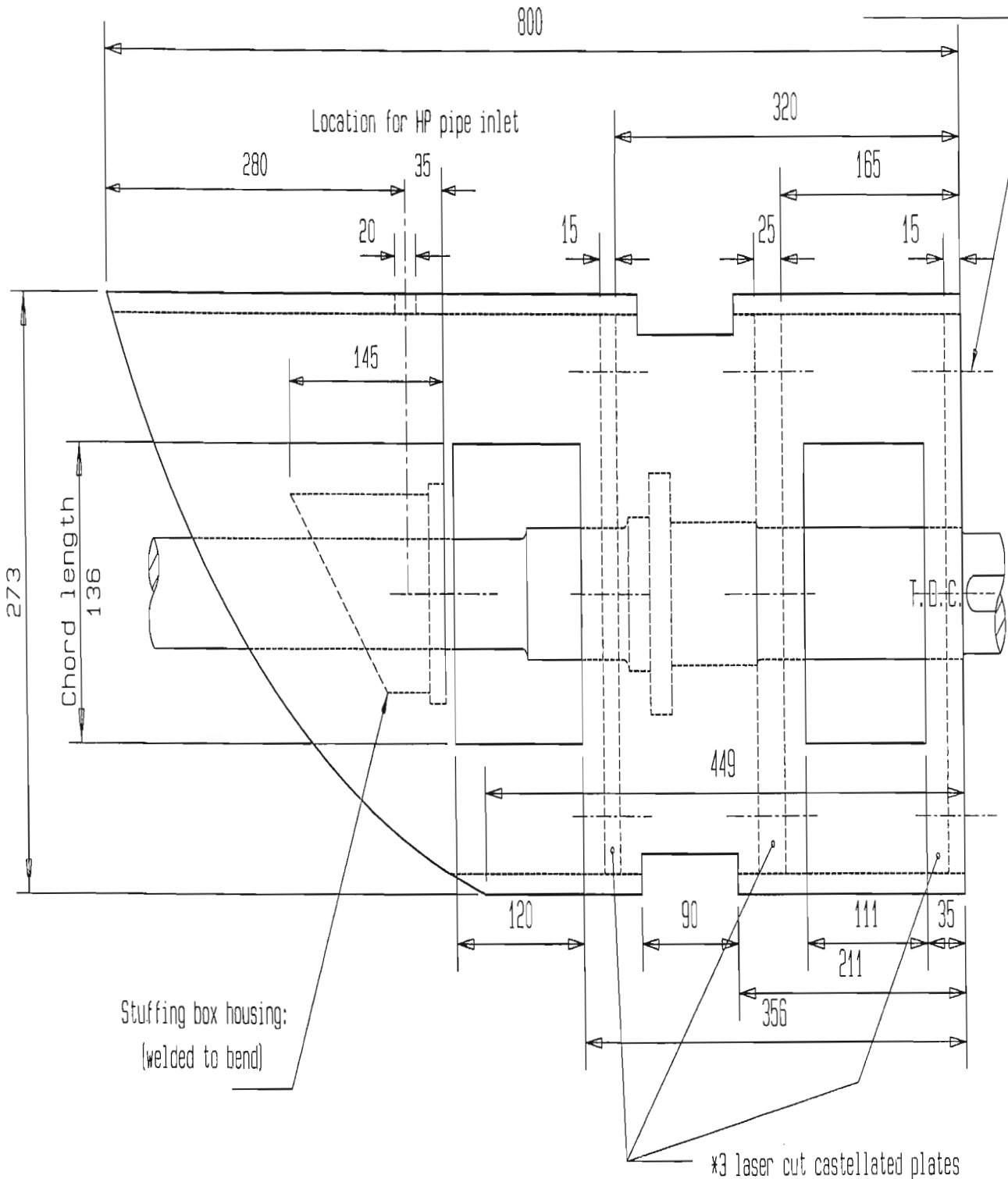
No.

11

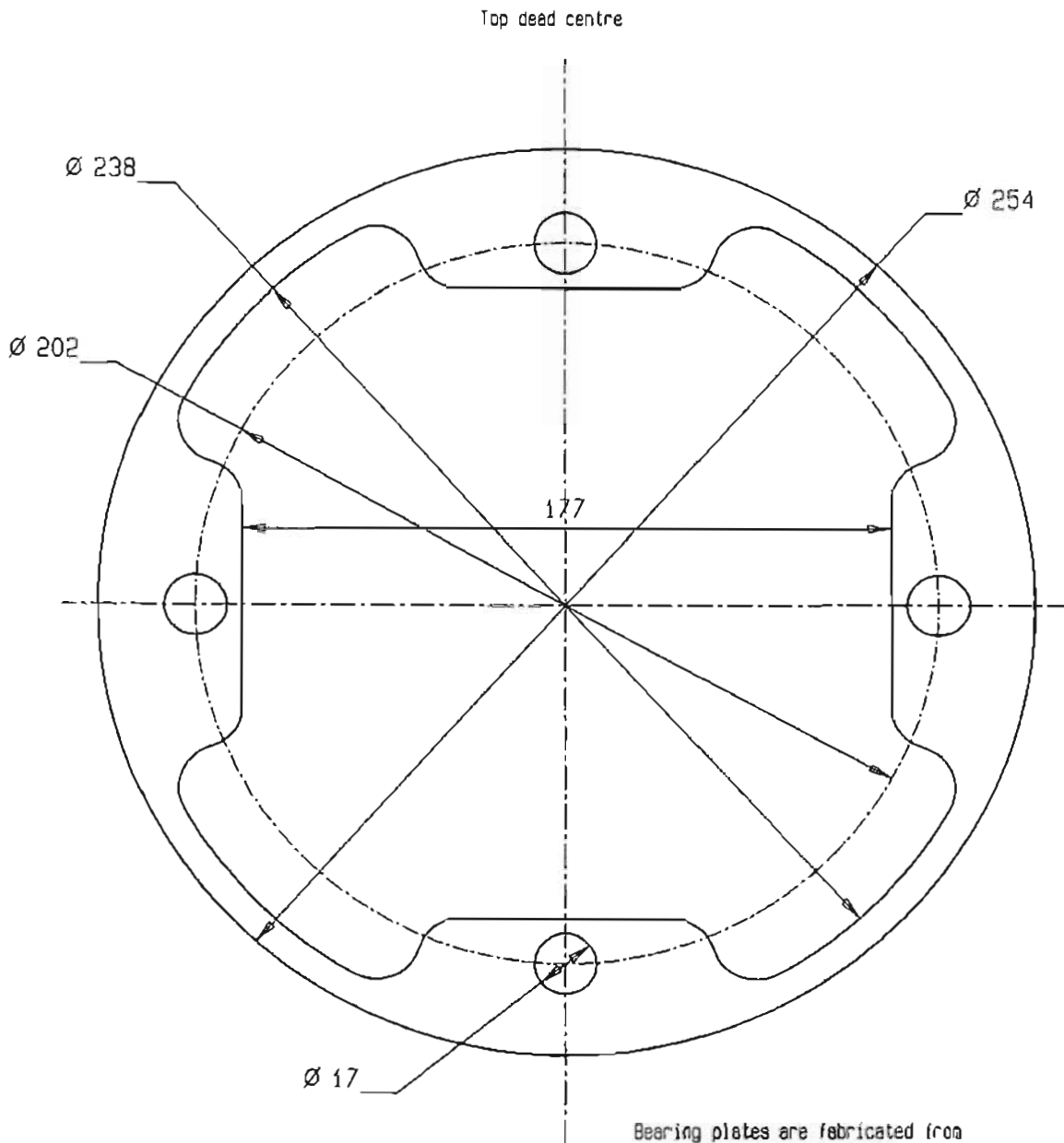


School of Mechanical Engineering

Centre line for M16 bolt holes  
 (@ P.C.D. = 202.23)



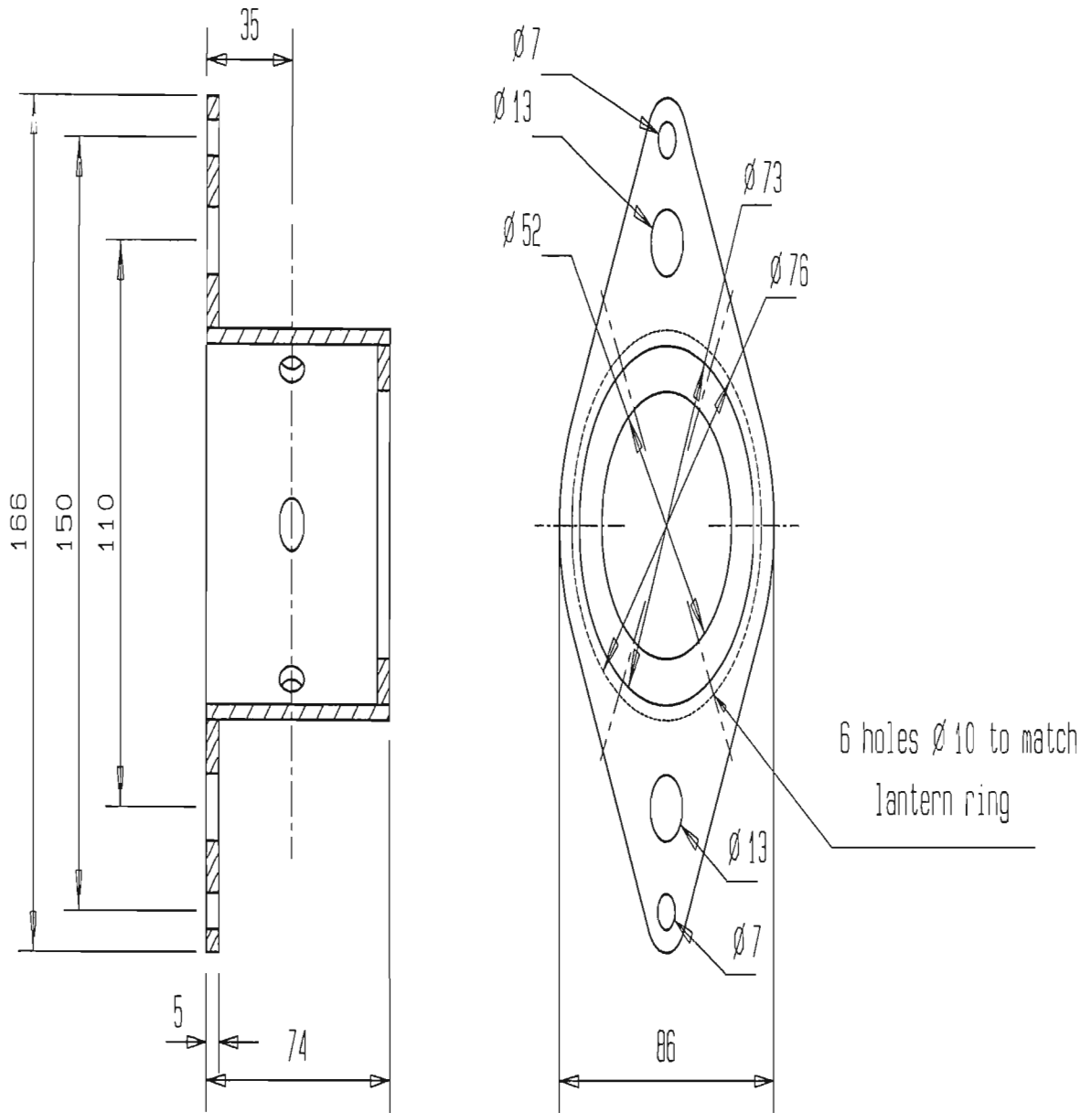
UNIVERSITY OF NATAL School of Mechanical Engineering		REV.	DATE	CHECKED	SCALE 1 : 4	UNITS : mm	PROJECT	No.
	Draftsperson				ESTIMATED MANUFACT. TIME:	STUDENT J RANDELHOFF	MSC THESIS	12
	Technician					SUPERVISOR PROF. GOJ SMITH	TITLE BEARING PEDESTAL	
W'Shop Manager								




Bearing plates are fabricated from  
laser cut plain carbon steel:  
to be supplied  
2 of 15mm, 1 of 25mm thickness

<b>UNIVERSITY OF NATAL</b> School of Mechanical Engineering		<b>PROJECT</b> MSC THESIS		No. 13	<b>TITLE</b> CASTELLATED PLATE	
	REV.	DATE	CHECKED	SCALE	1 : 2	UNITS : mm
Draftsperson				ESTIMATED MANUFACT. TIME:	STUDENT J RANDELHOFF	
Technician					SUPERVISOR PROF. GDJ SMITH	
W'Shop Manager						

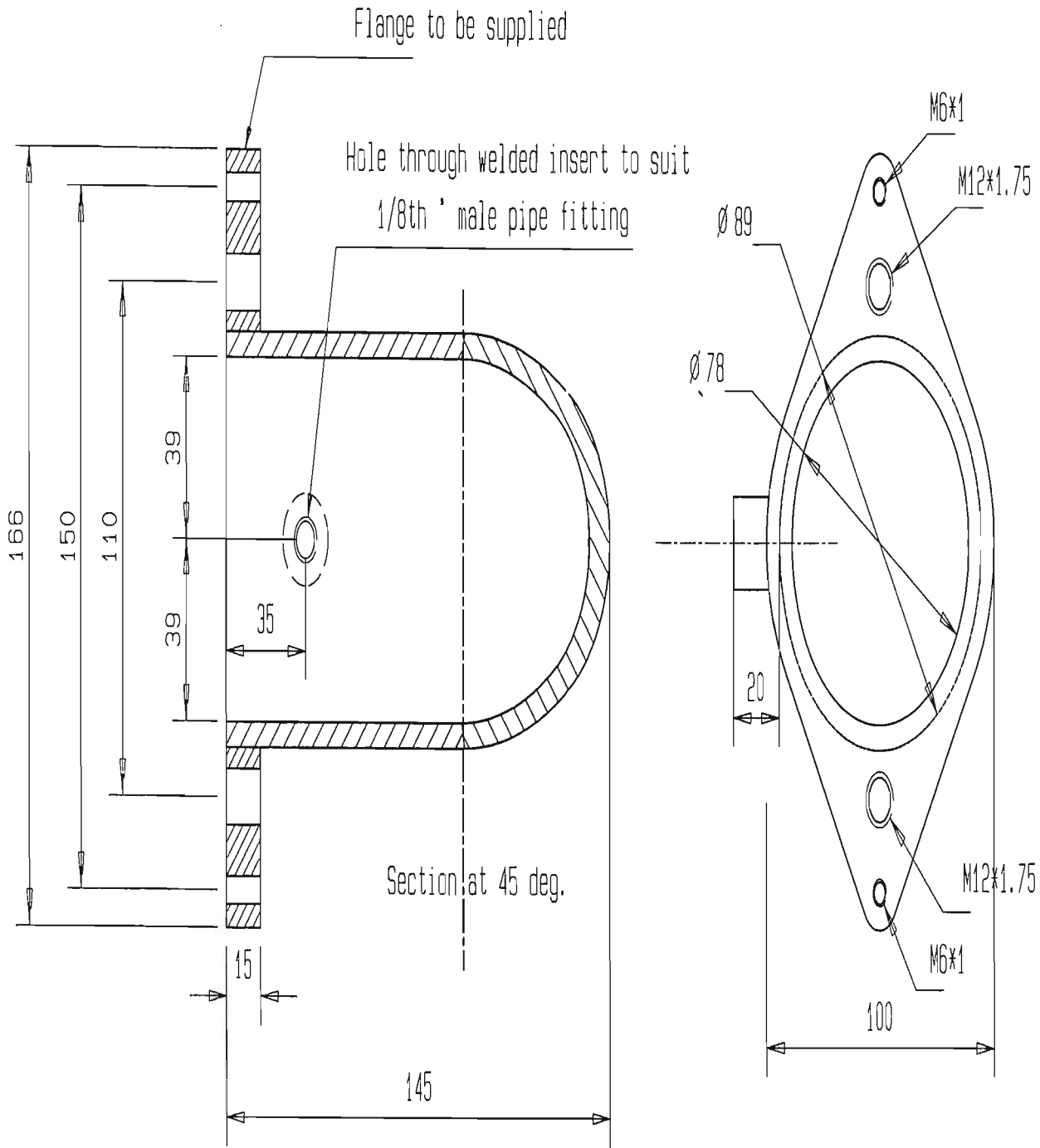
Stainless Steel packing housing insert:



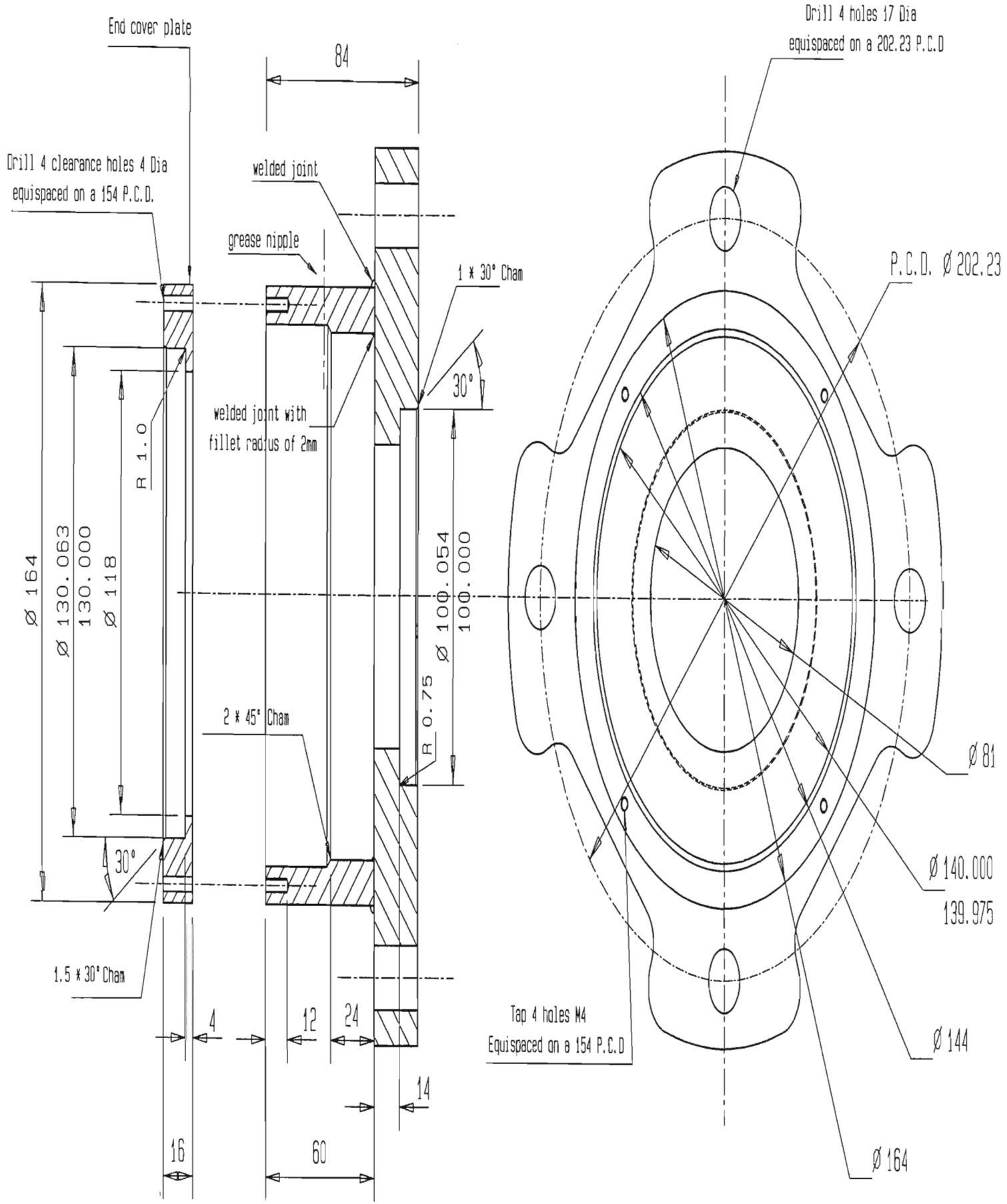
Flange and washer to be supplied

<b>UNIVERSITY OF NATAL</b> School of Mechanical Engineering		REV.	DATE	CHECKED	SCALE 1 : 2	UNITS : mm	PROJECT	No.
	Draftsperson				ESTIMATED MANUFACT. TIME:	STUDENT J RANDELHOFF	MSC THESIS	14
	Technician						TITLE	STUFFING BOX 
	WShop Manager				SUPERVISOR PROF. GDJ SMITH			

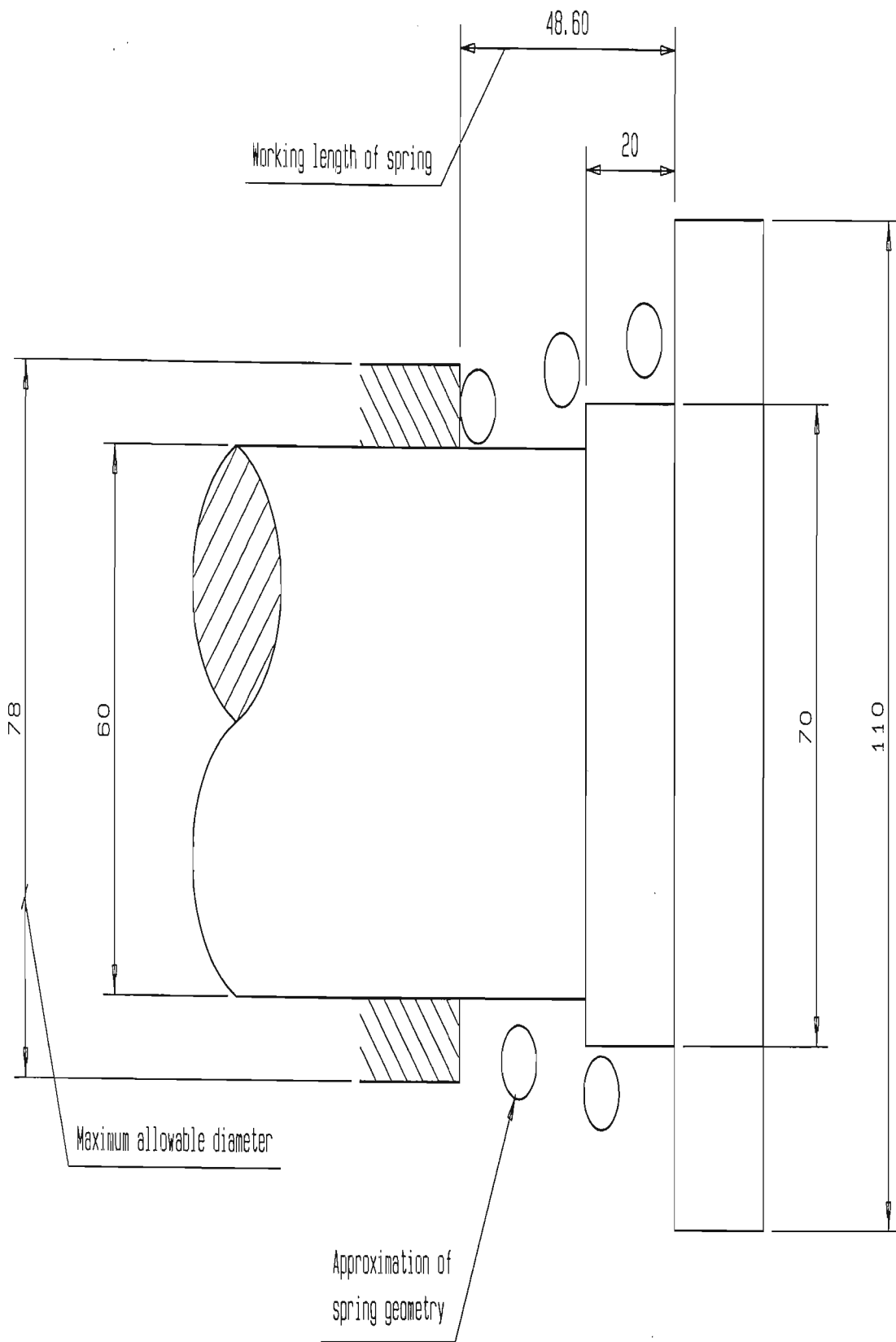




UNIVERSITY OF NATAL School of Mechanical Engineering		REV.	DATE	CHECKED	SCALE 1 : 2	UNITS : mm	PROJECT	No.	
	Draftsperson				ESTIMATED MANUFACT. TIME:	STUDENT J RANDELHOFF	MSC THESIS	15	
	Technician						TITLE	STUFFING BOX HOUSING	
	WShop Manager						SUPERVISOR PROF GOJ SMITH		



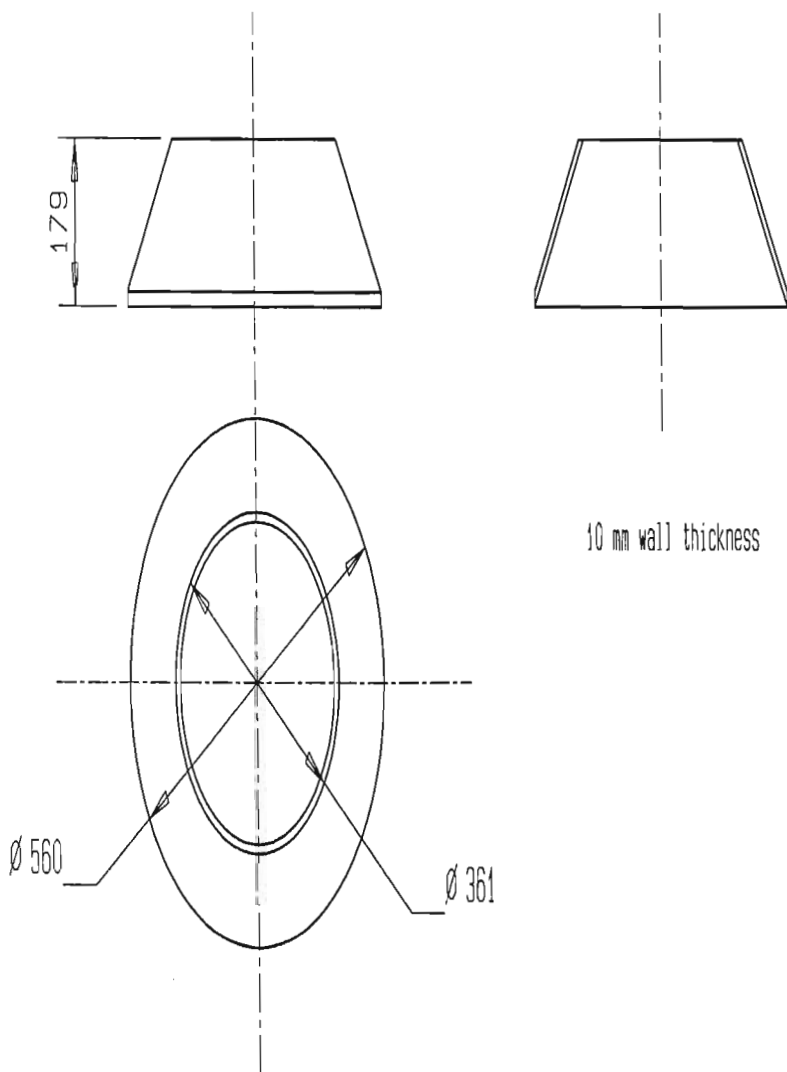
UNIVERSITY OF NATAL School of Mechanical Engineering	REV.	DATE	CHECKED	SCALE 1 : 2	UNITS : mm	PROJECT	No.
	Draftsperson			ESTIMATED MANUFACT. TIME:	STUDENT	MSC THESIS	16
	Technician				J RANDELHOFF	TITLE	
	WShop Manager				SUPERVISOR PROF. GDJ SMITH	THRUST BEARING HOUSING	



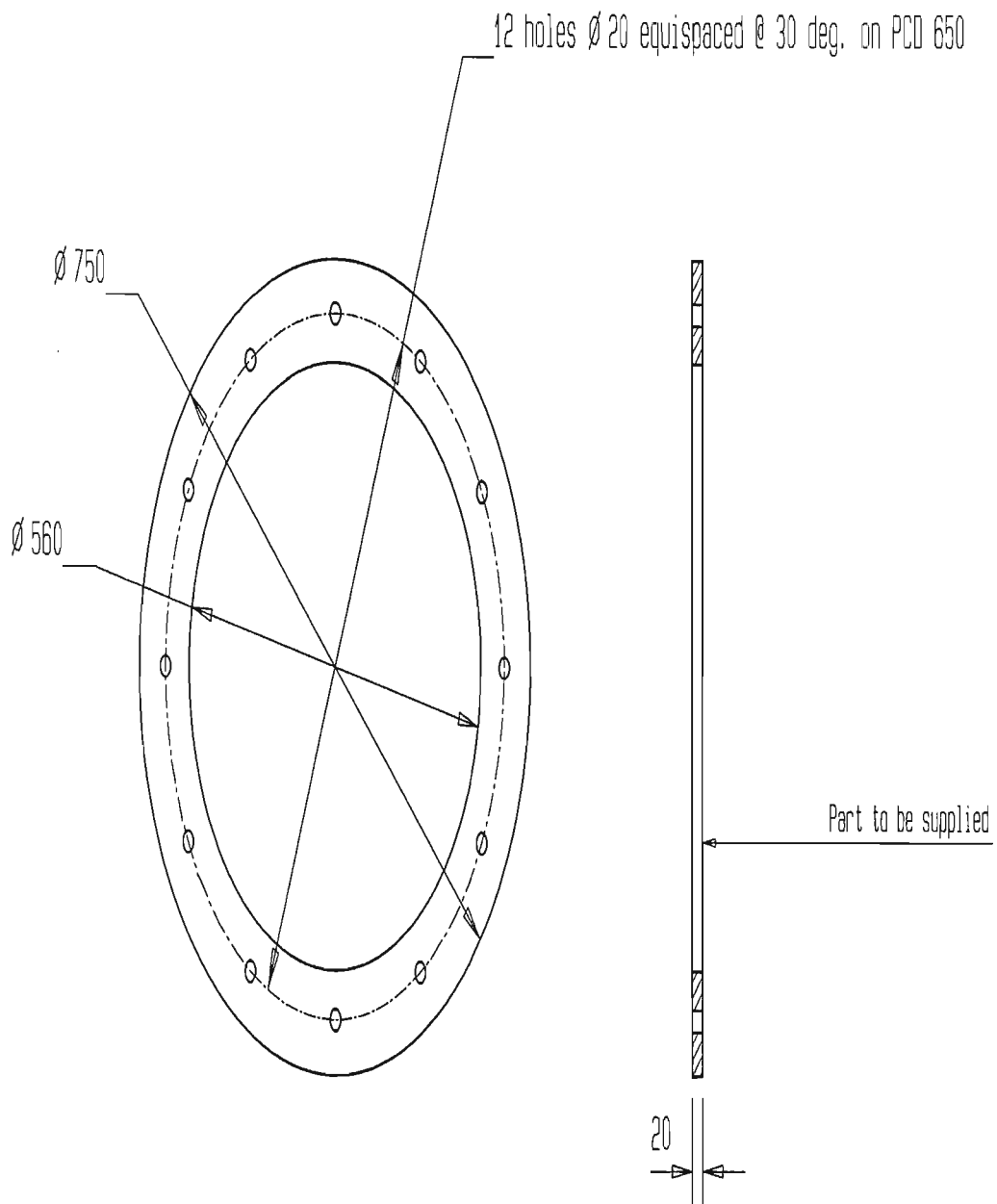
UNIVERSITY OF NATAL School of Mechanical Engineering		REV.	DATE	CHECKED	SCALE 1:1	UNITS : mm	PROJECT	No.
	Draftsperson				ESTIMATED MANUFACT. TIME:	STUDENT J. RANDELHOFF  SUPERVISOR PROF. GDJ SMITH	MSC THESIS	17
	Technician						TITLE	
	WShop Manager						PE-LOAD SPRING	



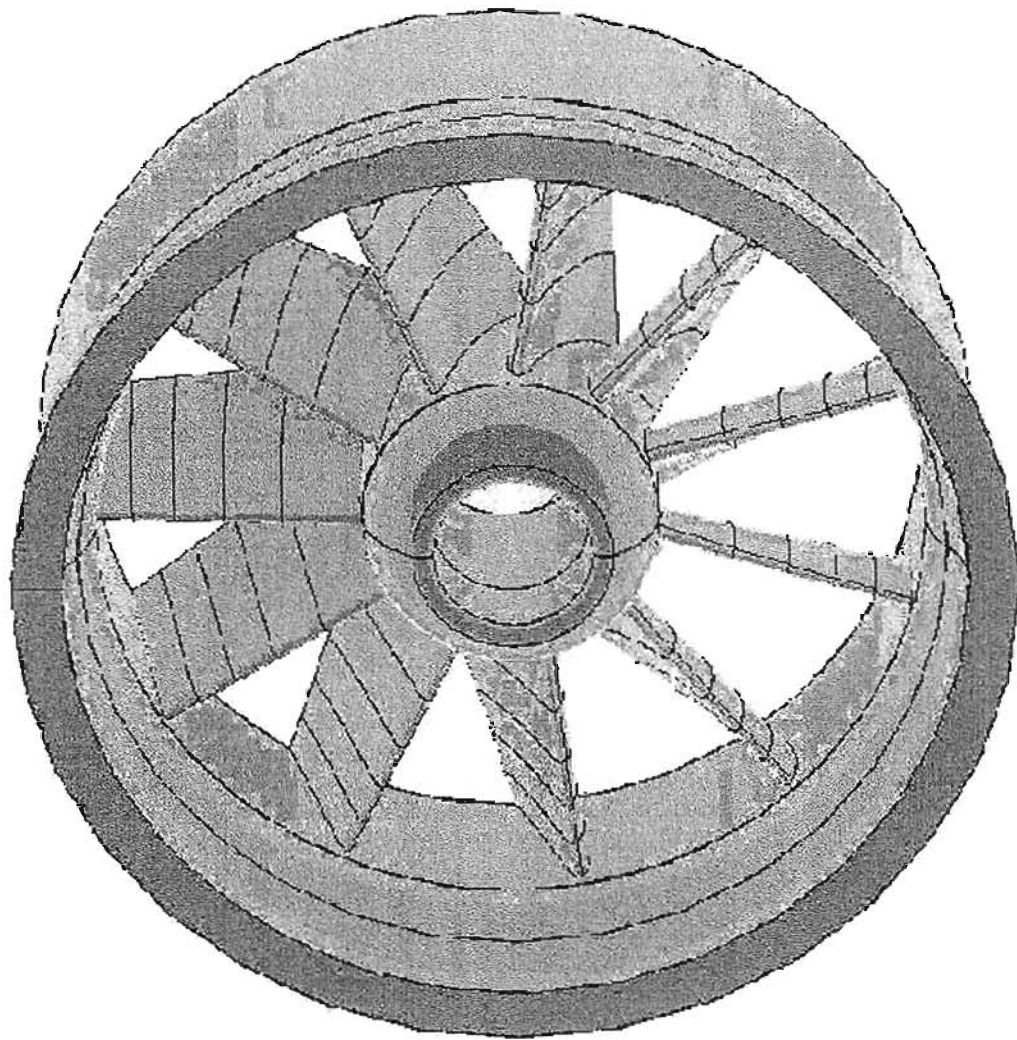
Chamfer to be machined parallel to the diffuser axis such that it forms a knife edge with the I.D.



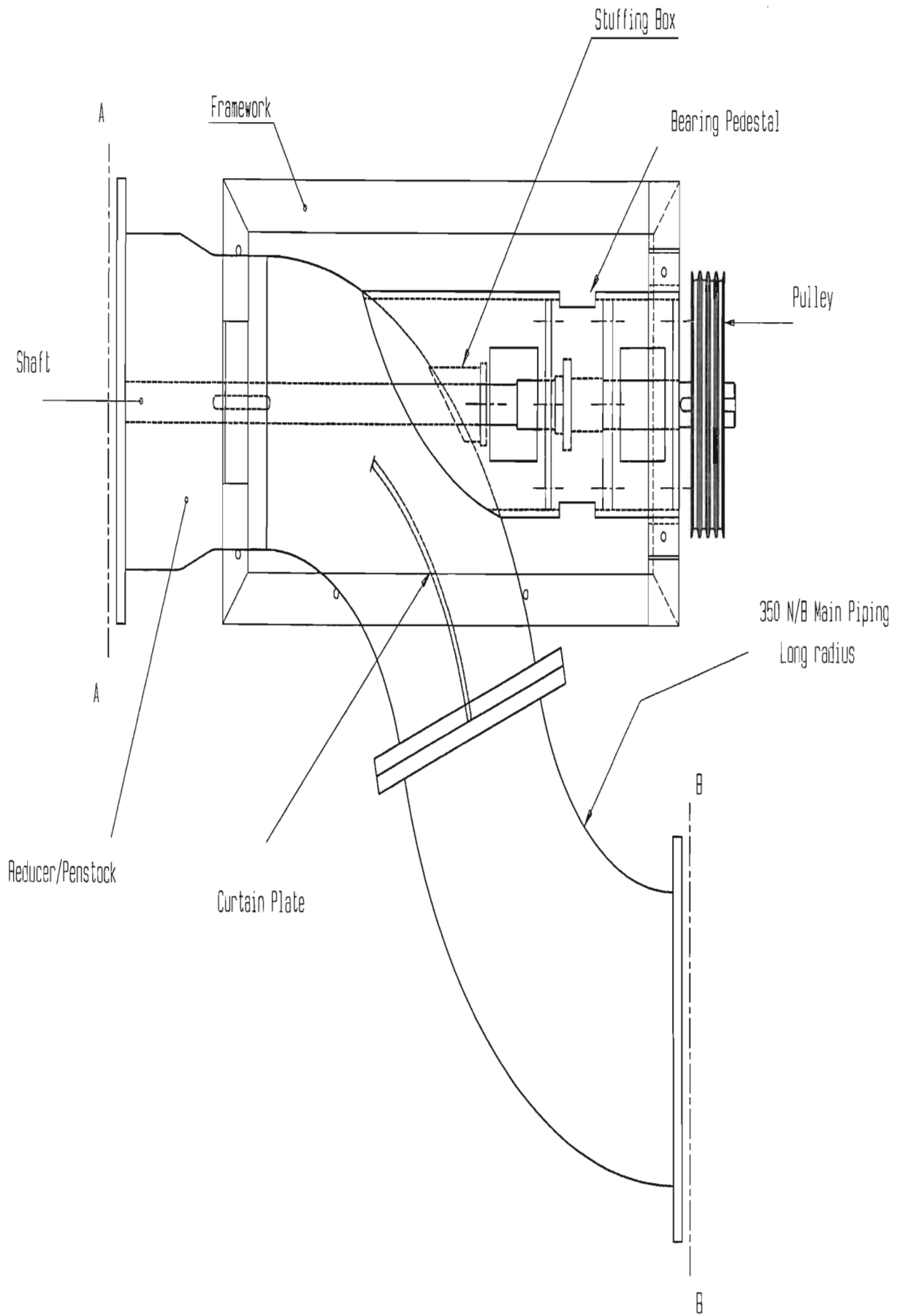
UNIVERSITY OF NATAL School of Mechanical Engineering		REV.	DATE	CHECKED	SCALE 1 : 12	UNITS : mm	PROJECT	No. 18
	Draftsperson				ESTIMATED MANUFACT. TIME:	STUDENT J RANDELHOFF	MSC THESIS	
	Technician					SUPERVISOR PROF. GOJ SMITH	TITLE	
	W'Shop Manager						DIFFUSER	



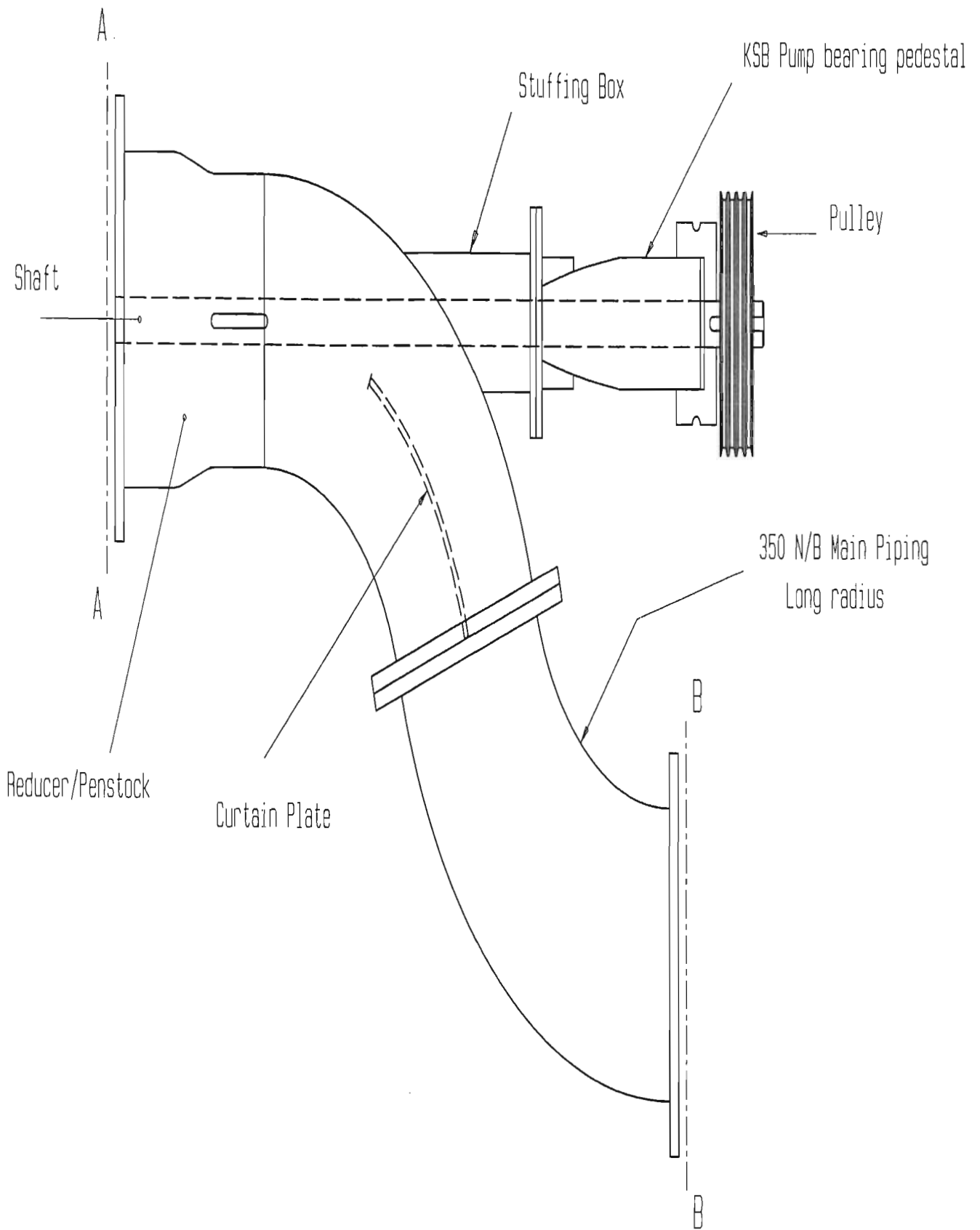
UNIVERSITY OF NATAL School of Mechanical Engineering		REV.	DATE	CHECKED	SCALE 1 : 10	UNITS : mm	PROJECT	No.
	Draftsperson				ESTIMATED MANUFACT. TIME:	STUDENT J RANDELHOFF SUPERVISOR PROF. GOJ SMITH	MSC THESIS	19
	Technician						TITLE	
	W'Shop Manager						DIFFUSER FLANGE	

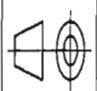


<b>UNIVERSITY OF NATAL</b>		<b>PROJECT</b>		<b>No.</b>	<b>TITLE</b>
School of Mechanical Engineering		MSC THESIS		20	STATOR WITH HOUSING
	<b>REV.</b>	<b>DATE</b>	<b>CHECKED</b>	<b>SCALE</b>	
Draftsperson				UNITS : mm	
Technician				<b>STUDENT</b>	J RANDELHOFF
W'Shop Manager				<b>SUPERVISOR</b>	PROF. GDJ SMITH
				<b>ESTIMATED MANUFACT. TIME:</b>	

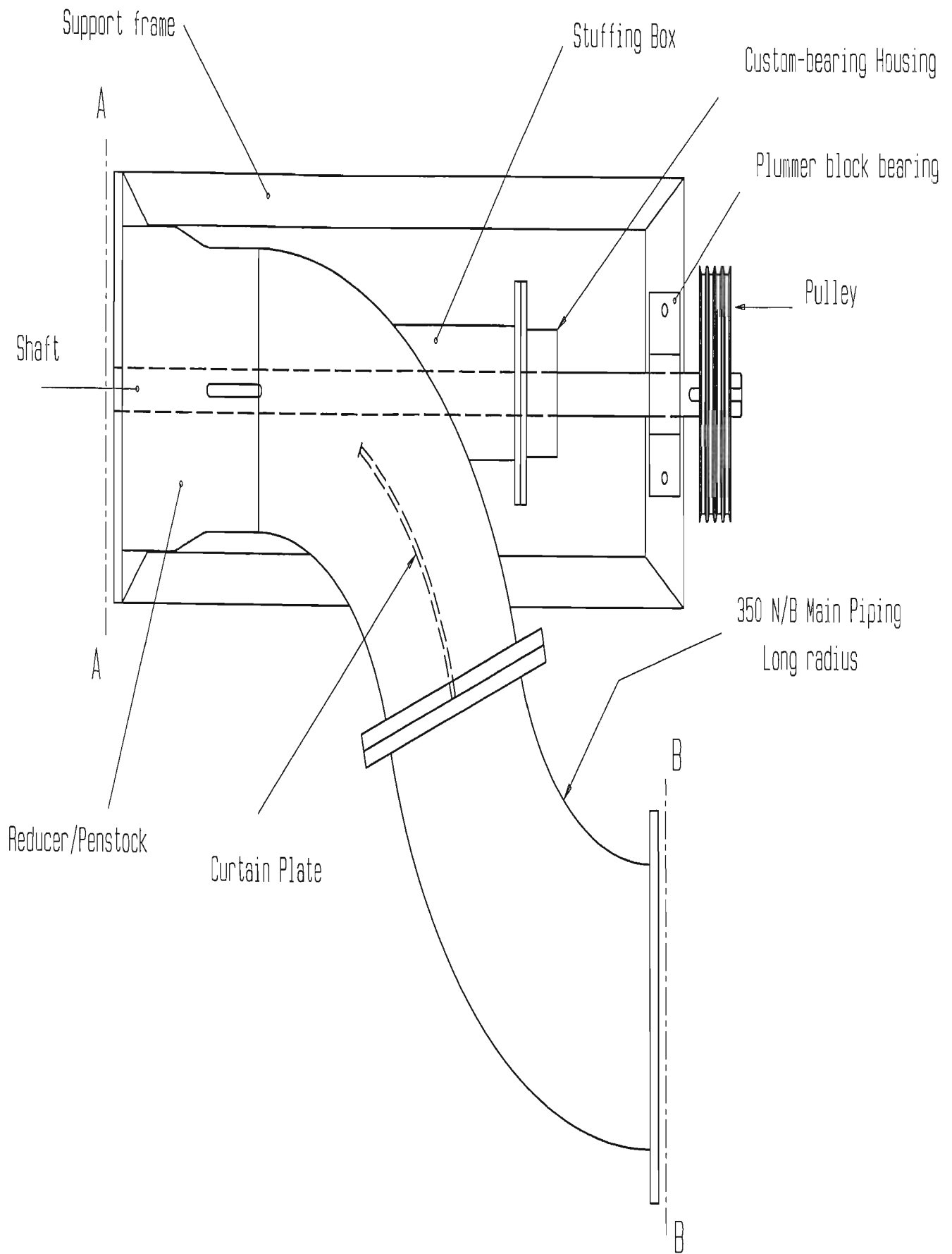


<b>UNIVERSITY OF NATAL</b> School of Mechanical Engineering		REV.	DATE	CHECKED	SCALE 1 : 10	UNITS : mm	PROJECT	No.
	Draftsperson				ESTIMATED MANUFACT. TIME:	STUDENT J. RANDELHOFF	MSC THESIS	21
	Technician						TITLE	
	W'Shop Manager					SUPERVISOR PROF. GOJ SMITH	ASSEMBLY	



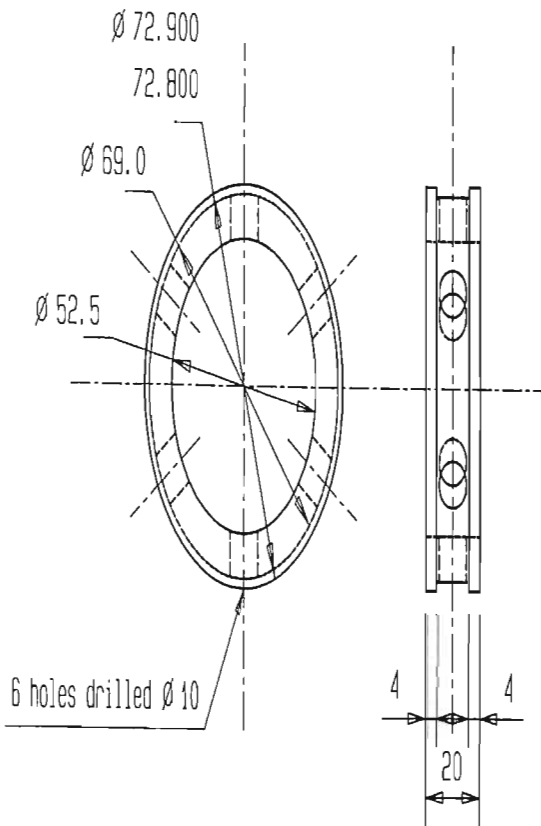
<b>UNIVERSITY OF NATAL</b> School of Mechanical Engineering		REV.	DATE	CHECKED	SCALE 1 : 10	UNITS : mm	PROJECT	No.
	Draftsperson				ESTIMATED MANUFACT. TIME:	STUDENT J RANDELHOFF	MSC THESIS	22
	Technician						TITLE	
	W'Shop Manager						STD BEARING ASSEMBLY	



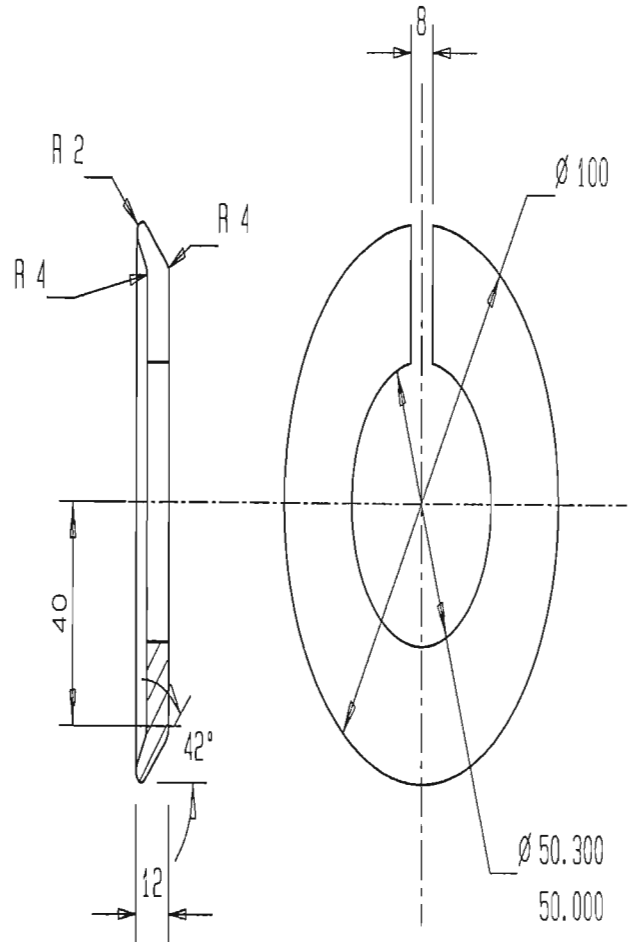


UNIVERSITY OF NATAL School of Mechanical Engineering		REV.	DATE	CHECKED	SCALE 1 : 10 ESTIMATED MANUFACT. TIME:	UNITS : mm	PROJECT	No.
	Draftsperson					STUDENT J RANDELHOFF	MSC THESIS	23
	Technician					SUPERVISOR PROF. GOJ SMITH	TITLE	
	W'Shop Manager					STD BEARING ASSEMBLY		

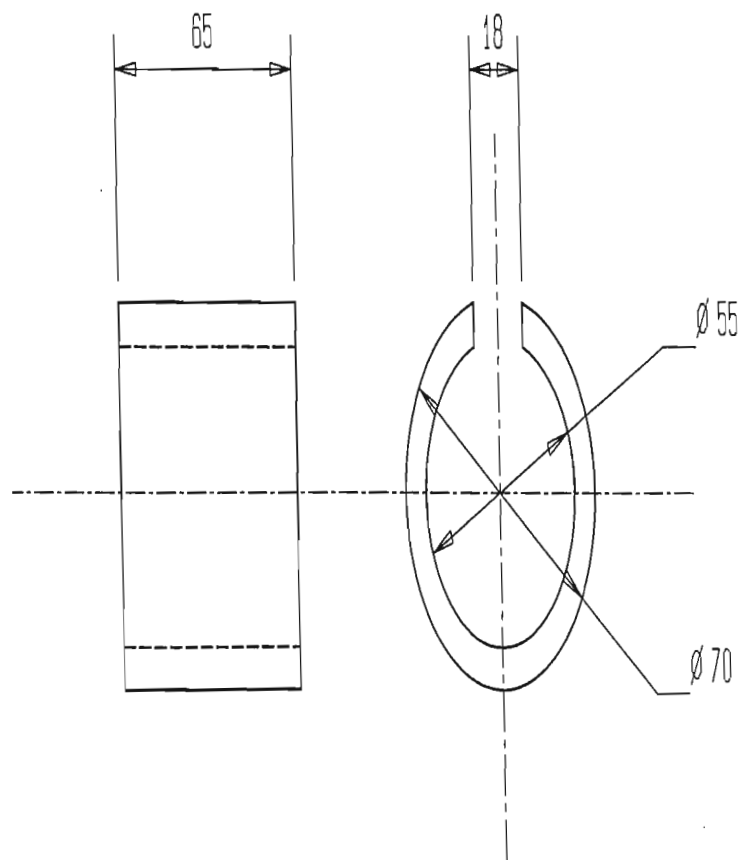
Lantern Ring



Slinger Ring



<b>UNIVERSITY OF NATAL</b> School of Mechanical Engineering		REV.	DATE	CHECKED	SCALE 1 : 2	UNITS : mm	PROJECT	No.
	Draftsperson				ESTIMATED MANUFACT. TIME:	STUDENT J RANDELHOFF	MSC THESIS	24
	Technician					SUPERVISOR PROF GOJ SMITH	TITLE LANTERN AND SLINGER	
	W'Shop Manager							



UNIVERSITY OF NATAL

School of Mechanical Engineering

	REV.	DATE	CHECKED
Draftsperson			
Technician			
W'Shop Manager			

SCALE 1 : 1  
ESTIMATED  
MANUFACT.  
TIME:

UNITS : mm  
STUDENT  
J RANDELHOFF  
SUPERVISOR  
PROF. GOJ SMITH

PROJECT  
MSC THESIS  
TITLE  
PTO BUSH

No.  
25

